

GEOCHEMISTRY OF SOME SULPHIDES AND SULPHO-SALTS
FROM PARYS MOUNTAIN, ANGLESEY

by

C. SIVAPRAKASH

A thesis submitted to the University of Aston in Birmingham in
partial fulfillment of the requirements for the award of the degree
of Master of Philosophy

May, 1977

Geochemistry of some sulphides and sulpho-salts from
Parys Mountain, Anglesey.

C. Sivaprakash

(Candidate for the M. Phil. degree, May, 1977)

SUMMARY

Sulphide mineralisation occurs at Parys Mountain, Anglesey, associated with Ordovician and Silurian sedimentary and volcanic rocks. Pyrite, chalcopyrite, sphalerite and galena are the sulphide minerals with minor quantities of arsenopyrite and pyrrhotite. Tetrahedrite-tennantites, and Pb and Bi sulpho-salts also occur as interstitial and fracture infillings in sulphides, mainly in pyrite. Pyritic mineralisation shows conformable features with the host rocks, whereas other sulphides and sulphosalts show epigenetic features.

Sulphides have been analysed for essential and trace elements namely Fe, S, Cu, Pb, Zn, Co, Ni, Ag, As, Sb, Sn, Ba, Mo, Te, Cd, Mn and Bi. Sphalerite and galena are comparatively more enriched in trace elements than pyrite and chalcopyrite. The Co/Ni ratio in pyrites is generally greater than 1.00, suggesting that the deposits are related to volcanism. Substantial quantities of Fe are present in sphalerites in solid solution.

Sulphosalts have been quantitatively identified by electron microprobe analysis to be tetrahedrite-tennantites, bournonites, kobellite, galenobismutite and lead sulpharsenides.

Unit cell edge measurements of sphalerite have been made by X-ray and electron diffraction, and a good linear relationship between mol% / FeS and unit cell edge is shown. Microhardness, reflectivity, infrared and d.t.a. data for sulphides are given - attempts to correlate the physical-optical characteristics with composition resulted in no significant conclusions, except the relation between microhardness and Fe content in sphalerite.

Diabantite, ripidolite, grochauite, clinocllore and aphrosiderite are the chlorite species occurring in the matrix associated with sulphide minerals; chlorite (1b species) has been identified in the matrix where no sulphide minerals occur.

The mineralogical and chemical results in the present study are interpreted to show that the mineralisation at Parys Mountain is a volcanogenic sedimentary process later enriched by hydrothermal processes.

Key words: Sulphide mineralogy, composition, trace-elements, sulpho-salts.

Acknowledgements

I am very grateful to Dr J. W. Gaskarth for his advice, patience, and supervision of this work and to Dr R. A. Ixer for his constant help, discussions and for critically reading the manuscript. I am also grateful to Dr D.J. Vaughan for his help and suggestions in the reflectivity studies, X-ray study of sphalerite and in the sulpho-salt studies.

I am grateful to Prof. D. D. Hawkes for providing the necessary facilities. I also thank all the members of the staff of the Department of Geological Sciences for their co-operation.

I express my gratitude to the technicians of the Departments of Geological Sciences, Metallurgy, and Chemistry for their technical assistance, especially to Mr D. Hodgson in the X-ray work, Mr R. Iver in the atomic absorption work, and to Mr S. Fuggle in the electron diffraction work. Mr J. H. Williams is thanked for his help throughout. My special thanks are due to Mr R. G. Howell of the Department of Metallurgy for his help during the electron-probe work and for providing the computer programme.

I am extremely grateful to the Ministry of Education and Social Welfare, Government of India for the award of a National Scholarship.

I am indebted to Dr N. F. M. Henry, University of Cambridge for kindly editing the draft during my absence on field work in India, and to Mrs J. Woodman for typing the whole thesis.

C. Sivaprakash

4 May 1977

List of Figures

- Fig. 1 Sketch Map of Anglesey to show the Parys Mountain Area
- Fig. 2 Simplified Geological map of Parys Mountain Area (after Thanasuthipithak, 1974)
- Fig. 3 Cross sections illustrating the structural interpretations at Parys Mountain
- Fig. 4 Sections illustrating the various lodes (after Manning, 1959)
- Fig. 5 Sketches of core and polished sections to show macroscopic features of the ore types
-
- Fig. 6a Size distribution of framboidal pyrites in sample A15/920 (180 frambooids)
- Fig. 6b Size distribution of framboidal pyrites in sample A15/941 (160 frambooids)
- Fig. 6c Size distribution of framboidal pyrites in samples H4/460 and H4/474
- Fig. 6d Plot of frequency against number of frambooids/cluster (sample H4/464)
- Fig. 7a Plot of microhardness (VHN) against wt% Fe in pyrite
- Fig. 7b Plot of microhardness against wt% Fe in chalcopyrite
- Fig. 7c Plot of microhardness against wt% Fe in sphalerite
- Fig. 7d Plot of microhardness against wt% As in galena
- Fig. 7e Plot of microhardness against wt% Bi in galena
- Fig. 8a Spectral reflectivity profiles of pyrite
- Fig. 8b Spectral reflectivity profiles of chalcopyrite
- Fig. 8c Spectral reflectivity profiles of sphalerite
- Fig. 8d Spectral reflectivity profiles of galena
- Fig. 9a Plot of Reflectivity (R%) at 589nm against wt% Fe in pyrite
- Fig. 9b Plot of Reflectivity (R%) at 589 nm against wt% Fe in sphalerite
- Fig. 9c Plot of Reflectivity (R%) at 589 nm against wt% As in galena
- Fig. 9d Plot of Reflectivity (R%) at 589nm against wt% Bi in galena

List of Figures (continued)

- Fig. 10 Infra-red spectra of pyrite
- Fig. 11 D. t. a. curves of pyrite
- Fig. 12 Infra-red spectra of chalcopyrite
- Fig. 13 D. t. a. curves of chalcopyrite
- Fig. 14 Plot of wt% Zn against wt% Fe in sphalerite
- Fig. 15 Plot of Mol% FeS against unit cell edges of sphalerite
- Fig. 16 Plot of Mol% CdS against unit cell edges of sphalerite
- Fig. 17 Infra-red spectra of sphalerite
- Fig. 18 Infra-red spectra of galena
- Fig. 19 Plot of wt% Sb against wt% As in tetrahedrite-tennantites showing the compositional break
- Fig. 20 Orthochlorites showing the species and variety boundaries (after Hey, 1954)
- Fig. 21 Infra-red spectra of chlorites

List of Tables

Table

1. Stratigraphic sequence at Parys Mountain
2. Classification of ore types
3. Summary of some mineral forms at Parys Mountain
4. Table showing the ore minerals at Parys Mountain
5. Summary of textures shown by ore minerals at Parys Mountain
6. Simplified paragenetic diagram of primary sulphides and sulpho-salts at Parys Mountain
7. Table to show the techniques employed and the nature of information obtained
8. Table showing the essential and trace-element composition of Pyrite (2 sheets)
9. Table showing the essential and trace-element composition of Chalcopyrite
10. Table showing the essential and trace-element composition of Sphalerite
11. Fe and Cd contents of Sphalerites
12. Table showing the essential and trace-element composition of Galena
13. Table showing the statistical data of Pyrite (in p. p. m. and %)
14. Table showing the statistical data of Chalcopyrite (in p. p. m. and %)
15. Table showing the statistical data of Sphalerite (in p. p. m. and %)
16. Table showing the statistical data of Galena (in p. p. m. and %)
17. Table showing the measured and calculated cell edges of Sphalerite
18. Table showing the differences in measured cell edges of Sphalerite by X-ray diffraction and by electron diffraction
19. Microhardness values of Pyrite
20. Microhardness values of Chalcopyrite
21. Microhardness values of Sphalerite
22. Microhardness values of Galena
23. Table showing the spectral reflectivity values of Pyrite in air
24. Table showing the spectral reflectivity values of Chalcopyrite in air
25. Table showing the spectral reflectivity values of Sphalerite in air
26. Table showing the spectral reflectivity values of Galena in air
27. Composition of Arsenopyrite

List of Tables (continued)

28. List of sulpho-salts found at Parys Mountain
29. Composition of Tetrahedrite - Tennantites
30. Table giving the atomic proportions for Tetrahedrite - Tennantite
(present study)
31. Composition and atomic proportions of Bournonite
32. Composition and atomic proportions of Kobellite
33. Composition and atomic proportions of Galenobismutite
34. Composition and atomic proportions of lead sulpharsenides
35. X-ray powder diffraction data for Diabantite
36. X-ray powder diffraction data for Ripidolite
37. X-ray powder diffraction data for Clinocllore
38. X-ray powder diffraction data for Aphrosiderite
39. X-ray powder diffraction data for Grochauite
40. X-ray powder diffraction data for Chlorite 1b
41. Standards used for microprobe analysis

List of Plates

- | | |
|----------------|---|
| Plates I - III | Photomicrographs |
| Plate IV | X-ray images showing distribution of Sb-As in
Tetrahedrite-Tennantites |

LIST OF CONTENTS

Summary		Page
Acknowledgements		
List of Figures		
List of Tables		
List of Plates		
Chapter 1 Introduction		1
1.1	Geology of Parys Mountain	1
1.2	Mineralisation	2
1.3	Summary of geological events at Parys Mountain	3
1.4	The present investigation	3
Chapter 2 Mineralogy and Paragenesis		5
2.1	Introduction	5
2.2	Microscopic features	5
2.2.1	Pyrite	5
2.2.1.1	Euhedral-subhedral pyrite	6
2.2.1.2	Anhedral pyrite	6
2.2.1.3	Framboidal pyrite	6
2.2.2	Chalcopyrite	7
2.2.3	Sphalerite	7
2.2.4	Galena	8
2.2.5	Tetrahedrite-tennantite	8
2.2.6	Bournonite	8
2.2.7	Lead sulpharsenides	8
2.2.8	Bismuth sulpho-salts	9
2.3	Textural features	9
2.4	Paragenesis	9
2.5	Stratiform features of Parys Mountain ores	9
Chapter 3 Sulphide Investigations		11
3.1	Introduction	11
3.2	Pyrite	11
3.2.1	Composition	11
3.2.2	Physical-optical characteristics	13
3.2.2.1	Microhardness	13
3.2.2.2	Reflectivity	14
3.2.2.3	Infra-red studies	14
3.2.2.4	Differential thermal analysis	14
3.3	Chalcopyrite	15
3.3.1	Composition	15
3.3.2	Physical-optical characteristics	16
3.3.2.1	Microhardness	16
3.3.2.2	Reflectivity	16
3.3.2.3	Infra-red studies	16
3.3.2.4	Differential thermal analysis	17
3.4	Sphalerite	17
3.4.1	Composition	17
3.4.2	Unit-cell edge measurements of sphalerite	19
3.4.3	Physical-optical characteristics	21
3.4.3.1	Microhardness	21
3.4.3.2	Reflectivity	21
3.4.3.3	Infra-red studies	22

	Page
3.5 Galena	22
3.5.1 Composition	22
3.5.2 Physical-optical characteristics	23
3.5.2.1 Microhardness	23
3.5.2.2 Reflectivity	23
3.5.2.3 Infra-red studies	24
3.6 Arsenopyrite	24
3.7 Pyrrhotite	24
3.8 Summary and implications of sulphide investigations	24
Chapter 4 Sulpho-Salts	
4.1 Introduction	26
4.2 Tetrahedrite-tennantite	26
4.3 Bournonite	27
4.4 Bismuth sulpho-salts	28
4.5 Lead sulpharsenides	28
4.6 Implications of sulpho-salt geochemistry	29
Chapter 5 Wall Rock Studies	
5.1 Introduction	30
5.2 X-ray diffraction studies	30
5.3 Infra-red studies	31
Chapter 6 Discussion and Conclusions	
6.1 Discussion	32
6.1.1 Source and availability of elements	32
6.1.2 Environment of formation	33
6.1.3 Relationship with the host rocks	34
6.1.4 Post depositional characteristics	34
6.2 Summary of conclusions	34
Appendix 1 Sample Selection and Preparation	
Appendix 2 Some Laboratory Methods	
2.1 Atomic absorption spectrophotometry	37
2.2 Electron-probe microanalysis	37
2.3 Reflectivity	38
2.4 Indentation microhardness	39
2.5 Infra-red absorption spectroscopy	39
2.6 Differential thermal analysis	39
References	40
Tables	
Figures	
Plates	

CHAPTER 1

INTRODUCTION

1.1 Geology of Parys Mountain

Parys Mountain lies in the north-east corner of Anglesey (Fig. 1) in North Wales. Situated about 4 km south of Amlwch port it forms a prominent topographical ridge aligned in ENE-WSW direction, rising to over 150m above sea level.

The geology of Parys Mountain has been studied by many investigators for a number of reasons. Structurally and stratigraphically it is a very complex area (Manning, 1959; Bates, 1966) and hence the relationship between its sedimentary and volcanic rocks has been variously interpreted. Its mineral deposits have been compared with other mining fields in the southern Caledonides, such as Avoca (south-eastern Ireland), and Coniston (Lake District), because of similar age and comparable tectonic and stratigraphic positions (Williams, 1969; Fitton and Hughes, 1970; Wheatly, 1971a, b). It has a close analogy in its depositional environment to other conformable polymetallic deposits (Wheatly, 1971a), and the close relationship between mineralisation and petrology, especially the volcanic succession of the area, has been well exemplified (Thanasuthipithak, 1974).

The most comprehensive and detailed account of the geology of Parys Mountain was given by Greenly (1919). Later various aspects of its geology, namely stratigraphy, structure, lithology, and mineralisation, were described by Manning (1959), Derry (1961), Bates (1964, 1966), Hawkins (1966) and Wolfenden (1967) - in Thanasuthipithak (1974), Williams (1969), Wheatly (1971a, b) and Thanasuthipithak (1974). A simplified geological map after Thanasuthipithak (1974) is given as Fig. 2.

The general stratigraphic sequence and lithologies proved from the bore holes, and described by Hawkins (1966) and Thanasuthipithak (1974) is given in Table 1.

Parys Mountain is underlain by the Precambrian Mona complex (Fig. 2) which is represented by chlorite schists in the northern and eastern parts of the area, and by micaceous granitoid and quartzitic gneisses in the south. The Ordovician, best exposed in the northern side of the mountain consists entirely of Shales (Table 1). They were named as Parys Green Shales by Greenly (1919), Parys Shales by Hawkins (1966) and 'Slates' by Thanasuthipithak (1974) as they possess a well developed slaty cleavage.

Silurian rocks form the core of the mountain (Fig. 2) and consist of highly cleaved and silicified shales. Surrounding the core, except to the east, are exposures of highly silicified and sheared rocks forming a hair-pin shaped outcrop. These were called 'Felsites' by Greenly (1919) and were considered by him to be intrusive. Thanasuthipithak (1974) described these felsitic rocks as a succession of extrusive volcanic rocks of Ordovician age consisting of dacitic and rhyolitic volcanic fragmental rocks and some siliceous sinter, a similar conclusion to that of both Hawkins (1966) and Wheatly (1971).

The rocks of the Precambrian Mona Complex are thrust over younger rocks along several low angle thrust faults called the Carmel Head, Corwas, and Nebo Thrusts (Fig. 2).

Although the structural relationship between shales and 'felsitic' rocks and the resultant structure of Parys Mountain has been variously interpreted, it is now generally agreed that the structure is an east-north-easterly trending, single syncline overturned to the north, with shales in the core (Fig. 3) (Thanasuthipithak, 1974).

1.2 Mineralisation

The mineralised belt trends between 060° and 070° following the general strike of the enclosing strata and dips $30-50^{\circ}$ to the north. It extends for some 1500 m, and is some 400 m wide and has been worked to a depth of 300 m. The mineralisation occurs as a series of lenticular to tabular ore zones, in the folded sequences of Ordovician and Silurian sedimentary and volcanic rocks. The mineralisation is generally concentrated on both sides of the northern outcrops of the rhyolitic rocks. It is present both in the rhyolitic rocks and in the rocks which are in contact with them, namely the siliceous sinter, parts of the Ordovician slates in the north, and the Silurian slates on the south side of the northern limb (Fig. 4) (Thanasuthipithak, 1974). Based on the host rock and the mineralogy, four types of ores were distinguished by Wolfenden (1967) (in Thanasuthipithak, 1974), and a slightly different division was given by Wheatly (1971a). The former division is made use of in the present study. These ore types are given in Table 2 and the lodes in which they occur are shown in Fig. 4.

The origin of these mineral deposits was regarded by earlier workers to be epigenetic, based on the notion that the 'felsite' was intrusive and probably supplied hydrothermal ore-bearing fluids. Deposition was thought to have been modified by metasomatic pyritization,

chalcopyritization and some lead-zinc metasomatism (Greenly, 1919; Manning, 1959). The controls of ore deposition were thought to be both shear zones and lithological interfaces.

Wheatly (1971a, b) suggested that, at Parys Mountain as well as in other mining fields in the southern Caledonides (Avoca, south-east Ireland; Coniston, Lake District), the conformable lenticular, pyritic zones associated with volcanic sequences, reacted with later hydrothermal fluids to produce the complex galena-sphalerite-pyrite mineralization. He further suggested that the mineralisations in these fields, including Parys Mountain, have a pulsatory metasomatic sequence related to tectono-stratigraphic controls. The ore localisation was thought to have been controlled by suitable structures and the pyritic shale horizons. Thus, Wheatly concluded that the main mineralisation was of an epigenetic hydrothermal enrichment type on a 'prototype' syngenetic mineralisation.

Thanasuthipithak (1974) studied the relationship of mineralisation to petrology and concluded that because there was a close association of ore bodies as lenses and tabular bodies, generally conformable with the Ordovician volcanic host rocks, they could be interpreted to have synsedimentary-exhalative origin. According to him the deposits were later modified by remobilization of some sulphides to produce apparent epigenetic features during the Caledonian orogeny.

1.3 Summary of geological events at Parys Mountain

The main geological events including the mineralisation at Parys Mountain, according to Thanasuthipithak (1974), are a) Deposition of Ordovician sediments in a marine environment with volcanism producing acidic rocks, b) Continued Ordovician sedimentation with some mineralisation, c) Main stage volcanism with some mineralisation, d) Erosion, submergence and deposition of Silurian sediments, e) Deformation of sediments and volcanics during the Caledonian and Variscan orogenies along with remobilization of the sulphides.

1.4 The present investigation

It is hoped that further mineralogical and geochemical studies on sulphide minerals can supplement geochemical information and thus help the various interpretations on the genesis of Parys Mountain mineral deposits. Previous interpretations were based on structural, petrological and mineralogical observations and no investigation of the geochemistry of the ore minerals was made. Similarly no systematic and detailed

investigations of the composition of the ore minerals, trace element distribution patterns, partition behaviour of trace elements, if significant, have been made, and although sulpho-salt minerals were recognised, no quantitative determination of them have been made. Also no previous correlation has been done relating the observed quantitative and qualitative reflected light properties of the opaque minerals with composition.

In fact, there are only a few areas in the British Isles where the major and trace element geochemistry of the ore minerals has been investigated to interpret the metallogenesis. El Shazly (1951), El Shazly et al (1957), Bishara (1966), Kakar (1971) were the few to make systematic investigations on trace elements in sulphide minerals mainly sphalerite and galena. Trace elements in pyrite, chalcopyrite, sphalerite and galena mainly from Avoca and a few from the Parys Mountain, and Coniston areas were studied by Wheatly (1971a) who showed a similarity in trace element content in all these areas. The geochemical investigations at Parys Mountain by this author were however not detailed and systematic. He also pointed out that work in progress on the geochemical atlas of Great Britain has delineated an anomalous tin area associated with copper at Parys Mountain, the explanation for which is not properly understood.

The present study was a systematic one of the geochemistry of the ore minerals and some of the physical and optical characteristics of the sulphide minerals. To this end studies were made using electron probe microanalysis, atomic absorption spectrophotometry, X-ray diffraction, electron diffraction, quantitative and qualitative reflected light microscopy, infra-red spectroscopy and differential thermal analysis.

CHAPTER 2

MINERALOGY AND PARAGENESIS

2.1 Introduction

The mineralogy and paragenesis of sulphide and sulpho-salt minerals from Parys Mountain has been described by both Wheatly (1971a) and Thanasuthipithak (1974). A description of the textural and paragenetic features observed in 58 polished sections from bore holes not previously studied (bore hole numbers A15, 27, 19, 36A, 32; mainly of pyritic and Bluestone ore types) is given here in addition to descriptions of those observed in some sections previously studied by Thanasuthipithak (1974). Textural features and optical characters of the opaque minerals were examined in reflected light using a Reichert Zetopan Ore Microscope with a micrometer ocular for grain size measurement.

Pyrite is the most abundant of the sulphides followed by chalcopyrite, sphalerite, galena and minor quantities of microscopically identifiable tetrahedrite-tennantite, arsenopyrite, pyrrhotite, lead and bismuth sulpho-salts. Megascopically the specimens studied show 4 or 5 distinct forms. The general features of these forms and the corresponding ore types are summarized in Table 3, and Fig. 5 shows sketches of these forms.

2.2 Microscopic features

Only primary minerals are described here, although some secondary minerals, such as covellite and bornite, have been described by Wheatly (1971a) and Thanasuthipithak (1974). A list of ore minerals present, and their general characters are presented in Table 4. Pyrrhotite, from Parys Mountain, has been described by Wheatly (1971a) and Thanasuthipithak (1974), and arsenopyrite has been described by the latter author, but in the present study only their compositions have been determined and these are given in Chapter 3.

2.2.1 Pyrite

Pyrite is the most abundant of all the sulphides, and is most abundant in the pyritic ore type, being present both in the layered sulphide and in disseminated forms, and is relatively least abundant in the Bluestone Ore type. Pyrite grains show both primary fabrics, representing the original depositional features, and secondary fabrics representing deformational and recrystallised features. Euhedral-subhedral, anhedral and framboidal type pyrite grains comprise the primary type. Colloform pyrite was also described by Thanasuthipithak (1974). Cataclastic, radial and recrystallised textures comprise the secondary type.

2.2.1.1 Euhedral-Subhedral pyrite

This type is mainly associated with black shale and dacite as disseminations through the rock. The following three divisions can be made: a) Isolated simple pyrite euhedra in which the grain size varies from about 0.05 mm to about 2 mm with some chalcopyrite replacement at the margins. Pyrite euhedra are associated with rutile and in some instances are seen to replace it (Plate IA). It is therefore paragenetically later than rutile. b) Spherically arranged aggregates of pyrite cubes forming pseudomorphs after framboidal pyrite. As many as 14 pyrite euhedra are present forming a spherically arranged aggregate of pyrite cubes homogenised at the centre of the aggregate but retaining their cube outlines at the periphery (Plate IB). c) Pyritohedra with intense deformation textures, the pyrite grains being heavily fractured (Plate IC). In most instances the fractures are filled by other sulphides.

2.2.1.2 Anhedral pyrite

Anhedral pyrite is less abundant than the euhedral/subhedral type. It is generally fine-grained (0.01 mm to 0.05 mm) and forms allotriomorphic granular aggregates commonly enclosing euhedral pyrite which implies a generation gap between the two types.

2.2.1.3 Framboidal pyrite

Framboidal pyrite was seen mainly in the Bluestone ore type associated with galena-sphalerite mineralisation. Generally three kinds of framboids are present:- a) Isolated framboid microcrysts ranging in size from 2 microns to about 40 microns in diameter. Quantitative studies of framboid grain size were made and the distribution is seen to be positively skewed (Fig. 6). The maximum occurs at 30 microns and the majority of the framboids occur within 15 microns diameter. The size distribution is similar in sections from the different bore holes. There is some clustering of framboids and a plot of the number of framboids per cluster against frequency (Fig. 6d) shows an irregular pattern with the frequency maximum at 10 framboids/cluster. b) The second type has the framboidal grains in the form of a network whose interstices are infilled mainly by sulpho-salts. This feature was described as atoll texture (Thanasuthipithak, 1974) in which the framboidal grains are extensively replaced, enclosed, and cemented by tetrahedrites (Plate I E, F). c) The third type has the form of a recrystallised

aggregate. The framboids form clusters (Plate ID) and lose their form where they are joined. The loss of shape is attributed to the result of growth of later pyrite between the granules (Raybould, 1973).

In some specimens the core of the framboidal cluster is replaced by sphalerite, and in some instances by tetrahedrite. Radiating textures have also developed in some framboidal pyrites (Plate II C).

Some pyrite grains in the types described above are compositionally zoned (Plate II E). The radiating textures (Plate II C) and irregular fracturing (Plate I C) exhibited by some pyrites are interpreted as resulting from cataclasis. In most specimens the fractures are infilled by other minerals namely sphalerite, and tetrahedrite-tennantites. Pyrite is comparatively free from inclusions; however, in some grains, small quantities of chalcopyrite and some gangue material are present as inclusions.

Pyrite occurs in minor quantities as fine-grained anhedral to subhedral grains forming a distinct vein or fracture filling in the matrix.

2.2.2 Chalcopyrite

Chalcopyrite most commonly is anhedral in form. It occurs: a) as a fracture filling in and replacing euhedral to subhedral pyrites; b) as a matrix material enclosing the pyrite grains; c) as mutual intergrowths with sphalerite, galena and pyrite; d) isolated anhedra embedded in rock matrix; and e) as exsolution bodies in sphalerite. Little chalcopyrite is associated with euhedral pyrite with most being associated with other kinds of pyrite and with other sulphides.

Chalcopyrite, where it is associated with pyrite generally replaces it. It is replaced by sphalerite although there is depositional overlap shown by intergrowths with sphalerite and galena.

2.2.3 Sphalerite

Sphalerite most commonly occurs in the fine-grained Bluestone ore type. The grain size varies between 0.02 mm to 0.5 mm. It is present as anhedral and irregular grains intergrown with other sulphides mainly chalcopyrite, and in lesser quantities filling fractures in cataclastic pyrite.

Two types of sphalerites are recognised: a) sphalerite with exsolutions of chalcopyrite and b) sphalerite without exsolutions. The first type is far more abundant than the second. Both the types are intergrown with chalcopyrite. Bournonite is found as inclusions or

infillings in sphalerite. Sphalerite generally shows mutual replacement textures and intergrowths with galena (Plate II A and B) and this is interpreted to indicate co-deposition.

2.2.4 Galena

Galena is present mainly in the Bluestone ore and Copper ore types and is not present in the Pyritic ore type. The grain size varies from 0.05 mm to 0.2 mm. It forms allotriomorphic masses and most commonly is intergrown with sphalerite and chalcopyrite.

Mutual replacements of sphalerite and galena are also present. A little galena, however, clearly replaces sphalerite, and paragenetically is therefore later. Inclusions or infillings of some sulpho-salts are present in galena.

2.2.5 Tetrahedrite-tennantite

The tetrahedrite group is the most abundant of the sulpho-salts at Parys Mountain and it is found only in the Bluestone ore type. These minerals occur as a) fracture fillings in pyrite grains (Plate II D); b) an interstitial cementing matrix for some subhedral pyrite grains (Plates II E and III A); c) inclusions in some sphalerites and chalcopyrites along the peripheries of, and extensively replacing, pyrite framboids. The tennantite end member has a lower reflectivity value than that of tetrahedrite. The tetrahedrite has a reflectivity of between 34.3 and 36.5% at 589 nm in air, and tennantite between 29.5 and 31.7%. The microhardness value ranges 279-328 Kg/mm² for both minerals and their grain size varies from 0.005 mm to 0.01 mm.

2.2.6 Bournonite

Bournonite occurs as very small (grain size 30 microns) inclusions in sphalerite (Plate III B). The reflectivity is generally high (38 - 42%) but could not be precisely estimated because of the very small grain size.

2.2.7 Lead Sulpharsenides

These minerals generally are very similar to galena and it is very difficult to distinguish between them optically. They are distinguished from galena only by an absence of cleavages and triangular pits and by anisotropism (seen only in oil immersion). Electron microprobe analysis showed these minerals to be lead sulpharsenides. They are white in colour, have irregular shapes and generally occur replacing sphalerite and galena along with other sulpho-salts. The reflectivity values are similar to those for galena (about 39.3 - 43.5%) and the

microhardness was not determined because of the very small grain size (about 0.05 mm).

2.2.8 Bismuth sulpho-salts

These are very similar in appearance to the lead sulpho-salts; however, they have a more greyish white colour, are more anisotropic, and the reflectivity (34.5 - 37%) is slightly lower than that of the lead sulpharsenides. They were identified, from electron microprobe analyses, as kobellite and galenobismuthite. Grain shapes are anhedral and irregular and they are generally present only as infillings in other sulphides mainly sphalerite and pyrite.

Mutual replacements between the sulpho-salt minerals are absent and it is difficult to infer paragenetic differences between them. The occurrence as inclusions, and as interstitial infillings in sulphides, is interpreted to indicate that they are later than the sulphides.

2.3 Textural features

The textural relationships outlined fall into two distinct categories. To distinguish between them, here they are called: a) Primary fabrics - developed in the original precipitation or depositional processes, and b) Secondary fabrics - developed either superimposed on an original primary fabric (e.g. cataclastic texture in pyrite) or formed due to some epigenetic process (e.g. fracture infilling of sulpho-salts in pyrite). The two types of fabrics are summarized in Table 5.

2.4 Paragenesis

A simplified paragenetic diagram for the ore minerals, based on the textural relationships outlined above, is presented in Table 6. This is in general agreement with that of Wheatly (1971a) and that of Thanasuthipithak (1974). It should be noted that the information on pyrrhotite and arsenopyrite is from Thanasuthipithak (1974).

2.5 Stratiform features of Parys Mountain ores

Stanton (1972) described stratiform ores as those that occur as layers concordant with the stratification of the enclosing rocks. They are thus confined stratigraphically and occur in preferred horizons. A comparison of mineralogical features of Parys Mountain ores with those of New Brunswick described by Stanton (1959, 1960 Parts I and II) as a typical conformable stratiform deposit brings out the following coincident features:-

- a) Imperfect alignment of ore lenses parallel to the bedding plane or schistosity
- b) Dominance of pyrite as iron sulphide with pyrrhotite being very local and minor
- c) Dominance of sphalerite among non-ferrous minerals
- d) Galena, although important, is subordinate to sphalerite
- e) Presence of trace quantities of minerals such as arsenopyrite, tetrahedrite-tennantite and other sulpho-salts.

Further the close association of the ores with pyroclastic volcanic rocks, tuffs and siliceous sinter as one of the stratiform type characters (Stanton 1960 Part I) can also be demonstrated in case of Parys Mountain ores (Thanasuthipithak, 1974).

Stanton (1964) considered that the textural features observed in stratiform ores are not depositional but result from growth during diagenesis and metamorphism. This is supported by experimental studies (Stanton and Gorman 1968). This hypothesis can explain the isolated uninhibited growths of euhedral and framboidal pyrites and intergrowths of other minerals with mutual boundary configurations. It cannot, however, account for fracture and interstitial infillings because of the fact that availability of mineral matter at such vacant spaces cannot be a coincidence, but it is a depositional feature along the available channel ways.

At Parys Mountain, the association of mineralisation with characteristic acidic volcanic rocks, megascopic conformable characters, mineralogical assemblages, close similarities to well established stratiform deposits such as Avica, all point to the fact that it is a syn-sedimentary stratiform conformable mineralisation. Replacement fabrics and fracture and interstitial infillings, favour some deposition at a later date superimposed on the original minerals as a later process of epigenesis. Pyrite represents the major conformable mineralisation with a little chalcopyrite. Microscopic evidence suggests that the minor sulphides and sulpho-salts were deposited at a later date as a process of epigenesis.

CHAPTER 3

SULPHIDE INVESTIGATIONS

3.1 Introduction

The essential and trace element contents of the sulphide minerals and their physical and optical characteristics, namely the reflectivity, microhardness, infra-red spectra and differential thermal analysis were determined to see if they could be correlated with composition and/or to compare with the published data. Table 7 lists the techniques employed and the nature of information obtained from the various minerals.

Samples for the present study were obtained from diamond drill cores, and selection and preparation techniques are described in Appendix 1.

Analysis for essential and trace elements was done by Atomic Absorption Spectrophotometry (A. A. S.) and Electron Probe Microanalysis. Fe, Cu, Zn, Pb, Co, Ni, Mo, Ba, Cd and Te were analysed by A. A. S. This technique was used because of its high sensitivity and minimum interference from other elements for the elements determined (McLaughlin, 1967; Volborth, 1969) and its simplicity and rapidity of operation (Kahn, 1968; Angino and Billings, 1972). A Perkin Elmer model 460 Atomic Absorption Spectrophotometer was used for all analyses. Details of the technique and sample solution preparation method are given in Appendix 2.

Electron Probe Microanalysis was used to analyse the more finely grained sulphides which could not be recovered in the powdered form, and for the quantitative determination of the sulpho-salt minerals. Some 74 analyses were made on various sulphides and sulpho-salts from some 43 polished sections (Tables 8-12) for the elements Fe, S, Cu, Pb, Zn, Co, Ni, As, Sb, Bi, Mo, Sn, Ag, Cd, Mn and Se. Instrumental and analytical details are given in Appendix 2.

Techniques for reflectivity, microhardness measurements, and sample preparation, along with instrumental details of infra-red and differential thermal studies are given in Appendix 2.

3.2 Pyrite

3.2.1 Composition

Pyrite (FeS_2) has a theoretical composition of 46.6 wt% Fe and 53.4 wt% S. Specimens of euhedral, subhedral, anhedral, and

framboidal pyrites were analysed for both essential and trace elements by electron microprobe and atomic absorption spectrophotometry and the values are given in Table 8. S was not determined in the samples analysed by the latter technique. The mean, minimum and maximum values are given in Table 13. The Fe content was found to fall in the range from 43.16 to 48.25%, with a mean value of 45.01% which is lower than the theoretical one. The S content ranges from 52.35 to 55.38% with a mean of 54.14% which is slightly higher than the theoretical value.

Trace quantities of Cu, Pb, and Zn are present in nearly all the samples analysed. Cu is a common trace element in pyrite, and in the present study the majority of the samples contain less than 2000 ppm of Cu. The high quantities 1.08% and 1.27% of Cu measured in samples H 14/186, and A 15/971 respectively (Table 8) are probably due to some slight contamination by chalcopyrite. Pb and Zn have a similar distribution pattern with mean values close to each other (Mean Pb 482 ppm and mean Zn 528 ppm). The samples analysed by A. A. S. were free from galena and sphalerite and the analysis in the electron microprobe was done only on pure pyrite grains. Therefore Pb and Zn are probably present in solid solution. Zn, however, is not unexpected in pyrite as Fe and Zn commonly substitute for one another in many minerals.

Co and Ni were present in nearly all the samples. Co substitutes for Fe in the pyrite structure (Rankama and Sahama, 1950), and Ni can exist in solid solution in pyrite (Fleischer, 1955). In the present study these two elements were found in almost all the samples analysed by A. A. S., but they were present in quantities below measurable limits in the samples analysed by probe. Analysis by A. A. S. showed the Co content to range from 30 to 2075 ppm (Table 8) with the majority of the samples containing less than 800 ppm. Although the distribution of Ni is irregular it has the comparatively narrow range of 16-696 ppm. The Co content is thus generally higher than that of Ni.

The Co/Ni ratios determined are given in Table 8. The majority of them show Co/Ni ratios to be greater than 1. High Co values and a Co/Ni ratio > 1 were found to be characteristic of pyritic deposits associated with volcanism (Loftus-Hills and Solomon, 1967). Those deposits in which the Co/Ni ratio is < 1 for pyrites are considered to

be sedimentary in origin. Hawley, and Gavelin and Gabrielson, (in Fleischer, 1955) found separately that the Co content and the Co:Ni ratio were generally high in high temperature deposits. Analysis of Parys Mountain pyrites by Wheatly (1971a) showed a high Co content and Co/Ni ratio > 1.00 and so he concluded the deposits to be associated with volcanism. In the present study, since the majority of the samples showed a consistent Co/Ni ratio > 1.00 it is concluded that pyritic mineralisation is related to volcanism at Parys Mountain.

Notable quantities of As have been reported in pyrite (Rankama and Sahama, 1950). However, in the present study probe analyses showed As to be present in quantities below measurable limits except in 3 samples where it is greater than 0.1% (Table 8).

Cd occurs in pyrite in lower concentrations than in sphalerite (Vlasov, 1964). In the present study only about 40% of the samples analysed contain Cd and in quantities generally less than 1000 ppm.

Ba cannot usually substitute for Fe because of its larger ionic radius and is therefore not common in pyrite (Rankama and Sahama, 1950). In the present study, however, Ba was found in most of the samples analysed by A.A.S. although most of the samples contained below 500 ppm (Table 8).

Mo is not a common trace element in pyrite, though it was reported in syngenetic pyrites by El Shazly (1951). In the present study it was found in some 25% of the samples in quantities less than 500 ppm.

Te, because of physical and chemical similarities, commonly substitutes for S, and as much as 0.1% of Te has been reported in pyrites (Vlasov, 1964). In the present study the majority of the samples analysed by A. A. S. contain less than 200 ppm Te (Table 8). Te is relatively more common in pyrite than in other sulphides.

Other elements detected, although present in below measurable quantities by probe analysis, are Ag, Mn, Bi and in a few samples Se. Sb and Sn were looked for but were not detected.

3.2.2 Physical-optical characteristics

3.2.2.1 Microhardness

The microhardness values for the pyrites determined are given in Table 19. For a load of 100 gm Bowie and Taylor (1958) reported values of 1027-1240 kg/mm² for pyrite. Pyrite from Parys Mountain

has a hardness range of 1031-1483 kg/mm². Higher hardness values of 1186-1836 kg/mm² are quoted by Young and Millman (1964). The measurements made in the present study are thus well within this region. The indentations obtained were all fractured as has been observed by other authors. The weight percentages of Fe in pyrites were plotted against microhardness number (Fig. 7a); however, no relationship was found.

3.2.2.2 Reflectivity

Results of reflectivity measurements on pyrites in the wavelength region 400nm - 700nm at intervals of 20nm including 589nm are given in Table 23, and the spectral reflectivity profiles are shown in Fig. 6a. The profiles show a regular pattern generally increasing sharply with wave length until about 520nm and then increasing very gently (Singh, 1965). However, no significant differences could be observed with different types of pyrites namely the framboidal, euhedral, anhedral and subhedral pyrites (Fig. 8a). Reflectivity values at 589nm were plotted against weight percentage Fe in pyrite (Fig. 9a), but no conclusion could be drawn about their relationship.

3.2.2.3 Infrared studies

The infrared spectra produced for pyrite are given in Fig. 10. The pyrites show poor resolution, and this has been previously reported by Hunt et al (1950). The two absorptions shown by pyrite are in the wave length region 2.8-2.9 microns and 6.1-6.2 microns (Fig. 10). It can be seen in the figure that, compared to the sample A 15/924 which has Fe content of 43.98%, the two samples 36A/1617 and 32-1108, which have Fe content of 45.23% and 45.71% respectively, have more prominent absorptions in the wave length region 6.0-6.2 microns. In sample IM 6/1231, which has Fe content of 46.78%, the absorption in the wave length region 6.2 microns although more prominent than sample A 15/924, is less prominent than the other two samples. This probably indicates that variations in composition may have some role in the absorption patterns.

3.2.2.4 Differential thermal analysis (d.t.a.)

The d.t.a curves obtained for 6 pyrite samples are given in Fig. 11. Comparison with the curves obtained by Kopp and Kerr (1957) show that the present curves are in good agreement in that the pyrites show a broad exothermic peak in the region of 400-500°C. The endothermic

reactions are present at about 550°C. Samples studied have Fe content ranging from 43.19 to 46.78% but no significant differences in the exothermic or endothermic behaviour of these pyrites was observed.

3.3 Chalcopyrite

3.3.1 Composition

The theoretical composition of chalcopyrite in wt. percent. is 34.6% Cu, 30.4% Fe, and 35.0% S. In this study 19 samples were analysed and the results are given in Table 9. Out of these, 8 were analysed by A.A.S., and 11 by electron probe. Four samples analysed by the latter technique were also analysed by A.A.S. S was determined only in the probe analyses. The mean values for Cu, Fe and S of 34.53%, 29.62% and 35.78% (Table 14) respectively are close to the theoretical values given above, although there is a considerable range. The maximum frequency of Cu occurs in the range of 34-36%, Fe in the range of 29-31%, and S in the range of 36-37% (Table 9).

Zn was found in all the samples analysed, ranging from 1000 to 5600 ppm, with a mean around 1900 ppm; this is attributed to the closely associated sphalerite, which commonly occurs as small inclusions in chalcopyrite. However, chalcopyrite is structurally similar to sphalerite and some Zn may also be present in solid solution in the chalcopyrite structure.

As and Bi have been reported in chalcopyrite (Fleischer, 1955), and probe analyses in the present study show that most of the samples contain these two elements (Table 9). Three samples contain more than 0.1% As, and another 3 samples contain more than 0.1% Bi (Table 9). These samples are from the ore types in which arsenopyrite and bismuth sulpho-salts occur respectively. None of the samples which have a high As content contain arsenopyrite. The high As content does not result from contamination but probably is due to its presence in the structure of chalcopyrite. Bismuth sulpho-salts are present as very fine-grained minerals (Chapter 4) in some of the sections (H 4/491, IM 9/269) that have a high Bi content. Thus these minerals probably have contributed to the high Bi values in the form of tiny inclusions.

Co and Ni are present in most of the samples analysed. Analysis by A.A.S. showed that Co ranges from 60 to 710 ppm and Ni from 12 to 1060 ppm (Table 9). Trace quantities of Co and Ni are not unexpected

in chalcopyrite although Ni tends to be concentrated in pyrite relative to chalcopyrite (Vaughan 1971).

Cd commonly is present in chalcopyrite, although in lower quantities than in sphalerite, because of the structural similarities between them (Vlasov, 1964). Analysis by A.A.S. showed Cd to be present in the range of 98 to 446 ppm.

Pb was found in most of the samples analysed in the range of 313 to 1045 ppm.

Te was found in only a few samples, ranging from 55 to 192 ppm, probably substituting for S.

Ba (A.A.S. analysis) was found in quantities ranging from 165 to 1653 ppm, with a mean of 737 ppm. It is not a very common trace element in chalcopyrite and its presence in the chalcopyrites at Parys Mountain is difficult to explain.

Mo (A.A.S. analysis) was also found in some 50% of the samples, in quantities ranging from 28 to 510 ppm, with a mean of 217 ppm.

Ag, Mn, Sb, Se and Sn were all below the limits of measurement of the electron probe.

3.3.2 Physical-optical characteristics

3.3.2.1 Microhardness

Microhardness values measured for chalcopyrite are given in Table 20. This hardness range of 171-221 kg/mm² with perfect indentations, is in close agreement with that of 186-219 by Bowie and Taylor (1958). Weight %s of Fe in the chalcopyrites were plotted against microhardness number (Fig. 7b), however, as in the case of pyrite, the relationship is not pronounced.

3.3.2.2 Reflectivity

Reflectivity measurements for chalcopyrite in the wave length region 400-700nm including 589nm are given in Table 24. The spectral reflectivity profiles are given in Fig. 8b. Like pyrite, chalcopyrite also has a regular spectral reflectivity profile, generally increasing sharply with wave length until about 520nm and then increasing very gently. Reflectivity values at 589nm plotted against weight % Fe showed no relationship.

3.3.2.3 Infrared studies

The infrared spectra produced for chalcopyrite are given in Fig. 12.

Chalcopyrite has a poor resolution and one sample (A 15/1193) showed absorption in the vicinity of 6 and 7 microns region. In the two samples studied No. A 15/1193 has Cu 35.05%, Fe 32.37% and S 34.20% and the other (M 10/1521) has Cu 34.73%, Fe 27.73% and S 35.96%. The sample A 15/1193 has a very much higher Fe content than the other and this probably is responsible for its having a more pronounced absorption pattern in the region 2.85-2.9 and 6.0 microns regions.

3.3.2.4 Differential thermal analysis (d.t.a.)

The d.t.a. curves obtained for chalcopyrite are given in Fig. 13. The five samples studied showed marked exothermic behaviour in the vicinity of 450-460°C. as part of a broad exothermic reaction starting at 400°C and continuing up to 500°C. No significant differences in differential thermal behaviour with compositional variations were observed. The sample with a lower Fe content (sample M 10/1521 with Fe content 27.73) than the others (which have Fe contents ranging from 28.55% to 32.37%), has a smoother curve. This is probably because reactions with higher Fe contents become more vigorous than those with lower Fe content. Further detailed investigations are necessary for significant conclusions.

3.4 Sphalerite

3.4.1 Composition

Sphalerite has a theoretical composition of 67.10% Zn and 32.90% S by weight, but in nature this is not found because the sphalerite structure is remarkably tolerant of substitutions by Fe, Cd and Mn for Zn. Nearly all natural sphalerites are diadochic compounds of ZnS with FeS (up to 42%), Cd (up to 2%), and MnS (up to 9%) (Boyle and Jambor, 1963). Both Zn and S can be isomorphously replaced by substantial quantities of other elements (Vaughan, 1971). The Fe content in particular has received a very considerable attention (Kullerud, 1953; Kalliokoski, 1959; Sims and Barton, 1967; Benson, 1960; Barton and Skinner, 1967; Campbell and Ethier, 1974; Williams, 1974). Trace elements in sphalerite have also been studied in greater detail than in any other sulphide.

In all, 22 sphalerite samples were analysed by electron probe and A.A.S. The Zn content was found to range from 51.68% to 64.74% (Table 10), with a mean of 58.46% (Table 15), and the S content ranges

from 32.23% to 38.66% with a mean of 35.29%. The Fe content ranges from 0.67% to 18.32% (Tables 10 and 11) with a mean of 6.42%. In addition to the analyses listed in Table 10, Fe and Cd were also determined using electron probe on 4 samples to enable calculation of the cell edges (discussed later).

There is a good antipathetic relationship between Zn and Fe content (Fig. 14) allowing the interpretation that Fe has substituted for Zn. The Fe content is believed to be present in sphalerite in solid solution and is not due to any contamination because most of the samples analysed were pure grains.

Cd was found in all the samples analysed in quantities ranging from 215 ppm (A.A.S. analysis) to 0.33% (probe analysis) (Tables 10 and 11).

Cu is present in all samples in quantities ranging from less than 0.1% to 2.75% (Table 10) as analysed by probe and A.A.S. The very high Cu contents of some samples can probably be attributed to sub-microscopic inclusions or exsolutions of chalcopyrite, though the Cu content of sphalerite is present in variable quantities (Rankama and Sahama, 1950).

Pb was found in some 11 samples ranging from 286 ppm to 1468 ppm (Table 10). However, this is probably due to intimate admixtures with galena as has been reported elsewhere (Fleischer, 1955).

Co has been reported in sphalerite and in a very few instances Ni also has been reported (Fleischer, 1955). A.A.S. analysis of Parys Mountain sphalerites showed Co to be present in 5 samples ranging from 206 to 967 ppm and one probe analysis showed 0.1% of Co. Ni was found in 3 samples in the range of 340 ppm to 433 ppm.

Sb, As and Bi have been reported from sphalerites although in most instances only qualitatively (Fleischer, 1955). As and Bi are present in trace quantities (below 0.1%) in most of the Parys Mountain sphalerites analysed by probe, although 4 samples contained more than 0.1% As, and another two more than 0.1% Bi (Table 10). Sb was not detected. It is likely that these quantities are from sulpho-salts containing As and Bi admixed in the sphalerites.

Mn is present in most samples but below measurable limits (0.1%) by electron probe, and in only 3 samples was it found to be more than 0.1% (Table 10).

Ba was found in the samples analysed by A.A.S. ranging from 174 to 7222 ppm (Table 10). As in the case of other sulphides its presence is unexplained.

Mo was found in trace quantities and in a few instances more than 0.1% (Table 10).

Ag and Sn were found not to be present by electron probe.

3.4.2 Unit cell edge measurements of sphalerite

In the present study the reason for the measurement of unit cell edges was two-fold: 1) To investigate whether there is a linear relationship between Fe content and measured cell edges of sphalerite by X-ray diffraction; 2) To investigate the possibility of using a single crystal electron diffraction technique to obtain Fe content in the same way as in X-ray diffraction, if confirmed that there is a linear relationship between cell edge and Fe content.

Kullerud (1953) reported that the effect of FeS (and the other common trace impurities MnS and CdS) is to cause an increase in the unit cell dimensions in a linear way. This then allows for accurate measurements of cell dimension to be used as an indicator of Fe content. Skinner (1961) presented an equation for this:

$$a = 5.4093 + 0.000456 X + 0.00424 Y + 0.00202 Z$$

where X, Y and Z are the contents of FeS, CdS and MnS in mol% and a is the cell edge in angstroms. Krause, and Van Aswegen and Verleger (in Boyle and Jambor, 1963) have, however, reported that Fe content has no increasing effect on unit cell edge and Williams (1965) has argued that the equation is the least squares fit to the experimental data and is therefore subject to possible error. The concept is, however, supported by Boyle and Jambor (1963) and by Evans et al (1968), and is used in this study.

The unit cell dimensions of 17 sphalerite specimens were measured using a Debye-Scherrer Powder Camera (114.59 mm diameter) fitted to a Phillips Norelco X-ray Diffractometer with Ni filtered $\text{CuK}\alpha$ radiation ($\lambda = 1.5405 \text{ \AA}$). No correction for film shrinkage was applied and the diffraction patterns were measured on a Central Scientific Instruments' Linear Comparator with a vernier having a least count of 0.05 mm (Straumanis' method as described by Zussman, 1967). X-ray diffraction angles (θ) calculated by this method were tabulated and the

interplanar spacings were read from tables. Corresponding hkl values were obtained from an X-ray diffraction data file (Berry, 1974), and unit cell edges calculated.

Unit cell edges of sphalerite were also calculated by substituting the mol% values of FeS, MnS and CdS in the equation by Skinner (1961). In general there is a good agreement between measured and calculated cell edges (Table 17) but there is a systematic trend of measured edges being greater than calculated edges, as also noticed by Evans et al (1968); Skinner 1961, found the opposite. A plot of measured cell edges against measured Fe content (mol% FeS) (Fig. 15) shows a good linear relationship between the two. This is interpreted to show that unit cell edge increases with increasing Fe content. The increase in cell edge at lower Fe contents is very pronounced, however, as higher values for Fe content are reached the rate of increase is less pronounced and the curve flattens out slightly. This observation is in agreement with the observations of Boyle and Jambor (1963), although it is a little less pronounced than that found by Evans et al (1968). It is concluded from these results that the accurate measurement of cell edge can be utilised to obtain FeS content. Mol% CdS plotted against cell edge showed no significant relationship (Fig. 16), because the electron probe was not able to measure accurately the trace quantities of Cd present in sphalerite. Mol% Mn was not plotted against cell edge as the data was insufficient.

Cell edge measurements were also made on 12 sphalerite samples by an electron diffraction technique for comparison purposes. Specimens were prepared using the technique described by McConnell (1967) and single crystal electron diffraction patterns were obtained using a Jeol JEM 100 B Transmission Electron Microscope at 100 kV. The diffraction patterns in each case were photographed and the 'd' spacings were calculated using the formula

$$d_{hkl} = \frac{\text{c.f.}}{\sqrt{hkl}}$$

where d_{hkl} is the lattice interplanar spacing

\sqrt{hkl} is the measured distance from origin 000 to spot hkl on the electron diffraction photograph. c.f. is the Camera Factor, a constant

provided (which depends on the camera length (L) and the wave length of the electron beam (λ) (c.f. = λL).

hkl values were obtained from X-ray powder file and the cell dimensions calculated as in the case of X-ray diffraction.

The cell edges measured are given in Table 18 and it can be seen that all the electron diffraction measurements are higher than those from X-ray diffraction. This is a systematic error in the electron diffraction measurements, probably resulting from an inaccuracy in the assumed Camera Factor. The accuracy could be improved by estimating this Camera Factor at the time of measurement by using an internal standard. Provided an internal standard is used an electron diffraction technique for cell edge measurement has many advantages:

- 1) It requires less sample than that required by X-ray diffraction;
- 2) Diffraction patterns can be obtained from several selected spots on a specimen and the Fe content obtained from several measurements might be used to indicate variations in Fe content within a specimen;
- 3) Diffraction patterns can be readily seen and photographed immediately and thus it is much quicker than X-ray diffraction;
- 4) Very sharp reflections can be obtained, unlike X-ray powder patterns where measurements are sometimes inaccurate because of obscure reflections and blackening of the film in the back reflection region.

3.4.3 Physical-optical characteristics

3.4.3.1 Microhardness

The microhardness data for sphalerite show it to have a range of 148-240 Kg/mm² (Table 21). The weight % of Fe in sphalerite was plotted against microhardness number (Fig. 7c), because it had been noticed by previous workers that an increase in Fe content of sphalerite increased its microhardness (Young and Millman, 1964; Bishara, 1966; Vaughan, 1971). In the present study, a good linear relationship between Fe content and microhardness was seen (Fig. 7c).

3.4.3.2 Reflectivity

Results of the reflectivity measurements in the wave length region 400 nm-700 nm including 589 nm are given in Table 25, and the spectral reflectivity profiles are shown in Fig. 8c. Sphalerite in this study was

seen to have maximum reflectivity in the wave length region 480-500 nm, as has been reported by Gray and Millman (1962) for sphalerites. In many grains little variation was observed with wave length, but generally the values decrease with increase in wave length. Reflectivity values at 589 nm plotted against weight% Fe in sphalerite (Fig. 9b) showed no significant relation.

3.4.3.3 Infrared studies

The infrared spectra for sphalerite are shown in Fig. 17, and compared with other sulphides, show good resolution. All the sphalerites show clearly two absorption peaks in the vicinity of 2.8-3.0 microns wave length. The 5 samples studied had Fe contents ranging from 1.59% to 18.32% (Fig. 17), and unlike pyrite and chalcopyrite, no differences in absorption patterns with varying Fe content were observed.

3.5 Galena

3.5.1 Composition

The theoretical composition of galena is 86.6 wt% Pb and 13.4 wt% S. Twelve samples were analysed, and the Pb content found to range from 80.15% to 87.15% (Table 12), with the majority of the samples containing between 82 and 86% Pb. All galenas analysed except one (A 15/1193) have a lower than theoretical Pb content, and have considerable As and Bi contents. The S content ranges from 13.85 wt% to 15.75 wt% (Probe analysis).

As, Sb and Bi are common trace elements in galena (Rankama and Sahama, 1950) and these elements were looked for in the specimens analysed by electron probe. As was found to range from 0.1wt% to 2.85 wt% with a mean of 1.48 wt%. Bi ranges from 0.27 wt% to 3.49 wt% with a mean of 1.58 wt% (Tables 12 and 16), and more than 0.1 wt% Sb was found in all samples. As and Bi sulpho-salts are present in very fine-grained sizes in most of the sections analysed by probe and high values in these analyses are thus probably due to some submicroscopic admixtures of these minerals with the galena. However, since As, Bi and Sb are common in galena, it is likely that they are also present in solid solution. No further information was gained in this study.

Ag is a common trace element in galena (Fleischer, 1955) and it was detected in all the samples analysed by probe and 4 samples were found to contain more than 0.1 wt% (Table 12). As there are no Ag

sulphides in the specimens analysed, the Ag content is not due to contamination but probably is present in solid solution.

Cu, Fe and Zn are all present generally above 1000 ppm or 0.1 wt% (Table 12). Cu occurs in lower quantities than in sphalerites. Fe and Zn although reported by previous workers in galenas, were probably due to contamination by pyrite and sphalerite (Fleischer, 1955). Most of the samples in the present study contain Fe and Zn (Table 12) (Probe and A.A.S. analysis) above 0.1 wt%.

Cd was found in most of the samples in quantities generally below 1000 ppm (Table 12). In 2 samples it was found to be 0.11 wt%. Goldschmidt (in Vlasov, 1964) suggested that admission of Cd into galena is due to the Cd-Pb isomorphism, and trace quantities of Cd in Parys Mountain galenas are probably present in solid solution.

Co and Ni are present only in trace quantities (Table 12) and in the samples analysed by A.A.S. they were found to be below 500 ppm.

Sn was detected in most probe analyses and 3 samples contain more than 0.1 wt% (Table 12).

Ba was measured by A.A.S. in 3 samples and it was found to be present below 500 ppm (Table 12). Its presence as in the other sulphides is difficult to account for.

Mo was also found in a few samples and 2 probe analyses showed more than 0.1 wt% (Table 12).

Te was measured in 4 samples by A.A.S. and was found to be below 100 ppm (Table 12). It has probably substituted for S.

3.5.2 Physical-optical characteristics

3.5.2.1 Microhardness

The measured values for microhardness of galena have a range of 61.7-107 kg/mm² (Table 22) in contrast to Bowie and Taylor's (1958) measurements of 71-84 kg/mm². The wider range in microhardness of Parys Mountain galenas probably results from the presence of considerable quantities of As and Bi. Weight %s of As and Bi were plotted against microhardness (Figs. 7d, e) and there appears to be slight linear relationship between them, though this needs confirmation by more data.

3.5.2.2 Reflectivity

Reflectivity measurements in the wave length region 400 nm-700 nm,

including 589 nm are given in Table 26, and the spectral reflectivity profiles are shown in Fig. 8d. Galena is a highly reflecting species and it shows irregular spectral profiles as reported by Gray and Millman (1962). Reflectivity % at 589 plotted against weight % As and weight % Bi showed no significant relationship probably because of insufficient data. (Fig. 9c, d).

3.5.2.3 Infrared studies

The infrared spectra produced for galena show poor resolution with broad absorption peaks between 2.8 and 3.0 microns wave length and one absorption peak in the vicinity of 6.0 micron wave length region (Fig. 18). No significant difference in absorption pattern was seen between the two samples studied, although one sample (19-424) contains 2.24% of As and the other (sample H 4/491) has only 0.10%, and both of them have nearly similar quantities of Bi (Table 12).

3.6 Arsenopyrite

Two grains of arsenopyrite were analysed by electron probe and the results are listed in Table 27 along with the theoretical value for the ideal formula FeAsS.

Compared with theoretical composition the Parys Mountain arsenopyrite has less As content but more Fe. Co, Ni, Cu, Pb and Zn are present in trace quantities (below measurable limits by electron probe).

3.7 Pyrrhotite

One pyrrhotite grain was analysed by electron probe and it has the following composition

	Fe	S	Co	Ni	Cu	Pb	Zn	Total
M 10/1521	57.33	40.91	tr	tr	1.30	tr	-	99.55

The high Cu content is difficult to account for from a single analysis and no further information was obtained in the present study.

3.7 Summary and implications of sulphide investigations

Investigations on Parys Mountain sulphide minerals have the following significant features:-

- 1) Analysis by electron probe on inclusion free areas showed the presence of substantial quantities of trace elements probably in solid solution.
- 2) The generalisation could be made that Co is concentrated in pyrite relative to other sulphides. Co and Ni are more common in pyrite and chalcopyrite than in sphalerite and galena.

- 3) Cd is concentrated in sphalerite relative to other sulphides, and there is a wide range of Fe content in sphalerites.
- 4) As, Bi and Ag are concentrated in galena relative to other sulphides. Sn is also present in galena but is absent in others.
- 5) Mo is concentrated more in sphalerite and galena than in pyrite and chalcopyrite. Ba is concentrated in chalcopyrite relative to pyrite. The significance of these two elements is not clear.
- 6) Correlation of trace element assemblage with the different types of the same mineral are inconclusive, such as between euhedral, anhedral and framboidal types in case of pyrite (Table 8), and in sphalerite grains those with exsolutions and without exsolutions (Table 10).
- 7) Concentration profiles for essential and trace elements were observed while analysing the sulphides by electron probe. It was noticed that variations of essential and trace elements within the same grain were more pronounced in case of sphalerite and galena than in the case of pyrite and chalcopyrite.
- 8) The Co/Ni ratio in pyrites (> 1) relates the deposits to volcanism
 High quantities of Cu in pyrites have been used by Frenzel and Ottemann (1967) in Fiji deposits to indicate a subvolcanic origin. High quantities of Cu in some Parys Mountain pyrites may be related to volcanism, though in some, contamination by inclusions is likely.
- 9) High Ag, Sb and Bi in galena indicate high temperature of formation as low quantities of these have been reported only from low temperature deposits (Fleischer, 1955; El Shazly et al 1957). Marshall and Joensuu (1961) also found that galenas having poor trace element assemblage predominantly form at lowest temperatures and vice versa. From this point of view the Parys Mountain galenas may throw some light on temperature of formation. However, it requires more data to draw any conclusions on this.
- 10) A linear relationship was observed between Fe content and unit cell edges of sphalerite and between microhardness and Fe content in sphalerite.
- 11) Attempts to correlate composition with some physical and optical characteristics of the sulphides allowed no significant conclusions, although some of this was due to insufficient data.

CHAPTER 4 SULPHO-SALTS

4.1 Introduction

The sulpho-salt minerals are intimately associated with the major sulphides at Parys Mountain. Their optical properties and textural relationships with the sulphides have been discussed elsewhere (Chapter 2). Their physical and optical characteristics are so similar that they are difficult to identify and distinguish optically (Uytenbogaardt and Burke, 1971) and so electron probe microanalysis is the most common method used for their mineralogical determination.

Most of the commonly known sulpho-salts contain one or more of the following elements - Fe, Co, Ni, Cu, Ag, Zn, Hg, Sn, Pb, Mo together with one or more of As, Sb and Bi; S is an essential constituent. These chemically complex sulpho-salts are commonly 'patterned' structurally after the simple sulphides (Ross, 1955) and are modifications of the cubic or hexagonal close packing structures. The sulpho-salt minerals present at Parys Mountain are listed in Table 28 along with their theoretical formulae. In addition to those listed, bismuthinite was reported by Thanasuthipithak (1974).

4.2 Tetrahedrite-tennantite

Many workers do not regard the tetrahedrite-tennantite group of minerals as sulpho-salts and there is considerable disagreement in assigning a chemical formula to them. Springer (1969), from the analyses of world wide material, concluded that the general formula $(\text{Cu, Ag, Fe, Zn, Hg})_3 (\text{As, Sb, Bi, Te})\text{S}_{3.25}$ is valid for tetrahedrite although the majority corresponds to $(\text{CuAg})_{2.50} (\text{Fe Zn})_{0.50} (\text{As Sb})\text{S}_{3.25}$. Later Maske and Skinner (1971) proposed a formula $\text{Cu}_{12+x}^{\text{As}}\text{S}_{13}^{\text{Sb}}$ where $0 \leq x \leq 1.72$ and $0 \leq y \leq 0.08$ for tennantite. Skinner et al (1972) proposed $\text{Cu}_{12+x}^{\text{Sb}}\text{S}_{13}^{\text{As}}$ for tetrahedrite where $0 \leq x \leq 1.92$ and $-0.02 \leq y \leq 0.27$. This complexity is due to extensive substitutions in the structure where Zn, Ag, Hg, Pb, Ni or Co as well as Fe may replace Cu in quantities ranging up to 16% (Vaughan, 1971).

Complex substitutions can occur in tetrahedrite partly because Cu occurs in both mono and divalent states. The first type is tetrahedrally co-ordinated with three S atoms in unusual planar groups (Riley, 1974). Cu in these sites can be replaced by Ag and Hg. In the second type Cu, which is in 3-fold co-ordination in the structure, can be replaced by Zn and Fe (Vaughan, 1971). Other substitutions involve Sb, which can be

completely or partly replaced by As and in minor quantities by Bi, Sn and Ge (Ramdohr, 1969). This complexity is well exemplified by the Parys Mountain minerals (Table 29).

Analyses of 6 tetrahedrites and 3 tennantites from Parys Mountain are shown in Table 29, and these represent the average analysis taken from 2 or 3 points in each grain. The atomic proportions (Table 30) were calculated by making the total of Cu + Ag + Fe + Zn equal to 12, Sb + As + Bi equal to 4 and obtaining the relative proportion for S based on the total of these two groups (Petruk et al., 1971). Analyses of tetrahedrites from Parys Mountain and Avoca, reported by Wheatly (1971a) are given in Table 29, for comparison.

Comparison of the compositions determined in the present study with those reported by Wheatly (1971a) (Table 29) shows that Ag content in Parys Mountain minerals in the present study is low, the maximum Ag value being 1.28 wt% from bore hole H4/491 (Bluestone ore) as compared to Wheatly's maximum Ag value of 5.4 wt%. The Fe content in the present study ranges from 3.16 to 10.18 wt% and is higher than that shown by Wheatly's (1971a) analyses. The zinc content ranges from 1.29 to 8.18 wt% and this range is quite in agreement with the analyses of Wheatly (1971a). All tetrahedrites contain some As and tennantites some Sb (X-ray images in Plate IV). Cu and Sb contents are in good agreement with Wheatly's (1971a) analyses. Bi is observed in both tetrahedrites and tennantites, the maximum content being 1.42 wt% from bore hole 27-145. There is a compositional break between tetrahedrite and tennantite as shown in Fig. 19. Such break was also noticed by Wheatly (1971a) at Avoca.

Deviations from the stoichiometric formula are illustrated by the atomic proportions of S given in Table 30. Such deviations have been noted in analyses elsewhere (Petruk et al., 1971) and are considered to be the result of complex metal substitutions with the whole complex forming an extensive solid solution series.

4.3 Bournonite

The theoretical formula for bournonite is CuPbSbS_3 . Analyses of specimens from Parys Mountain, Avoca and Idaho are compared with the theoretical values in Table 31, along with atomic proportions for the analyses in the present study.

The compositions and atomic proportions are at variance with the stoichiometric values. This is especially true of specimen 2 (sample M 10/1548) which contains appreciable quantities of Bi, Fe and Zn and has a Cu content very much higher than the theoretical value. The analysis of specimen (H4/465) however is in good agreement with the theoretical values and with the analyses of Avoca minerals (Wheatly 1971a). Analyses of specimens from Parys Mountain show As to be present in considerable quantities probably substituting for Sb. A solid solution series exists between Sb end member (Bournonite) and the As end member seligmannite (CuPbAsS_3) and this is considered to account for the As content in Parys Mountain analyses.

4.4 Bismuth sulpho-salts

Kobellite ($\text{Pb}(\text{Bi}, \text{Sb})_2\text{S}_5$) and galenobismuthite PbBi_2S_4 were identified at Parys Mountain in the Bluestone ore type. Kobellite is a disordered Bi-Sb-Pb sulpho-salt of composition $\text{Pb}_{6-x}(\text{Bi}, \text{Sb})_{7+x}(\text{Fe}, \text{Cu})\text{S}_{17.5}$ with $0 < x < 1$ (Weunsch, 1974). Weight percentages and atomic proportions for kobellite and galenobismuthite are given in Tables 32 and 33 along with theoretical values and some comparative analyses.

Comparison with theoretical composition shows the analytical data on Parys Mountain kobellite to be in good agreement with theoretical compositions. As is present substituting for Sb, and appreciable quantities of Cu and Fe are also present in the Parys Mountain kobellites. The deviation in composition from the theoretical composition of Parys Mountain galenobismuthite is due to a high Zn content which is probably present in solid solution.

4.5 Lead sulpharsenides

Mineral grains optically very similar to galena with high As values are classed here as lead sulpharsenide minerals. Analyses of these and calculated atomic proportions are presented in Table 34.

Chang and Bever (1973) have outlined the various disagreements on formulae for the lead sulpharsenide group of minerals. The calculated atomic proportions (Table 34) roughly correspond to jordanite which has a formula $\text{Pb}_{14}\text{As}_7\text{S}_{23}$ or $\text{Pb}_{13}\text{As}_7\text{S}_{23}$. However, since there is no standard and accepted formula for jordanite, Parys Mountain

minerals are classed as lead sulpharsenides only, rather than comparing them to any of the theoretical formulae.

4.6 Implications of sulpho-salt geochemistry

The complexity and uncertainty of the sulpho-salt geochemistry at Parys Mountain is due to the extremely local and minor abundance of these minerals and their fine grain size. Textural relationships with the major sulphides as outlined in Chapter 2 suggest that they are later than the conformable pyritic mineralisation. There is no geochemical evidence from sulpho-salt studies to assign any environment or temperature of formation for the Parys Mountain mineralisation.

Experimental studies by Maske and Skinner (1971) showed that the ideal composition for tennantite $\text{Cu}_{12}\text{As}_4\text{S}_{13}$ is probable only at lower temperature, i. e. below 300°C , and above this temperature, it deviates. Chang and Bever (1973) pointed out that lead sulpho-salt minerals are essentially restricted to hypogene deposits, particularly in the mesothermal intensity range. Minerals such as galenobismuthite have been described as occurring in high temperature areas ($550 - 610^\circ\text{C}$) of volcanic fumaroles in the Lipari Islands (Palache et al., 1944 in Craig, 1967). Czernanske and Hall (1975) have reported that the Darwin lead-zinc-Silver deposit where lead sulpho-salts occur, is a high temperature deposit.

If comparisons are made with Parys Mountain minerals, then a high temperature, at least a relatively higher temperature phase than earlier conformable pyritic mineralisation has to be assigned for the Parys Mountain sulpho-salts. Nevertheless, strong similarities in mineralogy, host rock geology and sulpho-salt assemblage exist between Parys Mountain deposits and the Kuroko deposits of Japan (Lambert and Sato, 1974) which are not considered to be of high temperature mineralisation.

CHAPTER 5

WALL ROCK STUDIES

5.1 Introduction

Despite the widespread occurrence of chlorite associated with mineralisation areas, little use has been made of its development in mapping metal distributions (Tuddenham and Lyon, 1959), and zoning in mineral deposits. In the present study 12 chlorites from wall rocks in mineralised sections, and 6 from non-mineralised sections, were studied, using X-ray diffraction techniques to identify them and to determine any differences which might be present between the different sections. Eight of the chlorites from the mineralised sections and 3 from non-mineralised ones were also subjected to infra-red absorption spectroscopy to discover any differences that might be present. Of the chlorites from mineralised sections 11 were largely from materials associated with pyritic and chalcopyritic mineralisation and in one case with sphaleritic mineralisation (sample IM 9/269).

5.2 X-ray diffraction studies

Powder samples used were either obtained from rock chips which were ground in a tungsten carbide mill or directly from the core samples using a vibrating needle.

Diffraction patterns were obtained on a Phillips Norelco X-ray diffractometer, with Ni filtered $\text{CuK}\alpha$ radiation, and quartz as an internal standard. The measured 'd' spacings of the chlorites are given in Tables 35 to 40. It was noticed that, while there is a variation in chlorite species from place to place in the case of the mineralised sections, in general there was no variation in specimens from the non-mineralised sections. A variation in chlorite species was also noticed in mineralised sections from the same bore hole (bore holes 36A and IM 6) (Tables 35, 36 & 38 to 40). Diabantite, clinochlore and grochaulte varieties of chlorite were found mainly associated with pyritic mineralisation with some chalcopyrite and sphalerite. Ripidolite was found associated with pyrite and chalcopyrite, and aphrosiderite with pyrite. Chlorite 1b species was found in all the non-mineralised sections studied. Comparison of the chlorites at Parys Mountain with the classification of the chlorites given by Hey (1954) as in Fig. 20 shows

that they are closely related varieties in terms of Si, total iron and Fe/(Fe + Mg). These different varieties of chlorites which have slightly different compositions probably are the result of the wall rock alteration associated with epigenetically formed sulphides. The differences may have been caused by the proposed secondary hydrothermal sulphide mineralisation rather than by the early sedimentary pyrite mineralisation. Determination of composition of chlorites in terms of major and trace elements and the identification of the species by X-ray study on a greater number of samples would be a useful investigation to find whether the above observation is localized or whether it is a general feature with the mineral deposits at Parys Mountain. This is particularly important in establishing the relative ages of mineralisation and metamorphism because pre-metamorphism chlorites would likely be destroyed.

5.3 Infra-red studies

Specimens used were 11 chlorites directly recovered from core samples and free from other minerals such as quartz. These were subjected to infra-red absorption spectroscopy, using the technique described in Chapter 3, and the spectra obtained were compared with those obtained by Tuddenham and Lyon (1959). They all fall under group 1 of the classification proposed by the above authors in that each spectrum has one strong absorption band in the wave length region between 9.3 and 11.0 microns and two to three clearly visible absorption bands between 2.6 and 3.0 microns (Fig. 21). It was, however, not possible to distinguish the chlorites from mineralised and non-mineralised sections because no significant differences in absorption patterns were seen.

CHAPTER 6

DISCUSSION AND CONCLUSIONS

6.1 Discussion

The mineralogical, textural and geochemical features discussed in the previous chapters can be used to add to discussion of the metallogenesis of these sulphide minerals. Interpretations of mineralisation should account for (a) Source and availability of various essential and trace elements, (b) Mode of transportation and availability of sites for precipitation or deposition (environment of formation), (c) Genetic relationship with the host rocks, (d) Post depositional characteristics. These are discussed below for Parys Mountain in the light of information derived in this study.

6.1.1 Source and availability of elements

As outlined in Chapter 2, the Parys Mountain deposits can be considered as stratiform type based on field, megascopic and mineralogical characteristics. These stratiform deposits, because of a close association with a volcanic succession, and generally having a Co:Ni ratio of > 1 , are thought to be related to volcanism. Hutchinson (1973) defined volcanogenic sulphide deposits as strata bound lenticular bodies of massive pyrite mineralisation, containing variable amounts of chalcopyrite, sphalerite and galena in layered volcanic rocks. They are believed to have been formed subsequently by volcanic fumarolic activity which occurred periodically during volcanism. The Parys Mountain deposits have close similarities to the Type II of Hutchinson (1973), in metals, volcanic rocks, volcanic activity, tectonic position and geological age.

Hutchinson Classification Type II is as follows:-

Type II	Pb-Zn-Cu Pyrite
Associated volcanics	Intermediate to felsic, calc-alkaline volcanic suites; andesite, dacite-rhyolite tuff etc.
Type of volcanism	Felsic centres of explosive, Pyroclastic and ignimbritic activity. Subaqueous to subaerial.
Associated sediments	Epiclastic predominates
Tectonic position	Later eugeosynclinal orogenic stage
Examples	Mt. Isa (Proterozoic) New Brunswick (Ordovician)

Petrological studies by Thanasuthipithak (1974) has established the presence of all these characteristics at Parys Mountain and that the volcanics belong to an orogenic-calcalkaline magma series formed in a continental margin/ island arc environment.

That many of the world's economically workable sulphide deposits have been derived from volcanic processes is firmly established by many workers throughout the world. Detailed discussions of individual deposits are given in Stanton (1960), (1965), Hutchinson (1965), Krauskopf (1967), Schermerchorn (1970), Ferguson and Lambert (1972), Lusk (1972), Goosens (1972), Constantinove and Govett (1973), Sillitoe (1973), Strauss and Madel (1973), Roberts (1975), Thurlow et al., (1975), Spence and Spence (1975), Spence (1975), Jenks (1975) and Angus and Davis (1976).

6.1.2 Environment of formation

Many of the volcanogenic deposits quoted above, though related to volcanism are thought to have been formed by an interplay of volcanic-sedimentary or volcanic-hydrothermal processes. It has to be postulated that there existed a sedimentary volcanic basin at Parys Mountain in which thick volcanic products accumulated. The sulphide metallic phases, mainly iron sulphide from volcanic emanations, were also deposited along with the volcanic successions within certain restricted environments. Thanasuthipithak (1974) called such a process 'syndimentary-exhalative'. However, as pointed out by Anderson and Nash (1972) the word 'exhalative' implies vapour transport and there is no evidence at Parys Mountain that the metals were carried in the vapour phase. Alternative terms given by Anderson and Nash (1972) are volcanogene-sedimentaire, volcano-sedimentaire, and submarine volcanic sedimentary. The term volcanogenic-sedimentary (Ilavsky 1976) is perhaps the most suitable for the Parys Mountain mineralisation.

However, microscopic features discussed in Chapter 2 suggest that the mineralisation at Parys Mountain was not a single simple episode. Although much of the copper ore has been removed by previous mining operations, its paragenesis is clear and it is only the pyritic mineralisation that has obvious conformable or syngenetic features. The lead-zinc sulphides and sulpho-salts are later and they apparently show features of deposition from a multi-component hydrothermal system, though they could have resulted as complex substitutions in other sulphides. Where

deposition has occurred from such a system the mobility of ore metals is in decreasing order as experimentally given by Barnes and Czernansky (1967) Pb-Cu-Zn-Sn-Ni-Fe-Co; (this coincides with the general paragenesis). All these epigenetic minerals were formed in fractures, and interstitial infillings and replacements of the earlier pyritic mineralisation.

6.1.3 Relationship with the host rocks

As outlined above the pyritic mineralisation is reported to be conformable and syngenetic with the host volcanic succession. Epigenetic mineralisation though, complex mineralogically, shows some crosscutting features consistent with later formation or remobilisation, presumably during metamorphism.

6.1.4 Post depositional characteristics

The earlier pyritic mineralisation shows post depositional characteristics mainly the evidence of deformation and remobilisation. These are the cataclastic textures, fracturing recrystallisation of framboid pyrites, etc. which became vacant sites for the subsequent epigenetic mineralisation. Either both these phases, or the earlier pyritic mineralisation, were remobilised during the Caledonian orogeny (Thanasuthipithak, 1974).

Both in the earlier syngenetic mineralisation and later hydrothermal deposition the source for the metallic sulphide is believed to have been volcanic. This repetition of ore formation is not uncommon in volcanogenic sulphide deposits.

It can therefore be concluded that the Parys Mountain mineralisation is consistent with a volcanogenic-sedimentary deposit of a stratiform type later enriched by hydrothermal processes. This deposit was later remobilised during the Caledonian orogeny to produce many of the crosscutting features.

6.2 Summary of conclusions

In the present study of mineralogy and geochemistry of Parys Mountain sulphides and sulpho-salt minerals, the following conclusions are reached:

- 1) The mineralogy, paragenesis and association with a volcanic succession of rocks allow the interpretation that the deposit is both stratiform and conformable associated with volcanism. An earlier synsedimentary pyritic mineralisation has been enriched by an epigenetic

complex sulphide and sulpho-salt mineralisation.

- 2) The deviations in composition of the major sulphide minerals pyrite, chalcopyrite, sphalerite and galena from their stoichiometry are interpreted as due to presence of appreciable quantities of trace elements and complex substitutions.
- 3) Pyrite and chalcopyrite have relatively low trace element content and they mainly contain Co, Ni, Ba, As, Pb, Zn, also Cu in pyrite. The Co/Ni ratio in pyrites is generally > 1 . This is interpreted to indicate that the deposits are related to volcanism.
- 4) Sphalerite and galena are rich in As, Ag, Bi, Sb contained in solid solutions.
- 5) The iron content in sphalerite varies widely, and this is interpreted as being due to solid solution.
- 6) Measurements of cell edge of sphalerites, using both electron diffraction and X-ray diffraction techniques, showed it to vary linearly with iron content. Electron diffraction is thus an alternative method for measuring the iron content of sphalerites.
- 7) There is a good relationship between iron content and microhardness in sphalerite. However, this was found not to apply to the other sulphides, namely pyrite and chalcopyrite.
- 8) The chlorite group minerals, diabantite, ripidolite, grochauite, and aphrosiderite were formed in wall rocks at the contacts of the mineralisation. Chlorite 1b species was found in non-mineralised sections.

APPENDIX I

SAMPLE SELECTION AND PREPARATION

All the sulphide samples studies were taken from the diamond drill cores including some previously studied by Thanasuthipithak (1974), and only fresh looking material was selected. Two types of samples were required: a) sections of mineralised parts for polishing (reflected light microscopy, reflectivity, microhardness, and electron probe measurements); b) powdered sulphide minerals for chemical analyses, infrared and differential thermal studies. In the latter case, only mineral grains which were sufficiently coarse (average size $>$ about one mm) to be liberated with considerable amount of purity were selected. More finely grained minerals were analysed by electron probe on polished sections.

Sulphide mineral grains were liberated directly from the core specimen using an electrically vibrating needle. They were then thoroughly washed using acetone and distilled water and dried. They were examined under a binocular microscope and impurities were removed by hand. In some instances a heavy-liquid technique was used (Muller, 1967) to separate less coarse grained sulphides from fine grained gangue. In some cases the core chip was polished on a coarse grade abrasive paper to allow grain boundaries to be clearly seen before the grain was liberated. Most of the sphalerite samples were recovered in this way.

A certain amount of mineral impurity was, however, unavoidable. This was especially true of sphalerites and pyrites with some chalcopyrite exsolutions. Also some very fine grained gangue inclusions in sulphide minerals could not be separated.

APPENDIX 2

LABORATORY METHODS

2.1 Atomic Absorption Spectrophotometry (A. A. S.)

Solutions for A.A.S. were prepared by dissolving the sulphide samples in concentrated HCl and concentrated HNO_3 (Strasheim et al. 1960; in Angino and Billings, 1972). About 200 mg of powder was weighed accurately into a conical flask and 8 to 10 ml of concentrated HCl was added. This was allowed to stand for approximately one hour for the initial reaction to take place before adding 8 to 10 ml of concentrated HNO_3 . This method was used in preference to direct use of aquaregia to prevent basic nitrates being formed on the surface of the sulphide grains (Dolezal et al. 1968, in Ghosh, 1972). After adding HNO_3 some 3 hours were allowed for a clear solution to form. The solutions were stirred and then transferred to 150 or 250 ml volumetric flasks, made up to volume with double distilled water, and quickly transferred to polythene bottles. The solutions were analysed within three days of preparation because elements present in low concentrations are lost by absorption on to the sides of the bottle, if stored for longer periods.

Standards were prepared from stock solutions containing 1000 ppm of the element in each case. These stock solutions, except Mo were supplied from BDH Chemicals Limited. The Mo standard was prepared by dissolving 1.840g of ammonium paramolybdate ($(\text{NH}_4)_6\text{Mo}_7\text{O}_{24}\cdot 4\text{H}_2\text{O}$) in 1 litre of 1% ammonium hydroxide (NH_4OH), for 1000 ppm concentration.

Analyses for Cd, Co, Cu, Fe, Ni, Pb, Te and Zn were done using an air acetylene flame, and Mo and Ba were determined using a nitrous oxide acetylene flame. An integrated period of 0.5 seconds was allowed for each aspiration. At the beginning of each run, standard solutions were aspirated starting from lower concentration to higher concentration, followed by the sample solution. At least 4 readings were taken for each sample solution. The mean of these concentrations was taken and from it the weight % in the sample was calculated.

2.2 Electron probe microanalysis

Analyses were done on carbon coated polished sections and in some instances on the sections mounted in conducting bakelite. The standards used were either pure metals/elements or compounds (Table 41).

Analyses were done using a Cambridge Microscan V with a constant accelerating potential of 15 kV, a sample current of 0.3 mA and a beam current of 0.05 mA. The crystals used were PET (Pentaerythritol) and LiF (Lithium fluoride). Both crystals were used because readings were obtained simultaneously in two separate channels thus allowing two elements to be determined simultaneously. Counting rates were measured for intervals of 10 seconds. Peak intensities for various elements determined in each grain were read at least twice, and the mean taken. Similarly background readings also were taken at least twice.

A dead time correction was applied for counts more than 2000/second, though for count rates below 10,000 counts /second, the error is considered to be less than 1% (Adler, 1970). Dead counts were read from the graph supplied and were added to the measured counts. The concentration after applying dead time was calculated using the formula

$$\text{Wt \%} = \frac{\text{Peak-Background} + \text{Dead time (counts/second) of specimen} \times C}{\text{Peak-Background} + \text{Dead time (counts/second) of standard}}$$

where C is the weight percentage of the element in the standard.

The measured concentrations were subjected to corrections described by Long (1967), Adler (1970). Corrections for Atomic Number (Z), Fluorescence and Absorbance, were made using a computer programme produced in the Department of Metallurgy, University of Aston.

2.3 Reflectivity

Measurements of reflectivity were made on a Reichert Zetopan Ore Microscope equipped with a reflex microphotometer (Singh, 1965). Comparative quantitative measurements were made against Tungsten Titanium Carbide (WTiC) and silicon carbide (SiC), standards with reflectivity being calculated from the formula

$$R_{\lambda} \% \text{ of Mineral} = \frac{\text{Deflection Value of Mineral}}{\text{Deflection Value of Standard}} \times K$$

where K = calibrated reflectivity % of standard

λ = monochromatic wave length

R% = Reflectivity percentage

All measurements unless otherwise specified were made at a wave length of 589 nm in air. A glare correction was applied before calculating R% to compensate for reflections from the back of the objective (Bowie and Henry, 1964).

2.4 Indentation microhardness

Measurements of microhardness were made with a Leitz Durimet Microscope with an attached indenter. Varying loads of 50, 200 and 300 gm were applied to obtain a sharp indentation and an indentation time of 30 seconds was allowed for each specimen. The diagonals of the projected impression on the polished surface were measured using a travelling micrometer ocular. The hardness number was calculated using the formula

$$\text{VHN} = \frac{1854.4 \times L}{d^2}$$

where VHN = Vickers microhardness number in kg/mm^2

L = Load applied

d = Indentation diagonal

2.5 Infrared Absorption Spectroscopy

Samples for infrared studies were prepared by potassium bromide pellet method (Tuddenham and Lyon, 1959; and Lyon, 1967). Spectra were obtained on a Perkin-Elmer 237 Grating Infra red Spectrophotometer in the wave number region $600\text{-}4000 \text{ cm}^{-1}$.

2.6 Differential Thermal Analysis

Analyses were made on samples of pyrite and chalcopyrite on a Dupont-900 Differential Analyser using a sample preparation technique described by McLaughlin (1967). Glass beads were used as standard. A heating rate of $50^\circ\text{C}/\text{minute}$ was applied, with the scale for chart paper of $100^\circ/\text{inch}$.

Sulphides contain corrosive elements such as S and As (Kopp and Kerr, 1957). Special techniques of diluting the samples with alumina to avoid corrosion by S or As were not employed because the maximum temperature reached was only 600°C .

REFERENCES

- Adler, I., (1970) X-ray emission spectrography in geology: in Methods in geochemistry and geophysics: Elsevier Publishing Company, Amsterdam, London and New York.
- Anderson, C. A., and Nash, J. T., (1972) Geology of the massive sulphide deposits at Jerome, Arizona - a re-interpretation: Econ. Geol., V. 67, pp. 845-863.
- Angino, E. E. and Billings, G. K., (1972) Atomic absorption spectrometry in geology: in Methods in geochemistry and geophysics: Elsevier Publishing Company, Amsterdam, London and New York.
- Angus, J. G. and Davis, G. R., (1976) Base metal enrichment in volcanic sublimates and secondary alteration products from Vesuvius and Vulcano: Mineralog. Mag., V. 40, pp. 481-486.
- Barnes, H. L. and Czernansky, G. K., (1967) Solubilities and transport of ore minerals: in Barnes, H. L., ed., Geochemistry of hydrothermal ore deposits: pp. 334-378. Holt, Rinehart and Winston Inc., New York/Chicago.
- Barton, P. B. and Skinner, B. J., (1967) Sulphide mineral stabilities: in Barnes, H. L., ed., Geochemistry of hydrothermal ore deposits: pp. 236-326. Holt, Rinehart and Winston, Inc., New York/Chicago.
- Bates, D. E. B., (1966) The geology of Parys Mountain: Welsh geol. quart., V. 2, pp. 27-29.
- Berry, L. G., (1940) Studies of mineral sulpho-salts IV: Galenobismuthite and 'lillianite': Am. Mineralogist, V. 25, pp. 726-734.
- Berry, L. G., (1974) Selected powder diffraction data for minerals. Joint Comm. Powder Diffraction Standards, Swarthmore, Penn., U. S. A.
- Bishara, W. W., (1966) Studies on trace and minor elements in sphalerite and galena from the Northern Pennine Ore field: Ph. D. thesis, Leeds University.
- Bowie, S. H. U. and Henry, N. F. M., (1964) Quantitative measurements with the Reflecting Polarising Microscope: Trans. Instn. of Min. Met., V. 73, pp. 467-478.
- Bowie, S. H. U. and Taylor, K., (1958) A system of ore mineral identification: Min. Mag., V. 99, pp. 265-277.

- Boyle, R. W. and Jambor, J. L., (1963) The geochemistry and geothermometry of sphalerites in the lead-zinc-silver lodes of the Keno Hill - Galena Hill area, Yukon: *Can. Min.*, V. 7, pp. 479-496.
- Campbell, F. A. and Ethier, V. G., (1974) Sulphur isotopes, iron content of sphalerites and ore textures in the Anvil ore body, Canada: *Econ. Geol.*, V. 69, pp. 482-493.
- Chang, L. L. Y. and Bever, J. E., (1973) Lead sulpho-salt minerals: Crystal Structures, stability relations and paragenesis: *Minerals, Sci. & Eng.*, V. 5, pp. 181-191.
- Constantinou, G., and Govett, G. J. S., (1973) Geology, geochemistry and genesis of Cyprus sulphide deposits: *Econ. Geol.* V. 68, pp. 843-858.
- Craig, J. R., (1967) Phase relations and mineral assemblages in the Ag-Bi-Pb-S system: *Miner. Deposita*, V. 1, pp. 278-306.
- Czemanske, G. K., and Hall, W., (1975) Mineralogy of the Darwin lead-silver-zinc deposit: *Econ. Geol.*, V. 70, pp. 1092-1110.
- El Shazly, E. M., (1951) The application of spectrographic analysis of minerals to the metallogenesis of lead-zinc ores: Ph. D. thesis, University of London.
- El Shazly, E. M., Webb, J. S. and Williams, D., (1957) Trace elements in sphalerite, galena and associated minerals from the British Isles: *Trans. Instn. Min. Met.*, V. 66, pp. 241-271.
- Evans, T. L., Campbell, F. A. and Krouse, H. R., (1968) A reconnaissance study of some Western Canadian lead-zinc deposits: *Econ. Geol.*, V. 63, pp. 349-359.
- Ferguson, J., and Lambert, I. B., (1972) Volcanic exhalations and metal enrichments at Matupi Harbour, New Britain, Territorial Protectorate of New Guinea: *Econ. Geol.*, V. 67, pp. 25-37.
- Fitton, J. G., and Hughes, D. J., (1970) Volcanism and plate tectonics in the British Ordovician: *Earth and Planetary Sci. Letters*, V. 8, pp. 223-228.
- Fleischer, M., (1955) Minor elements in some sulphide minerals: *Econ. Geol. 50th Anniv. Vol.*, pp. 970-1024.
- Frenzel, G., and Ottemann, J., (1967) Eine sulfidparagenese mit Kupferhaltigen Zonarpyrit von Nukundamu/Fiji: *Miner. Deposita*, V. 1, pp. 307-316.

- Ghosh, A.K., (1972) Trace element geochemistry and genesis of the copper ore deposits of the Singbhum shear zone, Eastern India: *Miner. Deposita* V. 6, pp. 292-313.
- Goosens, P.J., (1972) An exhalative volcanic iron sulphide stratabound deposit, near San Fernando, Azuay Province, Ecuador: *Econ. Geol.* V. 67, pp. 469-480.
- Gray, I.M., and Millman, A.P. (1962). Reflection characteristics of ore minerals: *Econ. Geol.* V. 51, pp. 325-349.
- Greenly, E., (1919) The geology of Anglesey: *Mem. Geol. Surv. Gt. Br.*, 2 vols.
- Hall, W.E., and Czernianske, G.K., (1972) Mineralogy and trace element content of the Wood River lead-silver deposits, Blaine County, Idaho: *Econ. Geol.*, V. 67, pp. 350-361.
- Hawkins, T.R.W., (1966) Bore holes at Parys Mountain near Amlwch, Anglesey: *Bull. Geol. Surv. Gt. Br.*, No. 24, pp. 7-18.
- Hey, H.M., (1954) A new review of the chlorites: *Mineralog. Mag.*, V. 30, pp. 277-292.
- Hunt, J.M., Wisherd M.P., & Bonham, L.C. (1950) Infrared absorption spectra of minerals and their inorganic compounds: *Analyt. chem.*, V. 22, pp. 1478-1497.
- Hutchinson, R.W., (1965) Genesis of Canadian massive sulphides re-considered by comparison to Cyprus deposits: *Can. Inst. Min. Met. Bull.*, V. 58, pp. 972-986.
- Hutchinson, R.W., (1973) Volcanogenic sulphide deposits and their metallogenic significance: *Econ. Geol.*, V. 68, pp. 1223-1246.
- Jenks, W.F., (1975) Origins of some massive pyritic ore deposits of western Europe: *Econ. Geol.*, V. 70, pp. 488-498.
- Kahn, L.H., (1968) Principles and practice of atomic absorption: *Advances in Chemistry series*, No. 73, pp. 183-229.
- Kakar, S.K., (1971) A study of the trace elements associated with lead-zinc ores of mid-Wales: Ph. D. thesis, University of Wales.

- Kalliokoski, J., (1959) Sphalerite temperatures from the Brunswick and Nigadoo deposits, New Brunswick, Canada: (Abst) Geol. Soc. Am. Bull., V. 70, p. 1626.
- Kopp, O. C., and Kerr, P. F., (1957) Differential Thermal Analyses of sulphides and arsenides: Am. Mineralogist, V. 42, pp. 445-454.
- Krauskopf, K. B., (1967) Source rocks for metal bearing fluids: in Barnes, H. L., ed., Geochemistry of hydrothermal ore deposits: pp. 1-28, Holt, Rinehart and Winston, Inc., New York/Chicago.
- Kullerud, G., (1953) The FeS-ZnS system - a geological thermometer: Norsk. Geol. Tidsskr., V. 32, pp. 61-147.
- Lambert, I. B., and Sato, T., (1974) The kuroko and associated ore deposits of Japan: A Review of their features and metallogenesis. Econ. Geol., V. 69, pp. 1215-1236.
- Loftus-Hills, G., and Solomon, M., (1967) Cobalt, nickel and selenium in sulphides as indicators of ore genesis: Miner. Deposita, V. 2, pp. 228-242.
- Long, J. V. P., (1967) Electron probe microanalysis: in Zussman, J., ed., Physical methods in determinative mineralogy., pp. 215-260. Academic Press, London, New York.
- Lusk, J., (1972) Examination of volcanic exhalative and biogenic origins for sulphur in the stratiform massive sulphide deposits of New Brunswick: Econ. Geol., V. 67, pp. 169-183.
- Manning, W., (1959) The Parys and Mona mines in Anglesey: in Future of non-ferrous mining in Great Britain and Ireland: Proceedings of the Symposium, Inst. Min. Met., London.
- McConnell, J. D. C., (1967) Electron microscopy and electron diffraction: in Zussman, J., ed., Physical methods in determinative mineralogy, pp. 335-370, Academic Press, London and New York.
- McLaughlin, R. J. W., (1967) Thermal techniques: in Zussman, J., ed., Physical methods in determinative mineralogy, pp. 405-444, Academic Press, London and New York.
- McLaughlin, R. J. W., (1967) Atomic absorption spectroscopy: in Zussman, J., ed., Physical methods in determinative mineralogy, pp. 475-486, Academic Press, London and New York.

- Muller, L. D., (1967) Laboratory methods of mineral separation: in Zussman, J., ed., Physical methods in determinative mineralogy, pp. 1-30, Academic Press, London and New York.
- Nash, T., (1975) Geochemical studies in the Park city district: Econ. Geol., V. 70, pp. 1038-1049.
- Petruk, W., and staff (1971) Characteristics of the sulphides: in Berry, L.G., ed., The Silver-arsenide deposits of the Cobalt-Gowganda region, Ontario., The Canadian Mineralogist, V. 2., pp. 196-231.
- Ramdohr, P., (1969) Ore minerals and their intergrowths: Oxford, Pergamon Press.
- Rankama, K., and Sahama, Th.G., (1950) Geochemistry: University of Chicago Press, Chicago.
- Raybould, J.G., (1973) The study of framboidal pyrites: Lithos, V. 6, pp. 175-182.
- Riley, J. F., (1974) The tetrahedrite-freibergite series with reference to the Mount Isa Pb-Zn-Ag ore body: Miner. Deposita, V. 9, pp. 117-124.
- Roberts, R.G., (1975) The geological setting of the Mattagami Lake mine, Quebec: A volcanogenic massive sulphide deposit: Econ. Geol., V. 70, pp. 115-129.
- Ross, V., (1957) Geochemistry, crystal structure and mineralogy, of the sulphides: Econ. Geol., V. 52, pp. 755-774.
- Schermerhorn, L. J.G., (1970) The deposition of volcanics and pyrite in Iberian pyrite belt: Miner. Deposita, V. 5, pp. 273-279.
- Sillitoe, R. H., (1973) Environments of formation of volcanogenic massive sulphide deposits: Econ. Geol., V. 68, pp. 1321-1336.
- Sims, P.K., and Barton, P.B., Jr., (1961) Some aspects of the geochemistry of sphalerite, Central City district, Colorado: Econ. Geol., V. 56, pp. 1221-1237.
- Singh, D. S., (1965) Measurement of spectral reflectivity with the Reichert Microphotometer: Trans. Inst. Min. Met., V. 74, pp. 901-916.
- Skinner, B. J., (1961) Unit cell edges of natural and synthetic sphalerites: Am. Mineralogist, V. 46, pp. 1399-1411.

- Skinner, B. J., Luce, F. D., and Makovicky, E., (1972) Studies of the Sulfosalts of Copper III: Phases and Phase relations in the system Cu-Sb-S; *Econ. Geol.*, V. 67, pp. 924-938.
- Spence, C. D., (1975) Volcanogenic features of the Vauze sulfide deposit, Noranda, Quebec: *Econ. Geol.*, V. 70, pp. 102-114.
- Spence, C. D., and de Rosen Spence, A. F., (1975) The place of sulfide mineralisation in the volcanic sequence at Noranda, Quebec: *Econ. Geol.*, V. 70, pp. 90-101.
- Springer, G., (1969) Electron probe analyses of tetrahedrite: *Neues, Jahr. Min. Mt.*, pp. 24-32.
- Stanton, R. L., (1960) General features of the conformable 'pyritic' ore bodies, Parts I & II: *Canadian Min. Metall. Bull.*, No. 573, pp. 24-29 and No. 574, pp. 66-74.
- Stanton, R. L., (1965) Mineral interfaces in stratiform ores: *Trans. Inst. Min. Met.*, V. 74, pp. 46-79.
- Stanton, R. L., (1972) *Ore Petrology*: New York, McGraw-Hill.
- Stanton, R. L., and Gorman, H., (1968) A phenomenological study of grain boundary migration in some common sulphides: *Econ. Geol.*, V. 63, pp. 907-923.
- Strauss, G. K., and Madel, J., (1974) Geology of massive sulphide deposits in the Spanish-Portuguese pyrite belt: *Geol. Rundschau*, V. 63, pp. 191-211.
- Suffel, G. G., (1965) Remarks on some sulphide deposits in volcanic extrusives: *Can. Inst. Min. Met. Bull.*, V. 58, pp. 1057-1063.
- Thanasuthipithak, T., (1974) Relationship of mineralisation to petrology at Parys Mountain, Anglesey: Ph. D. thesis, University of Aston in Birmingham.
- Thurlow, J. G., Swanson, E. A., and Strong, D. F., (1975) Geology and lithochemochemistry of the Buchans polymetallic sulfide deposits, New Foundland: *Econ. Geol.*, V. 70, pp. 130-144.
- Tuddenham, W. M., and Lyon, J. R. P., (1959) Relation of infrared spectra and chemical analysis for some chlorites and related minerals: *Analyt. Chem.* 31, p. 377.
- Uytenbogaardt, W., and Burke, E. A. J., (1971) Tables for microscopic identification of ore minerals: Elsevier Publishing Company, Amsterdam, London and New York.

- Vaughan, D. J., (1971) Aspects of structure and bonding in the iron sulphides and related minerals: D. Phil., thesis, University of Oxford.
- Vlosov, K. A., (1964) Geochemistry and mineralogy of rare elements and genetic types of their deposits: Vol. 1, Geochemistry of rare elements. Jerusalem: Israel programme for scientific translations.
- Volborth, A., (1969) Elemental analysis in geochemistry Part A. Major elements: Methods in geochemistry and geophysics. Elsevier Publishing Company, Amsterdam, London and New York.
- Wager, L. R., and Brown, G. M., (1960) Collection and preparation of material for analysis: in Smales, A. A., Wager, L. R., ed., Methods in geochemistry. Interscience Publishers Inc., New York and London.
- Weunsch, B. J., (1974) Determination, relationships and classification of sulphide mineral structures: in Ribbe, P. H. (editor) Sulphide mineralogy. Min. Soc. Amer. Short course Notes 1, pp. W1-W20.
- Wheatly, C. J. V., (1971a) Economic geology of the Avoca mineralised belt, S. E. Ireland, and Parys Mountain, Anglesey: Ph. D. thesis, University of London.
- Wheatly, C. J. V., (1971b) Aspects of metallogenesis within the Southern Caledonides of Great Britain and Ireland: Trans. Inst. Min. Met., V. 80, pp. B 211-223.
- Williams, K. L., (1965) Determinations of the iron content of sphalerite: Econ. Geol., V. 60, pp. 1740-1747.
- Williams, K. L., (1974) Composition of sphalerites at Zeehan, Tasmania: Econ. Geol., V. 69, pp. 657-672.
- Young, B. B., and Millman, A. P., (1964) Microhardness and deformation characteristics of ore minerals: Trans. Inst. Min. Metall., V. 73, pp. 437-466.
- Zussman, J., (1967) X-ray diffraction: in Zussman, J., ed., Physical methods in determinative mineralogy. Academic Press, London and New York., pp. 261-334.

Table 1 Stratigraphic sequence at Parys Mountain

Age	(Hawkins, 1966)		(Thanasuthipithak, 1974)	
	Lithology	Thickness	Lithology	Thickness
Silurian	Grey shales with graptolites		Dark-grey to black slates	
Ordovician	Fine-grained sediments with a few occurrences of tuff in felsitic zone of silicification	600 ft	unconformity ?	
			Rhyolitic volcanic rocks	200m
			Grey to greenish-grey slates	600m
	Parys shales	720 ft		
	Black shales			
	* Grey shales weathering to brown and green			
	Grey micaceous shales with beds of sedimentary breccia	1200 ft		
----- Carmel Head Thrust -----				
Pre-Cambrian	Amlwch beds Pale-green phyllites		Chlorite schists, micaceous and granitoid gneisses, quartzitic gneisses.	

* Note: These are the Parys Green Shales of Greenly

Table 2. Classification of Ore Types.

Author	Mineralisation Type	Host rock or matrix	Mineralogy		Example
			Major	Minor	
Wolfenden (1967) (in Thanasuthipithak 1974)	Copper ore	Northern rhyolites and its contacts	Pyrite Chalcopyrite	Sphalerite Galena	Great ore Opencast lode, Hill Side open case, Black rock lode
	Bluestone ore	Dacite, silicified silurian slates and in rhyolites in contact with Ordovician slates	Argentiferous galena, Sphalerite	Chalcopyrite Pyrite	Clay shaft lode Black rock lode
	Pyritic ore	Within rhyolitic rocks	Pyrite	Chalcopyrite	Golden venture lode Carreg-y-doll lode, Middle lode, South branch lode North discovery lode
	Low grade Galena-Sphalerite ore	Disseminated in Ordovician slates	Galena Sphalerite		Not mined because of low grade
Wheatly 1971a	Pyritic zone	Black shale (Ordovician slates)	Pyrite Chalcopyrite	Pyrrhotite Sphalerite Galena	Disseminated in shale units
	Siliceous zone	Shales and tuffs (silicified Silurian slates and rhyolitic tuffs + siliceous sinter)	Pyrite Chalcopyrite Sphalerite Galena	Pyrrhotite Tetra- hedrite Bismuth- inite Native Bismuth	Carreg-y-doll, Golden Venture lode Charlotte lode, North discovery lode.
	Lead-zinc zone	Shales and tuffs	Sphalerite Galena Pyrite Chalcopyrite	Tetra- hedrite Bournon- ite	Morfa-dee and Black rock lodes, clay shaft lodes (Bluestone)
	Veins	Shales, tuffs and lavas	Galena, Sphalerite Chalcopyrite	Tetra- hedrite	Great cross Cowis Carreg-y-doll lode.

Table 3 Summary of some mineral forms at Parys Mountain

Ore Type	Form	Description	Minerals		Grain size/dmsns	Matrix/host matrix
			Major	Minor		
Pyritic ore	a) Layered sulphide form	Continuous and discontinuous layers conformable with the quartz and chloritic matrix parallel to foliation of the host rock. Some layers have a lenticular shape, major lens made up of smaller lenses giving rise to enechelon arrangement	Pyrite Chalcopyrite	Sphalerite	Thickness of the layer 2mm-1 cm.	Quartz-chloritic rocks
	b) Disseminated form	Well developed euhedral and subhedral pyrite grains disseminated in host rock.	Pyrite	Chalcopyrite	0.3mm-2 mm	Black shale, Dacite
Copper ore	a) Massive form	Irregular, coarse granular intergrowths	Pyrite Chalcopyrite	Sphalerite Galena	0.5cm to even 2cm in case of pyrite	Quartz is the main matrix
	b) Vein and stockwork form	Intersecting continuous and discontinuous veins of chalcopyrite	Chalcopyrite	Pyrite	Average width of the vein about 5 mm	Siliceous rocks
Blue-stone ore	Fine-grained	Microscopic granular intergrowths	Sphalerite Galena Chalcopyrite Pyrite	Sulphosalts	Average size < 1 mm	Shales and tuffs (Siliceous/sinter)

Table 4 Table showing the ore minerals at Parys Mountain

Name	Form	Microhardness range (Kg/mm ²)	Reflectivity % range at 589nm (air)	Special association
Pyrite	Euhedral, subhedral anhedral and fram- boidal	1027 - 1483	45.9 - 56.5	Euhedral pyrite with rutile
Chalco- pyrite	Anhedral, allotrio- morphic	174 - 221	38.2 - 42.6	
Sphaler- ite	Anhedral, rounded and as intergrowths with chalcopyrite	148 - 240	16.3 - 22.1	
Galena	Anhedral, sometimes intergrows with sphalerite	61 - 201	37.3 - 41.3	
Arseno- pyrite	Euhedral to subhedral	-	-	
Pyrrho- tite	Anhedral, irregular	-	-	
Tetra- hedrite- Tennantite	Fracture and interstitial infillings mainly in pyrite	279- 328	34.3 - 36.5 (Tetra- hedrite) 29.5 - 31.7 (Tennan- tite)	Pyrite
Bourn- onite	Inclusions - white in colour and anisotropic	-	-	Sphalerite
Lead sulpho- salts	Inclusions and intergrowths with mainly sphalerite and galena	-	39.3 - 43.5	Sphalerite and galena
Bismuth sulpho- salts	Interstitial infillings in pyrite, sphalerite	-	-	

Table 5 Summary of Textures shown by ore minerals at Parys Mountain

Texture	Primary		Texture	Secondary	
	Description	Mineral/s		Description	Mineral/s
1) Panidiomorphic	Euhedral grains	Pyrite	1) Cataclastic	Fractures and other deformative features are present	Pyrite
2) Framboidal	A spherical or subspherical aggregate of pyrite granules or microcrysts	Pyrite	2) Vein filling	A distinct and narrow filling of pyrite in the matrix in the form of a vein	Pyrite
3) Allotriomorphic granular	Irregular and anhedral grains	Pyrite Chalcopyrite Sphalerite Galena & sulphosalts	3) Interstitial fillings	Later formed minerals are present in the interstitial spaces of the previously formed grains	Sphalerite in Pyrite Tetra- hedrite - Tennan- tite in Pyrite
4) Mutual intergrowths	The two minerals are usually intergrown with no distinct boundary between them		4) Replacement	Later formed minerals replace previously formed minerals along peripheries	Chalcopyrite replaces pyrite
			5) Recrystallisation and homogenisation	An aggregate of framboidal or euhedral grains homogenised at the centre, retaining their respective outlines at the periphery	Pyrites

Table 6 Simplified Paragenetic diagram of Primary Sulphides and Sulpho-salts at Parys Mountain

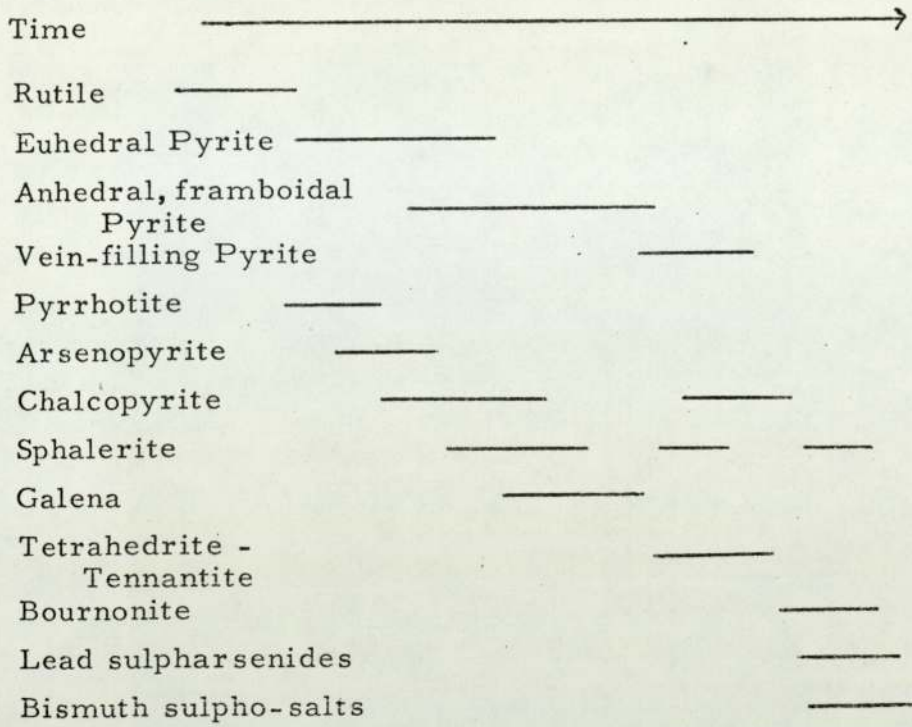


Table 7 Table to show the techniques employed and the nature of information obtained

Name of the technique	No. of samples	Minerals	Information
Reflected Light Microscopy	58	Sulphides and Sulpho-salts	Identification, Description and Paragenesis
Reflectivity	71 grains	a) Sulphides	a) Plotting of spectral reflectivity profiles.
		b) Sulpho-salts	b) For identification
Microhardness	56 grains	Sulphides	Quantitative measurement
X-ray diffraction (Powder Camera)	17	Sphalerite	Unit cell measurement
Electron diffraction	12	Sphalerite	Unit cell measurement
Atomic Absorption spectrophotometry	55	Sulphides	Major and trace element analysis
Electron Probe Microanalysis	74	Sulphides and Sulpho-salts	Major and trace element analysis
Infra-red absorption spectroscopy	13	Sulphides	To compare with published data and to see if related to composition
Differential thermal analysis	11	Pyrite, Chalcopyrite	To compare with published data and to see if related to composition

Explanation for Tables 8 - 12

A. A. S.	Atomic Absorption Spectrophotometry
EPMA	Electron Probe Microanalysis
A	Anhedral
F	Framboidal
E	Euhedral
S	Subhedral
X	Not determined
XX	Looked for but not detected
tr	traces

Results of EPMA are quoted in %

Results of A. A. S. are quoted in ‰ for essential elements, and in parts per million for trace elements. Where EPMA and AAS analyses have both been done on the same sample, the analyses for essential elements are those done by EPMA and the trace elements unless quoted in ‰ are those analysed by A.A.S.

Table 8 Table showing the essential and trace element composition of Pyrite

Sl. No.	Sample No.	Method	Type of grain	Fe	S	Total	As	Ba	Cd	Co	Cu	Mo	Ni	Pb	Te	Zn	Co/ Ni
1	A15/911	AAS	A	44.56	x	x	x	xx	xx	39	2873	xx	xx	107	49	414	-
2	A15/916	"	A	43.16	x	x	x	386	xx	66	1025	xx	46	208	52	502	1.43
3	A15/924	EPMA & AAS	F	43.98	54.65	0.16	xx	235	xx	1900	300	xx	400	xx	30	1400	4.75
4	A15/928	AAS	F	46.93	x	x	x	645	128	222	335	xx	37	38	133	41	6.00
5	A15/935	"	A	44.32	x	x	x	761	216	683	760	xx	47	429	15	22	14.53
6	A15/953	"	F	43.73	x	x	x	xx	xx	742	650	xx	349	1300	xx	141	2.13
7	A15/971	"	A	43.36	x	x	x	171	105	125	12715	46	158	808	xx	171	0.79
8	A15/980	"	E	44.84	x	x	x	108	91	340	454	37	253	535	23	874	1.30
9	A15/1193	"	A	43.55	x	x	x	150	76	206	348	193	16	411	xx	280	12.88
10	IM6/516' 6"	"	E	45.56	x	x	x	349	xx	xx	137	241.	97	390	68	289	-
11	IM6/770	"	S	44.97	x	x	x	148	xx	455	380	256	541	xx	xx	698	0.84
12	IM6/1044' 8"	"	S	44.64	x	x	x	205	xx	590	540	39	79	595	31	210	7.47
13	IM6/1101	"	S	47.15	x	x	x	103	xx	143	2575	xx	208	500	55	51	0.69
14	IM6/1108	"	S	46.33	x	x	x	xx	xx	105	120	13	84	873	88	30	1.25
15	IM6/1160	"	S	45.57	x	x	x	267	33	583	568	19	696	536	24	204	0.84
16	IM6/1179	"	A	44.96	x	x	x	105	xx	958	957	168	556	485	27	1854	1.72
17	IM6/1231	"	S	46.78	x	x	x	112	xx	487	479	xx	50	293	xx	325	9.74
18	IM6/1393	"	A	44.19	x	x	x	xx	45	795	2487	442	xx	316	xx	48	-
19	36A/1611	"	A	44.88	x	x	x	394	xx	36	2875	xx	xx	xx	128	71	-
20	36A/1617	"	A	45.23	x	x	x	268	xx	99	1563	xx	xx	xx	132	518	-
21	32-1108	"	E	45.71	x	x	x	827	275	697	340	xx	59	361	xx	108	11.81
22	32-1198	"	E	44.42	x	x	x	388	46	1486	379	xx	667	150	xx	190	2.23

Sl No.	Sample Number	Method	Type of grain	Fe	S	Total	As	Ba	Cd	Co	Cu	Mo	Ni	Pb	Te	Zn	Co/ Ni
23	HMA/1510	AAS	A	48.25	x	x	x	xx	xx	136	200	120	133	697	xx	629	1.02
24	H ₄ 3A/1837	"	A	47.65	x	x	x	130	xx	789	210	xx	50	804	xx	125	15.78
25	A14/1534	"	S	45.91	x	x	x	xx	xx	36	9767	xx	19	490	79	17	1.89
26	H14/186	EPMA & AAS	A	44.64	53.97	98.61	x	125	xx	2075	10800	xx	185	305	230	3280	11.22
27	H14/265	"	A	43.60	55.38	98.98	0.21	xx	320	268	tr	xx	563	152	xx	202	0.48
28	IM9/264	EPMA	S	46.56	52.88	99.44	0.11	x	tr	tr	tr	tr	tr	tr	x	0.28	
29	IM9/269	"	A	44.89	53.61	98.50	tr	x	xx	tr	0.12	tr	tr	1300	x	tr	
30	IM9/285	"	A	44.30	54.62	98.92	tr	x	tr	tr	0.10	tr	tr	tr	x	tr	
31	IM9/288	AAS	A	43.75	x	x	x	xx	260	83	2875	230	552	156	39	148	0.15
32	IM9/292' 6"	EPMA & AAS	A	43.19	54.97	98.16	tr	x	249	160	1260	68	276	589	36	380	0.58
33	IM9/294' 6"	EPMA	A	43.61	54.82	98.43	tr	x	tr	tr	0.11	tr	tr	tr	x	tr	
34	IM9/364' 6"	AAS	S	44.85	x	x	x	195	180	69	tr	100	410	440	169	260	0.17
35	M10/1512	EPMA	A	44.11	54.53	98.64	tr	x	0.10	tr	0.12	tr	tr	tr	x	tr	
36	M10/1540	EPMA	A	45.53	54.17	99.70	tr	x	0.13	tr	tr	tr	tr	tr	x	tr	
37	M10/1548	"	A	44.73	53.34	98.07	tr	x	0.11	tr	tr	xx	tr	tr	x	tr	
38	M10/1589	"	A	44.89	53.28	98.17	tr	x	tr	tr	tr	xx	tr	tr	x	tr	
39	M10/1599	"	A	46.84	52.35	99.19	tr	x	0.10	tr	tr	xx	tr	tr	x	tr	
40	M10/1608	"	A	44.38	54.69	99.07	tr	x	tr	0.12	tr	xx	tr	xx	x	tr	
41	H4/456	"	F	45.37	55.07	100.44	tr	x	tr	tr	tr	xx	xx	xx	x	xx	
42	H4/464	"	F	44.72	53.34	98.06	tr	x	tr	tr	tr	xx	xx	xx	x	tr	
43	H4/465	"	F	44.77	53.66	98.43	tr	x	tr	tr	tr	xx	xx	tr	x	xx	
44	H4/474	"	F	45.96	54.68	100.64	tr	x	tr	tr	tr	xx	xx	xx	x	tr	
45	C4/960	"	A	45.19	54.37	99.56	xx	x	tr	tr	tr	tr	tr	tr	x	xx	

Table 9 Table showing the essential and trace element composition of Chalcopyrite

Sl. No.	Sample Number	Method	Cu	Fe	S	Total	As	Ba	Bi	Cd	Co	Mo	Ni	Pb	Te	Zn
1	A15/920	AAS	34.37	31.16	x	x	924	x	xx	133	28	41	xx	xx	680	
2	A15/965	AAS	36.11	29.36	x	x	276	x	xx	60	140	12	325	62	395	
3	A15/1193	EPMA & AAS	35.05	32.37	34.20	101.62	tr	576	xx	250	405	510	500	155	55	2140
4	M10/1410	AAS	34.59	29.92	x	x	1653	x	xx	440	260	690	410	xx	1790	
5	M10/1521	EPMA & AAS	34.73	27.73	35.96	98.42	0.27	1385	xx	tr	710	tr	726	xx	74	1895
6	M10/1589	EPMA	35.81	28.15	36.15	100.11	tr	x	0.13	tr	tr	xx	tr	tr	x	tr
7	A14/1534	AAS	33.87	30.98	x	x	260	x	180	275	405	122	820	192	1388	
8	IM6/762	"	33.70	30.12	x	x	742	x	235	344	280	215	285	xx	696	
9	IM6/1392	"	32.40	30.34	x	x	210	x	446	486	85	190	1045	xx	851	
10	IM6/1393	EPMA	33.66	31.19	34.85	99.70	0.12	x	xx	tr	tr	tr	tr	x	tr	
11	H4/464	EPMA & AAS	34.64	30.15	36.58	101.37	0.11	xx	tr	211	410	300	510	tr	xx	345
12	H4/465	EPMA	34.72	25.80	36.49	97.01	tr	x	tr	tr	tr	tr	tr	tr	x	2100
13	H4/491	EPMA & AAS	34.54	27.75	36.61	98.90	tr	165	0.24	198	625	tr	446	656	xx	911
14	H4/581	EPMA	35.19	32.12	33.29	100.60	tr	x	tr	tr	tr	xx	tr	tr	x	0.38
15	IM9/264	"	32.07	29.25	36.93	98.25	tr	x	tr	xx	tr	xx	tr	tr	x	0.27
16	IM9/269	"	37.09	28.76	35.61	101.46	tr	x	0.13	xx	tr	xx	tr	tr	x	0.56
17	H14/171	AAS	32.27	30.69	x	-	x	368	x	98	290	xx	1060	316	xx	1100
18	H14/186	EPMA	35.25	32.81	32.81	100.54	xx	x	xx	tr	tr	xx	tr	tr	x	0.47
19	H43A/855	AAS	35.25	28.55	x	x	1526	x	xx	236	xx	xx	xx	313	xx	1295

Table 10 Table showing the essential and trace element composition of Sphalerite

Sl No.	Sample number	Method	Zn	Fe	S	Total	As	Fa	Bi	Cd	Co	Cu	Mn	Mo	Ni	Pb	Te	Type
1	H4/456	EPMA & AAS	58.99	4.21	35.27	98.47	0.12	2189	tr	0.17	206	2980	tr	xx	xx	1468	105	Exsolutions of Chalcopyrite present
2	H4/460	"	64.74	1.12	34.63	100.49	0.10	7222	tr	0.12	668	15360	tr	285	433	1286	xx	"
3	H4/467	AAS	53.01	13.77	x		x	1383	x	876	967	3157	x	xx	385	315	16	"
4	H4/473	EPMA	61.70	1.16	35.59	98.45	tr	x	xx	0.15	tr	0.33	xx	xx	xx	0.11	x	"
5	H4/474	"	54.87	12.47	32.23	99.57	tr	x	xx	0.13	tr	2.28	0.10	0.12	xx	0.14	x	"
6	H4/481	"	56.12	9.12	35.83	101.07	tr	x	0.14	0.13	tr	0.26	xx	0.12	xx	xx	x	"
7	H4/491	EPMA & AAS	51.68	14.21	35.28	101.17	tr	174	0.11	0.28	tr	4600	tr	2100	tr	286	149	"
8	IM9/283	EPMA	64.31	1.65	34.33	100.29	tr	x	tr	tr	tr	0.65	tr	tr	tr	0.12	x	"
9	IM9/285	"	60.43	2.75	37.08	100.26	tr	x	tr	0.11	tr	0.30	tr	tr	tr	tr	x	"
10	IM9/285'2"	EPMA & AAS	61.84	2.86	35.67	100.37	tr	1088	tr	388	tr	2870	tr	tr	tr	tr	x	"
11	IM9/292'6"	EPMA	62.66	1.59	35.19	99.44	0.12	x	tr	tr	xx	0.18	tr	xx	xx	tr	x	"
12	IM9/294'	"	62.07	5.09	33.94	101.10	tr	x	tr	tr	xx	0.40	tr	xx	xx	tr	x	"
13	IM9/294'6"	EPMA & AAS	61.87	2.96	36.15	100.98	tr	569	tr	215	135	1088	xx	565	340	85	260	"
14	IM6/1160	EPMA	54.56	11.58	35.61	101.75	xx	x	xx	0.12	xx	0.22	tr	xx	xx	0.12	x	No exsolutions
15	IM6/1392	EPMA	52.11	10.65	38.16	100.92	tr	x	xx	0.14	tr	0.10	tr	xx	xx	tr	x	"
16	M10/1548	"	62.78	3.73	32.97	99.48	0.37	x	xx	0.11	0.10	0.13	tr	tr	tr	tr	x	Exsolutions present
17	M10/1589	"	52.91	10.87	36.91	100.69	tr	x	tr	0.12	tr	2.75	tr	tr	xx	tr	x	"
18	A15/971	"	53.81	12.56	35.58	101.95	tr	x	tr	tr	tr	1.08	0.13	tr	xx	tr	x	"
19	A15/1193	"	58.56	2.39	38.66	99.61	tr	x	tr	tr	tr	tr	tr	tr	xx	tr	x	No exsolutions
20	A15/1194	AAS	57.91	2.19	x	-	x	168	x	228	886	330	x	384	xx	190	53	"
21	27-145	EPMA	55.26	11.78	32.98	100.02	tr	x	tr	tr	tr	0.47	tr	tr	xx	tr	x	Exsols pre-sent
22	H14/265	EPMA & AAS	63.82	2.77	33.74	100.33	tr	413	tr	1600	tr	4020	0.10	tr	tr	990	x	"

Table 11 Fe and Cd contents of Sphalerites

Sample	Fe%	Cd%
H 4/581	2.03	< 0.1
IM 9/269	18.32	0.33
IM 6/1044'8"	8.77	0.11
M 10/1512	1.69	0.18

Table 12. Table showing the essential and trace element composition of Galena

Sl. No.	Sample Number	Method	Pb	S	Total	Ag	As	Ba	Bi	Cd	Co	Cu	Fe	Mo	Ni	Sb	Sn	Te	Zn
1	H4/464	EPMA	81.61	14.87	96.48	0.12	2.33	x	1.18	0.11	xx	1.17	0.39	0.11	xx	0.21	tr	x	0.29
2	H4/474	"	83.88	15.75	99.63	0.11	1.78	x	0.34	tr	tr	0.10	0.12	0.12	tr	0.11	tr	x	0.21
3	H4/491	EPMA & AAS	83.12	15.65	98.77	tr	0.10	233	0.27	xx	xx	0.29	0.12	6.80	tr	0.10	tr	xx	0.59
4	H4/581	EPMA	80.15	15.13	95.28	tr	2.85	x	0.37	tr	tr	0.38	tr	xx	tr	0.15	tr	x	0.54
5	IM9/269	AAS	84.77	x		x	x	xx	x	xx	238	359	487	xx	xx	x	x	27	3188
6	IM9/283	AAS	85.14	x		x	x	455	x	775	xx	5680	1025	xx	xx	x	x	69	1164
7	IM9/294'16"	EPMA & AAS	85.19	14.60	99.83	0.28	1.26	xx	0.98	683	497	6100	913	386	145	0.19	0.13	15	2200
8	H14/265	EPMA	82.28	14.87	97.15	0.15	0.17	x	3.49	tr	tr	tr	0.11	xx	xx	0.37	tr	x	0.18
9	19-424	"	83.68	14.81	98.49	tr	2.24	x	0.38	tr	tr	0.14	tr	tr	tr	0.16	tr	x	0.15
10	A15/1193	AAS	87.75	x		x	x	396	x	412	xx	933	1236	xx	210	x	x	19	2130
11	M10/1584	EPMA	81.25	13.85	95.10	tr	1.18	x	3.17	0.11	tr	1.65	tr	tr	xx	0.14	0.13	x	0.26
12	M10/1589	"	83.19	14.67	97.86	tr	tr	x	1.07	tr	xx	0.14	tr	xx	xx	0.41	0.11	x	0.12

Table 13. Table showing the statistical data of Pyrite (in p.p.m. & %)

	Fe%	S%	As	Ba	Cd	Co	Cu	Mo	Ni	Pb	Te	Zn
Mean	45.01	54.14	-	314	395	523	1946	138	264	482	78	528
Minimum	42.83	52.35	-	103	33	30	120	13	16	38	15	17
Maximum	48.25	55.38	-	827	1300	2075	1,271	442	696	1300	230	3280

Table 14. Table showing the statistical data of Chalcopyrite (in p.p.m. & %)

	Cu%	Fe%	S%	As	Ba	Bi	Cd	Co	Mo	Ni	Pb	Te	Zn
Mean	34.50	29.85	35.38	-	737	0.16%	231	401	217	410	481	95	1907
Minimum	32.40	25.80	32.48	-	165	1000	-	60	28	12	1000	55	1000
Maximum	37.09	32.81	36.93	-	1653	0.24%	446	710	510	1060	1045	192	5600

Table 15. Table showing the statistical data of Sphalerite (in p.p.m. & %)

	Cu%	Fe%	S%	As	Ba	Bi	Cd	Co	Cu	Mn	Mo	Ni	Pb	Te
Mean	58.46	6.43	35.29	0.17%	1651	0.12%	1190	588	5996	1157	951	382	874	116
Minimum	51.68	1.12	32.23	1000	168	1000	215	206	3.30%	1000	285	340	190	16
Maximum	64.74	18.32	38.66	0.37%	7222	0.13%	2780	1000	2.75%	1300	2100	433	1468	260

Table 16 Table showing the statistical data for Galena (in p. p. m. & %)

	Pb(%)	S(%)	Ag	As	Ba	Bi	Cd	Co	Cu	Fe	Mo	Ni	Sb	Sn	Te	Zn
Mean	83.50	14.91	16.50	1.48%	361	1.25%	820	367	4310	1378	841	202	0.20%	0.12%	33	2674
Minimum	80.15	13.85	1000	1.68%	233	0.27%	412	238	359	487	386	145	0.10%	1000	15	1164
Maximum	87.75	15.75	2800	2.85%	455	3.49%	1130	497	1.65%	3900	1200	260	0.37%	0.12%	69	5860

Table 17 Table showing the measured and calculated cell edges of Sphalerite

Sl. No.	Sample Number	Measured edge in Å	Calculated edge Å	Difference Å
1	H4/456	5.4146	5.4135	-0.0011
2	H4/460	5.4113	5.4107	-0.0006
3	H4/467	5.4221	5.4211	-0.0010
4	H4/473	5.4120	5.4108	-0.0012
5	H4/474	5.4194	5.4202	+0.0008
6	H4/481	5.4162	5.4172	+0.0010
7	H4/491	5.4201	5.4220	+0.0019
8	H4/581	5.4135	5.4109	-0.0026
9	IM6/1044'8"	5.4206	5.4169	-0.0037
10	IM6/1160	5.4198	5.4193	-0.0005
11	IM9/269	5.4249	5.4259	+0.0010
12	IM9/283	5.4118	5.4107	-0.0011
13	IM9/285'2"	5.4125	5.4118	-0.0007
14	IM9/292'6"	5.4114	5.4106	-0.0008
15	IM9/294'6"	5.4127	5.4118	-0.0009
16	M10/1512	5.4106	5.4114	+0.0008
17	H14/265	5.4152	5.4124	-0.0028

Table 18 Table showing the differences in measured cell edges of Sphalerite by X-ray diffraction and electron diffraction

Sl, No.	Sample number	X-ray diffraction Å	Electron diffraction Å	Difference Å
1	H4/456	5.4146	5.4284	0.0138
2	H4/460	5.4113	5.4226	0.0113
3	H4/491	5.4171	5.4248	0.0077
4	IM9/269	5.4249	5.4367	0.0118
5	IM9/283	5.4118	5.4320	0.0202
6	IM9/285'2"	5.4125	5.4177	0.0052
7	IM9/292'6"	5.4114	5.4236	0.0122
8	IM9/294'6"	5.4127	5.4381	0.0254
9	H14/265	5.4202	5.4207	0.0005
10	M10/1512	5.4106	5.4242	0.0136
11	19-424	* 5.4240	5.4196	0.0044
12	A15/1193	* 5.4115	5.4224	0.0109

* calculated edges

Table 19 Microhardness values of Pyrite

Sl. No.	Sample number	VHN kg/mm ²	Sl. No.	Sample number	VHN kg/mm ²
1	A15/916	1031	9	M10/1548	1097
2	A15/924	1037	10	M10/1589	1123
3	A15/971	1052	11	H14/186	1118
4	IM6/1044'8"	1063	12	M10/1599	1155
5	IM6/1160	1185	13	C4/960	1110
6	36A/1617	1123	14	H4/464	1168
7	H43A/1837'	1483	15	H14/265	1107
8	M10/1540	1089	16	32-1108	1063

Table 20 Microhardness values of Chalcopyrite

Sl. No.	Sample number	VHN kg/mm ²	Sl. No.	Sample number	VHN kg/mm ²
1	A15/920	203	7	IM9/264	221
2	A15/1193	210	8	M10/1548	197
3	A14/1534	201	9	M10/1589	187
4	M10/1521	201	10	H4/465	174
5	M10/1512	187	11	H4/491	194
6	H14/186	194	12	H4/171	210

Table 21 Microhardness values of Sphalerite

Sl. No.	Sample number	VHN kg/mm ²	Sl. No.	Sample number	VHN kg/mm ²
1	A15/971	230	11	IM9/288	206
2	IM6/1160	215	12	M10/1589	195
3	IM9/269	237	13	H4/465	148
4	19-424	203	14	M10/1548	175
5	M10/1512	161	15	H4/481	190
6	A15/1194	172	16	H4/474	210
7	H4/474	195	17	IM9/294'6"	172
8	H4/491	240	18	IM9/285	186
9	IM9/285'2"	168	19	H4/456	203
10	M10/1584	198			

Table 22 Microhardness values of Galena

Sl. No.	Sample number	VHN kg/mm ²	Sl. No.	Sample number	VHN kg/mm ²
1	19-424	61.7	5	H4/491	67.7
2	H4/464	107	6	M10/1584	201
3	H4/474	104	7	IM9/283	96.5
4	A15/1194	77.9	8	H14/265	87.8

Table 23 Table showing the spectral reflectivity values of Pyrite (R% air)

Section No.	400	420	440	460	480	500	520	540	560	580	589	600	620	640	660	680	700
A15/924	41.05	46.1	47.5	50.05	51.8	52.0	52.7	55.0	55.15	56.23	56.45	57.8	56.2	57.3	57.6	57.8	57.7
A15/980	42.5	45.20	45.5	45.18	47.5	48.2	49.3	49.6	49.8	50.25	52.1	52.5	52.6	53.8	53.9	53.8	53.7
A15/971	35.05	36.8	37.9	40.10	42.5	43.2	45.05	46.8	47.5	49.0	49.8	50.15	51.2	52.5	54.1	54.6	55.3
A14/1534	36.10	37.6	39.8	42.5	43.6	46.0	47.5	49.0	49.65	49.75	51.38	52.1	53.4	55.6	55.2	55.3	55.25
27-145	42.5	44.3	47.0	48.3	49.5	50.25	50.05	51.2	52.1	52.1	52.3	52.1	52.5	53.2	53.8	54.0	54.8
H43A/1855	34.8	36.7	37.2	38.3	41.8	42.9	45.6	47.5	48.3	50.6	52.1	52.35	53.68	54.8	54.95	55.0	54.86
32-1108	34.3	37.9	40.15	41.6	42.65	45.73	46.85	46.65	46.75	46.89	47.5	50.05	50.10	50.10	5.05	50.05	51.00
32-1198	36.0	37.5	39.8	42.5	45.05	47.8	48.5	50.05	50.10	50.5	52.01	52.25	52.20	51.85	51.80	51.8	50.75
H14/265	32.5	36.2	37.3	39.4	40.03	41.6	42.5	43.6	45.80	47.2	47.8	48.3	49.6	49.5	49.9	50.05	50.20
H4/456	36.2	41.8	42.6	43.2	45.05	46.7	47.5	48.3	50.15	52.6	53.9	54.8	55.05	55.10	55.20	55.15	55.20
H14/	36.25	37.5	37.8	40.16	41.68	42.5	43.6	45.2	46.25	46.8	47.6	47.8	49.3	50.2	52.6	52.3	52.2
19-424	38.12	40.10	42.3	42.7	44.3	45.6	46.2	47.6	48.3	48.9	49.2	50.12	50.15	49.8	50.2	49.5	50.05
A15/953	42.5	43.4	47.5	48.2	51.6	52.6	54.8	55.1	55.2	56.2	56.3	56.8	56.4	52.5	57.2	57.6	57.3
A15/950	37.0	37.5	39.5	40.25	45.06	46.3	47.5	49.3	47.25	50.15	50.30	52.2	55.0	55.25	55.6	55.3	55.75
A15/	34.8	35.2	36.8	36.9	37.5	40.2	41.5	42.2	43.8	45.0	46.3	49.8	51.3	52.6	52.7	52.6	53.9
32-1269	33.6	37.6	39.5	42.5	45.0	47.5	50.2	51.8	52.5	52.8	53.6	54.9	55.2	55.1	55.3	55.6	55.4
IM6/1101	35.0	37.8	41.8	44.8	47.5	47.8	51.3	51.85	52.6	53.6	52.8	55.05	55.61	55.3	55.4	55.6	55.0
A15/1193	32.6	34.6	39.6	42.5	45.0	47.2	49.6	49.8	50.1	51.2	51.8	52.5	52.6	52.7	52.9	54.0	55.0
IM6/1160	32.5	35.6	40.04	42.6	45.10	47.5	49.8	50.1	50.25	52.5	52.7	54.0	55.0	55.2	55.05	55.10	55.2
A15/941	36.8	37.5	39.8	42.3	42.8	46.8	47.9	50.0	50.10	50.15	51.28	52.20	52.5	52.8	52.4	52.3	52.0
IM6/231	34.3	35.0	36.2	37.2	40.02	40.35	42.5	42.6	44.8	46.35	47.21	47.75	48.3	48.4	48.2	48.3	49.5
A15/916	38.35	40.05	44.3	47.5	48.3	50.1	50.2	52.5	52.7	53.6	54.8	55.0	55.6	55.2	54.9	54.8	54.6
IM6/1392	34.8	35.0	40.35	42.6	46.3	46.2	47.5	47.8	47.9	50.25	50.20	53.2	52.5	53.2	53.1	53.6	53.78
H4/474	33.6	35.0	36.2	37.8	38.3	40.5	42.5	45.0	45.8	46.9	46.92	46.85	47.25	47.05	46.55	47.2	47.4
A15/935	33.8	36.8	38.6	42.6	47.5	48.9	51.6	52.6	53.78	54.2	53.98	54.5	55.2	55.1	52.8	52.3	52.6

	400	420	440	460	480	500	520	540	560	580	589	600	620	640	660	680	700
IM6/779	34.85	37.5	40.2	42.5	45.1	47.5	48.6	49.3	49.35	50.6	50.53	51.26	52.5	52.7	52.8	52.3	52.6
IM 9/36412"	32.15	34.68	37.3	39.8	41.9	42.5	44.6	45.7	45.6	46.8	47.6	47.8	48.4	49.6	50.2	50.2	50.3
M10/1548	36.18	37.39	40.15	42.5	45.2	45.6	47.8	47.5	49.5	50.2	50.3	52.5	52.6	53.4	54.8	53.6	53.2
A15/965	33.5	35.7	37.8	40.2	42.5	43.6	44.2	45.6	45.2	45.7	45.9	50.2	51.2	52.3	50.25	50.15	51.2
36.A/1611	32.3	35.2	37.5	38.2	39.6	46.1	41.8	42.6	42.75	44.5	44.8	45.6	45.8	47.3	48.4	49.5	49.8
H4/491	32.2	35.0	37.5	41.5	42.6	44.2	45.5	47.5	48.4	50.5	51.6	52.5	53.6	53.8	53.65	53.78	53.6
M10/1610	34.8	34.6	40.2	42.6	46.8	47.5	50.2	51.8	52.6	54.6	54.5	54.7	55.2	55.3	55.0	55.2	55.4
IM9/292'6"	32.6	35.0	37.5	39.8	42.5	46.8	47.2	47.5	48.6	50.2	52.3	52.2	54.8	54.6	53.8	53.2	53.5

Table 24 Table showing the spectral reflectivity values of Chalcopyrite (R% air)

Section No.	400	420	440	460	480	500	520	540	560	580	589	600	620	640	660	680	700
32-1198	24.48	27.54	29.04	31.71	34.58	37.11	38.23	39.45	40.05	40.25	41.33	41.39	40.66	39.68	39.45	38.66	38.73
A15/1193	25.92	28.85	31.00	33.44	35.40	36.49	37.44	37.79	38.81	39.12	40.36	39.60	38.31	36.8	36.65	36.03	35.93
IM6/1393	22.75	24.26	26.28	28.54	29.91	31.13	31.32	33.38	34.56	36.15	38.21	38.66	37.81	36.65	36.2	34.75	34.2
A15/924	28.7	29.10	31.8	32.7	34.10	35.71	37.19	38.14	38.37	39.83	40.36	41.18	38.31	36.8	36.5	36.2	35.85
A15/943	21.91	22.95	24.60	27.45	30.10	34.76	35.68	36.61	37.31	38.25	38.65	39.30	40.31	39.58	37.61	37.5	36.31
H14/186	25.10	28.78	29.9	30.31	31.15	32.36	35.29	35.86	36.16	36.24	38.34	39.47	40.69	39.68	39.32	38.58	36.8
A15/965	20.40	22.56	25.08	27.81	30.44	32.38	33.98	34.39	36.35	37.12	38.88	38.56	37.34	38.31	36.62	36.12	35.2
IM6/779	28.15	29.28	30.36	31.38	32.67	34.73	36.01	37.28	37.92	39.13	40.62	39.47	40.31	39.8	38.86	38.05	36.9
H4/456	23.53	28.01	29.36	30.35	31.29	32.75	33.51	35.91	37.53	38.62	40.55	39.47	40.31	41.4	40.38	39.68	39.7
H43A/ 1855	27.35	28.45	28.86	29.81	30.34	33.76	35.29	36.94	37.92	39.6	41.35	40.44	40.75	40.4	40.2	39.65	39.3
H4/491	26.16	27.36	28.71	29.30	30.16	31.35	33.69	34.85	32.83	39.65	41.02	41.37	40.31	40.6	40.4	40.2	39.3
M10/1410	23.6	24.2	26.8	29.80	30.34	33.76	36.29	38.94	39.92	40.15	42.61	43.85	43.05	42.83	42.65	41.85	40.38

Table 25 Table showing the spectral reflectivity values of Sphalerite (R% in air)

Section No.	400	420	440	460	480	500	520	540	560	580	589	600	620	640	660	680	700
IM9/294' 6"	16.85	16.9	17.01	17.55	17.42	17.96	17.53	17.55	17.00	17.25	17.05	19.57	18.36	20.3	19.8	19.6	18.9
H4/456	19.2	18.9	18.8	18.9	18.62	18.78	17.53	17.6	17.37	17.25	17.60	18.85	18.64	18.32	18.8	20.3	20.6
IM9/285' 2"	18.35	18.2	17.85	17.83	17.79	16.52	16.32	15.89	15.81	16.35	17.7	16.32	17.8	19.32	20.3	19.46	19.3
A15/980	16.85	16.73	16.15	15.84	14.85	14.86	15.25	15.4	15.92	15.66	16.35	17.94	15.87	14.53	14.83	15.63	14.89
27-145	18.85	18.80	18.68	18.62	18.07	17.65	17.79	17.74	17.83	17.72	17.89	19.65	18.13	20.3	19.8	19.6	19.3
32-1198	22.24	22.20	22.16	22.04	21.95	21.87	22.31	22.04	22.29	22.25	22.13	23.92	22.67	23.07	20.32	19.87	19.6
19-424	16.85	16.76	16.64	16.58	16.11	16.66	16.40	16.50	16.07	16.95	16.98	17.08	15.87	14.53	13.53	13.6	13.3
A15/1193	19.31	19.25	19.05	18.72	19.91	18.80	17.93	18.28	18.79	17.72	17.92	17.65	18.13	19.23	20.3	19.6	19.4
IM6/1393	18.4	18.3	17.4	16.78	16.4	16.11	15.21	15.86	15.92	15.66	16.78	17.08	15.87	14.83	15.33	13.53	13.53
H14/265	19.15	19.03	18.8	18.6	18.6	17.89	17.35	17.63	17.65	17.43	17.35	17.28	16.87	16.47	17.15	17.6	17.6

Table 26 Table showing the spectral reflectivity values of Galena (R% air)

Section No.	400	420	440	460	480	500	520	540	560	580	589	600	620	640	660	680	700
H4 A14/456	32.95	33.45	32.80	32.8	32.15	32.00	31.92	32.38	34.16	35.86	37.31	37.31	38.15	37.7	35.57	34.2	33.2
19-424	43.31	43.15	43.05	42.66	40.65	38.85	39.29	38.91	38.37	37.83	38.3	39.6	37.39	41.4	40.8	41.2	40.5
A15/1193	45.92	45.24	45.15	45.05	45.24	43.95	42.38	41.71	40.57	39.45	40.25	41.18	36.13	36.8	36.5	37.2	36.68
H4/491	43.93	43.65	43.35	42.84	42.64	41.96	41.35	41.39	41.08	40.68	41.32	42.36	43.06	46.0	45.8	45.63	44.83
M10/1584	38.75	38.65	38.3	36.09	35.19	35.69	33.26	32.79	32.73	32.74	32.47	31.87	33.22	34.42	36.35	33.2	31.2

Table 27

Composition of Arsenopyrite

	M 10/1599 %	M 10/1608 %	Theoretical composition %
Fe	36.06	37.11	34.30
As	42.78	43.23	46.01
Co	tr	tr	
Ni	tr	tr	
Cu	tr	tr	
Pb	tr	tr	
Zn	tr	tr	
S	20.76	21.25	19.69
Total	99.60	101.59	100.00

Table 28 List of Sulpho-salts found at Parys Mountain

General classification	Name	Theoretical formula
Copper Sulpho-salts	Tetrahedrite-Tennantite	$(\text{Cu Fe Zn Hg})_{12}$ $(\text{Sb As})_4\text{S}_{13}$
Copper-Lead Sulpho-salt	Bournonite	Pb Cu Sb S_3
Lead Bismuth Sulpho-salts	Galenobismuthite Kobellite	$\text{Pb Bi}_2\text{S}_4$ $\text{Pb (Bi, Sb)}_2\text{S}_5$
Lead Sulpharsenides	Lead Sulpharsenide	Pb-As-S (varying)

Table 29 Composition of Tetrahedrite - Tennantites

Sample No.	1	2	3	4	5	6	7	8	9	10	11	12	13
	H4/473	H4/464	H4/456a	H4/456b	27-145	H4/474	27-145	H4/491	M10/1548				
Element Cu	34.35	36.12	33.76	36.31	39.67	32.39	37.88	31.61	28.78	34.7	32.6	34.4	34.9
Ag	0.1	tr	0.31	tr	0.55	tr	0.23	1.28	xx	3.1	5.4	1.8	2.6
Fe	9.54	8.42	10.18	9.61	6.05	4.31	7.04	8.31	3.16	1.7	1.3	4.9	3.9
Zn	2.38	1.29	5.36	2.23	4.24	8.18	4.69	5.15	1.29	5.7	6.1	2.6	2.5
Sb	24.77	28.52	23.35	22.85	22.12	23.67	tr	1.38	0.12	25.1	28.2	29.8	29.8
As	2.1	3.2	2.1	4.48	1.18	3.28	22.16	24.29	41.57	2.7	0.8	1.1	0.8
Bi	0.32	0.89	0.67	tr	xx	xx	1.42	0.87	xx	-	-	-	-
S	25.45	23.25	26.18	25.03	23.32	26.66	27.47	24.63	25.12	25.2	24.5	25.0	24.7
Total	99.01	98.69	101.91	100.51	97.75	98.49	100.91	97.52	100.04	98.2	98.9	99.6	99.2

tr - traces xx not detected

1 - 6 Parys Mountain Tetrahedrites (Present Study)

7 - 9 Parys Mountain Tennantites (Present Study)

10 Parys Mountain Tetrahedrite Hill Side open cast, Bluestone adit dump (Analyst: Wheatly 1971a)

11 Parys Mountain Tetrahedrite, Morfa-du Ida Shafi dump (Analyst: Wheatly 1971a)

12 West Avoca Tetrahedrite, South Lode. (Analyst: Wheatly 1971a)

13 East Avoca Tetrahedrite (Analyst: Wheatly 1971a).

Table 30 Table giving the atomic proportions for Tetrahedrites-Tennantites (Present Study)

	T e t r a h e d r i t e s				T e n n a n t i t e s				
	H4/473	H4/464	H4/456a	H4/456b	27-145	H4/474	27-145	H4/491	M10/1548
Cu	8.66	9.23	7.99	10.59	9.33	8.59	8.99	8.10	10.27
Ag	0.01	-	0.04	-	0.07	-	0.03	0.19	-
Fe	2.73	2.44	2.74	1.05	1.62	1.30	1.90	2.42	1.28
Zn	0.58	0.32	1.23	0.37	0.97	2.10	1.08	1.28	0.45
Sb	3.49	3.33	3.44	3.03	3.53	3.26	0.00	0.13	-
As	0.48	0.61	0.50	0.97	0.47	0.74	3.90	3.82	3.99
Bi	0.02	0.06	0.06	-	-	-	0.09	0.05	0.00
S	12.93	11.37	12.79	13.95	11.54	13.90	12.48	11.42	11.50

Table 31 Composition and atomic proportions of Bournonite

	Composition						Atomic Proportions	
	1	2	3	4	5	6	1	2
Cu	15.22	20.72	13.0	13.6	14.2	12.3	1.37	1.58
Pb	39.81	43.86	42.4	44.6	43.8	42.9	1.10	1.03
Sb	22.84	16.17	24.9	22.7	22.7	25.3	1.07	0.64
As	2.49	3.67	-	-			0.19	0.24
Bi	0.12	0.22	-	-			0.00	0.00
Fe	xx	0.25	-	-			-	0.02
Zn	0.16	0.14	-	-			0.01	0.01
S	18.17	15.62	19.7	19.3	20.5	19.6	3.25	2.46
Total	98.81	100.65	100.0	100.2	101.2	100.1		

1. Parys Mountain, H4/465 (Present Study)
2. Parys Mountain, M10/1548 (Present Study)
3. Theoretical Composition
4. East Avoca, Tigroney (Analyst: Wheatly, 1971a)
5. No. 1A, draw point, Avoca (Analyst: Wheatly, 1971a)
6. Wood river Lead Silver deposit, Idaho (Analysts: Hall and Czernanske, 1972)

Table 32 Composition and atomic proportions of Kobellite

	Composition				Atomic Proportions	
	1	2	3	4	1	2
Pb	40.26	43.18	44.4	47.1	5.51	8.77
Cu	2.86	2.19	-	0.9	1.27	1.45
Bi	30.22	32.15	29.9	32.1	4.10	6.47
Sb	6.12	4.23	8.6	4.5	1.43	1.46
Fe	3.12	1.29	-	-	0.65	0.97
As	1.31	0.88	-	-	0.05	0.00
S	17.18	16.19	17.2	15.7	15.20	21.25
Total	101.07	100.11	100.1	100.3		

1. Parys Mountain H4/474
2. Parys Mountain M10/1548
3. Theoretical Composition
4. West Avoca (Analyst: Wheatly, 1971a)

Table 33 Composition and atomic proportions of Galenobismuthite

	Composition				Atomic Proportions
	1	2	3	4	1
Bi	43.16	55.5	54.69	58.0	1.47
Cu	3.18	-			0.36
Pb	26.47	27.5	27.65	24.7	0.83
Zn	10.12				1.10
Fe	0.39				0.00
S	13.78	17.0	17.35	17.0	3.06
	97.10	100.0	99.69	99.7	

1. Parys Mountain H4/474
2. Theoretical Composition
3. Type Material (Analyst: Sjogren (1878) in Berry, 1940)
4. Bally Coog, Avoca (Analyst: Wheatly, 1971a)

Table 34 Composition and atomic proportions of Lead Sulpharsenides

	Composition		Atomic Proportions	
	1	2	1	2
Cu	0.18	0.28	0.03	0.06
Pb	69.68	68.18	3.17	4.21
Sb	0.13	0.05	0.01	0.00
As	13.24	15.37	1.66	2.63
Fe	0.16	0.38	0.03	0.09
Zn	1.88	0.19	0.27	0.04
Bi	xx	xx		
S	13.82	14.38	4.06	5.75
Total	99.09	98.83		

1. Parys Mountain 19-424
2. Parys Mountain M10/1589

Table 35 X-ray Powder diffraction data for Diabantite

d Å (from Tables 7-171)	hkl	d Å measured
7.08	002	7.081
3.541	004	3.541
2.458	132, 20 $\bar{3}$	2.458
2.271	132, 20 $\bar{4}$	2.276
1.829	13 $\bar{6}$, 205	1.829
1.550	33 $\bar{1}$, 060	1.542
1.360	334, 065, 336	1.368

Table 36 X-ray Powder diffraction data for Ripidolite

d Å (from Tables 7-76)	hkl	d Å measured
14.1	001	14.119
7.07	002	7.076
4.724	003	4.720
3.537	004	3.534
2.599	(131, 20 $\bar{2}$)	2.600
2.450	132, 20 $\bar{3}$	2.452
1.826	13 $\bar{6}$, 205	1.826
1.665	13 $\bar{7}$, 206	1.666
1.547	33 $\bar{1}$, 060	1.546

Table 37 X-ray Powder diffraction data for Clinocllore

d Å from Tables 19-749	hkl	d Å measured
14.3	001	14.348
7.12	002	7.115
3.56	004	3.559
2.435	132	2.438
2.255	133	2.256
1.535	24 $\bar{5}$, 060	1.536

Table 38 X-ray Powder diffraction data for Aphrosiderite

d Å from Tables 2-243	hkl	d Å measured
7.05	002	7.047
3.52	004	3.527
2.83	005	2.822
2.67	200	2.672
1.559	060	1.559

Table 39 X-ray Powder diffraction data for Grochautite

d Å from Tables 7-165	hkl	d Å measured
14.0	001	14.029
7.08	002	7.081
3.545	004	3.545
2.543	13 $\bar{2}$, $\bar{2}$ 01	2.544
2.842	005	2.844

Table 40

X-ray powder data for Chlorite 1b

d(Å) from Tables 16-351	hkl	d Å measured
14.4	001	14.392
7.15	002	7.155
2.475	20 $\bar{3}$	2.470
2.29	20 $\bar{4}$	2.287
1.548	060	1.549

- 35 36A/1617 (Pyrite with little chalcopyrite), IM6/1044'8" (Pyrite), 36A/1611 (Pyrite)
- 36 36A/1670 (Pyrite), M10/1630 (Pyrite), A15/941 (Pyrite with little chalcopyrite), M10/1410 (Chalcopyrite with some pyrite)
- 37 IM9/269 (Sphalerite with some pyrite), 32-1198 (Pyrite with little sphalerite)
- 38, 39 IM6/1231 (Pyrite), IM6/1365 (Pyrite, Chalcopyrite with little sphalerite; in this section only grochauite is present)
- 40 IM6/1359, 36A/1525, 6-527, H17A/1510, H43A/1845 (non-mineralised sections).

Table 41

Standards used for Microprobe Analysis

Element	Standard	Radiation
Ag	Pure Metal	Ag K_{α}
As	Pure Element	As K_{α}
Bi	Pure Metal	Bi L_{α}
Cd	Pure Metal	Cd L_{α}
Co	Pure Metal	Co K_{α}
Cu	Pure Metal	Cu K_{α}
Fe	FeS ₂ 46.55% Fe	Fe K_{α}
Mn	Pure Metal	Mn K_{α}
Mo	Pure Metal	Mo L_{α}
Ni	Pure Metal	Ni K_{α}
Pb	PbS 86.62% Pb	Pb M_{α}
S	FeS ₂ 53.45% S	S K_{α}
Sb	Pure Element	Sb L_{α}
Se	No Standard available	-
Sn	Pure Metal	Sn K_{α}
Zn	Pure Metal	Zn K_{α}

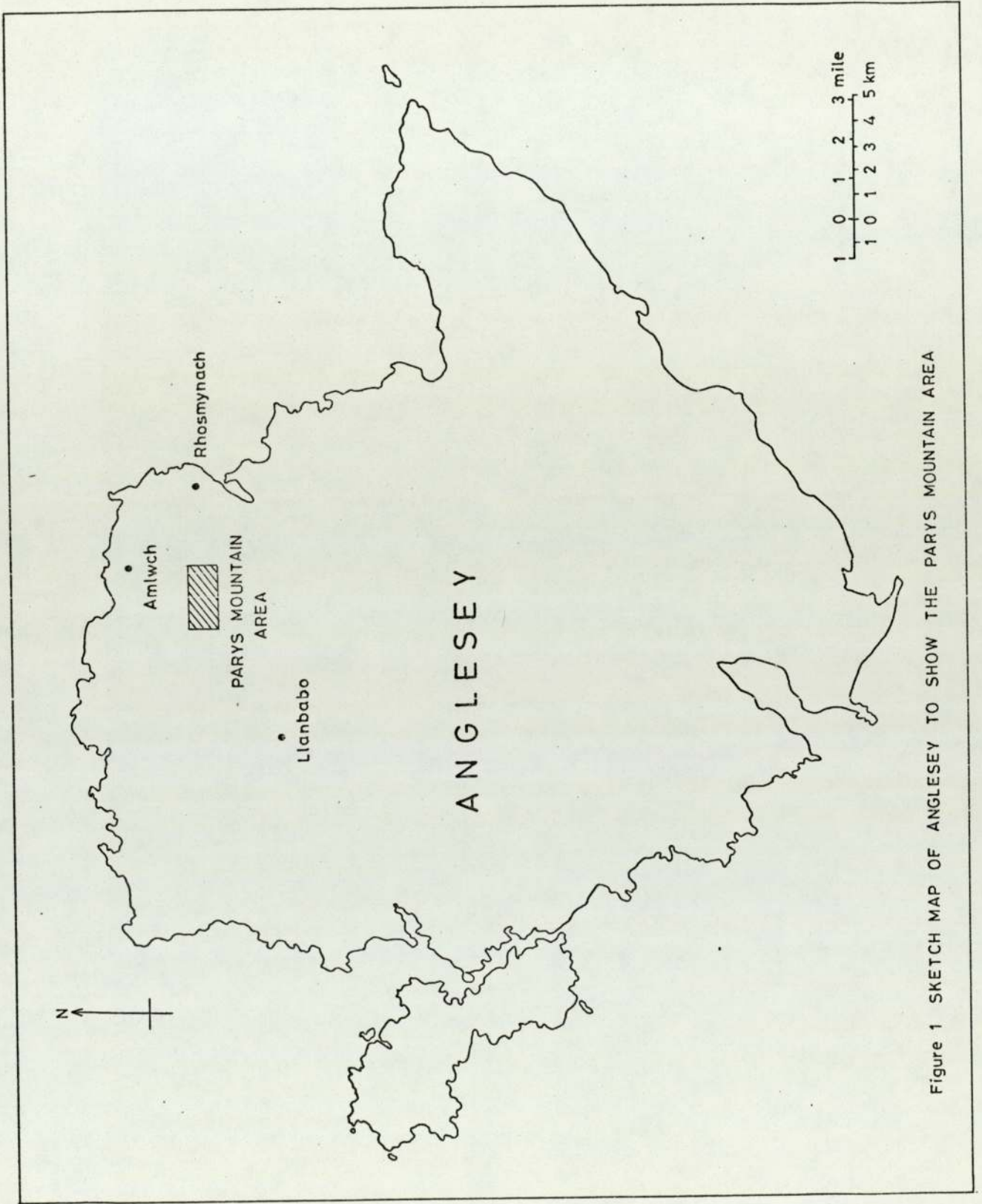
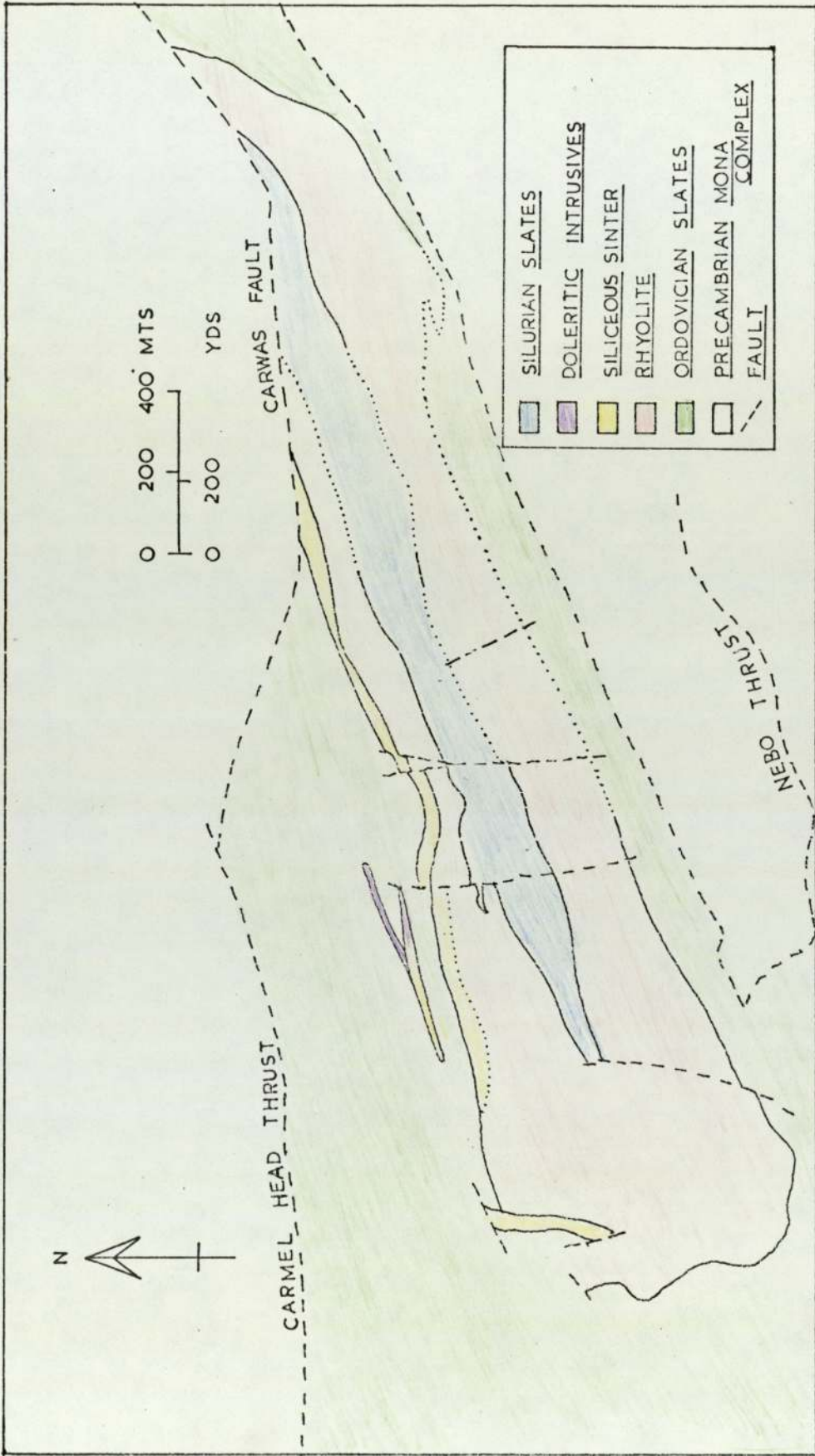


Figure 1 SKETCH MAP OF ANGLESEY TO SHOW THE PARYS MOUNTAIN AREA

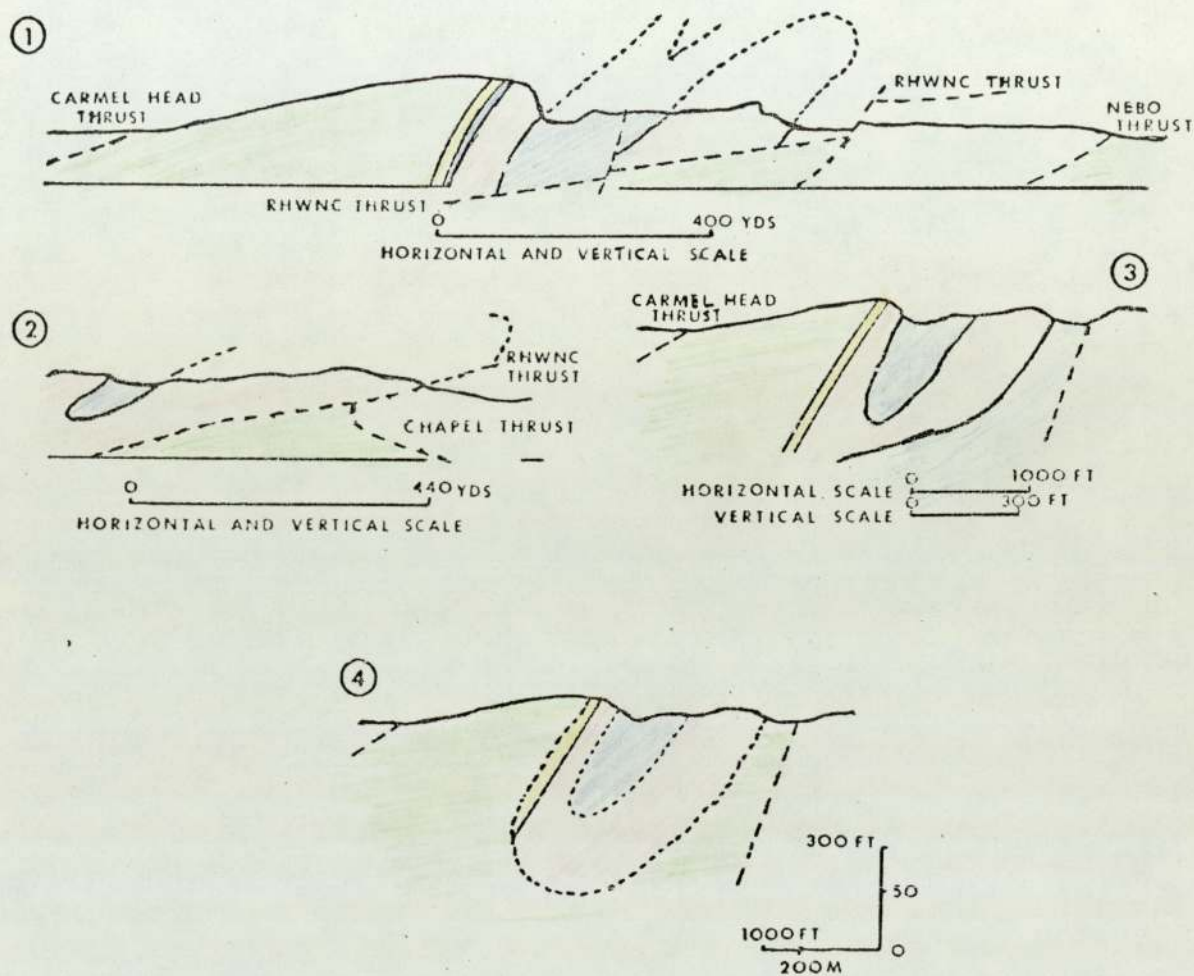
FIGURE 2



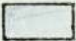
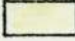
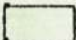
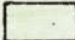

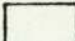
Simplified Geological map of Parys Mountain Area (after Thanasuthipithak, 1974)

FIGURE 3

CROSS SECTIONS ILLUSTRATING THE STRUCTURAL INTERPRETATIONS OF PARYS MOUNTAIN



- ① SECTION THROUGH THE CENTRAL PART OF PARYS MOUNTAIN (AFTER GREENLY 1919)
- ② SECTION THROUGH THE WESTERN END OF PARYS MOUNTAIN (AFTER GREENLY 1919)
- ③ SECTION THROUGH THE CENTRAL PART OF PARYS MOUNTAIN (AFTER MANNING 1959)
- ④ SECTION THROUGH THE CENTRAL PART OF PARYS MOUNTAIN AFTER THANASUTHIPITHAK 1974
(cf. WHEATLEY, 1971)

	SILURIAN SLATE		SILICEOUS SINTER
	DACITE		ORDOVICIAN SLATE
	RHYOLITE		PRECAMBRIAN MONA COMPLEX

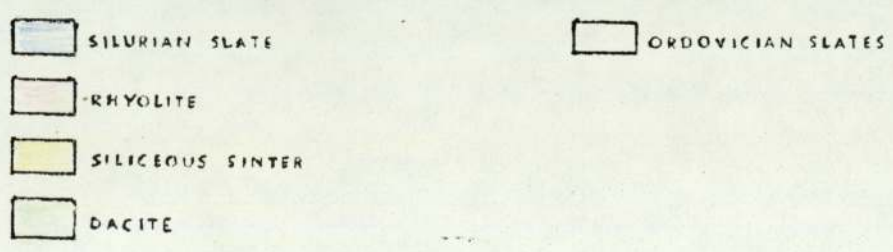
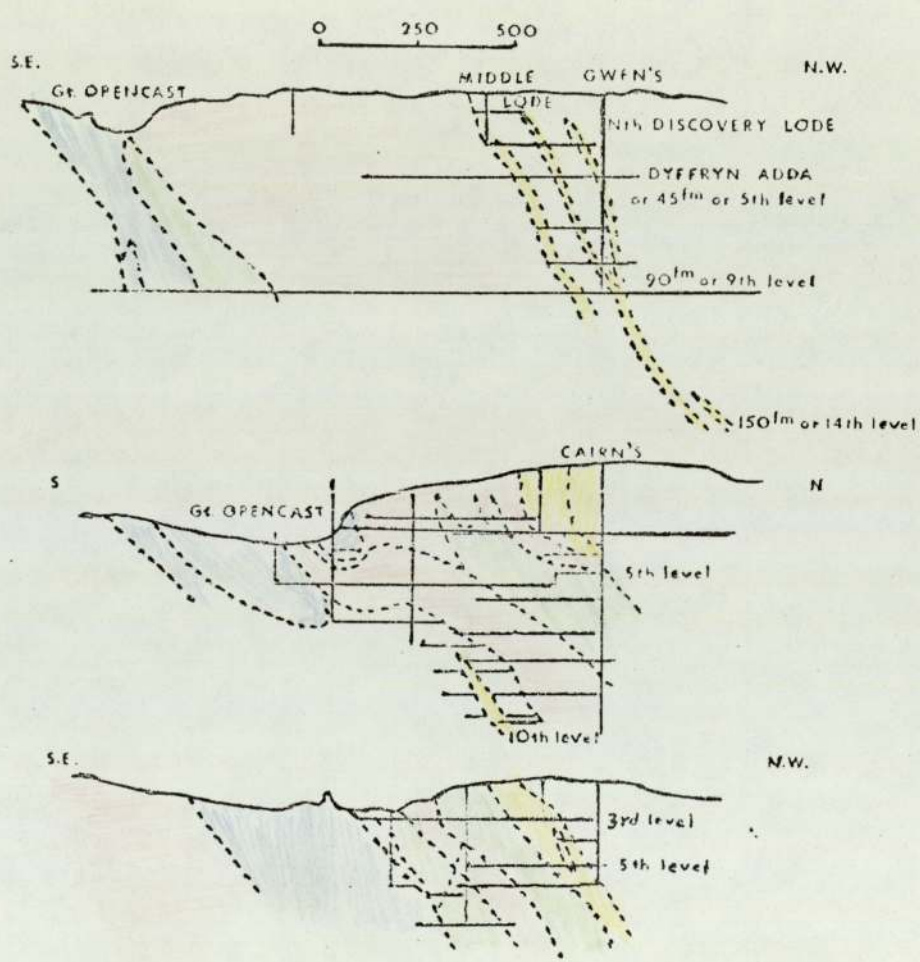
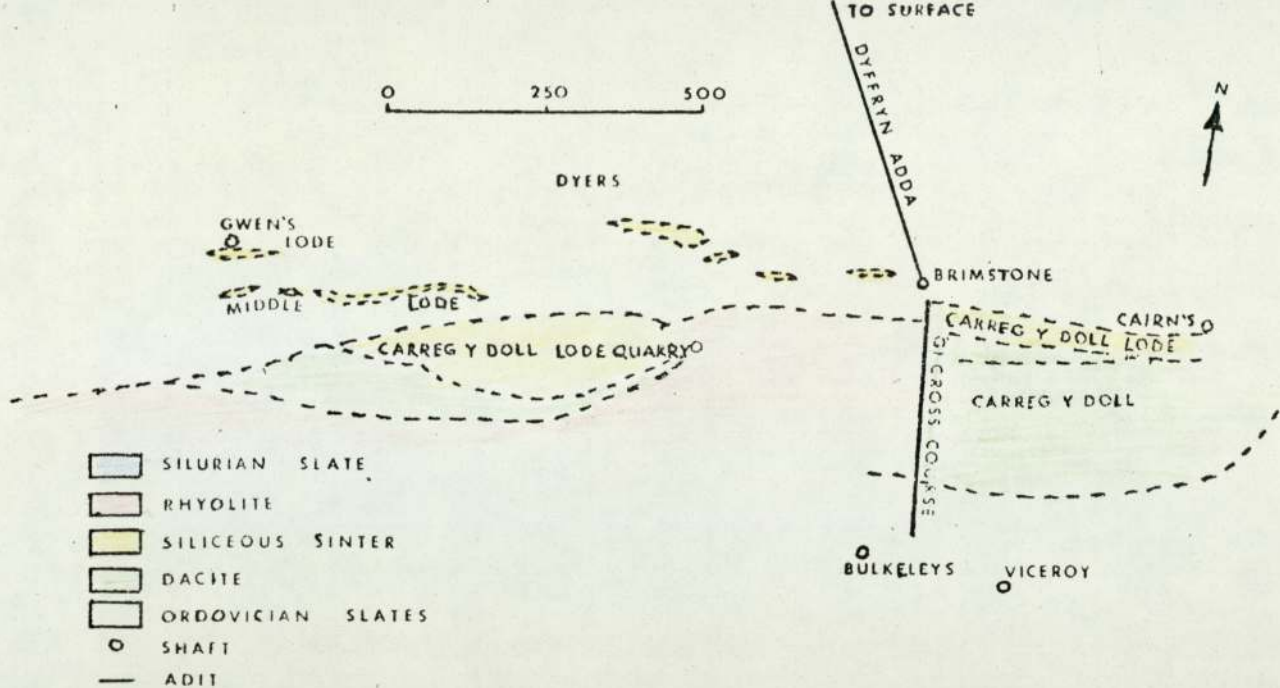
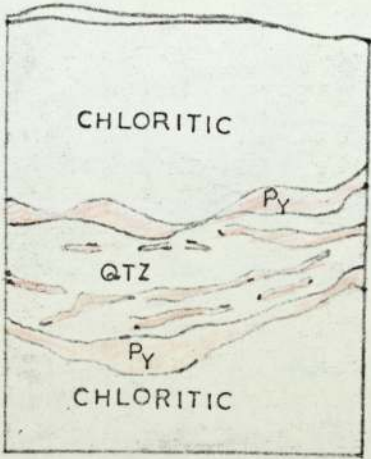


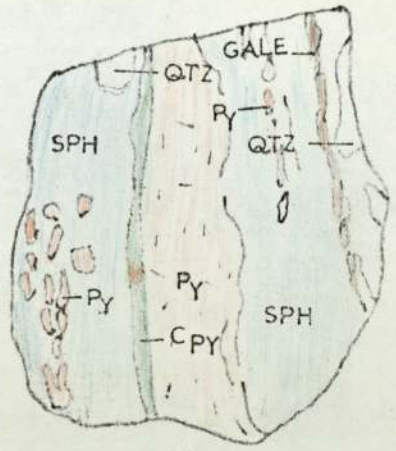
Figure 4

Sections illustrating the various lodes (after Manning, 1959)

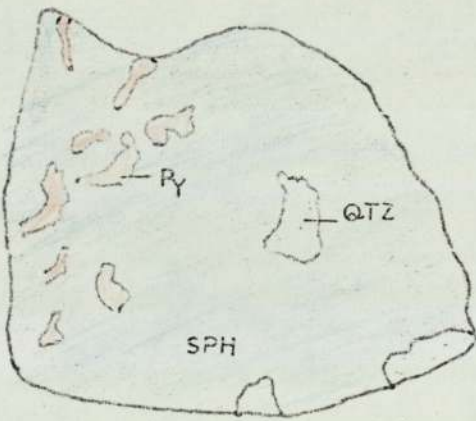
FIGURE 5



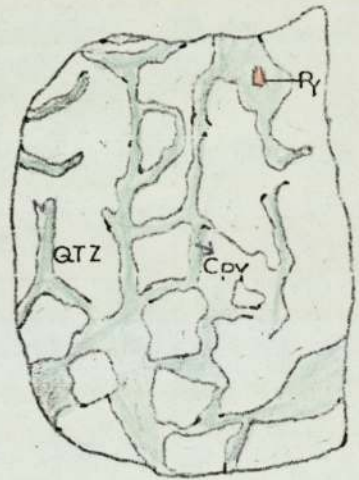
A



B



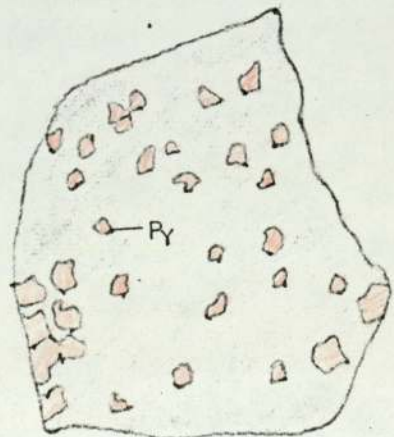
C



D



E



F

1 CM

Fig. 6a

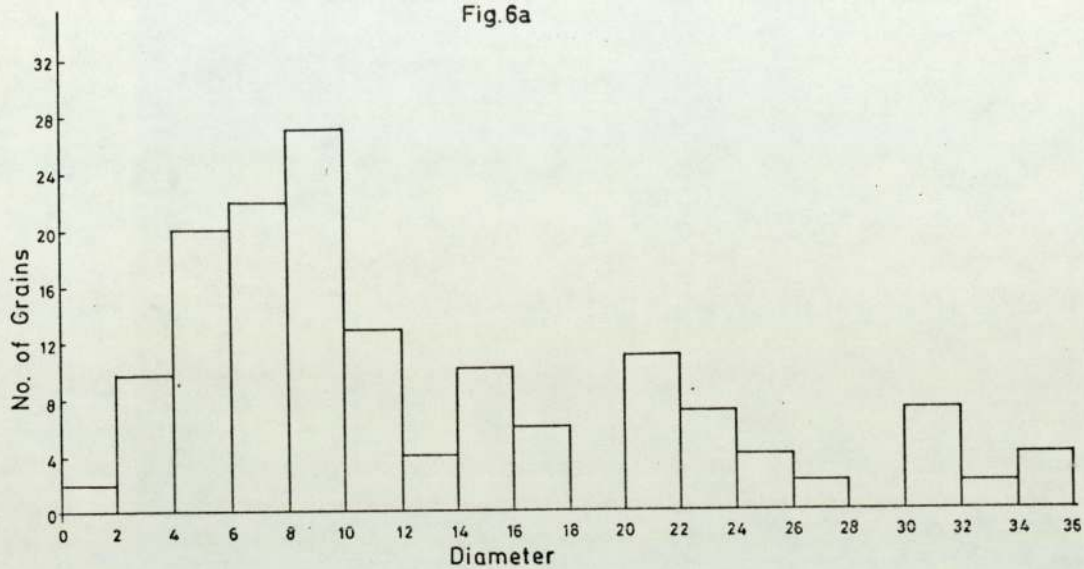


Fig. 6b

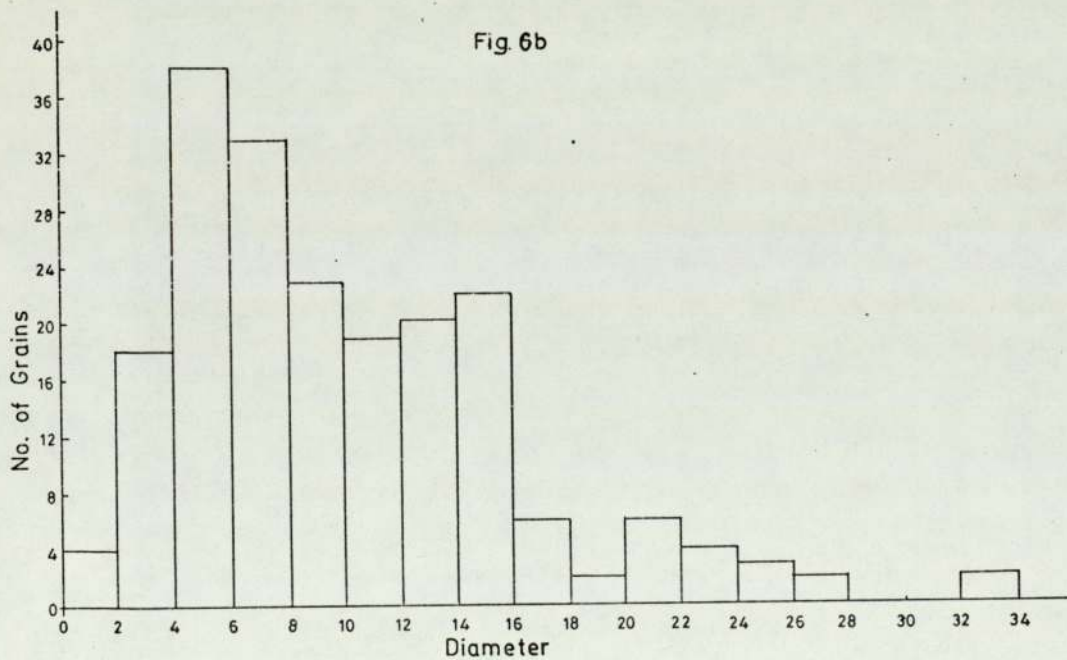


Fig. 6a Size distribution of framboidal pyrites in sample A15/920 (180 frambooids)

Fig. 6b Size distribution of framboidal pyrites in sample A15/941 (160 frambooids)

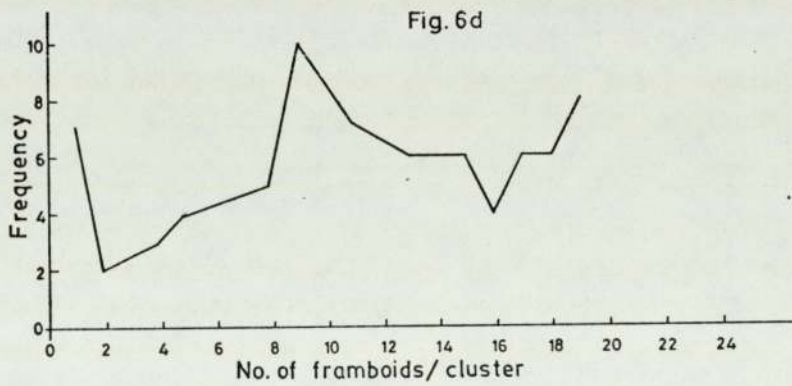
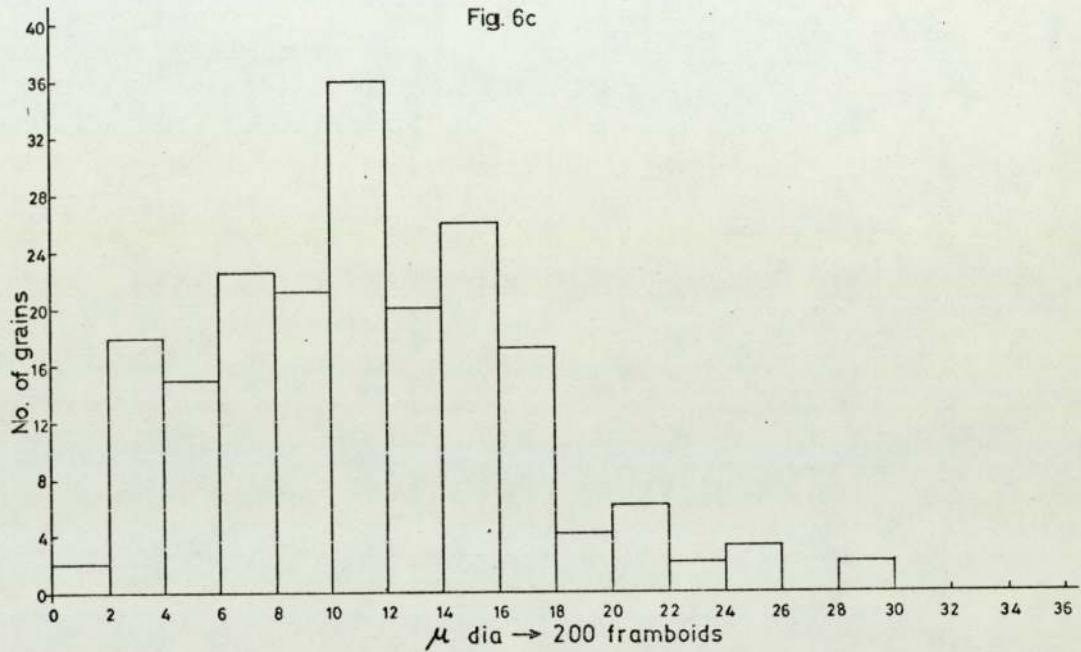


Fig. 6c Size distribution of framboidal pyrites in samples H4/460 and H4/474

Fig. 6d Plot of frequency against number of frambooids/cluster (sample H4/464)

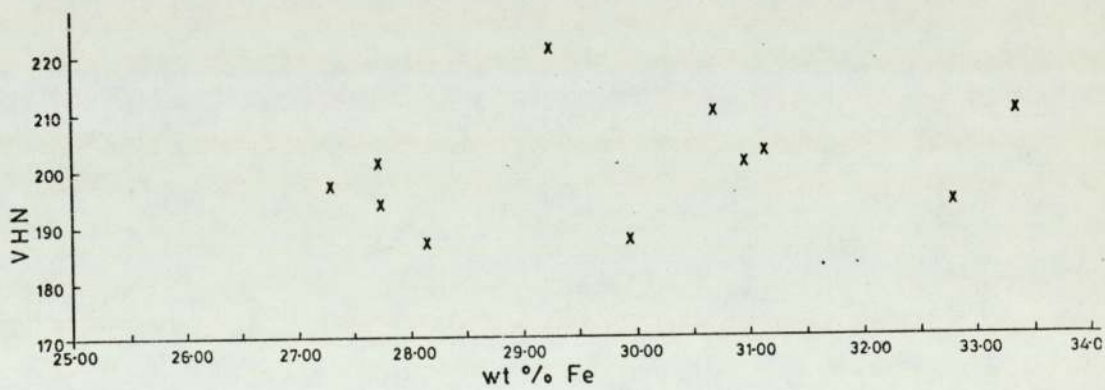
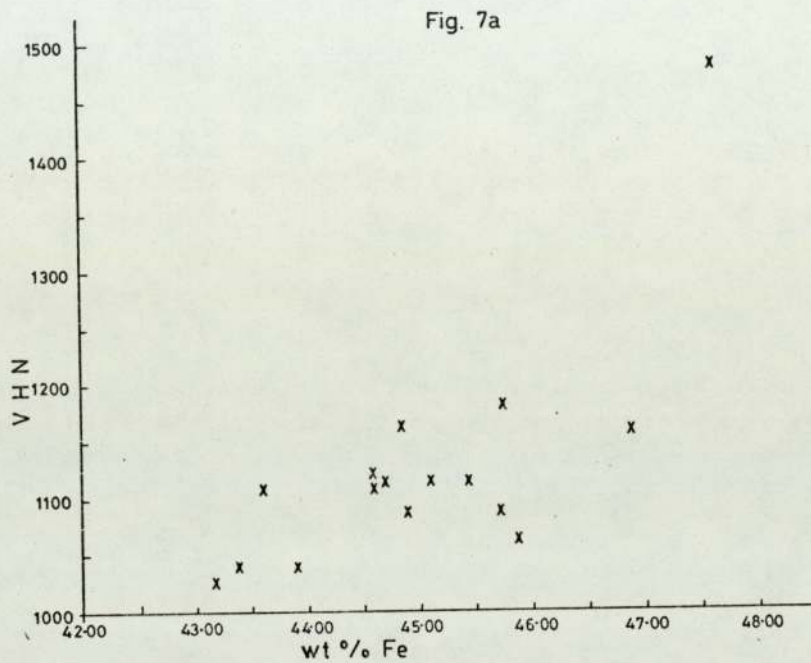


Fig. 7a Plot of microhardness (VHN) against wt% Fe in pyrite
 Fig. 7b Plot of microhardness (VHN) against wt% Fe in chalcopyrite

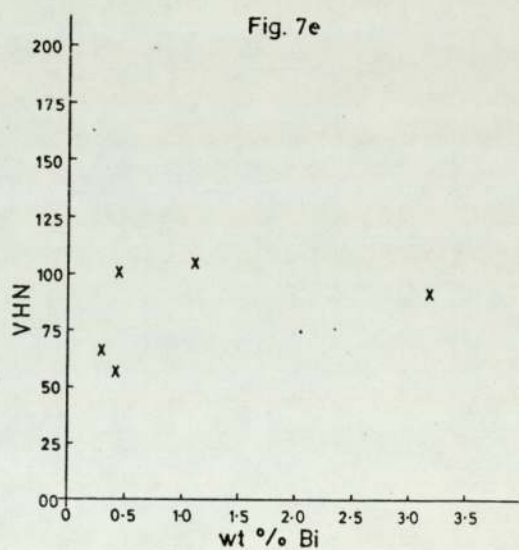
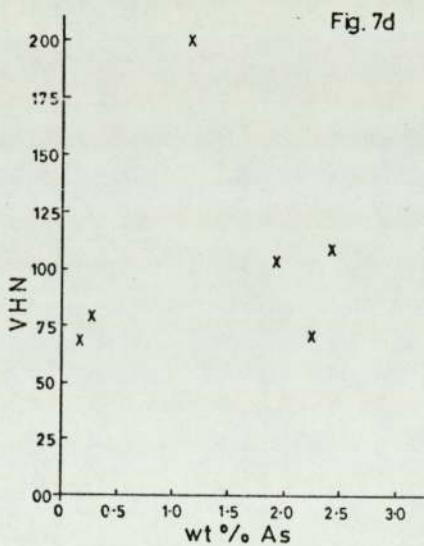
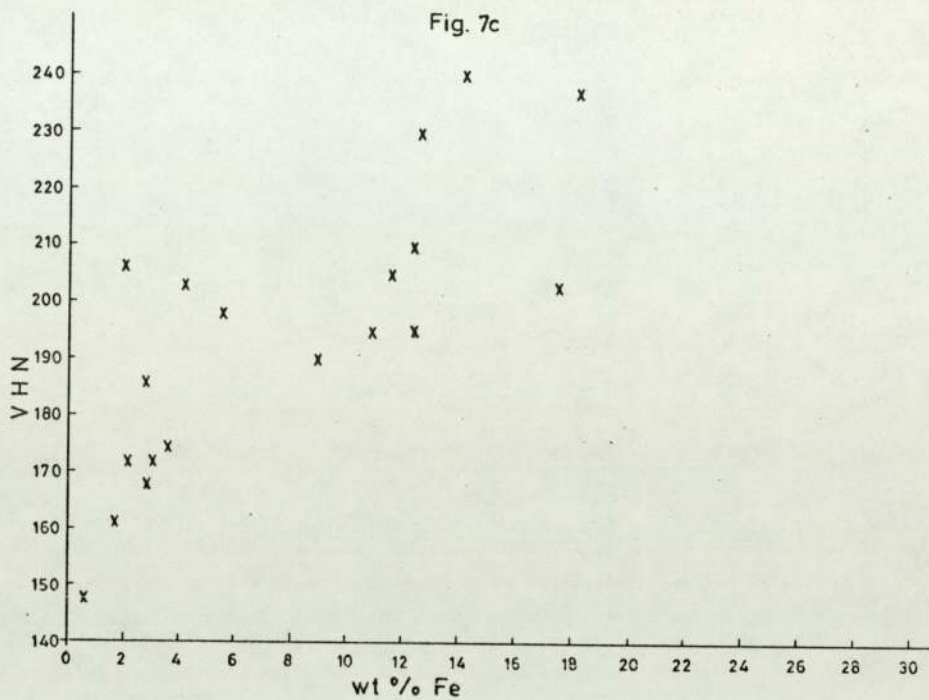


Fig. 7c Plot of microhardness (VHN) against wt% Fe in sphalerite
 Fig. 7d Plot of microhardness (VHN) against wt% As in galena
 Fig. 7e Plot of microhardness (VHN) against wt% Bi in galena

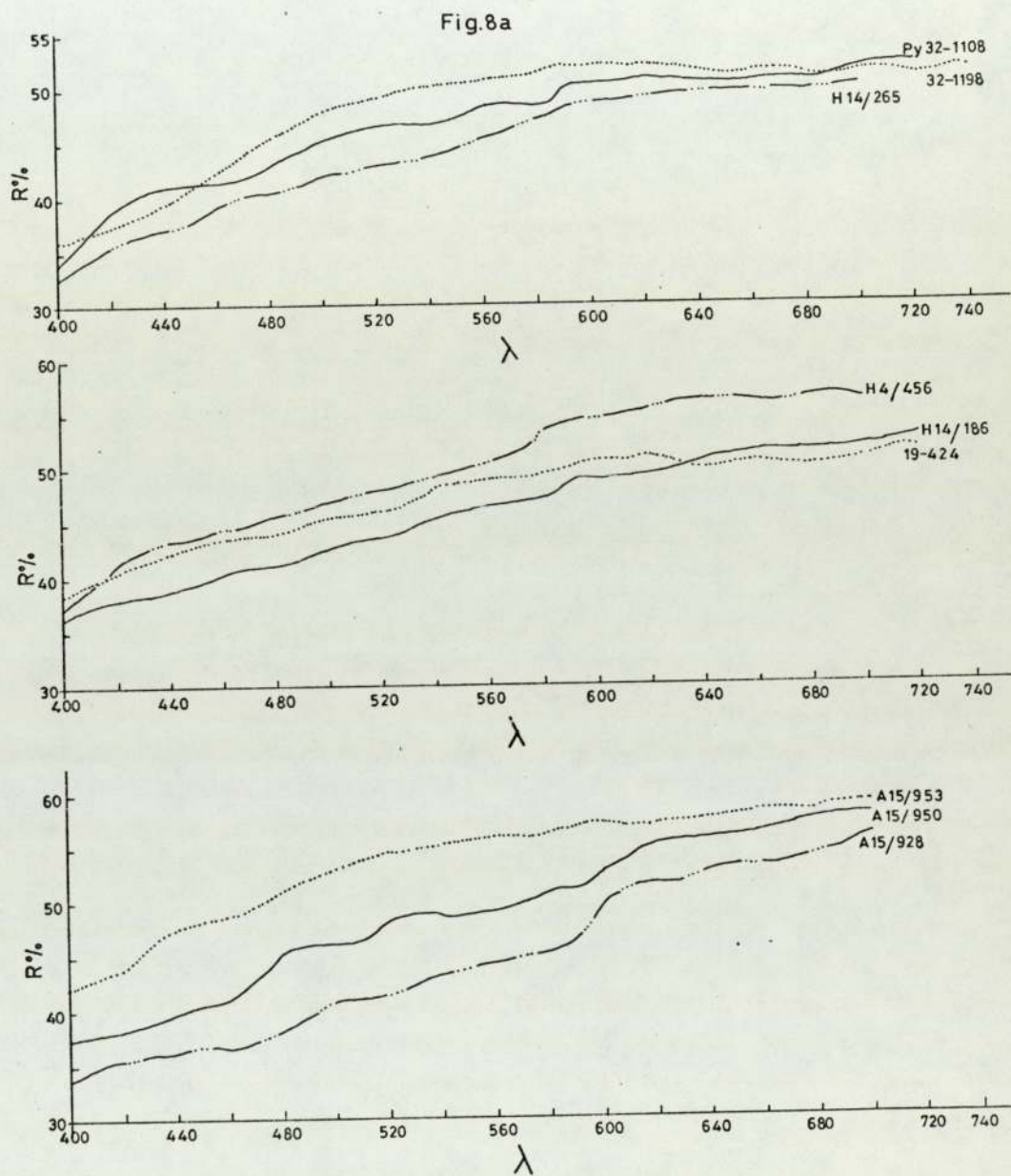


Fig. 8a Spectral reflectivity profiles of pyrite R% - Reflectivity; (air)
 λ - wave length
 32-1108, 32-1198 Euhedral pyrites; H 14/265, H14/186, 19-424,
 A 15/950, M 10/1630, all anhedral pyrites; H 4/456, A 15/953,
 A 15/928 Framboidal pyrites

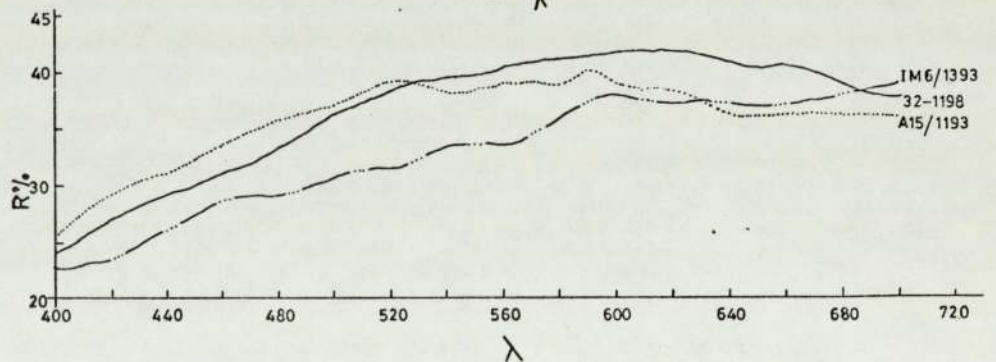
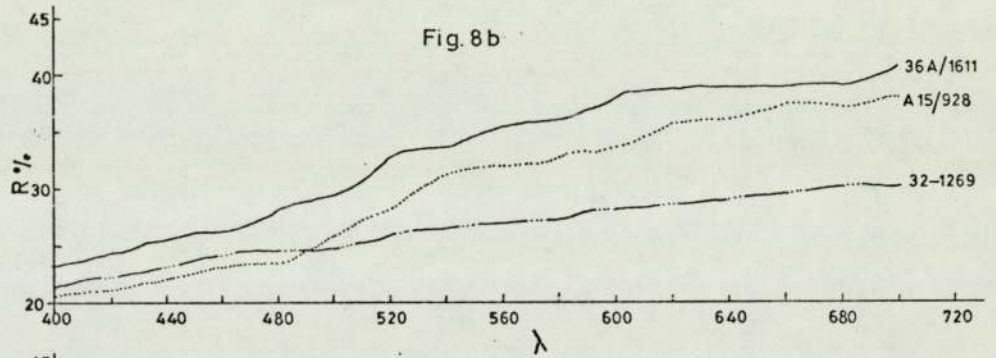
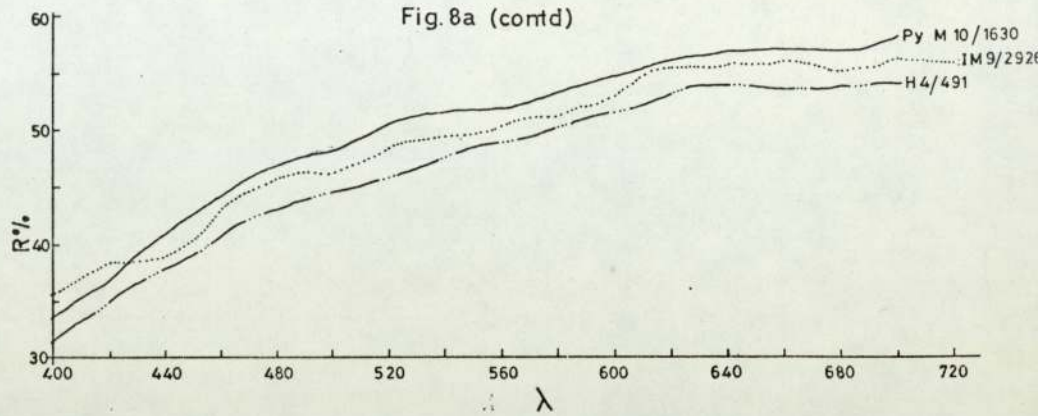


Fig. 8b Spectral reflectivity profiles of chalcopyrite (sample number is given at the end of each curve)
 R% - Reflectivity (air)
 λ - Wave length

Fig. 8c

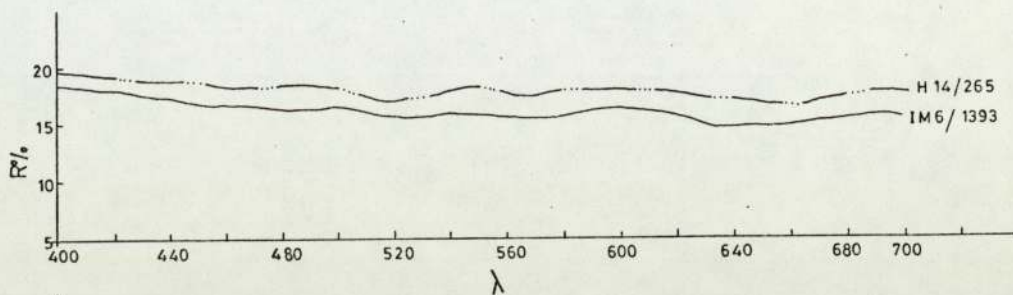


Fig. 8d

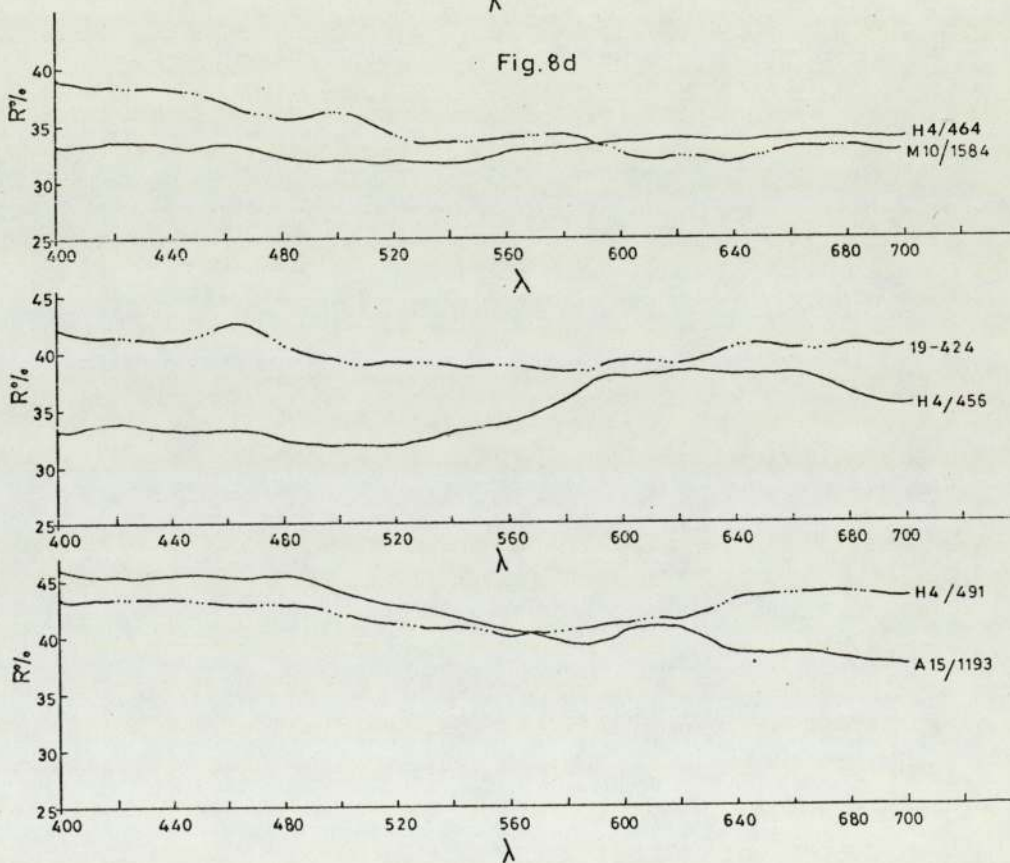


Fig. 8c Spectral reflectivity profiles of sphalerite
Fig. 8d Spectral reflectivity profiles of galena
R% - Reflectivity (air)
λ - Wave length
Sample number is given at the end of each curve.

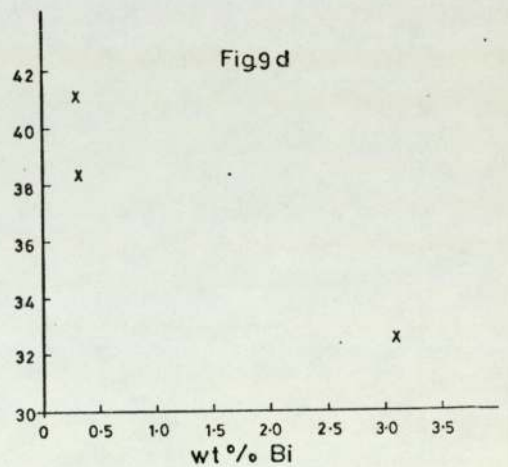
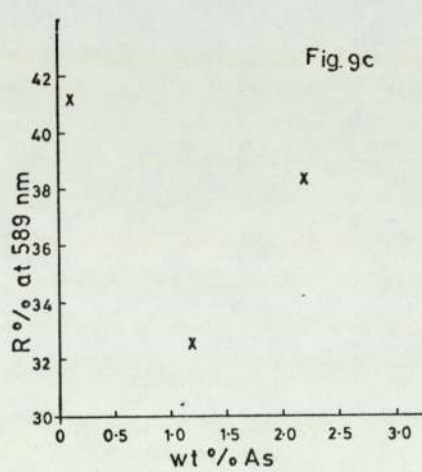
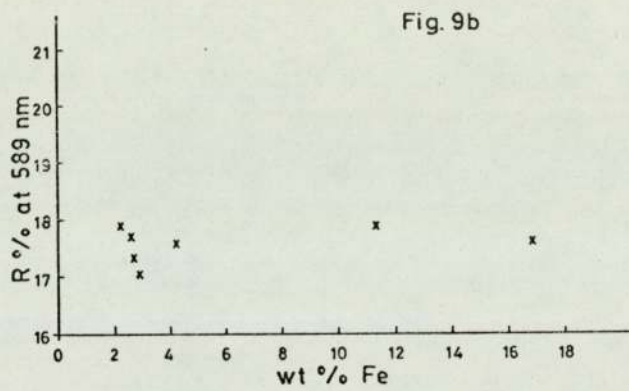
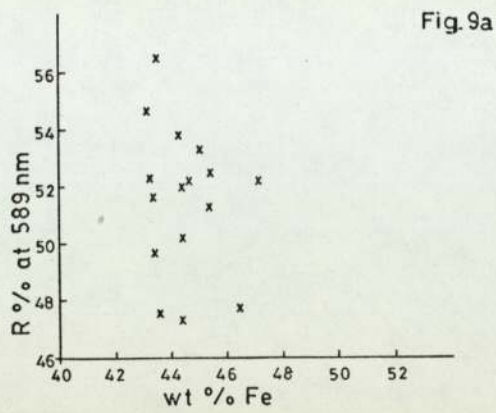
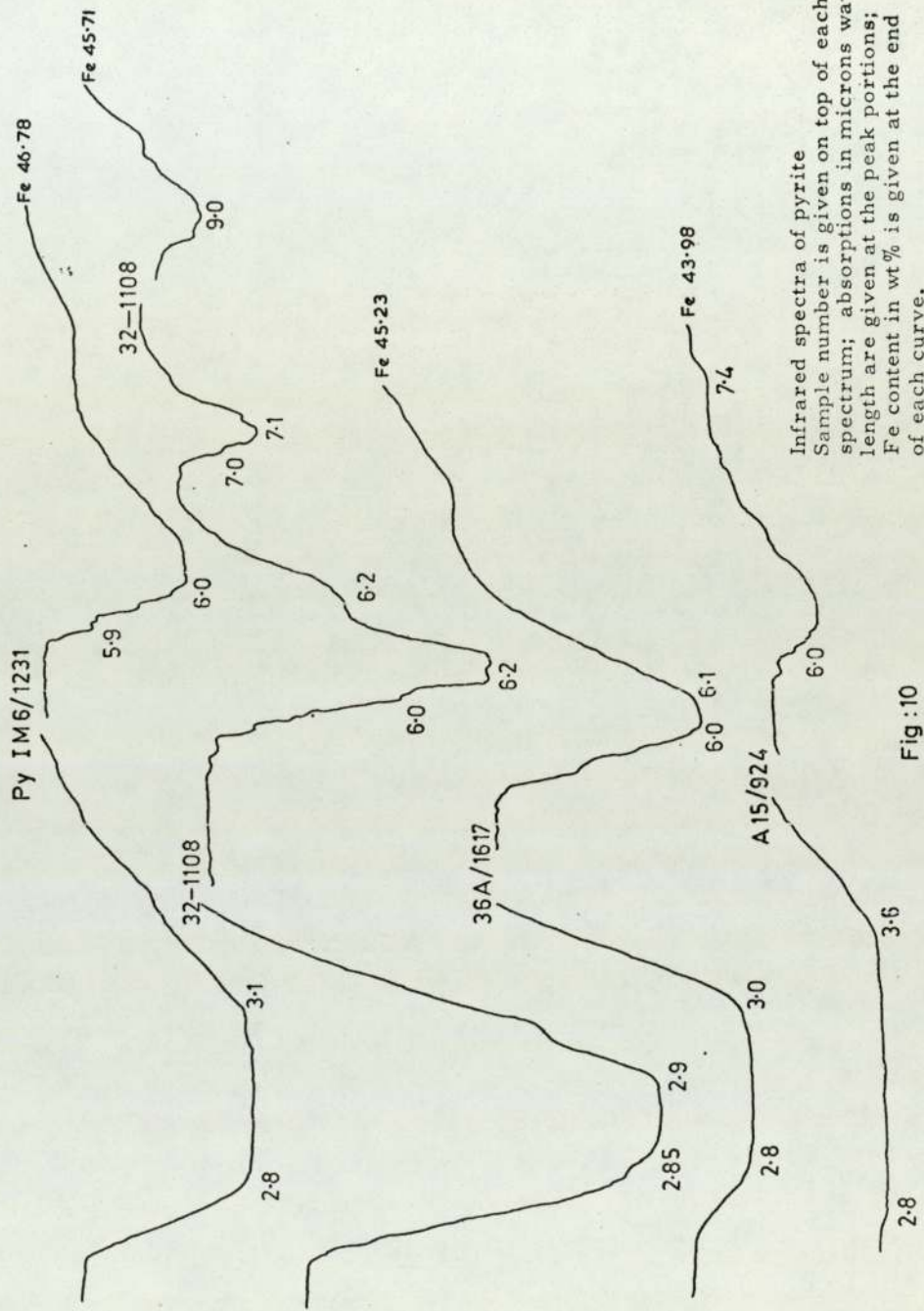


Fig. 9a Plot of Reflectivity (R%) at 589nm against wt% Fe in pyrite
 Fig. 9b Plot of Reflectivity (R%) at 589nm against wt% Fe in sphalerite
 Fig. 9c Plot of Reflectivity (R%) at 589nm against wt% As in galena
 Fig. 9d Plot of Reflectivity (R%) at 589nm against wt% Bi in galena



Infrared spectra of pyrite
 Sample number is given on top of each
 spectrum; absorptions in microns wave
 length are given at the peak portions;
 Fe content in wt% is given at the end
 of each curve.

Fig:10

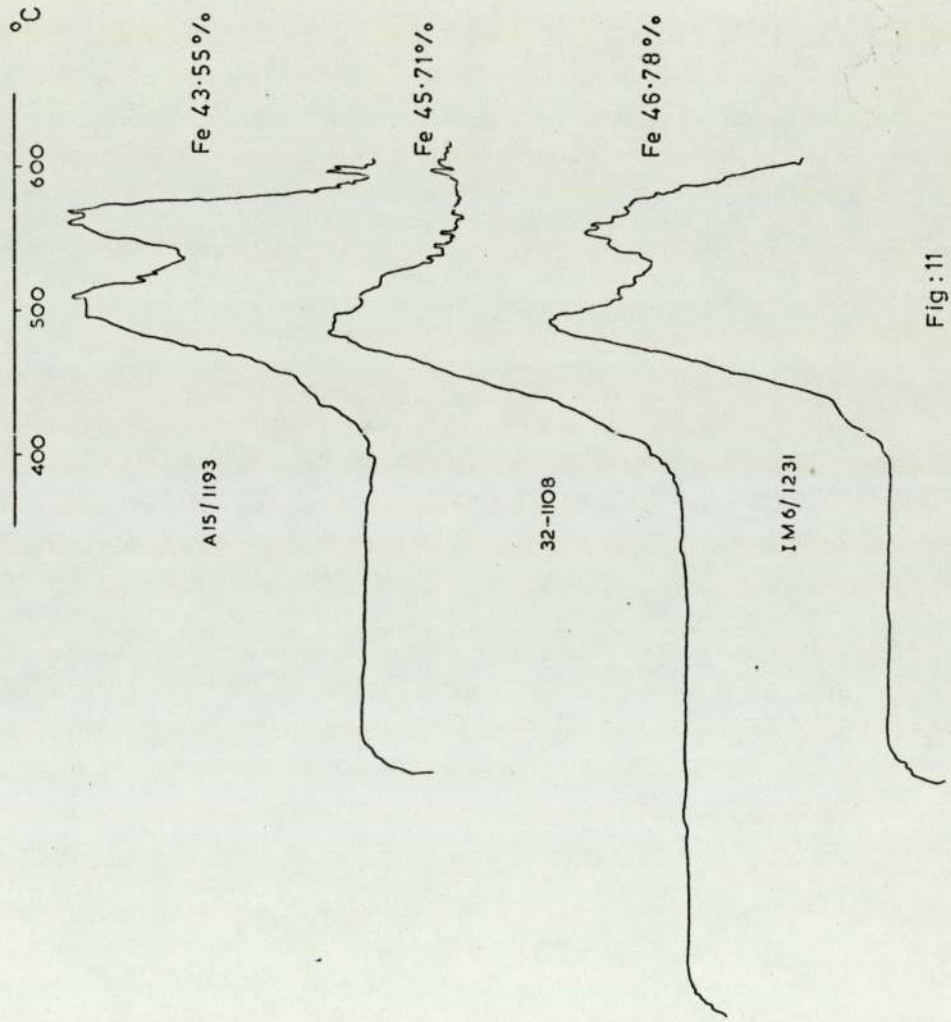
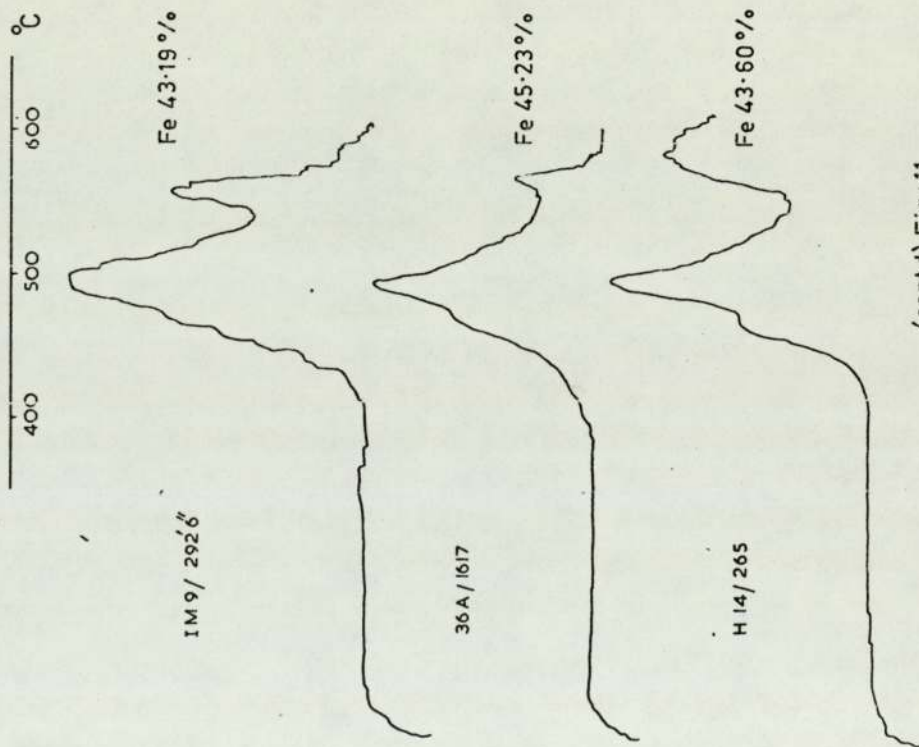


Fig: 11

D.t.a. curves of pyrite. Sample numbers are given at the left hand side of each curve; Fe content in wt% is given at the right hand side of each curve.



(contd) Fig : 11

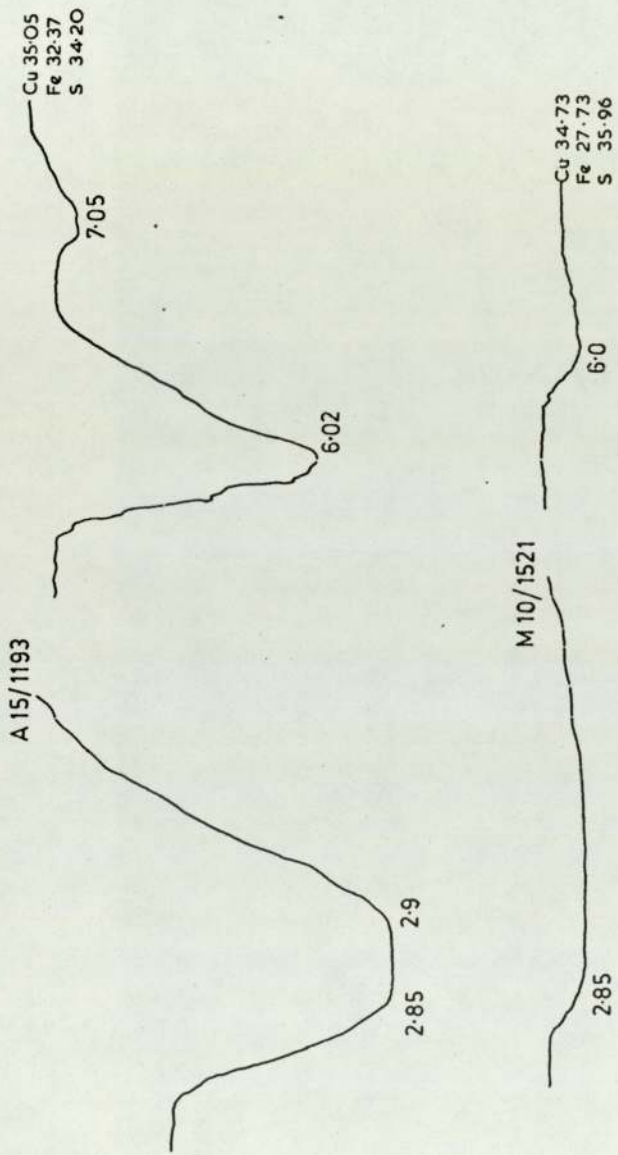


Fig :12

Infrared spectra of chalcopyrite. Sample number is given on top of each spectrum. Absorptions in microns wave length are given at peak portions. Composition in wt% is given at the end of each spectrum.

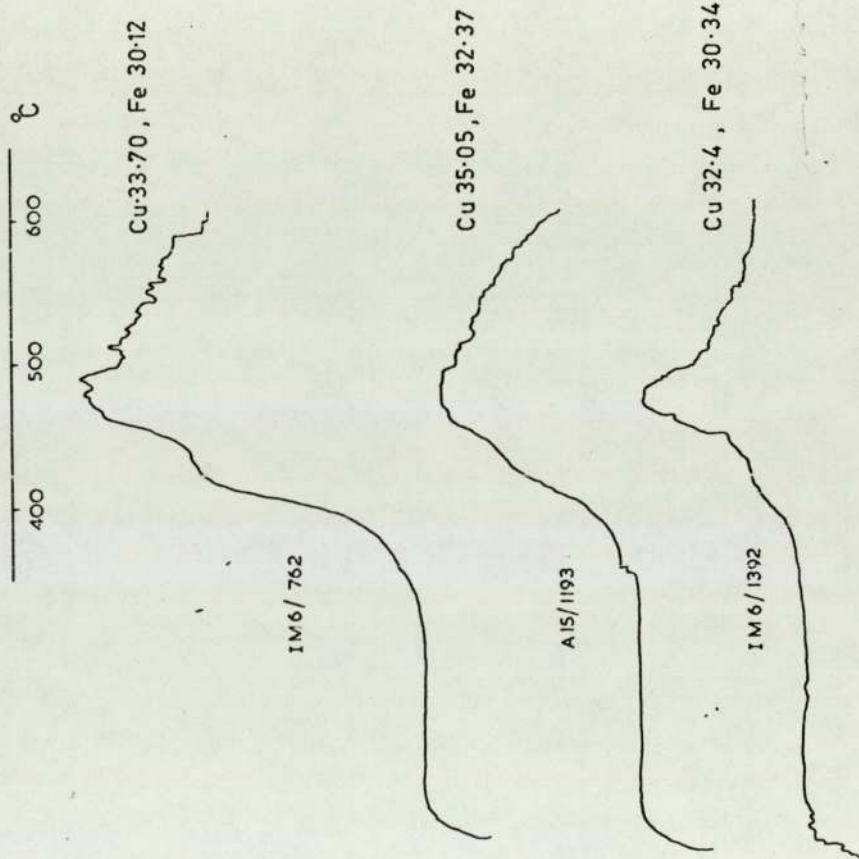
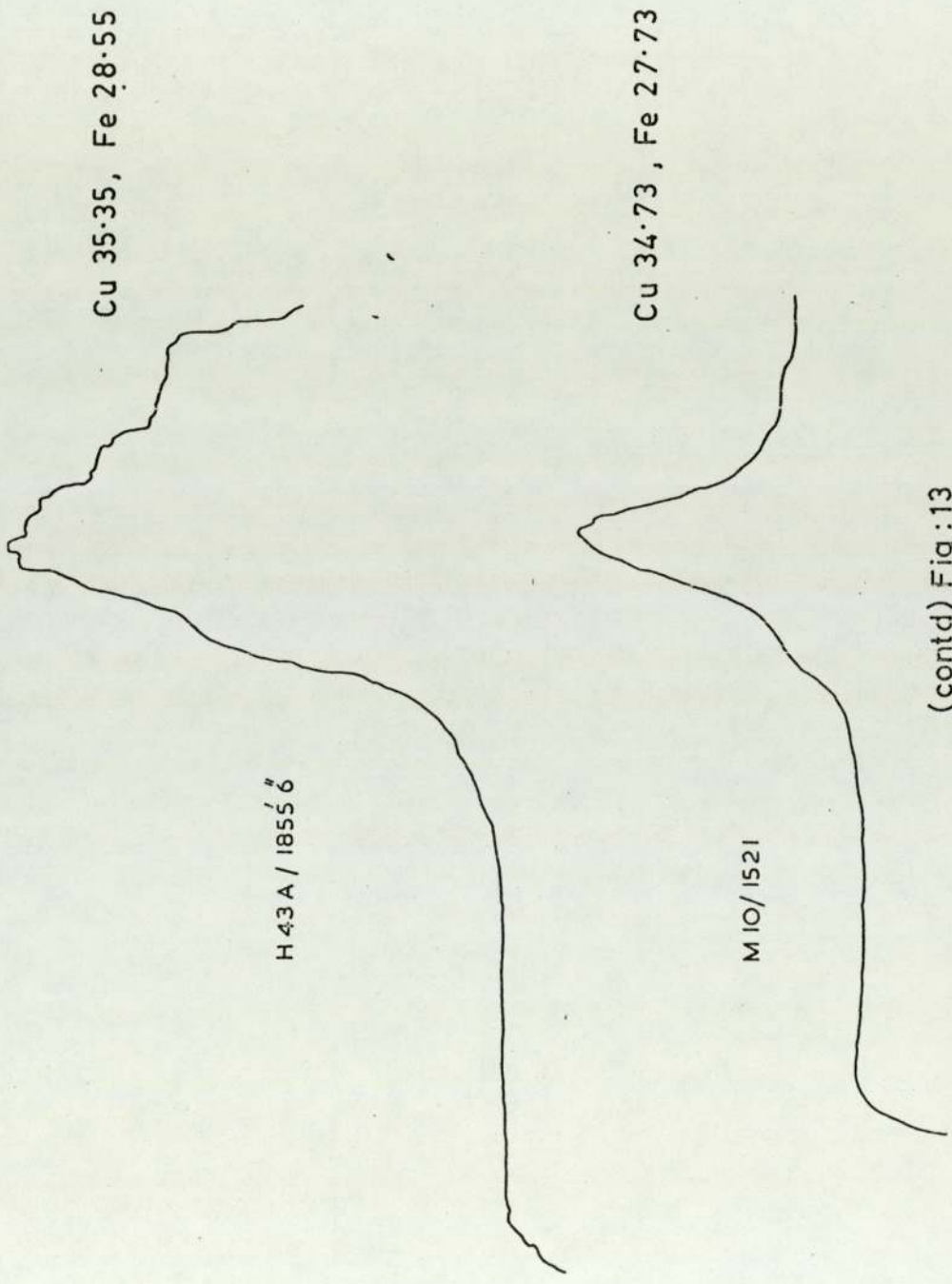


Fig:13

D. t. a. curves of chalcopyrite. Sample number is given at the left hand side of each curve. Wt% Cu and Fe are given at the right hand side of each curve.

400 500 600 °C



(contd) Fig : 13

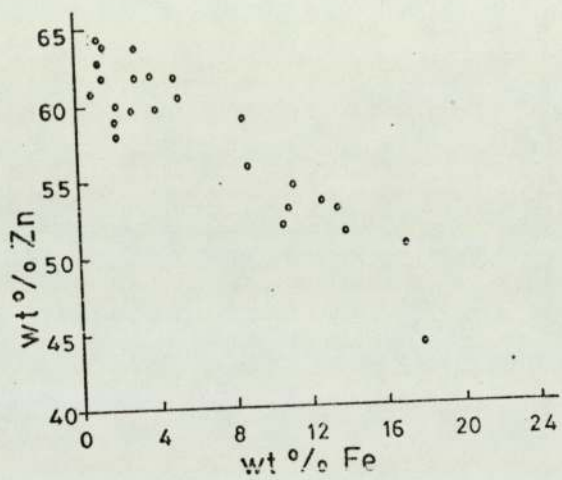


Fig.14

Plot of wt% Zn against wt% Fe in sphalerite

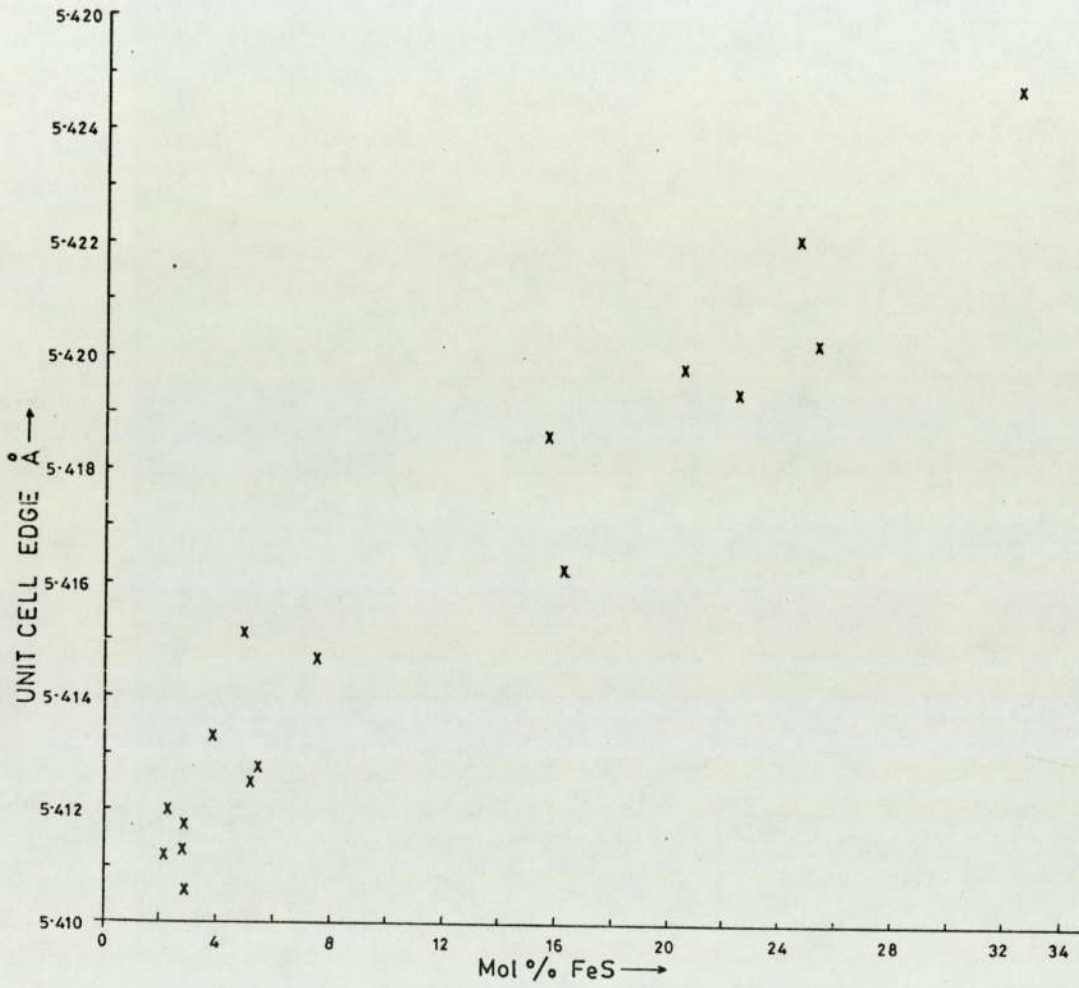


Fig. 15

Plot of Mol % FeS against unit cell edges of sphalerite

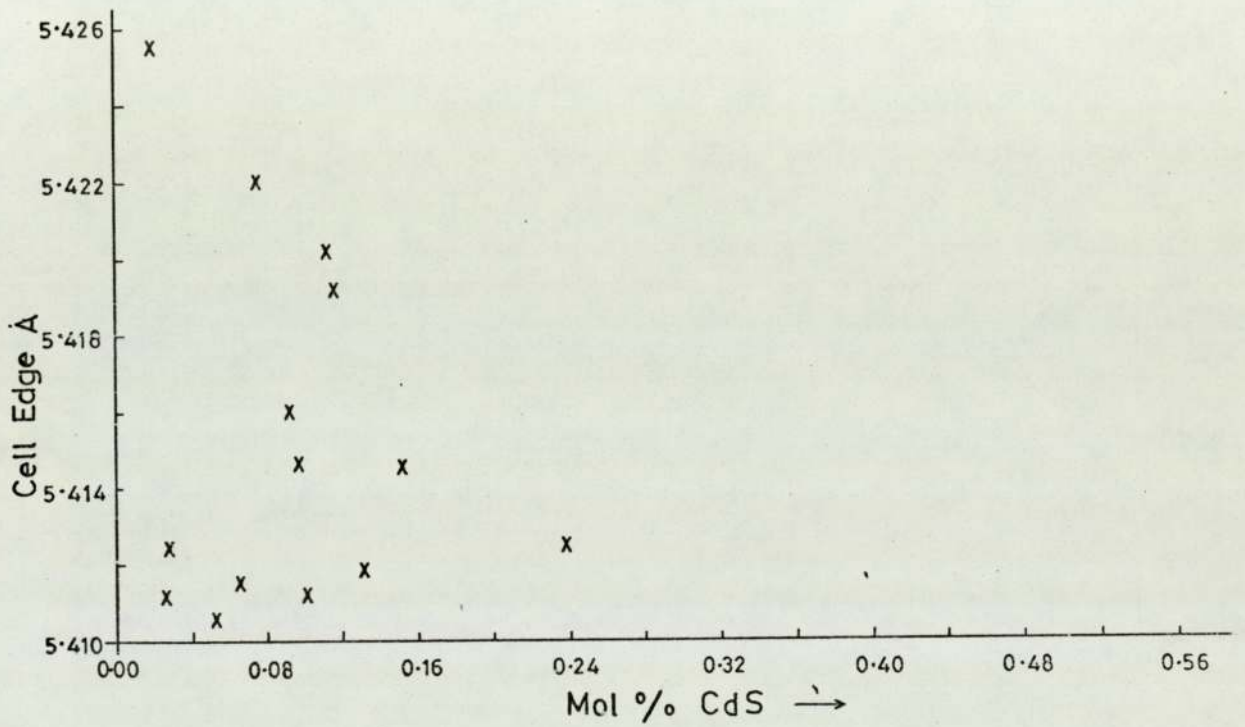
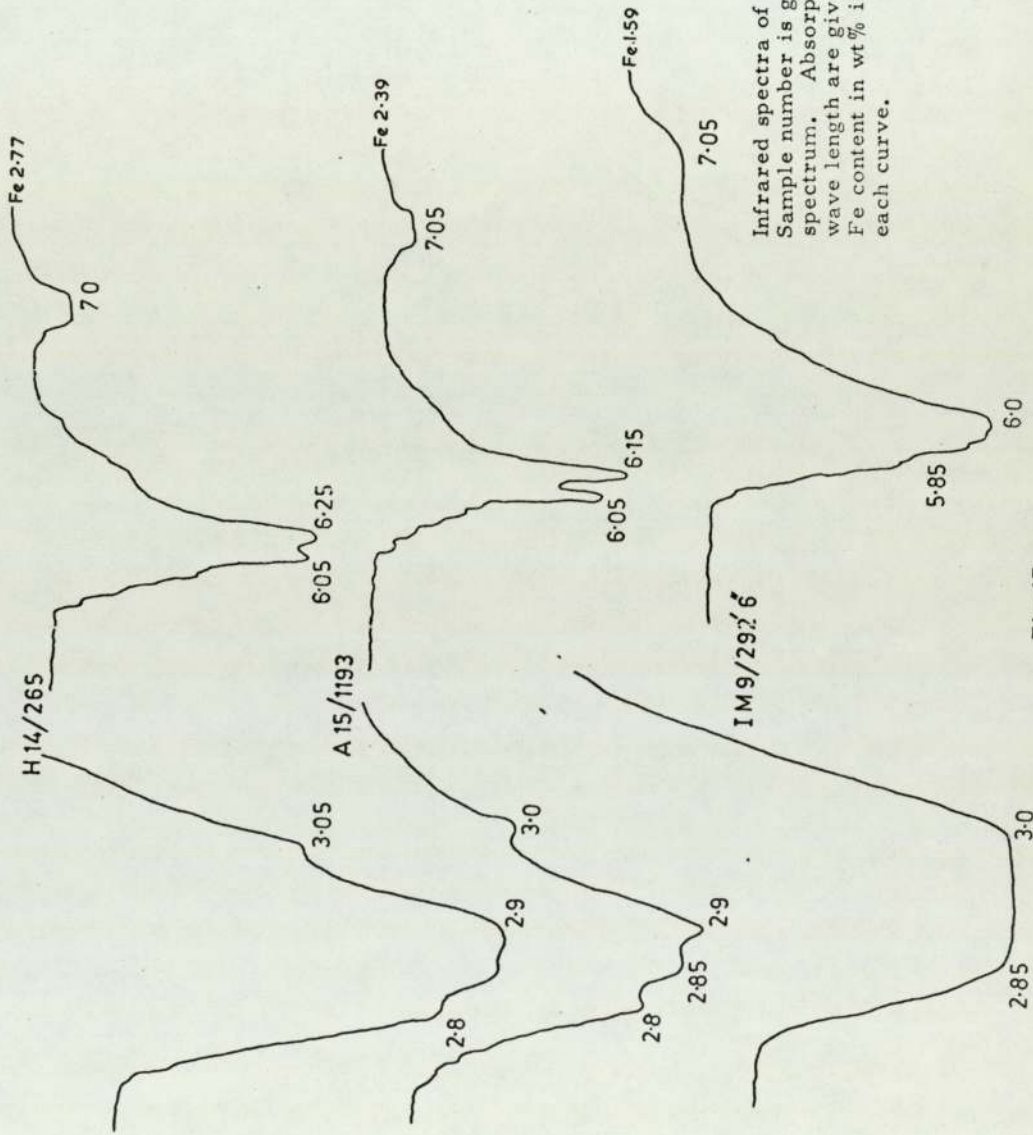


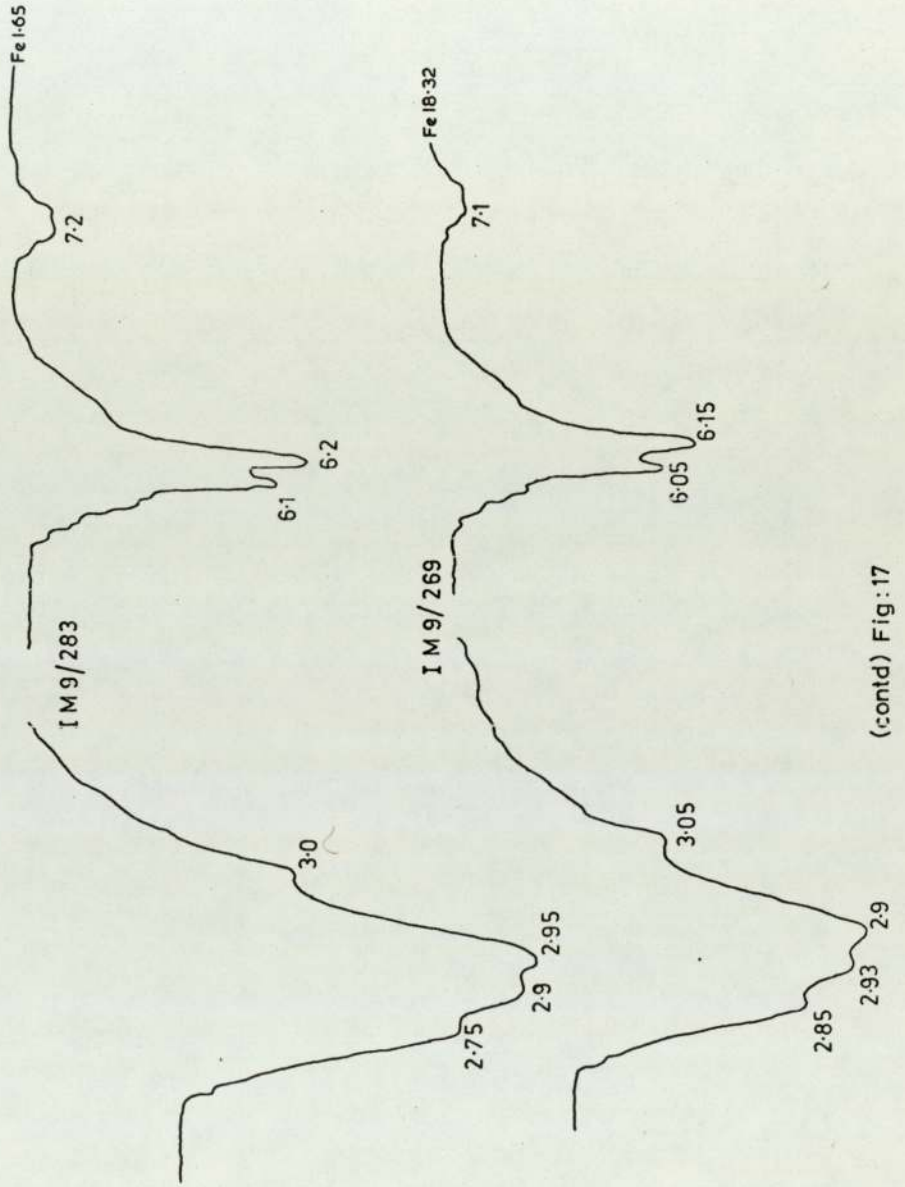
Fig. 16

Plot of Mol% CdS against unit cell edges of sphalerite



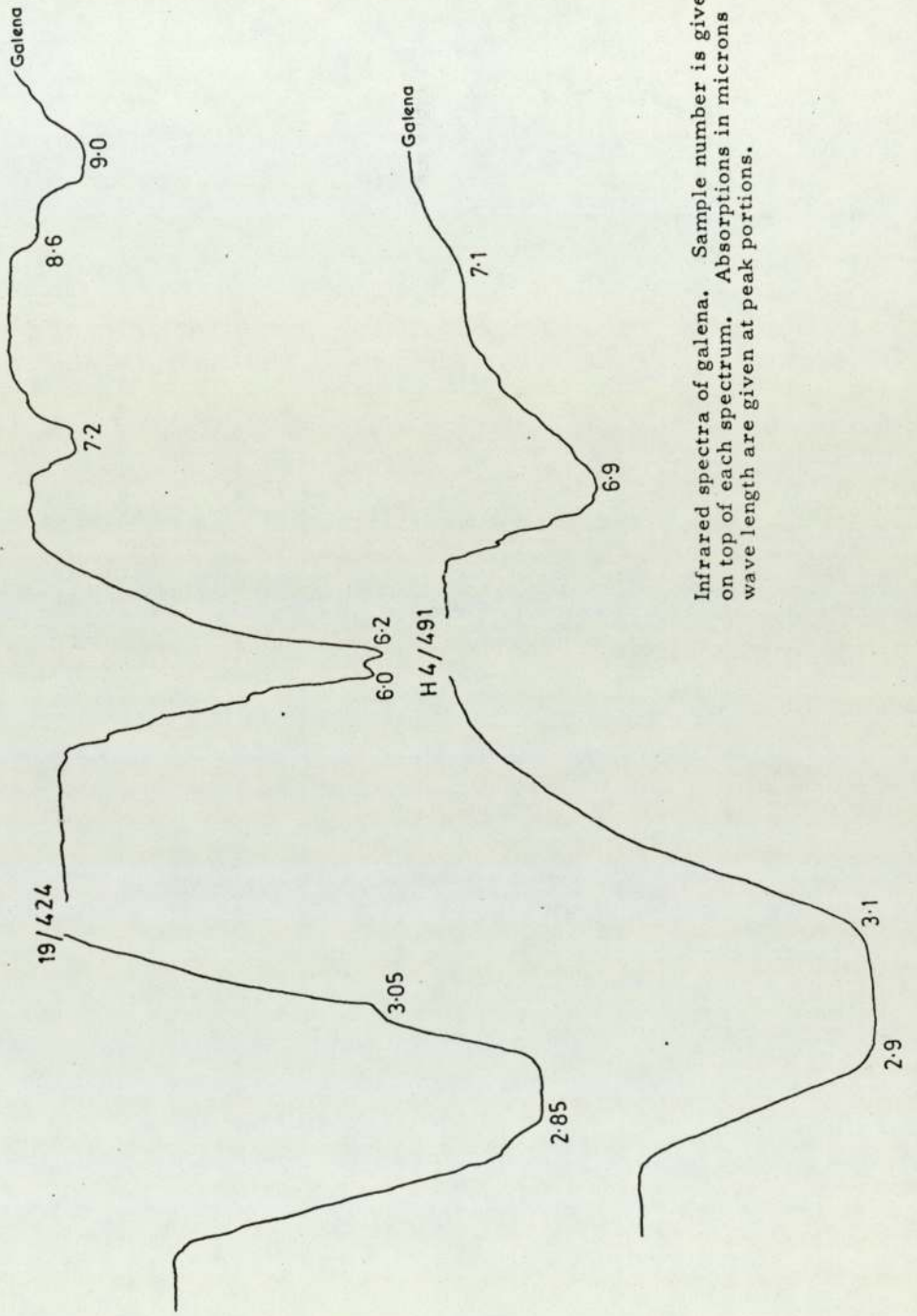
Infrared spectra of sphalerite.
 Sample number is given on top of each spectrum. Absorptions in microns wave length are given at the peak portions. Fe content in wt% is given at the end of each curve.

Fig:17



(contd) Fig: 17

Fig: 18



Infrared spectra of galena. Sample number is given on top of each spectrum. Absorptions in microns wave length are given at peak portions.

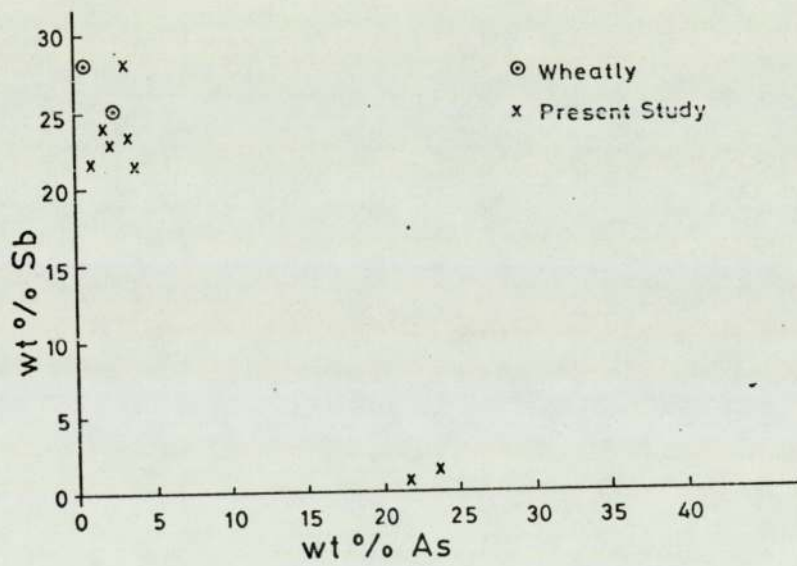
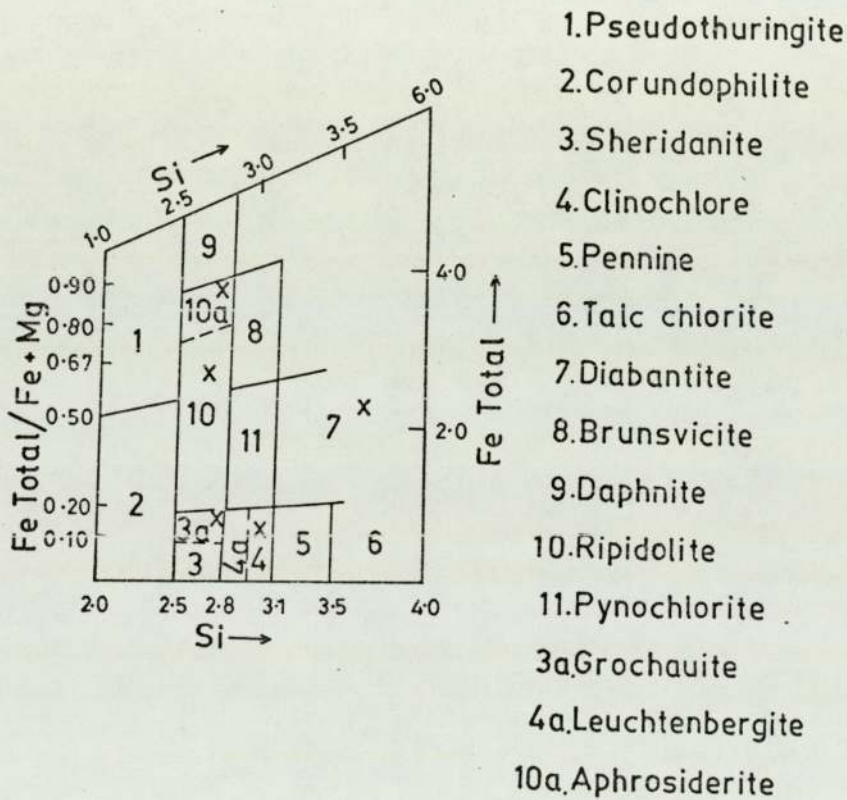


Fig.19

Plot of wt% Sb against wt% As in tetrahedrite-tennantites showing the compositional break.

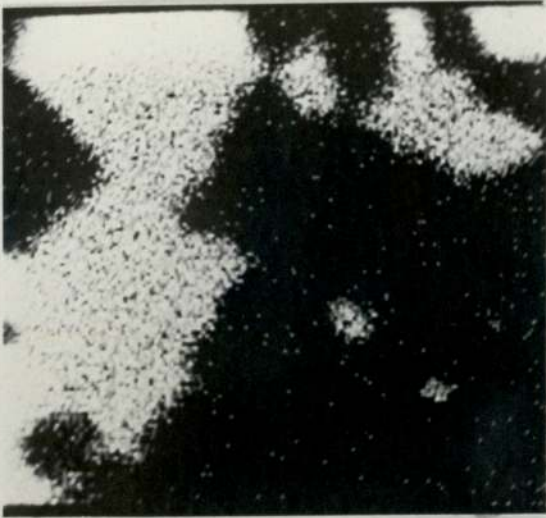
Fig. 20



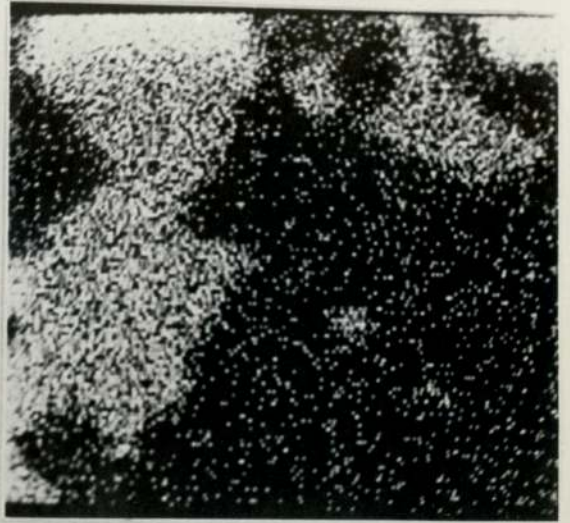
Orthochlorites showing the species and variety boundaries (after Hey, 1954)
 X - shows the Parys Mountain Species

PLATE IV

A



B



C



D

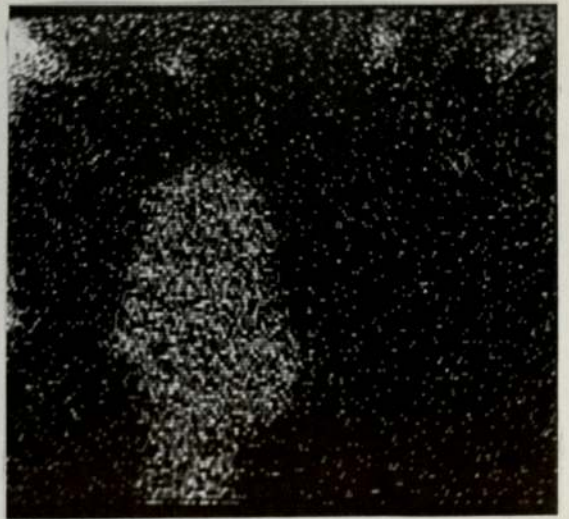


Plate IV X-ray images

A-B Tetrahedrite in sample 27-145

A - Sb L_α

B - As K_α

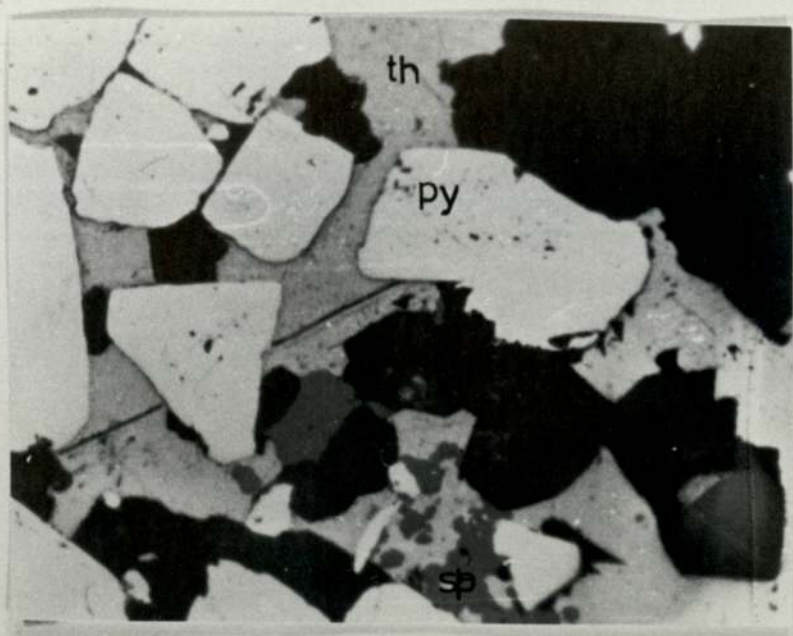
C-D Tennantite in sample 27-145

C - As K_α

D - Sb L_α

PLATE III

A



B

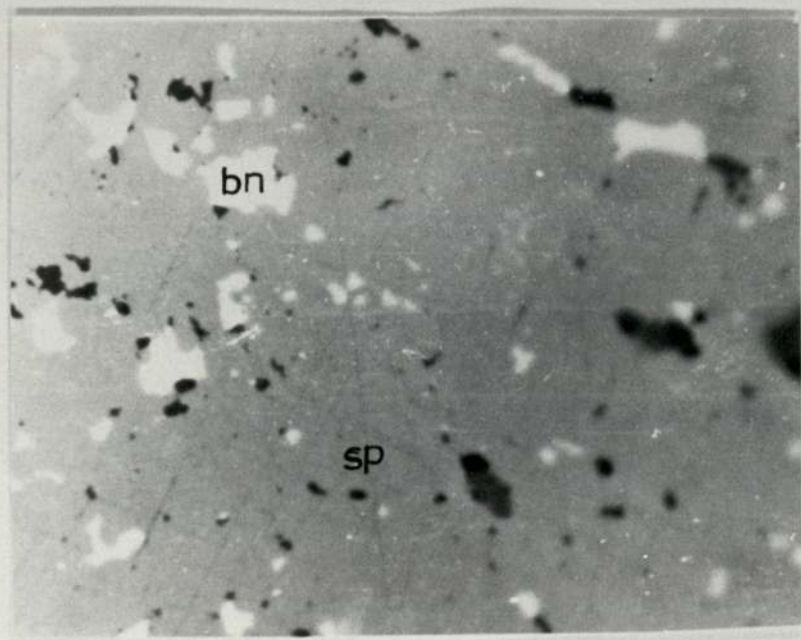
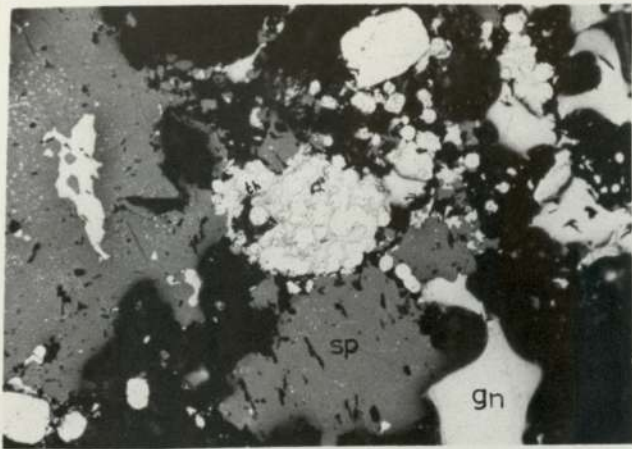


Plate III Photomicrographs

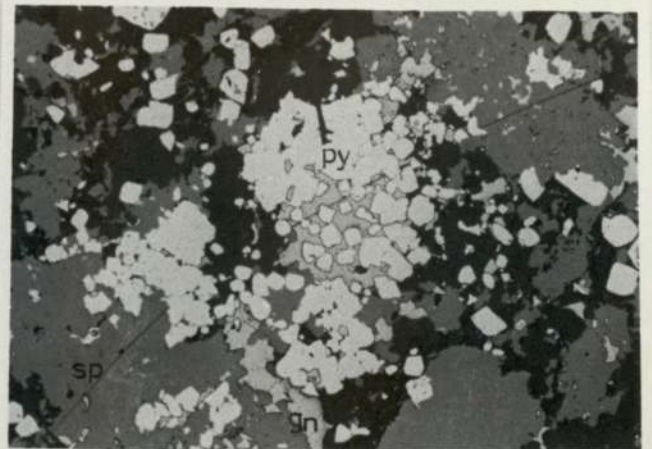
- A Sample from bore hole 27 at 145 feet depth. Tetra-
hedrite (th) forming the interstitial and fracture
infillings of pyrite. 16 x (air)
- B Sample from bore hole H4 at 465 feet depth.
Sphalerite (sp) with inclusions/infillings of
bournonite (bn). 40 x (oil)

PLATE II

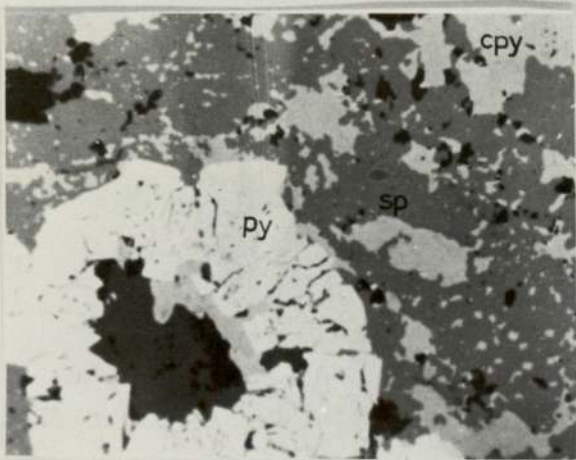
A



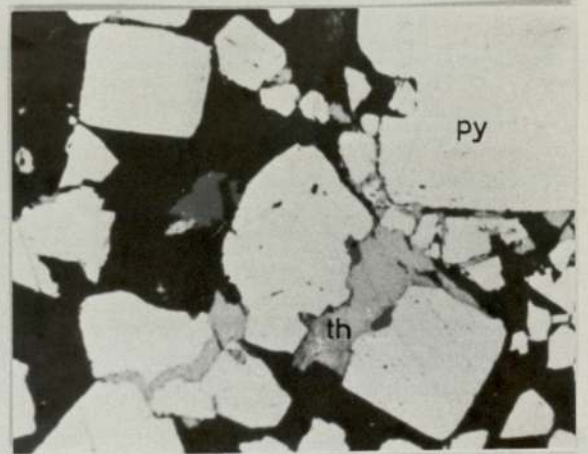
B



C



D



E

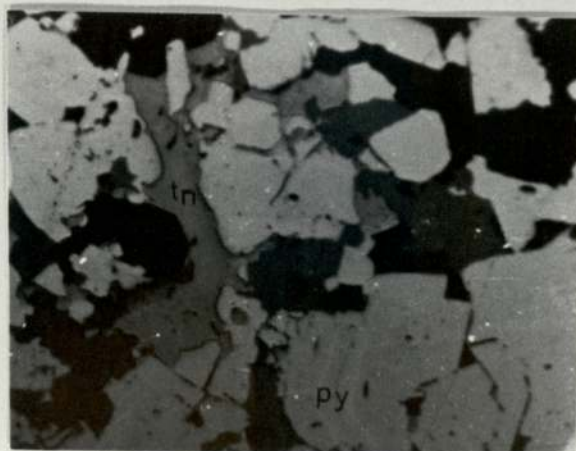
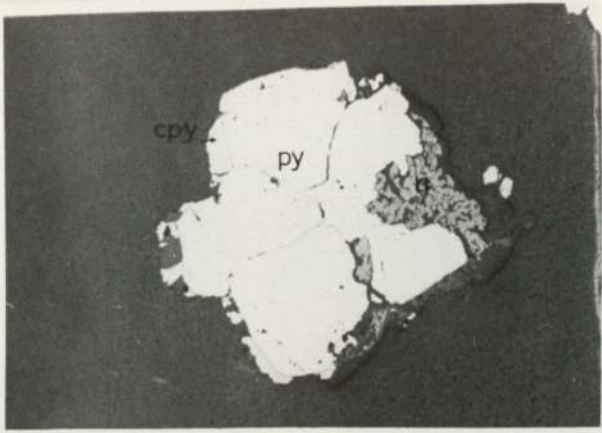


Plate II Photomicrographs

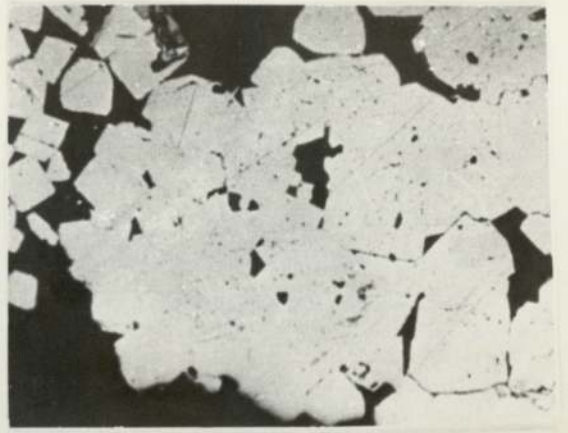
- A-B Sample from bore hole H4 at 474 feet depth. Sphalerites (sp) showing intergrowths with galena (gn). Galena and tetrahedrites forming interstitial matrix for pyrites. 16 x (oil)
- C Sample from bore hole IM6 at 1392 feet depth. Pyrite (py) showing the radiating texture. Chalcopyrite (cpy) and sphalerite (sp) show intergrowth textures. Chalcopyrite is also seen replacing the core of the pyrite and filling in its fractures. 16 x (air)
- D Sample from bore hole 27 at 145 feet depth. Tetrahedrite (th) forming the interstitial and fracture infillings of pyrite. 16 x (air)
- E Sample from bore hole 27 at 145 feet depth. Pyrite (bottom centre) showing zoning. Tennantite (tn) is filling in the interstitial spaces of pyrite. 16 x (air)

PLATE I

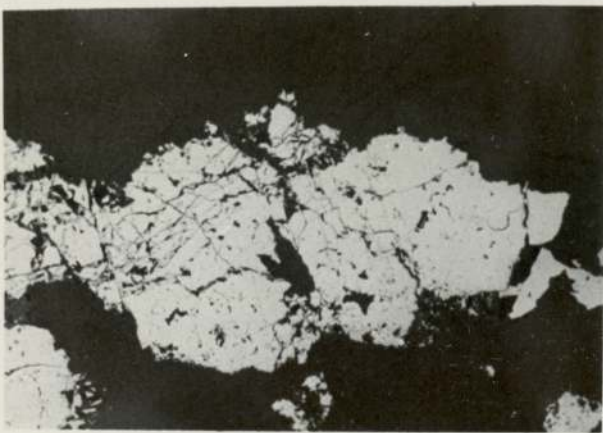
A



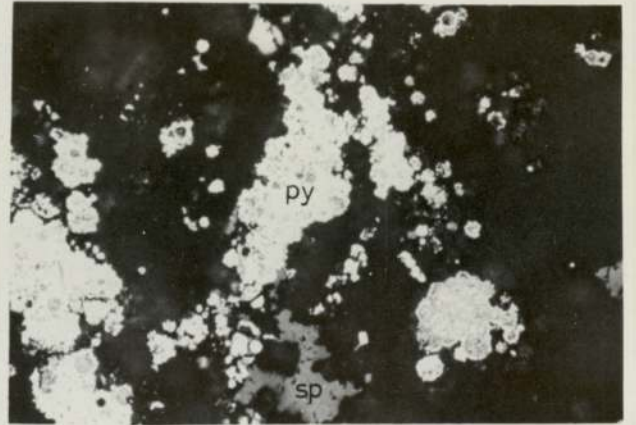
B



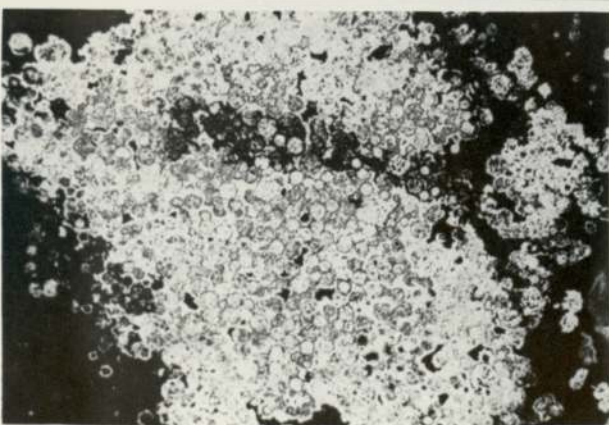
C



D



E



F

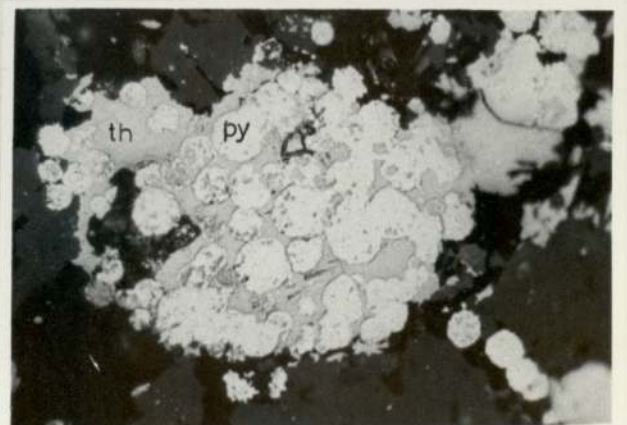
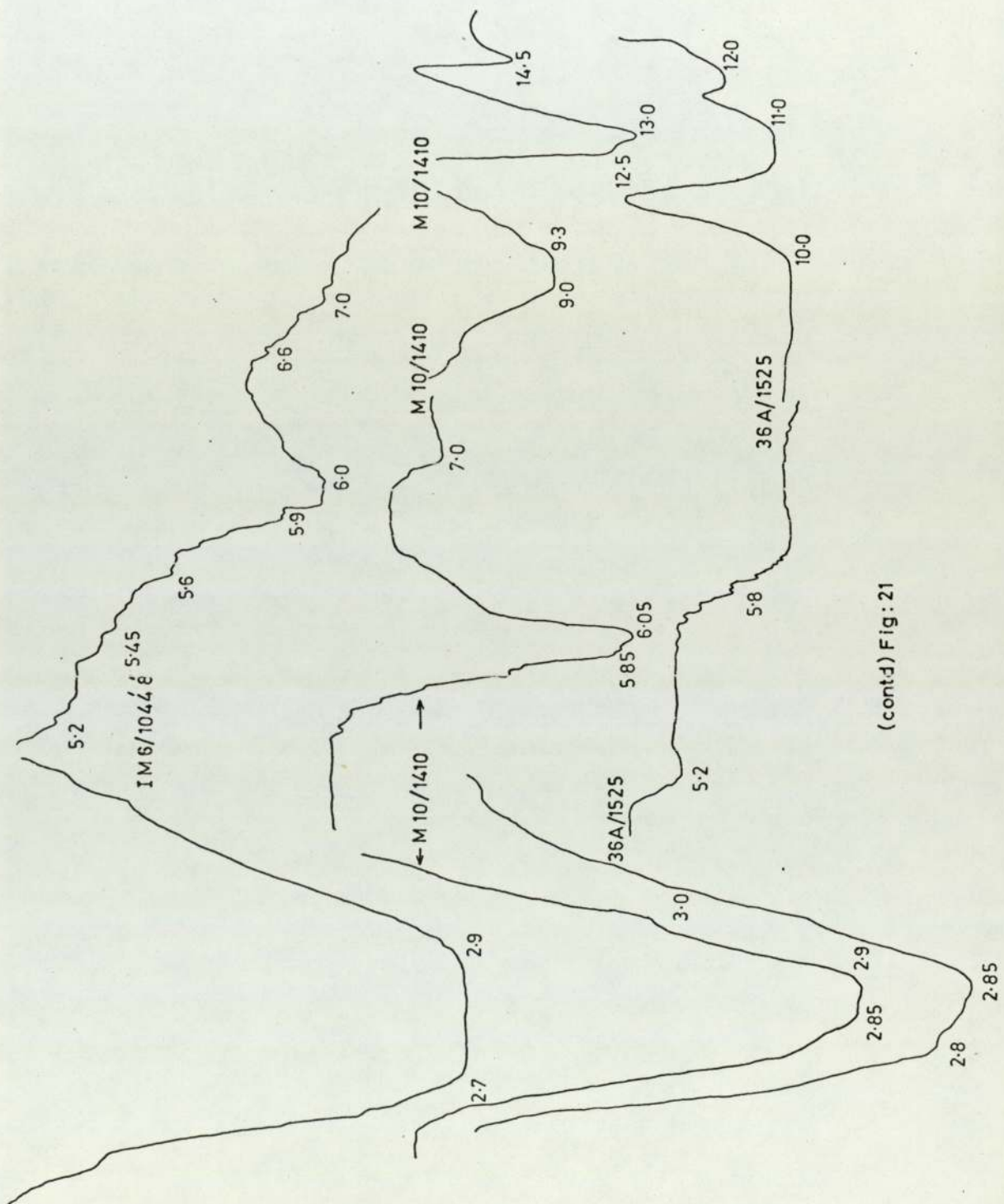
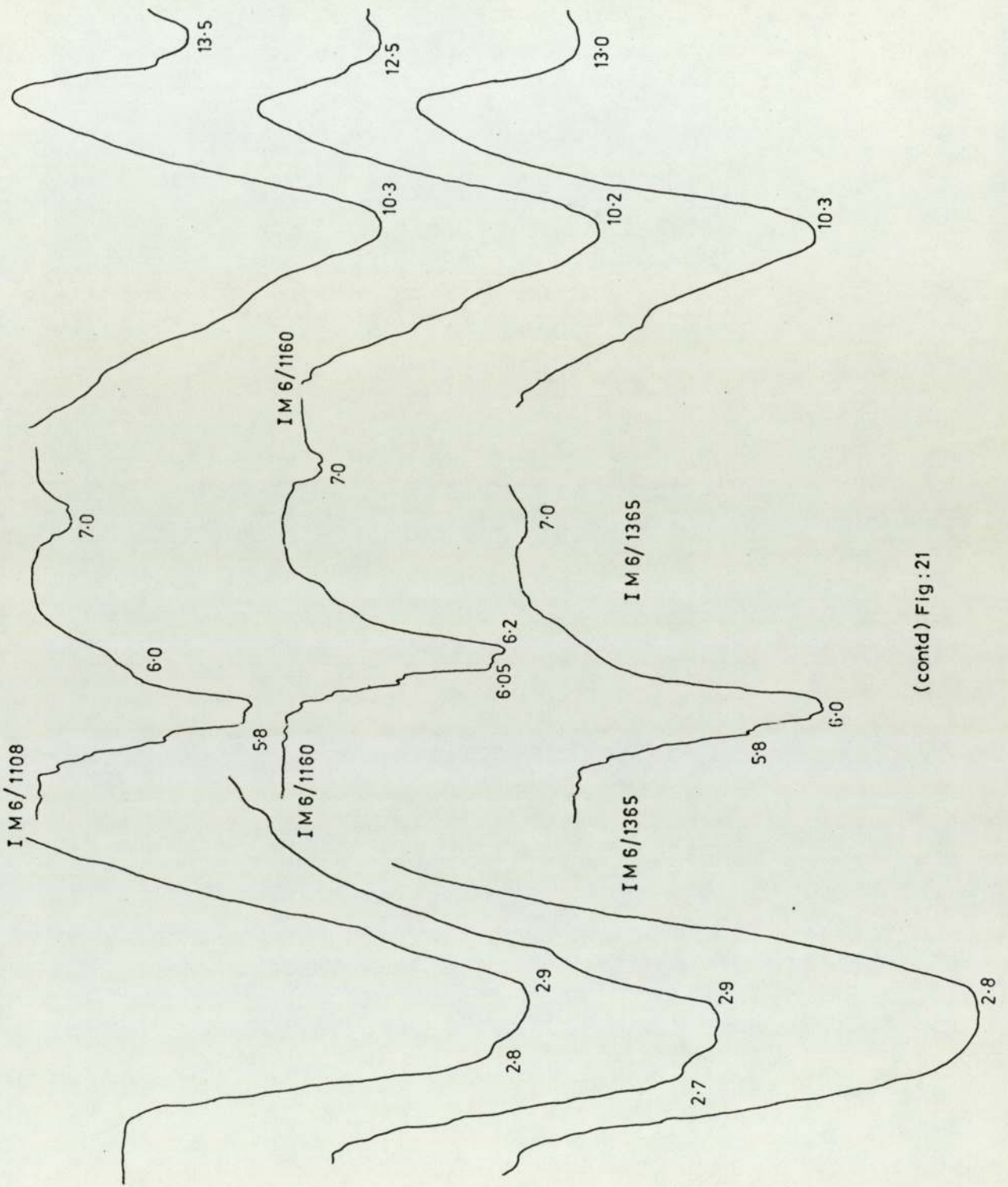


Plate I Photomicrographs

- A Sample from bore hole 32 at 1198 feet depth. Pyrite (py) associated with rutile (rt). Chalcopyrite rims pyrite and replaces it at grain boundaries.
4 x (air)
- B Sample from bore hole 27 at 145 feet depth. Aggregate of euhedral pyrites homogenised at the centre of the aggregate but retaining the cubic outlines at the periphery.
4 x (air)
- C Sample from bore hole A 15 at 1193 feet depth. Pyrite showing intense fractures developed due to cataclasis.
4 x (air)
- D Sample from bore hole H 4 at 464 feet depth. Framboidal pyrites (py) forming clusters. Sphalerite (sp) is also seen.
16 x (oil)
- E Sample from bore hole H4 at 464 feet depth. Framboidal pyrites showing atoll textures with tetrahedrite-tennantite forming the interstitial infillings.
16 x (oil)
- F Sample from bore hole H4 at 474 feet depth. Framboidal pyrites (py) with interstitial infillings of tetrahedrite (th).
16 x (oil)



(contd) Fig: 21



(contd) Fig : 21

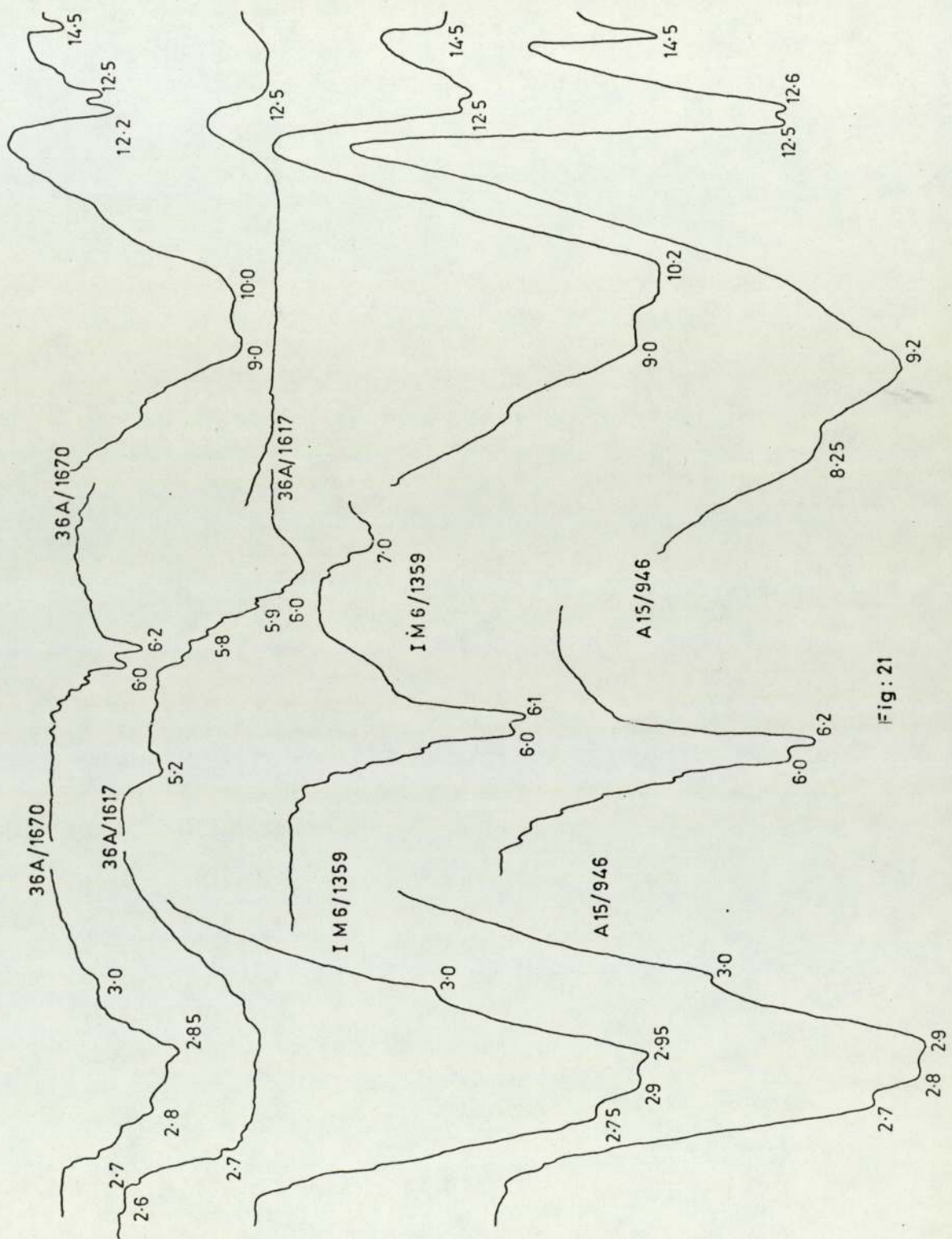


Fig: 21

Fig. 21 Infrared spectra of chlorites.
36A/1670, A15/946, M10/1410 Ripidolite
36A/1617, IM6/1044'8" Diabantite
IM6/1359, 36A/1525 Chlorite 1b
IM6/1365 Aphrosiderite and grochauite
IM6/1108, IM6/1160 Chlorites (species not identified)

Sample number is given on top of each spectrum; absorptions in microns wave length are given at the peak portions.

GEOCHEMISTRY OF SOME SULPHIDES AND SULPHO-SALTS
FROM PARYS MOUNTAIN, ANGLESEY

by

C. SIVAPRAKASH

A thesis submitted to the University of Aston in Birmingham in
partial fulfillment of the requirements for the award of the degree
of Master of Philosophy

May, 1977

Geochemistry of some sulphides and sulpho-salts from
Parys Mountain, Anglesey.

C. Sivaprakash

(Candidate for the M. Phil. degree, May, 1977)

SUMMARY

Sulphide mineralisation occurs at Parys Mountain, Anglesey, associated with Ordovician and Silurian sedimentary and volcanic rocks. Pyrite, chalcopyrite, sphalerite and galena are the sulphide minerals with minor quantities of arsenopyrite and pyrrhotite. Tetrahedrite-tennantites, and Pb and Bi sulpho-salts also occur as interstitial and fracture infillings in sulphides, mainly in pyrite. Pyritic mineralisation shows conformable features with the host rocks, whereas other sulphides and sulphosalts show epigenetic features.

Sulphides have been analysed for essential and trace elements namely Fe, S, Cu, Pb, Zn, Co, Ni, Ag, As, Sb, Sn, Ba, Mo, Te, Cd, Mn and Bi. Sphalerite and galena are comparatively more enriched in trace elements than pyrite and chalcopyrite. The Co/Ni ratio in pyrites is generally greater than 1.00, suggesting that the deposits are related to volcanism. Substantial quantities of Fe are present in sphalerites in solid solution.

Sulphosalts have been quantitatively identified by electron microprobe analysis to be tetrahedrite-tennantites, bournonites, kobellite, galenobismutite and lead sulpharsenides.

Unit cell edge measurements of sphalerite have been made by X-ray and electron diffraction, and a good linear relationship between mol% / FeS and unit cell edge is shown. Microhardness, reflectivity, infrared and d.t.a. data for sulphides are given - attempts to correlate the physical-optical characteristics with composition resulted in no significant conclusions, except the relation between microhardness and Fe content in sphalerite.

Diabantite, ripidolite, grochauite, clinocllore and aphrosiderite are the chlorite species occurring in the matrix associated with sulphide minerals; chlorite (1b species) has been identified in the matrix where no sulphide minerals occur.

The mineralogical and chemical results in the present study are interpreted to show that the mineralisation at Parys Mountain is a volcanogenic sedimentary process later enriched by hydrothermal processes.

Key words: Sulphide mineralogy, composition, trace-elements, sulpho-salts.

Acknowledgements

I am very grateful to Dr J. W. Gaskarth for his advice, patience, and supervision of this work and to Dr R. A. Ixer for his constant help, discussions and for critically reading the manuscript. I am also grateful to Dr D.J. Vaughan for his help and suggestions in the reflectivity studies, X-ray study of sphalerite and in the sulpho-salt studies.

I am grateful to Prof. D. D. Hawkes for providing the necessary facilities. I also thank all the members of the staff of the Department of Geological Sciences for their co-operation.

I express my gratitude to the technicians of the Departments of Geological Sciences, Metallurgy, and Chemistry for their technical assistance, especially to Mr D. Hodgson in the X-ray work, Mr R. Iver in the atomic absorption work, and to Mr S. Fuggle in the electron diffraction work. Mr J. H. Williams is thanked for his help throughout. My special thanks are due to Mr R. G. Howell of the Department of Metallurgy for his help during the electron-probe work and for providing the computer programme.

I am extremely grateful to the Ministry of Education and Social Welfare, Government of India for the award of a National Scholarship.

I am indebted to Dr N. F. M. Henry, University of Cambridge for kindly editing the draft during my absence on field work in India, and to Mrs J. Woodman for typing the whole thesis.

C. Sivaprakash

4 May 1977

List of Figures

- Fig. 1 Sketch Map of Anglesey to show the Parys Mountain Area
- Fig. 2 Simplified Geological map of Parys Mountain Area (after Thanasuthipithak, 1974)
- Fig. 3 Cross sections illustrating the structural interpretations at Parys Mountain
- Fig. 4 Sections illustrating the various lodes (after Manning, 1959)
- Fig. 5 Sketches of core and polished sections to show macroscopic features of the ore types
-
- Fig. 6a Size distribution of framboidal pyrites in sample A15/920 (180 frambooids)
- Fig. 6b Size distribution of framboidal pyrites in sample A15/941 (160 frambooids)
- Fig. 6c Size distribution of framboidal pyrites in samples H4/460 and H4/474
- Fig. 6d Plot of frequency against number of frambooids/cluster (sample H4/464)
- Fig. 7a Plot of microhardness (VHN) against wt% Fe in pyrite
- Fig. 7b Plot of microhardness against wt% Fe in chalcopyrite
- Fig. 7c Plot of microhardness against wt% Fe in sphalerite
- Fig. 7d Plot of microhardness against wt% As in galena
- Fig. 7e Plot of microhardness against wt% Bi in galena
- Fig. 8a Spectral reflectivity profiles of pyrite
- Fig. 8b Spectral reflectivity profiles of chalcopyrite
- Fig. 8c Spectral reflectivity profiles of sphalerite
- Fig. 8d Spectral reflectivity profiles of galena
- Fig. 9a Plot of Reflectivity (R%) at 589nm against wt% Fe in pyrite
- Fig. 9b Plot of Reflectivity (R%) at 589 nm against wt% Fe in sphalerite
- Fig. 9c Plot of Reflectivity (R%) at 589 nm against wt% As in galena
- Fig. 9d Plot of Reflectivity (R%) at 589nm against wt% Bi in galena

List of Figures (continued)

- Fig. 10 Infra-red spectra of pyrite
- Fig. 11 D. t. a. curves of pyrite
- Fig. 12 Infra-red spectra of chalcopyrite
- Fig. 13 D. t. a. curves of chalcopyrite
- Fig. 14 Plot of wt% Zn against wt% Fe in sphalerite
- Fig. 15 Plot of Mol% FeS against unit cell edges of sphalerite
- Fig. 16 Plot of Mol% CdS against unit cell edges of sphalerite
- Fig. 17 Infra-red spectra of sphalerite
- Fig. 18 Infra-red spectra of galena
- Fig. 19 Plot of wt% Sb against wt% As in tetrahedrite-tennantites showing the compositional break
- Fig. 20 Orthochlorites showing the species and variety boundaries (after Hey, 1954)
- Fig. 21 Infra-red spectra of chlorites

List of Tables

Table

1. Stratigraphic sequence at Parys Mountain
2. Classification of ore types
3. Summary of some mineral forms at Parys Mountain
4. Table showing the ore minerals at Parys Mountain
5. Summary of textures shown by ore minerals at Parys Mountain
6. Simplified paragenetic diagram of primary sulphides and sulpho-salts at Parys Mountain
7. Table to show the techniques employed and the nature of information obtained
8. Table showing the essential and trace-element composition of Pyrite (2 sheets)
9. Table showing the essential and trace-element composition of Chalcopyrite
10. Table showing the essential and trace-element composition of Sphalerite
11. Fe and Cd contents of Sphalerites
12. Table showing the essential and trace-element composition of Galena
13. Table showing the statistical data of Pyrite (in p. p. m. and %)
14. Table showing the statistical data of Chalcopyrite (in p. p. m. and %)
15. Table showing the statistical data of Sphalerite (in p. p. m. and %)
16. Table showing the statistical data of Galena (in p. p. m. and %)
17. Table showing the measured and calculated cell edges of Sphalerite
18. Table showing the differences in measured cell edges of Sphalerite by X-ray diffraction and by electron diffraction
19. Microhardness values of Pyrite
20. Microhardness values of Chalcopyrite
21. Microhardness values of Sphalerite
22. Microhardness values of Galena
23. Table showing the spectral reflectivity values of Pyrite in air
24. Table showing the spectral reflectivity values of Chalcopyrite in air
25. Table showing the spectral reflectivity values of Sphalerite in air
26. Table showing the spectral reflectivity values of Galena in air
27. Composition of Arsenopyrite

List of Tables (continued)

28. List of sulpho-salts found at Parys Mountain
29. Composition of Tetrahedrite - Tennantites
30. Table giving the atomic proportions for Tetrahedrite - Tennantite
(present study)
31. Composition and atomic proportions of Bournonite
32. Composition and atomic proportions of Kobellite
33. Composition and atomic proportions of Galenobismutite
34. Composition and atomic proportions of lead sulpharsenides
35. X-ray powder diffraction data for Diabantite
36. X-ray powder diffraction data for Ripidolite
37. X-ray powder diffraction data for Clinocllore
38. X-ray powder diffraction data for Aphrosiderite
39. X-ray powder diffraction data for Grochauite
40. X-ray powder diffraction data for Chlorite 1b
41. Standards used for microprobe analysis

List of Plates

- | | |
|----------------|---|
| Plates I - III | Photomicrographs |
| Plate IV | X-ray images showing distribution of Sb-As in
Tetrahedrite-Tennantites |

LIST OF CONTENTS

Summary	Page
Acknowledgements	
List of Figures	
List of Tables	
List of Plates	
Chapter 1 Introduction	
	1
1.1 Geology of Parys Mountain	1
1.2 Mineralisation	2
1.3 Summary of geological events at Parys Mountain	3
1.4 The present investigation	3
Chapter 2 Mineralogy and Paragenesis	
	5
2.1 Introduction	5
2.2 Microscopic features	5
2.2.1 Pyrite	5
2.2.1.1 Euhedral-subhedral pyrite	6
2.2.1.2 Anhedral pyrite	6
2.2.1.3 Framboidal pyrite	6
2.2.2 Chalcopyrite	7
2.2.3 Sphalerite	7
2.2.4 Galena	8
2.2.5 Tetrahedrite-tennantite	8
2.2.6 Bournonite	8
2.2.7 Lead sulpharsenides	8
2.2.8 Bismuth sulpho-salts	9
2.3 Textural features	9
2.4 Paragenesis	9
2.5 Stratiform features of Parys Mountain ores	9
Chapter 3 Sulphide Investigations	
	11
3.1 Introduction	11
3.2 Pyrite	11
3.2.1 Composition	11
3.2.2 Physical-optical characteristics	13
3.2.2.1 Microhardness	13
3.2.2.2 Reflectivity	14
3.2.2.3 Infra-red studies	14
3.2.2.4 Differential thermal analysis	14
3.3 Chalcopyrite	15
3.3.1 Composition	15
3.3.2 Physical-optical characteristics	16
3.3.2.1 Microhardness	16
3.3.2.2 Reflectivity	16
3.3.2.3 Infra-red studies	16
3.3.2.4 Differential thermal analysis	17
3.4 Sphalerite	17
3.4.1 Composition	17
3.4.2 Unit-cell edge measurements of sphalerite	19
3.4.3 Physical-optical characteristics	21
3.4.3.1 Microhardness	21
3.4.3.2 Reflectivity	21
3.4.3.3 Infra-red studies	22

	Page
3.5 Galena	22
3.5.1 Composition	22
3.5.2 Physical-optical characteristics	23
3.5.2.1 Microhardness	23
3.5.2.2 Reflectivity	23
3.5.2.3 Infra-red studies	24
3.6 Arsenopyrite	24
3.7 Pyrrhotite	24
3.8 Summary and implications of sulphide investigations	24
Chapter 4 Sulpho-Salts	
4.1 Introduction	26
4.2 Tetrahedrite-tennantite	26
4.3 Bournonite	27
4.4 Bismuth sulpho-salts	28
4.5 Lead sulpharsenides	28
4.6 Implications of sulpho-salt geochemistry	29
Chapter 5 Wall Rock Studies	
5.1 Introduction	30
5.2 X-ray diffraction studies	30
5.3 Infra-red studies	31
Chapter 6 Discussion and Conclusions	
6.1 Discussion	32
6.1.1 Source and availability of elements	32
6.1.2 Environment of formation	33
6.1.3 Relationship with the host rocks	34
6.1.4 Post depositional characteristics	34
6.2 Summary of conclusions	34
Appendix 1 Sample Selection and Preparation	
Appendix 2 Some Laboratory Methods	
2.1 Atomic absorption spectrophotometry	37
2.2 Electron-probe microanalysis	37
2.3 Reflectivity	38
2.4 Indentation microhardness	39
2.5 Infra-red absorption spectroscopy	39
2.6 Differential thermal analysis	39
References	40
Tables	
Figures	
Plates	

CHAPTER 1

INTRODUCTION

1.1 Geology of Parys Mountain

Parys Mountain lies in the north-east corner of Anglesey (Fig. 1) in North Wales. Situated about 4 km south of Amlwch port it forms a prominent topographical ridge aligned in ENE-WSW direction, rising to over 150m above sea level.

The geology of Parys Mountain has been studied by many investigators for a number of reasons. Structurally and stratigraphically it is a very complex area (Manning, 1959; Bates, 1966) and hence the relationship between its sedimentary and volcanic rocks has been variously interpreted. Its mineral deposits have been compared with other mining fields in the southern Caledonides, such as Avoca (south-eastern Ireland), and Coniston (Lake District), because of similar age and comparable tectonic and stratigraphic positions (Williams, 1969; Fitton and Hughes, 1970; Wheatly, 1971a, b). It has a close analogy in its depositional environment to other conformable polymetallic deposits (Wheatly, 1971a), and the close relationship between mineralisation and petrology, especially the volcanic succession of the area, has been well exemplified (Thanasuthipithak, 1974).

The most comprehensive and detailed account of the geology of Parys Mountain was given by Greenly (1919). Later various aspects of its geology, namely stratigraphy, structure, lithology, and mineralisation, were described by Manning (1959), Derry (1961), Bates (1964, 1966), Hawkins (1966) and Wolfenden (1967) - in Thanasuthipithak (1974), Williams (1969), Wheatly (1971a, b) and Thanasuthipithak (1974). A simplified geological map after Thanasuthipithak (1974) is given as Fig. 2.

The general stratigraphic sequence and lithologies proved from the bore holes, and described by Hawkins (1966) and Thanasuthipithak (1974) is given in Table 1.

Parys Mountain is underlain by the Precambrian Mona complex (Fig. 2) which is represented by chlorite schists in the northern and eastern parts of the area, and by micaceous granitoid and quartzitic gneisses in the south. The Ordovician, best exposed in the northern side of the mountain consists entirely of Shales (Table 1). They were named as Parys Green Shales by Greenly (1919), Parys Shales by Hawkins (1966) and 'Slates' by Thanasuthipithak (1974) as they possess a well developed slaty cleavage.

Silurian rocks form the core of the mountain (Fig. 2) and consist of highly cleaved and silicified shales. Surrounding the core, except to the east, are exposures of highly silicified and sheared rocks forming a hair-pin shaped outcrop. These were called 'Felsites' by Greenly (1919) and were considered by him to be intrusive. Thanasuthipithak (1974) described these felsitic rocks as a succession of extrusive volcanic rocks of Ordovician age consisting of dacitic and rhyolitic volcanic fragmental rocks and some siliceous sinter, a similar conclusion to that of both Hawkins (1966) and Wheatly (1971).

The rocks of the Precambrian Mona Complex are thrust over younger rocks along several low angle thrust faults called the Carmel Head, Corwas, and Nebo Thrusts (Fig. 2).

Although the structural relationship between shales and 'felsitic' rocks and the resultant structure of Parys Mountain has been variously interpreted, it is now generally agreed that the structure is an east-north-easterly trending, single syncline overturned to the north, with shales in the core (Fig. 3) (Thanasuthipithak, 1974).

1.2 Mineralisation

The mineralised belt trends between 060° and 070° following the general strike of the enclosing strata and dips $30-50^{\circ}$ to the north. It extends for some 1500 m, and is some 400 m wide and has been worked to a depth of 300 m. The mineralisation occurs as a series of lenticular to tabular ore zones, in the folded sequences of Ordovician and Silurian sedimentary and volcanic rocks. The mineralisation is generally concentrated on both sides of the northern outcrops of the rhyolitic rocks. It is present both in the rhyolitic rocks and in the rocks which are in contact with them, namely the siliceous sinter, parts of the Ordovician slates in the north, and the Silurian slates on the south side of the northern limb (Fig. 4) (Thanasuthipithak, 1974). Based on the host rock and the mineralogy, four types of ores were distinguished by Wolfenden (1967) (in Thanasuthipithak, 1974), and a slightly different division was given by Wheatly (1971a). The former division is made use of in the present study. These ore types are given in Table 2 and the lodes in which they occur are shown in Fig. 4.

The origin of these mineral deposits was regarded by earlier workers to be epigenetic, based on the notion that the 'felsite' was intrusive and probably supplied hydrothermal ore-bearing fluids. Deposition was thought to have been modified by metasomatic pyritization,

chalcopyritization and some lead-zinc metasomatism (Greenly, 1919; Manning, 1959). The controls of ore deposition were thought to be both shear zones and lithological interfaces.

Wheatly (1971a, b) suggested that, at Parys Mountain as well as in other mining fields in the southern Caledonides (Avoca, south-east Ireland; Coniston, Lake District), the conformable lenticular, pyritic zones associated with volcanic sequences, reacted with later hydrothermal fluids to produce the complex galena-sphalerite-pyrite mineralization. He further suggested that the mineralisations in these fields, including Parys Mountain, have a pulsatory metasomatic sequence related to tectono-stratigraphic controls. The ore localisation was thought to have been controlled by suitable structures and the pyritic shale horizons. Thus, Wheatly concluded that the main mineralisation was of an epigenetic hydrothermal enrichment type on a 'prototype' syngenetic mineralisation.

Thanasuthipithak (1974) studied the relationship of mineralisation to petrology and concluded that because there was a close association of ore bodies as lenses and tabular bodies, generally conformable with the Ordovician volcanic host rocks, they could be interpreted to have synsedimentary-exhalative origin. According to him the deposits were later modified by remobilization of some sulphides to produce apparent epigenetic features during the Caledonian orogeny.

1.3 Summary of geological events at Parys Mountain

The main geological events including the mineralisation at Parys Mountain, according to Thanasuthipithak (1974), are a) Deposition of Ordovician sediments in a marine environment with volcanism producing acidic rocks, b) Continued Ordovician sedimentation with some mineralisation, c) Main stage volcanism with some mineralisation, d) Erosion, submergence and deposition of Silurian sediments, e) Deformation of sediments and volcanics during the Caledonian and Variscan orogenies along with remobilization of the sulphides.

1.4 The present investigation

It is hoped that further mineralogical and geochemical studies on sulphide minerals can supplement geochemical information and thus help the various interpretations on the genesis of Parys Mountain mineral deposits. Previous interpretations were based on structural, petrological and mineralogical observations and no investigation of the geochemistry of the ore minerals was made. Similarly no systematic and detailed

investigations of the composition of the ore minerals, trace element distribution patterns, partition behaviour of trace elements, if significant, have been made, and although sulpho-salt minerals were recognised, no quantitative determination of them have been made. Also no previous correlation has been done relating the observed quantitative and qualitative reflected light properties of the opaque minerals with composition.

In fact, there are only a few areas in the British Isles where the major and trace element geochemistry of the ore minerals has been investigated to interpret the metallogenesis. El Shazly (1951), El Shazly et al (1957), Bishara (1966), Kakar (1971) were the few to make systematic investigations on trace elements in sulphide minerals mainly sphalerite and galena. Trace elements in pyrite, chalcopyrite, sphalerite and galena mainly from Avoca and a few from the Parys Mountain, and Coniston areas were studied by Wheatly (1971a) who showed a similarity in trace element content in all these areas. The geochemical investigations at Parys Mountain by this author were however not detailed and systematic. He also pointed out that work in progress on the geochemical atlas of Great Britain has delineated an anomalous tin area associated with copper at Parys Mountain, the explanation for which is not properly understood.

The present study was a systematic one of the geochemistry of the ore minerals and some of the physical and optical characteristics of the sulphide minerals. To this end studies were made using electron probe microanalysis, atomic absorption spectrophotometry, X-ray diffraction, electron diffraction, quantitative and qualitative reflected light microscopy, infra-red spectroscopy and differential thermal analysis.

CHAPTER 2

MINERALOGY AND PARAGENESIS

2.1 Introduction

The mineralogy and paragenesis of sulphide and sulpho-salt minerals from Parys Mountain has been described by both Wheatly (1971a) and Thanasuthipithak (1974). A description of the textural and paragenetic features observed in 58 polished sections from bore holes not previously studied (bore hole numbers A15, 27, 19, 36A, 32; mainly of pyritic and Bluestone ore types) is given here in addition to descriptions of those observed in some sections previously studied by Thanasuthipithak (1974). Textural features and optical characters of the opaque minerals were examined in reflected light using a Reichert Zetopan Ore Microscope with a micrometer ocular for grain size measurement.

Pyrite is the most abundant of the sulphides followed by chalcopyrite, sphalerite, galena and minor quantities of microscopically identifiable tetrahedrite-tennantite, arsenopyrite, pyrrhotite, lead and bismuth sulpho-salts. Megascopically the specimens studied show 4 or 5 distinct forms. The general features of these forms and the corresponding ore types are summarized in Table 3, and Fig. 5 shows sketches of these forms.

2.2 Microscopic features

Only primary minerals are described here, although some secondary minerals, such as covellite and bornite, have been described by Wheatly (1971a) and Thanasuthipithak (1974). A list of ore minerals present, and their general characters are presented in Table 4. Pyrrhotite, from Parys Mountain, has been described by Wheatly (1971a) and Thanasuthipithak (1974), and arsenopyrite has been described by the latter author, but in the present study only their compositions have been determined and these are given in Chapter 3.

2.2.1 Pyrite

Pyrite is the most abundant of all the sulphides, and is most abundant in the pyritic ore type, being present both in the layered sulphide and in disseminated forms, and is relatively least abundant in the Bluestone Ore type. Pyrite grains show both primary fabrics, representing the original depositional features, and secondary fabrics representing deformational and recrystallised features. Euhedral-subhedral, anhedral and framboidal type pyrite grains comprise the primary type. Colloform pyrite was also described by Thanasuthipithak (1974). Cataclastic, radial and recrystallised textures comprise the secondary type.

2.2.1.1 Euhedral-Subhedral pyrite

This type is mainly associated with black shale and dacite as disseminations through the rock. The following three divisions can be made: a) Isolated simple pyrite euhedra in which the grain size varies from about 0.05 mm to about 2 mm with some chalcopyrite replacement at the margins. Pyrite euhedra are associated with rutile and in some instances are seen to replace it (Plate IA). It is therefore paragenetically later than rutile. b) Spherically arranged aggregates of pyrite cubes forming pseudomorphs after framboidal pyrite. As many as 14 pyrite euhedra are present forming a spherically arranged aggregate of pyrite cubes homogenised at the centre of the aggregate but retaining their cube outlines at the periphery (Plate IB). c) Pyritohedra with intense deformation textures, the pyrite grains being heavily fractured (Plate IC). In most instances the fractures are filled by other sulphides.

2.2.1.2 Anhedral pyrite

Anhedral pyrite is less abundant than the euhedral/subhedral type. It is generally fine-grained (0.01 mm to 0.05 mm) and forms allotriomorphic granular aggregates commonly enclosing euhedral pyrite which implies a generation gap between the two types.

2.2.1.3 Framboidal pyrite

Framboidal pyrite was seen mainly in the Bluestone ore type associated with galena-sphalerite mineralisation. Generally three kinds of framboids are present:- a) Isolated framboid microcrysts ranging in size from 2 microns to about 40 microns in diameter. Quantitative studies of framboid grain size were made and the distribution is seen to be positively skewed (Fig. 6). The maximum occurs at 30 microns and the majority of the framboids occur within 15 microns diameter. The size distribution is similar in sections from the different bore holes. There is some clustering of framboids and a plot of the number of framboids per cluster against frequency (Fig. 6d) shows an irregular pattern with the frequency maximum at 10 framboids/cluster. b) The second type has the framboidal grains in the form of a network whose interstices are infilled mainly by sulpho-salts. This feature was described as atoll texture (Thanasuthipithak, 1974) in which the framboidal grains are extensively replaced, enclosed, and cemented by tetrahedrites (Plate I E, F). c) The third type has the form of a recrystallised

aggregate. The framboids form clusters (Plate ID) and lose their form where they are joined. The loss of shape is attributed to the result of growth of later pyrite between the granules (Raybould, 1973).

In some specimens the core of the framboidal cluster is replaced by sphalerite, and in some instances by tetrahedrite. Radiating textures have also developed in some framboidal pyrites (Plate II C).

Some pyrite grains in the types described above are compositionally zoned (Plate II E). The radiating textures (Plate II C) and irregular fracturing (Plate I C) exhibited by some pyrites are interpreted as resulting from cataclasis. In most specimens the fractures are infilled by other minerals namely sphalerite, and tetrahedrite-tennantites. Pyrite is comparatively free from inclusions; however, in some grains, small quantities of chalcopyrite and some gangue material are present as inclusions.

Pyrite occurs in minor quantities as fine-grained anhedral to subhedral grains forming a distinct vein or fracture filling in the matrix.

2.2.2 Chalcopyrite

Chalcopyrite most commonly is anhedral in form. It occurs: a) as a fracture filling in and replacing euhedral to subhedral pyrites; b) as a matrix material enclosing the pyrite grains; c) as mutual intergrowths with sphalerite, galena and pyrite; d) isolated anhedra embedded in rock matrix; and e) as exsolution bodies in sphalerite. Little chalcopyrite is associated with euhedral pyrite with most being associated with other kinds of pyrite and with other sulphides.

Chalcopyrite, where it is associated with pyrite generally replaces it. It is replaced by sphalerite although there is depositional overlap shown by intergrowths with sphalerite and galena.

2.2.3 Sphalerite

Sphalerite most commonly occurs in the fine-grained Bluestone ore type. The grain size varies between 0.02 mm to 0.5 mm. It is present as anhedral and irregular grains intergrown with other sulphides mainly chalcopyrite, and in lesser quantities filling fractures in cataclastic pyrite.

Two types of sphalerites are recognised: a) sphalerite with exsolutions of chalcopyrite and b) sphalerite without exsolutions. The first type is far more abundant than the second. Both the types are intergrown with chalcopyrite. Bournonite is found as inclusions or

infillings in sphalerite. Sphalerite generally shows mutual replacement textures and intergrowths with galena (Plate II A and B) and this is interpreted to indicate co-deposition.

2.2.4 Galena

Galena is present mainly in the Bluestone ore and Copper ore types and is not present in the Pyritic ore type. The grain size varies from 0.05 mm to 0.2 mm. It forms allotriomorphic masses and most commonly is intergrown with sphalerite and chalcopyrite.

Mutual replacements of sphalerite and galena are also present. A little galena, however, clearly replaces sphalerite, and paragenetically is therefore later. Inclusions or infillings of some sulpho-salts are present in galena.

2.2.5 Tetrahedrite-tennantite

The tetrahedrite group is the most abundant of the sulpho-salts at Parys Mountain and it is found only in the Bluestone ore type. These minerals occur as a) fracture fillings in pyrite grains (Plate II D); b) an interstitial cementing matrix for some subhedral pyrite grains (Plates II E and III A); c) inclusions in some sphalerites and chalcopyrites along the peripheries of, and extensively replacing, pyrite framboids. The tennantite end member has a lower reflectivity value than that of tetrahedrite. The tetrahedrite has a reflectivity of between 34.3 and 36.5% at 589 nm in air, and tennantite between 29.5 and 31.7%. The microhardness value ranges 279-328 Kg/mm² for both minerals and their grain size varies from 0.005 mm to 0.01 mm.

2.2.6 Bournonite

Bournonite occurs as very small (grain size 30 microns) inclusions in sphalerite (Plate III B). The reflectivity is generally high (38 - 42%) but could not be precisely estimated because of the very small grain size.

2.2.7 Lead Sulpharsenides

These minerals generally are very similar to galena and it is very difficult to distinguish between them optically. They are distinguished from galena only by an absence of cleavages and triangular pits and by anisotropism (seen only in oil immersion). Electron microprobe analysis showed these minerals to be lead sulpharsenides. They are white in colour, have irregular shapes and generally occur replacing sphalerite and galena along with other sulpho-salts. The reflectivity values are similar to those for galena (about 39.3 - 43.5%) and the

microhardness was not determined because of the very small grain size (about 0.05 mm).

2.2.8 Bismuth sulpho-salts

These are very similar in appearance to the lead sulpho-salts; however, they have a more greyish white colour, are more anisotropic, and the reflectivity (34.5 - 37%) is slightly lower than that of the lead sulpharsenides. They were identified, from electron microprobe analyses, as kobellite and galenobismuthite. Grain shapes are anhedral and irregular and they are generally present only as infillings in other sulphides mainly sphalerite and pyrite.

Mutual replacements between the sulpho-salt minerals are absent and it is difficult to infer paragenetic differences between them. The occurrence as inclusions, and as interstitial infillings in sulphides, is interpreted to indicate that they are later than the sulphides.

2.3 Textural features

The textural relationships outlined fall into two distinct categories. To distinguish between them, here they are called: a) Primary fabrics - developed in the original precipitation or depositional processes, and b) Secondary fabrics - developed either superimposed on an original primary fabric (e.g. cataclastic texture in pyrite) or formed due to some epigenetic process (e.g. fracture infilling of sulpho-salts in pyrite). The two types of fabrics are summarized in Table 5.

2.4 Paragenesis

A simplified paragenetic diagram for the ore minerals, based on the textural relationships outlined above, is presented in Table 6. This is in general agreement with that of Wheatly (1971a) and that of Thanasuthipithak (1974). It should be noted that the information on pyrrhotite and arsenopyrite is from Thanasuthipithak (1974).

2.5 Stratiform features of Parys Mountain ores

Stanton (1972) described stratiform ores as those that occur as layers concordant with the stratification of the enclosing rocks. They are thus confined stratigraphically and occur in preferred horizons. A comparison of mineralogical features of Parys Mountain ores with those of New Brunswick described by Stanton (1959, 1960 Parts I and II) as a typical conformable stratiform deposit brings out the following coincident features:-

- a) Imperfect alignment of ore lenses parallel to the bedding plane or schistosity
- b) Dominance of pyrite as iron sulphide with pyrrhotite being very local and minor
- c) Dominance of sphalerite among non-ferrous minerals
- d) Galena, although important, is subordinate to sphalerite
- e) Presence of trace quantities of minerals such as arsenopyrite, tetrahedrite-tennantite and other sulpho-salts.

Further the close association of the ores with pyroclastic volcanic rocks, tuffs and siliceous sinter as one of the stratiform type characters (Stanton 1960 Part I) can also be demonstrated in case of Parys Mountain ores (Thanasuthipithak, 1974).

Stanton (1964) considered that the textural features observed in stratiform ores are not depositional but result from growth during diagenesis and metamorphism. This is supported by experimental studies (Stanton and Gorman 1968). This hypothesis can explain the isolated uninhibited growths of euhedral and framboidal pyrites and intergrowths of other minerals with mutual boundary configurations. It cannot, however, account for fracture and interstitial infillings because of the fact that availability of mineral matter at such vacant spaces cannot be a coincidence, but it is a depositional feature along the available channel ways.

At Parys Mountain, the association of mineralisation with characteristic acidic volcanic rocks, megascopic conformable characters, mineralogical assemblages, close similarities to well established stratiform deposits such as Avica, all point to the fact that it is a syn-sedimentary stratiform conformable mineralisation. Replacement fabrics and fracture and interstitial infillings, favour some deposition at a later date superimposed on the original minerals as a later process of epigenesis. Pyrite represents the major conformable mineralisation with a little chalcopyrite. Microscopic evidence suggests that the minor sulphides and sulpho-salts were deposited at a later date as a process of epigenesis.

CHAPTER 3

SULPHIDE INVESTIGATIONS

3.1 Introduction

The essential and trace element contents of the sulphide minerals and their physical and optical characteristics, namely the reflectivity, microhardness, infra-red spectra and differential thermal analysis were determined to see if they could be correlated with composition and/or to compare with the published data. Table 7 lists the techniques employed and the nature of information obtained from the various minerals.

Samples for the present study were obtained from diamond drill cores, and selection and preparation techniques are described in Appendix 1.

Analysis for essential and trace elements was done by Atomic Absorption Spectrophotometry (A. A. S.) and Electron Probe Microanalysis. Fe, Cu, Zn, Pb, Co, Ni, Mo, Ba, Cd and Te were analysed by A. A. S. This technique was used because of its high sensitivity and minimum interference from other elements for the elements determined (McLaughlin, 1967; Volborth, 1969) and its simplicity and rapidity of operation (Kahn, 1968; Angino and Billings, 1972). A Perkin Elmer model 460 Atomic Absorption Spectrophotometer was used for all analyses. Details of the technique and sample solution preparation method are given in Appendix 2.

Electron Probe Microanalysis was used to analyse the more finely grained sulphides which could not be recovered in the powdered form, and for the quantitative determination of the sulpho-salt minerals. Some 74 analyses were made on various sulphides and sulpho-salts from some 43 polished sections (Tables 8-12) for the elements Fe, S, Cu, Pb, Zn, Co, Ni, As, Sb, Bi, Mo, Sn, Ag, Cd, Mn and Se. Instrumental and analytical details are given in Appendix 2.

Techniques for reflectivity, microhardness measurements, and sample preparation, along with instrumental details of infra-red and differential thermal studies are given in Appendix 2.

3.2 Pyrite

3.2.1 Composition

Pyrite (FeS_2) has a theoretical composition of 46.6 wt% Fe and 53.4 wt% S. Specimens of euhedral, subhedral, anhedral, and

framboidal pyrites were analysed for both essential and trace elements by electron microprobe and atomic absorption spectrophotometry and the values are given in Table 8. S was not determined in the samples analysed by the latter technique. The mean, minimum and maximum values are given in Table 13. The Fe content was found to fall in the range from 43.16 to 48.25%, with a mean value of 45.01% which is lower than the theoretical one. The S content ranges from 52.35 to 55.38% with a mean of 54.14% which is slightly higher than the theoretical value.

Trace quantities of Cu, Pb, and Zn are present in nearly all the samples analysed. Cu is a common trace element in pyrite, and in the present study the majority of the samples contain less than 2000 ppm of Cu. The high quantities 1.08% and 1.27% of Cu measured in samples H 14/186, and A 15/971 respectively (Table 8) are probably due to some slight contamination by chalcopyrite. Pb and Zn have a similar distribution pattern with mean values close to each other (Mean Pb 482 ppm and mean Zn 528 ppm). The samples analysed by A. A. S. were free from galena and sphalerite and the analysis in the electron microprobe was done only on pure pyrite grains. Therefore Pb and Zn are probably present in solid solution. Zn, however, is not unexpected in pyrite as Fe and Zn commonly substitute for one another in many minerals.

Co and Ni were present in nearly all the samples. Co substitutes for Fe in the pyrite structure (Rankama and Sahama, 1950), and Ni can exist in solid solution in pyrite (Fleischer, 1955). In the present study these two elements were found in almost all the samples analysed by A. A. S., but they were present in quantities below measurable limits in the samples analysed by probe. Analysis by A. A. S. showed the Co content to range from 30 to 2075 ppm (Table 8) with the majority of the samples containing less than 800 ppm. Although the distribution of Ni is irregular it has the comparatively narrow range of 16-696 ppm. The Co content is thus generally higher than that of Ni.

The Co/Ni ratios determined are given in Table 8. The majority of them show Co/Ni ratios to be greater than 1. High Co values and a Co/Ni ratio > 1 were found to be characteristic of pyritic deposits associated with volcanism (Loftus-Hills and Solomon, 1967). Those deposits in which the Co/Ni ratio is < 1 for pyrites are considered to

be sedimentary in origin. Hawley, and Gavelin and Gabrielson, (in Fleischer, 1955) found separately that the Co content and the Co:Ni ratio were generally high in high temperature deposits. Analysis of Parys Mountain pyrites by Wheatly (1971a) showed a high Co content and Co/Ni ratio > 1.00 and so he concluded the deposits to be associated with volcanism. In the present study, since the majority of the samples showed a consistent Co/Ni ratio > 1.00 it is concluded that pyritic mineralisation is related to volcanism at Parys Mountain.

Notable quantities of As have been reported in pyrite (Rankama and Sahama, 1950). However, in the present study probe analyses showed As to be present in quantities below measurable limits except in 3 samples where it is greater than 0.1% (Table 8).

Cd occurs in pyrite in lower concentrations than in sphalerite (Vlasov, 1964). In the present study only about 40% of the samples analysed contain Cd and in quantities generally less than 1000 ppm.

Ba cannot usually substitute for Fe because of its larger ionic radius and is therefore not common in pyrite (Rankama and Sahama, 1950). In the present study, however, Ba was found in most of the samples analysed by A.A.S. although most of the samples contained below 500 ppm (Table 8).

Mo is not a common trace element in pyrite, though it was reported in syngenetic pyrites by El Shazly (1951). In the present study it was found in some 25% of the samples in quantities less than 500 ppm.

Te, because of physical and chemical similarities, commonly substitutes for S, and as much as 0.1% of Te has been reported in pyrites (Vlasov, 1964). In the present study the majority of the samples analysed by A. A. S. contain less than 200 ppm Te (Table 8). Te is relatively more common in pyrite than in other sulphides.

Other elements detected, although present in below measurable quantities by probe analysis, are Ag, Mn, Bi and in a few samples Se. Sb and Sn were looked for but were not detected.

3.2.2 Physical-optical characteristics

3.2.2.1 Microhardness

The microhardness values for the pyrites determined are given in Table 19. For a load of 100 gm Bowie and Taylor (1958) reported values of 1027-1240 kg/mm² for pyrite. Pyrite from Parys Mountain

has a hardness range of 1031-1483 kg/mm². Higher hardness values of 1186-1836 kg/mm² are quoted by Young and Millman (1964). The measurements made in the present study are thus well within this region. The indentations obtained were all fractured as has been observed by other authors. The weight percentages of Fe in pyrites were plotted against microhardness number (Fig. 7a); however, no relationship was found.

3.2.2.2 Reflectivity

Results of reflectivity measurements on pyrites in the wavelength region 400nm - 700nm at intervals of 20nm including 589nm are given in Table 23, and the spectral reflectivity profiles are shown in Fig. 6a. The profiles show a regular pattern generally increasing sharply with wave length until about 520nm and then increasing very gently (Singh, 1965). However, no significant differences could be observed with different types of pyrites namely the framboidal, euhedral, anhedral and subhedral pyrites (Fig. 8a). Reflectivity values at 589nm were plotted against weight percentage Fe in pyrite (Fig. 9a), but no conclusion could be drawn about their relationship.

3.2.2.3 Infrared studies

The infrared spectra produced for pyrite are given in Fig. 10. The pyrites show poor resolution, and this has been previously reported by Hunt et al (1950). The two absorptions shown by pyrite are in the wave length region 2.8-2.9 microns and 6.1-6.2 microns (Fig. 10). It can be seen in the figure that, compared to the sample A 15/924 which has Fe content of 43.98%, the two samples 36A/1617 and 32-1108, which have Fe content of 45.23% and 45.71% respectively, have more prominent absorptions in the wave length region 6.0-6.2 microns. In sample IM 6/1231, which has Fe content of 46.78%, the absorption in the wave length region 6.2 microns although more prominent than sample A 15/924, is less prominent than the other two samples. This probably indicates that variations in composition may have some role in the absorption patterns.

3.2.2.4 Differential thermal analysis (d.t.a.)

The d.t.a curves obtained for 6 pyrite samples are given in Fig. 11. Comparison with the curves obtained by Kopp and Kerr (1957) show that the present curves are in good agreement in that the pyrites show a broad exothermic peak in the region of 400-500°C. The endothermic

reactions are present at about 550°C. Samples studied have Fe content ranging from 43.19 to 46.78% but no significant differences in the exothermic or endothermic behaviour of these pyrites was observed.

3.3 Chalcopyrite

3.3.1 Composition

The theoretical composition of chalcopyrite in wt. percent. is 34.6% Cu, 30.4% Fe, and 35.0% S. In this study 19 samples were analysed and the results are given in Table 9. Out of these, 8 were analysed by A.A.S., and 11 by electron probe. Four samples analysed by the latter technique were also analysed by A.A.S. S was determined only in the probe analyses. The mean values for Cu, Fe and S of 34.53%, 29.62% and 35.78% (Table 14) respectively are close to the theoretical values given above, although there is a considerable range. The maximum frequency of Cu occurs in the range of 34-36%, Fe in the range of 29-31%, and S in the range of 36-37% (Table 9).

Zn was found in all the samples analysed, ranging from 1000 to 5600 ppm, with a mean around 1900 ppm; this is attributed to the closely associated sphalerite, which commonly occurs as small inclusions in chalcopyrite. However, chalcopyrite is structurally similar to sphalerite and some Zn may also be present in solid solution in the chalcopyrite structure.

As and Bi have been reported in chalcopyrite (Fleischer, 1955), and probe analyses in the present study show that most of the samples contain these two elements (Table 9). Three samples contain more than 0.1% As, and another 3 samples contain more than 0.1% Bi (Table 9). These samples are from the ore types in which arsenopyrite and bismuth sulpho-salts occur respectively. None of the samples which have a high As content contain arsenopyrite. The high As content does not result from contamination but probably is due to its presence in the structure of chalcopyrite. Bismuth sulpho-salts are present as very fine-grained minerals (Chapter 4) in some of the sections (H 4/491, IM 9/269) that have a high Bi content. Thus these minerals probably have contributed to the high Bi values in the form of tiny inclusions.

Co and Ni are present in most of the samples analysed. Analysis by A.A.S. showed that Co ranges from 60 to 710 ppm and Ni from 12 to 1060 ppm (Table 9). Trace quantities of Co and Ni are not unexpected

in chalcopyrite although Ni tends to be concentrated in pyrite relative to chalcopyrite (Vaughan 1971).

Cd commonly is present in chalcopyrite, although in lower quantities than in sphalerite, because of the structural similarities between them (Vlasov, 1964). Analysis by A.A.S. showed Cd to be present in the range of 98 to 446 ppm.

Pb was found in most of the samples analysed in the range of 313 to 1045 ppm.

Te was found in only a few samples, ranging from 55 to 192 ppm, probably substituting for S.

Ba (A.A.S. analysis) was found in quantities ranging from 165 to 1653 ppm, with a mean of 737 ppm. It is not a very common trace element in chalcopyrite and its presence in the chalcopyrites at Parys Mountain is difficult to explain.

Mo (A.A.S. analysis) was also found in some 50% of the samples, in quantities ranging from 28 to 510 ppm, with a mean of 217 ppm.

Ag, Mn, Sb, Se and Sn were all below the limits of measurement of the electron probe.

3.3.2 Physical-optical characteristics

3.3.2.1 Microhardness

Microhardness values measured for chalcopyrite are given in Table 20. This hardness range of 171-221 kg/mm² with perfect indentations, is in close agreement with that of 186-219 by Bowie and Taylor (1958). Weight %s of Fe in the chalcopyrites were plotted against microhardness number (Fig. 7b), however, as in the case of pyrite, the relationship is not pronounced.

3.3.2.2 Reflectivity

Reflectivity measurements for chalcopyrite in the wave length region 400-700nm including 589nm are given in Table 24. The spectral reflectivity profiles are given in Fig. 8b. Like pyrite, chalcopyrite also has a regular spectral reflectivity profile, generally increasing sharply with wave length until about 520nm and then increasing very gently. Reflectivity values at 589nm plotted against weight % Fe showed no relationship.

3.3.2.3 Infrared studies

The infrared spectra produced for chalcopyrite are given in Fig. 12.

Chalcopyrite has a poor resolution and one sample (A 15/1193) showed absorption in the vicinity of 6 and 7 microns region. In the two samples studied No. A 15/1193 has Cu 35.05%, Fe 32.37% and S 34.20% and the other (M 10/1521) has Cu 34.73%, Fe 27.73% and S 35.96%. The sample A 15/1193 has a very much higher Fe content than the other and this probably is responsible for its having a more pronounced absorption pattern in the region 2.85-2.9 and 6.0 microns regions.

3.3.2.4 Differential thermal analysis (d.t.a.)

The d.t.a. curves obtained for chalcopyrite are given in Fig. 13. The five samples studied showed marked exothermic behaviour in the vicinity of 450-460°C. as part of a broad exothermic reaction starting at 400°C and continuing up to 500°C. No significant differences in differential thermal behaviour with compositional variations were observed. The sample with a lower Fe content (sample M 10/1521 with Fe content 27.73) than the others (which have Fe contents ranging from 28.55% to 32.37%), has a smoother curve. This is probably because reactions with higher Fe contents become more vigorous than those with lower Fe content. Further detailed investigations are necessary for significant conclusions.

3.4 Sphalerite

3.4.1 Composition

Sphalerite has a theoretical composition of 67.10% Zn and 32.90% S by weight, but in nature this is not found because the sphalerite structure is remarkably tolerant of substitutions by Fe, Cd and Mn for Zn. Nearly all natural sphalerites are diadochic compounds of ZnS with FeS (up to 42%), Cd (up to 2%), and MnS (up to 9%) (Boyle and Jambor, 1963). Both Zn and S can be isomorphously replaced by substantial quantities of other elements (Vaughan, 1971). The Fe content in particular has received a very considerable attention (Kullerud, 1953; Kalliokoski, 1959; Sims and Barton, 1967; Benson, 1960; Barton and Skinner, 1967; Campbell and Ethier, 1974; Williams, 1974). Trace elements in sphalerite have also been studied in greater detail than in any other sulphide.

In all, 22 sphalerite samples were analysed by electron probe and A.A.S. The Zn content was found to range from 51.68% to 64.74% (Table 10), with a mean of 58.46% (Table 15), and the S content ranges

from 32.23% to 38.66% with a mean of 35.29%. The Fe content ranges from 0.67% to 18.32% (Tables 10 and 11) with a mean of 6.42%. In addition to the analyses listed in Table 10, Fe and Cd were also determined using electron probe on 4 samples to enable calculation of the cell edges (discussed later).

There is a good antipathetic relationship between Zn and Fe content (Fig. 14) allowing the interpretation that Fe has substituted for Zn. The Fe content is believed to be present in sphalerite in solid solution and is not due to any contamination because most of the samples analysed were pure grains.

Cd was found in all the samples analysed in quantities ranging from 215 ppm (A.A.S. analysis) to 0.33% (probe analysis) (Tables 10 and 11).

Cu is present in all samples in quantities ranging from less than 0.1% to 2.75% (Table 10) as analysed by probe and A.A.S. The very high Cu contents of some samples can probably be attributed to sub-microscopic inclusions or exsolutions of chalcopyrite, though the Cu content of sphalerite is present in variable quantities (Rankama and Sahama, 1950).

Pb was found in some 11 samples ranging from 286 ppm to 1468 ppm (Table 10). However, this is probably due to intimate admixtures with galena as has been reported elsewhere (Fleischer, 1955).

Co has been reported in sphalerite and in a very few instances Ni also has been reported (Fleischer, 1955). A.A.S. analysis of Parys Mountain sphalerites showed Co to be present in 5 samples ranging from 206 to 967 ppm and one probe analysis showed 0.1% of Co. Ni was found in 3 samples in the range of 340 ppm to 433 ppm.

Sb, As and Bi have been reported from sphalerites although in most instances only qualitatively (Fleischer, 1955). As and Bi are present in trace quantities (below 0.1%) in most of the Parys Mountain sphalerites analysed by probe, although 4 samples contained more than 0.1% As, and another two more than 0.1% Bi (Table 10). Sb was not detected. It is likely that these quantities are from sulpho-salts containing As and Bi admixed in the sphalerites.

Mn is present in most samples but below measurable limits (0.1%) by electron probe, and in only 3 samples was it found to be more than 0.1% (Table 10).

Ba was found in the samples analysed by A.A.S. ranging from 174 to 7222 ppm (Table 10). As in the case of other sulphides its presence is unexplained.

Mo was found in trace quantities and in a few instances more than 0.1% (Table 10).

Ag and Sn were found not to be present by electron probe.

3.4.2 Unit cell edge measurements of sphalerite

In the present study the reason for the measurement of unit cell edges was two-fold: 1) To investigate whether there is a linear relationship between Fe content and measured cell edges of sphalerite by X-ray diffraction; 2) To investigate the possibility of using a single crystal electron diffraction technique to obtain Fe content in the same way as in X-ray diffraction, if confirmed that there is a linear relationship between cell edge and Fe content.

Kullerud (1953) reported that the effect of FeS (and the other common trace impurities MnS and CdS) is to cause an increase in the unit cell dimensions in a linear way. This then allows for accurate measurements of cell dimension to be used as an indicator of Fe content. Skinner (1961) presented an equation for this:

$$a = 5.4093 + 0.000456 X + 0.00424 Y + 0.00202 Z$$

where X, Y and Z are the contents of FeS, CdS and MnS in mol% and a is the cell edge in angstroms. Krause, and Van Aswegen and Verleger (in Boyle and Jambor, 1963) have, however, reported that Fe content has no increasing effect on unit cell edge and Williams (1965) has argued that the equation is the least squares fit to the experimental data and is therefore subject to possible error. The concept is, however, supported by Boyle and Jambor (1963) and by Evans et al (1968), and is used in this study.

The unit cell dimensions of 17 sphalerite specimens were measured using a Debye-Scherrer Powder Camera (114.59 mm diameter) fitted to a Phillips Norelco X-ray Diffractometer with Ni filtered $\text{CuK}\alpha$ radiation ($\lambda = 1.5405 \text{ \AA}$). No correction for film shrinkage was applied and the diffraction patterns were measured on a Central Scientific Instruments' Linear Comparator with a vernier having a least count of 0.05 mm (Straumanis' method as described by Zussman, 1967). X-ray diffraction angles (θ) calculated by this method were tabulated and the

interplanar spacings were read from tables. Corresponding hkl values were obtained from an X-ray diffraction data file (Berry, 1974), and unit cell edges calculated.

Unit cell edges of sphalerite were also calculated by substituting the mol% values of FeS, MnS and CdS in the equation by Skinner (1961). In general there is a good agreement between measured and calculated cell edges (Table 17) but there is a systematic trend of measured edges being greater than calculated edges, as also noticed by Evans et al (1968); Skinner 1961, found the opposite. A plot of measured cell edges against measured Fe content (mol% FeS) (Fig. 15) shows a good linear relationship between the two. This is interpreted to show that unit cell edge increases with increasing Fe content. The increase in cell edge at lower Fe contents is very pronounced, however, as higher values for Fe content are reached the rate of increase is less pronounced and the curve flattens out slightly. This observation is in agreement with the observations of Boyle and Jambor (1963), although it is a little less pronounced than that found by Evans et al (1968). It is concluded from these results that the accurate measurement of cell edge can be utilised to obtain FeS content. Mol% CdS plotted against cell edge showed no significant relationship (Fig. 16), because the electron probe was not able to measure accurately the trace quantities of Cd present in sphalerite. Mol% Mn was not plotted against cell edge as the data was insufficient.

Cell edge measurements were also made on 12 sphalerite samples by an electron diffraction technique for comparison purposes. Specimens were prepared using the technique described by McConnell (1967) and single crystal electron diffraction patterns were obtained using a Jeol JEM 100 B Transmission Electron Microscope at 100 kV. The diffraction patterns in each case were photographed and the 'd' spacings were calculated using the formula

$$d_{hkl} = \frac{\text{c.f.}}{\sqrt{hkl}}$$

where d_{hkl} is the lattice interplanar spacing

\sqrt{hkl} is the measured distance from origin 000 to spot hkl on the electron diffraction photograph. c.f. is the Camera Factor, a constant

provided (which depends on the camera length (L) and the wave length of the electron beam (λ) (c.f. = λL).

hkl values were obtained from X-ray powder file and the cell dimensions calculated as in the case of X-ray diffraction.

The cell edges measured are given in Table 18 and it can be seen that all the electron diffraction measurements are higher than those from X-ray diffraction. This is a systematic error in the electron diffraction measurements, probably resulting from an inaccuracy in the assumed Camera Factor. The accuracy could be improved by estimating this Camera Factor at the time of measurement by using an internal standard. Provided an internal standard is used an electron diffraction technique for cell edge measurement has many advantages:

- 1) It requires less sample than that required by X-ray diffraction;
- 2) Diffraction patterns can be obtained from several selected spots on a specimen and the Fe content obtained from several measurements might be used to indicate variations in Fe content within a specimen;
- 3) Diffraction patterns can be readily seen and photographed immediately and thus it is much quicker than X-ray diffraction;
- 4) Very sharp reflections can be obtained, unlike X-ray powder patterns where measurements are sometimes inaccurate because of obscure reflections and blackening of the film in the back reflection region.

3.4.3 Physical-optical characteristics

3.4.3.1 Microhardness

The microhardness data for sphalerite show it to have a range of 148-240 Kg/mm² (Table 21). The weight % of Fe in sphalerite was plotted against microhardness number (Fig. 7c), because it had been noticed by previous workers that an increase in Fe content of sphalerite increased its microhardness (Young and Millman, 1964; Bishara, 1966; Vaughan, 1971). In the present study, a good linear relationship between Fe content and microhardness was seen (Fig. 7c).

3.4.3.2 Reflectivity

Results of the reflectivity measurements in the wave length region 400 nm-700 nm including 589 nm are given in Table 25, and the spectral reflectivity profiles are shown in Fig. 8c. Sphalerite in this study was

seen to have maximum reflectivity in the wave length region 480-500 nm, as has been reported by Gray and Millman (1962) for sphalerites. In many grains little variation was observed with wave length, but generally the values decrease with increase in wave length. Reflectivity values at 589 nm plotted against weight% Fe in sphalerite (Fig. 9b) showed no significant relation.

3.4.3.3 Infrared studies

The infrared spectra for sphalerite are shown in Fig. 17, and compared with other sulphides, show good resolution. All the sphalerites show clearly two absorption peaks in the vicinity of 2.8-3.0 microns wave length. The 5 samples studied had Fe contents ranging from 1.59% to 18.32% (Fig. 17), and unlike pyrite and chalcopyrite, no differences in absorption patterns with varying Fe content were observed.

3.5 Galena

3.5.1 Composition

The theoretical composition of galena is 86.6 wt% Pb and 13.4 wt% S. Twelve samples were analysed, and the Pb content found to range from 80.15% to 87.15% (Table 12), with the majority of the samples containing between 82 and 86% Pb. All galenas analysed except one (A 15/1193) have a lower than theoretical Pb content, and have considerable As and Bi contents. The S content ranges from 13.85 wt% to 15.75 wt% (Probe analysis).

As, Sb and Bi are common trace elements in galena (Rankama and Sahama, 1950) and these elements were looked for in the specimens analysed by electron probe. As was found to range from 0.1wt% to 2.85 wt% with a mean of 1.48 wt%. Bi ranges from 0.27 wt% to 3.49 wt% with a mean of 1.58 wt% (Tables 12 and 16), and more than 0.1 wt% Sb was found in all samples. As and Bi sulpho-salts are present in very fine-grained sizes in most of the sections analysed by probe and high values in these analyses are thus probably due to some submicroscopic admixtures of these minerals with the galena. However, since As, Bi and Sb are common in galena, it is likely that they are also present in solid solution. No further information was gained in this study.

Ag is a common trace element in galena (Fleischer, 1955) and it was detected in all the samples analysed by probe and 4 samples were found to contain more than 0.1 wt% (Table 12). As there are no Ag

sulphides in the specimens analysed, the Ag content is not due to contamination but probably is present in solid solution.

Cu, Fe and Zn are all present generally above 1000 ppm or 0.1 wt% (Table 12). Cu occurs in lower quantities than in sphalerites. Fe and Zn although reported by previous workers in galenas, were probably due to contamination by pyrite and sphalerite (Fleischer, 1955). Most of the samples in the present study contain Fe and Zn (Table 12) (Probe and A.A.S. analysis) above 0.1 wt%.

Cd was found in most of the samples in quantities generally below 1000 ppm (Table 12). In 2 samples it was found to be 0.11 wt%. Goldschmidt (in Vlasov, 1964) suggested that admission of Cd into galena is due to the Cd-Pb isomorphism, and trace quantities of Cd in Parys Mountain galenas are probably present in solid solution.

Co and Ni are present only in trace quantities (Table 12) and in the samples analysed by A.A.S. they were found to be below 500 ppm.

Sn was detected in most probe analyses and 3 samples contain more than 0.1 wt% (Table 12).

Ba was measured by A.A.S. in 3 samples and it was found to be present below 500 ppm (Table 12). Its presence as in the other sulphides is difficult to account for.

Mo was also found in a few samples and 2 probe analyses showed more than 0.1 wt% (Table 12).

Te was measured in 4 samples by A.A.S. and was found to be below 100 ppm (Table 12). It has probably substituted for S.

3.5.2 Physical-optical characteristics

3.5.2.1 Microhardness

The measured values for microhardness of galena have a range of 61.7-107 kg/mm² (Table 22) in contrast to Bowie and Taylor's (1958) measurements of 71-84 kg/mm². The wider range in microhardness of Parys Mountain galenas probably results from the presence of considerable quantities of As and Bi. Weight %s of As and Bi were plotted against microhardness (Figs. 7d, e) and there appears to be slight linear relationship between them, though this needs confirmation by more data.

3.5.2.2 Reflectivity

Reflectivity measurements in the wave length region 400 nm-700 nm,

including 589 nm are given in Table 26, and the spectral reflectivity profiles are shown in Fig. 8d. Galena is a highly reflecting species and it shows irregular spectral profiles as reported by Gray and Millman (1962). Reflectivity % at 589 plotted against weight % As and weight % Bi showed no significant relationship probably because of insufficient data. (Fig. 9c, d).

3.5.2.3 Infrared studies

The infrared spectra produced for galena show poor resolution with broad absorption peaks between 2.8 and 3.0 microns wave length and one absorption peak in the vicinity of 6.0 micron wave length region (Fig. 18). No significant difference in absorption pattern was seen between the two samples studied, although one sample (19-424) contains 2.24% of As and the other (sample H 4/491) has only 0.10%, and both of them have nearly similar quantities of Bi (Table 12).

3.6 Arsenopyrite

Two grains of arsenopyrite were analysed by electron probe and the results are listed in Table 27 along with the theoretical value for the ideal formula FeAsS.

Compared with theoretical composition the Parys Mountain arsenopyrite has less As content but more Fe. Co, Ni, Cu, Pb and Zn are present in trace quantities (below measurable limits by electron probe).

3.7 Pyrrhotite

One pyrrhotite grain was analysed by electron probe and it has the following composition

	Fe	S	Co	Ni	Cu	Pb	Zn	Total
M 10/1521	57.33	40.91	tr	tr	1.30	tr	-	99.55

The high Cu content is difficult to account for from a single analysis and no further information was obtained in the present study.

3.7 Summary and implications of sulphide investigations

Investigations on Parys Mountain sulphide minerals have the following significant features:-

- 1) Analysis by electron probe on inclusion free areas showed the presence of substantial quantities of trace elements probably in solid solution.
- 2) The generalisation could be made that Co is concentrated in pyrite relative to other sulphides. Co and Ni are more common in pyrite and chalcopyrite than in sphalerite and galena.

- 3) Cd is concentrated in sphalerite relative to other sulphides, and there is a wide range of Fe content in sphalerites.
- 4) As, Bi and Ag are concentrated in galena relative to other sulphides. Sn is also present in galena but is absent in others.
- 5) Mo is concentrated more in sphalerite and galena than in pyrite and chalcopyrite. Ba is concentrated in chalcopyrite relative to pyrite. The significance of these two elements is not clear.
- 6) Correlation of trace element assemblage with the different types of the same mineral are inconclusive, such as between euhedral, anhedral and framboidal types in case of pyrite (Table 8), and in sphalerite grains those with exsolutions and without exsolutions (Table 10).
- 7) Concentration profiles for essential and trace elements were observed while analysing the sulphides by electron probe. It was noticed that variations of essential and trace elements within the same grain were more pronounced in case of sphalerite and galena than in the case of pyrite and chalcopyrite.
- 8) The Co/Ni ratio in pyrites (> 1) relates the deposits to volcanism
 High quantities of Cu in pyrites have been used by Frenzel and Ottemann (1967) in Fiji deposits to indicate a subvolcanic origin. High quantities of Cu in some Parys Mountain pyrites may be related to volcanism, though in some, contamination by inclusions is likely.
- 9) High Ag, Sb and Bi in galena indicate high temperature of formation as low quantities of these have been reported only from low temperature deposits (Fleischer, 1955; El Shazly et al 1957). Marshall and Joensuu (1961) also found that galenas having poor trace element assemblage predominantly form at lowest temperatures and vice versa. From this point of view the Parys Mountain galenas may throw some light on temperature of formation. However, it requires more data to draw any conclusions on this.
- 10) A linear relationship was observed between Fe content and unit cell edges of sphalerite and between microhardness and Fe content in sphalerite.
- 11) Attempts to correlate composition with some physical and optical characteristics of the sulphides allowed no significant conclusions, although some of this was due to insufficient data.

CHAPTER 4

SULPHO-SALTS

4.1 Introduction

The sulpho-salt minerals are intimately associated with the major sulphides at Parys Mountain. Their optical properties and textural relationships with the sulphides have been discussed elsewhere (Chapter 2). Their physical and optical characteristics are so similar that they are difficult to identify and distinguish optically (Uytenbogaardt and Burke, 1971) and so electron probe microanalysis is the most common method used for their mineralogical determination.

Most of the commonly known sulpho-salts contain one or more of the following elements - Fe, Co, Ni, Cu, Ag, Zn, Hg, Sn, Pb, Mo together with one or more of As, Sb and Bi; S is an essential constituent. These chemically complex sulpho-salts are commonly 'patterned' structurally after the simple sulphides (Ross, 1955) and are modifications of the cubic or hexagonal close packing structures. The sulpho-salt minerals present at Parys Mountain are listed in Table 28 along with their theoretical formulae. In addition to those listed, bismuthinite was reported by Thanasuthipithak (1974).

4.2 Tetrahedrite-tennantite

Many workers do not regard the tetrahedrite-tennantite group of minerals as sulpho-salts and there is considerable disagreement in assigning a chemical formula to them. Springer (1969), from the analyses of world wide material, concluded that the general formula $(\text{Cu, Ag, Fe, Zn, Hg})_3 (\text{As, Sb, Bi, Te})\text{S}_{3.25}$ is valid for tetrahedrite although the majority corresponds to $(\text{CuAg})_{2.50} (\text{Fe Zn})_{0.50} (\text{As Sb})\text{S}_{3.25}$. Later Maske and Skinner (1971) proposed a formula $\text{Cu}_{12+x} \text{As}_{4+y} \text{S}_{13}$ where $0 \leq x \leq 1.72$ and $0 \leq y \leq 0.08$ for tennantite. Skinner et al (1972) proposed $\text{Cu}_{12+x} \text{Sb}_{4+y} \text{S}_{13}$ for tetrahedrite where $0 \leq x \leq 1.92$ and $-0.02 \leq y \leq 0.27$. This complexity is due to extensive substitutions in the structure where Zn, Ag, Hg, Pb, Ni or Co as well as Fe may replace Cu in quantities ranging up to 16% (Vaughan, 1971).

Complex substitutions can occur in tetrahedrite partly because Cu occurs in both mono and divalent states. The first type is tetrahedrally co-ordinated with three S atoms in unusual planar groups (Riley, 1974). Cu in these sites can be replaced by Ag and Hg. In the second type Cu, which is in 3-fold co-ordination in the structure, can be replaced by Zn and Fe (Vaughan, 1971). Other substitutions involve Sb, which can be

completely or partly replaced by As and in minor quantities by Bi, Sn and Ge (Ramdohr, 1969). This complexity is well exemplified by the Parys Mountain minerals (Table 29).

Analyses of 6 tetrahedrites and 3 tennantites from Parys Mountain are shown in Table 29, and these represent the average analysis taken from 2 or 3 points in each grain. The atomic proportions (Table 30) were calculated by making the total of Cu + Ag + Fe + Zn equal to 12, Sb + As + Bi equal to 4 and obtaining the relative proportion for S based on the total of these two groups (Petruk et al., 1971). Analyses of tetrahedrites from Parys Mountain and Avoca, reported by Wheatly (1971a) are given in Table 29, for comparison.

Comparison of the compositions determined in the present study with those reported by Wheatly (1971a) (Table 29) shows that Ag content in Parys Mountain minerals in the present study is low, the maximum Ag value being 1.28 wt% from bore hole H4/491 (Bluestone ore) as compared to Wheatly's maximum Ag value of 5.4 wt%. The Fe content in the present study ranges from 3.16 to 10.18 wt% and is higher than that shown by Wheatly's (1971a) analyses. The zinc content ranges from 1.29 to 8.18 wt% and this range is quite in agreement with the analyses of Wheatly (1971a). All tetrahedrites contain some As and tennantites some Sb (X-ray images in Plate IV). Cu and Sb contents are in good agreement with Wheatly's (1971a) analyses. Bi is observed in both tetrahedrites and tennantites, the maximum content being 1.42 wt% from bore hole 27-145. There is a compositional break between tetrahedrite and tennantite as shown in Fig. 19. Such break was also noticed by Wheatly (1971a) at Avoca.

Deviations from the stoichiometric formula are illustrated by the atomic proportions of S given in Table 30. Such deviations have been noted in analyses elsewhere (Petruk et al., 1971) and are considered to be the result of complex metal substitutions with the whole complex forming an extensive solid solution series.

4.3 Bournonite

The theoretical formula for bournonite is CuPbSbS_3 . Analyses of specimens from Parys Mountain, Avoca and Idaho are compared with the theoretical values in Table 31, along with atomic proportions for the analyses in the present study.

The compositions and atomic proportions are at variance with the stoichiometric values. This is especially true of specimen 2 (sample M 10/1548) which contains appreciable quantities of Bi, Fe and Zn and has a Cu content very much higher than the theoretical value. The analysis of specimen (H4/465) however is in good agreement with the theoretical values and with the analyses of Avoca minerals (Wheatly 1971a). Analyses of specimens from Parys Mountain show As to be present in considerable quantities probably substituting for Sb. A solid solution series exists between Sb end member (Bournonite) and the As end member seligmannite (CuPbAsS_3) and this is considered to account for the As content in Parys Mountain analyses.

4.4 Bismuth sulpho-salts

Kobellite ($\text{Pb}(\text{Bi}, \text{Sb})_2\text{S}_5$) and galenobismuthite PbBi_2S_4 were identified at Parys Mountain in the Bluestone ore type. Kobellite is a disordered Bi-Sb-Pb sulpho-salt of composition $\text{Pb}_{6-x}(\text{Bi}, \text{Sb})_{7+x}(\text{Fe}, \text{Cu})\text{S}_{17.5}$ with $0 < x < 1$ (Weunsch, 1974). Weight percentages and atomic proportions for kobellite and galenobismuthite are given in Tables 32 and 33 along with theoretical values and some comparative analyses.

Comparison with theoretical composition shows the analytical data on Parys Mountain kobellite to be in good agreement with theoretical compositions. As is present substituting for Sb, and appreciable quantities of Cu and Fe are also present in the Parys Mountain kobellites. The deviation in composition from the theoretical composition of Parys Mountain galenobismuthite is due to a high Zn content which is probably present in solid solution.

4.5 Lead sulpharsenides

Mineral grains optically very similar to galena with high As values are classed here as lead sulpharsenide minerals. Analyses of these and calculated atomic proportions are presented in Table 34.

Chang and Bever (1973) have outlined the various disagreements on formulae for the lead sulpharsenide group of minerals. The calculated atomic proportions (Table 34) roughly correspond to jordanite which has a formula $\text{Pb}_{14}\text{As}_7\text{S}_{23}$ or $\text{Pb}_{13}\text{As}_7\text{S}_{23}$. However, since there is no standard and accepted formula for jordanite, Parys Mountain

minerals are classed as lead sulpharsenides only, rather than comparing them to any of the theoretical formulae.

4.6 Implications of sulpho-salt geochemistry

The complexity and uncertainty of the sulpho-salt geochemistry at Parys Mountain is due to the extremely local and minor abundance of these minerals and their fine grain size. Textural relationships with the major sulphides as outlined in Chapter 2 suggest that they are later than the conformable pyritic mineralisation. There is no geochemical evidence from sulpho-salt studies to assign any environment or temperature of formation for the Parys Mountain mineralisation.

Experimental studies by Maske and Skinner (1971) showed that the ideal composition for tennantite $\text{Cu}_{12}\text{As}_4\text{S}_{13}$ is probable only at lower temperature, i. e. below 300°C , and above this temperature, it deviates. Chang and Bever (1973) pointed out that lead sulpho-salt minerals are essentially restricted to hypogene deposits, particularly in the mesothermal intensity range. Minerals such as galenobismuthite have been described as occurring in high temperature areas ($550 - 610^\circ\text{C}$) of volcanic fumaroles in the Lipari Islands (Palache et al., 1944 in Craig, 1967). Czernanske and Hall (1975) have reported that the Darwin lead-zinc-silver deposit where lead sulpho-salts occur, is a high temperature deposit.

If comparisons are made with Parys Mountain minerals, then a high temperature, at least a relatively higher temperature phase than earlier conformable pyritic mineralisation has to be assigned for the Parys Mountain sulpho-salts. Nevertheless, strong similarities in mineralogy, host rock geology and sulpho-salt assemblage exist between Parys Mountain deposits and the Kuroko deposits of Japan (Lambert and Sato, 1974) which are not considered to be of high temperature mineralisation.

CHAPTER 5

WALL ROCK STUDIES

5.1 Introduction

Despite the widespread occurrence of chlorite associated with mineralisation areas, little use has been made of its development in mapping metal distributions (Tuddenham and Lyon, 1959), and zoning in mineral deposits. In the present study 12 chlorites from wall rocks in mineralised sections, and 6 from non-mineralised sections, were studied, using X-ray diffraction techniques to identify them and to determine any differences which might be present between the different sections. Eight of the chlorites from the mineralised sections and 3 from non-mineralised ones were also subjected to infra-red absorption spectroscopy to discover any differences that might be present. Of the chlorites from mineralised sections 11 were largely from materials associated with pyritic and chalcopyritic mineralisation and in one case with sphaleritic mineralisation (sample IM 9/269).

5.2 X-ray diffraction studies

Powder samples used were either obtained from rock chips which were ground in a tungsten carbide mill or directly from the core samples using a vibrating needle.

Diffraction patterns were obtained on a Phillips Norelco X-ray diffractometer, with Ni filtered $\text{CuK}\alpha$ radiation, and quartz as an internal standard. The measured 'd' spacings of the chlorites are given in Tables 35 to 40. It was noticed that, while there is a variation in chlorite species from place to place in the case of the mineralised sections, in general there was no variation in specimens from the non-mineralised sections. A variation in chlorite species was also noticed in mineralised sections from the same bore hole (bore holes 36A and IM 6) (Tables 35, 36 & 38 to 40). Diabantite, clinochlore and grochaulte varieties of chlorite were found mainly associated with pyritic mineralisation with some chalcopyrite and sphalerite. Ripidolite was found associated with pyrite and chalcopyrite, and aphrosiderite with pyrite. Chlorite 1b species was found in all the non-mineralised sections studied. Comparison of the chlorites at Parys Mountain with the classification of the chlorites given by Hey (1954) as in Fig. 20 shows

that they are closely related varieties in terms of Si, total iron and Fe/(Fe + Mg). These different varieties of chlorites which have slightly different compositions probably are the result of the wall rock alteration associated with epigenetically formed sulphides. The differences may have been caused by the proposed secondary hydrothermal sulphide mineralisation rather than by the early sedimentary pyrite mineralisation. Determination of composition of chlorites in terms of major and trace elements and the identification of the species by X-ray study on a greater number of samples would be a useful investigation to find whether the above observation is localized or whether it is a general feature with the mineral deposits at Parys Mountain. This is particularly important in establishing the relative ages of mineralisation and metamorphism because pre-metamorphism chlorites would likely be destroyed.

5.3 Infra-red studies

Specimens used were 11 chlorites directly recovered from core samples and free from other minerals such as quartz. These were subjected to infra-red absorption spectroscopy, using the technique described in Chapter 3, and the spectra obtained were compared with those obtained by Tuddenham and Lyon (1959). They all fall under group 1 of the classification proposed by the above authors in that each spectrum has one strong absorption band in the wave length region between 9.3 and 11.0 microns and two to three clearly visible absorption bands between 2.6 and 3.0 microns (Fig. 21). It was, however, not possible to distinguish the chlorites from mineralised and non-mineralised sections because no significant differences in absorption patterns were seen.

CHAPTER 6

DISCUSSION AND CONCLUSIONS

6.1 Discussion

The mineralogical, textural and geochemical features discussed in the previous chapters can be used to add to discussion of the metallogenesis of these sulphide minerals. Interpretations of mineralisation should account for (a) Source and availability of various essential and trace elements, (b) Mode of transportation and availability of sites for precipitation or deposition (environment of formation), (c) Genetic relationship with the host rocks, (d) Post depositional characteristics. These are discussed below for Parys Mountain in the light of information derived in this study.

6.1.1 Source and availability of elements

As outlined in Chapter 2, the Parys Mountain deposits can be considered as stratiform type based on field, megascopic and mineralogical characteristics. These stratiform deposits, because of a close association with a volcanic succession, and generally having a Co:Ni ratio of > 1 , are thought to be related to volcanism. Hutchinson (1973) defined volcanogenic sulphide deposits as strata bound lenticular bodies of massive pyrite mineralisation, containing variable amounts of chalcopyrite, sphalerite and galena in layered volcanic rocks. They are believed to have been formed subsequently by volcanic fumarolic activity which occurred periodically during volcanism. The Parys Mountain deposits have close similarities to the Type II of Hutchinson (1973), in metals, volcanic rocks, volcanic activity, tectonic position and geological age.

Hutchinson Classification Type II is as follows:-

Type II	Pb-Zn-Cu Pyrite
Associated volcanics	Intermediate to felsic, calc-alkaline volcanic suites; andesite, dacite-rhyolite tuff etc.
Type of volcanism	Felsic centres of explosive, Pyroclastic and ignimbritic activity. Subaqueous to subaerial.
Associated sediments	Epiclastic predominates
Tectonic position	Later eugeosynclinal orogenic stage
Examples	Mt. Isa (Proterozoic) New Brunswick (Ordovician)

Petrological studies by Thanasuthipithak (1974) has established the presence of all these characteristics at Parys Mountain and that the volcanics belong to an orogenic-calcalkaline magma series formed in a continental margin/ island arc environment.

That many of the world's economically workable sulphide deposits have been derived from volcanic processes is firmly established by many workers throughout the world. Detailed discussions of individual deposits are given in Stanton (1960), (1965), Hutchinson (1965), Krauskopf (1967), Schermerchorn (1970), Ferguson and Lambert (1972), Lusk (1972), Goosens (1972), Constantinove and Govett (1973), Sillitoe (1973), Strauss and Madel (1973), Roberts (1975), Thurlow et al., (1975), Spence and Spence (1975), Spence (1975), Jenks (1975) and Angus and Davis (1976).

6.1.2 Environment of formation

Many of the volcanogenic deposits quoted above, though related to volcanism are thought to have been formed by an interplay of volcanic-sedimentary or volcanic-hydrothermal processes. It has to be postulated that there existed a sedimentary volcanic basin at Parys Mountain in which thick volcanic products accumulated. The sulphide metallic phases, mainly iron sulphide from volcanic emanations, were also deposited along with the volcanic successions within certain restricted environments. Thanasuthipithak (1974) called such a process 'syndimentary-exhalative'. However, as pointed out by Anderson and Nash (1972) the word 'exhalative' implies vapour transport and there is no evidence at Parys Mountain that the metals were carried in the vapour phase. Alternative terms given by Anderson and Nash (1972) are volcanogene-sedimentaire, volcano-sedimentaire, and submarine volcanic sedimentary. The term volcanogenic-sedimentary (Ilavsky 1976) is perhaps the most suitable for the Parys Mountain mineralisation.

However, microscopic features discussed in Chapter 2 suggest that the mineralisation at Parys Mountain was not a single simple episode. Although much of the copper ore has been removed by previous mining operations, its paragenesis is clear and it is only the pyritic mineralisation that has obvious conformable or syngenetic features. The lead-zinc sulphides and sulpho-salts are later and they apparently show features of deposition from a multi-component hydrothermal system, though they could have resulted as complex substitutions in other sulphides. Where

deposition has occurred from such a system the mobility of ore metals is in decreasing order as experimentally given by Barnes and Czernansky (1967) Pb-Cu-Zn-Sn-Ni-Fe-Co; (this coincides with the general paragenesis). All these epigenetic minerals were formed in fractures, and interstitial infillings and replacements of the earlier pyritic mineralisation.

6.1.3 Relationship with the host rocks

As outlined above the pyritic mineralisation is reported to be conformable and syngenetic with the host volcanic succession. Epigenetic mineralisation though, complex mineralogically, shows some crosscutting features consistent with later formation or remobilisation, presumably during metamorphism.

6.1.4 Post depositional characteristics

The earlier pyritic mineralisation shows post depositional characteristics mainly the evidence of deformation and remobilisation. These are the cataclastic textures, fracturing recrystallisation of framboid pyrites, etc. which became vacant sites for the subsequent epigenetic mineralisation. Either both these phases, or the earlier pyritic mineralisation, were remobilised during the Caledonian orogeny (Thanasuthipithak, 1974).

Both in the earlier syngenetic mineralisation and later hydrothermal deposition the source for the metallic sulphide is believed to have been volcanic. This repetition of ore formation is not uncommon in volcanogenic sulphide deposits.

It can therefore be concluded that the Parys Mountain mineralisation is consistent with a volcanogenic-sedimentary deposit of a stratiform type later enriched by hydrothermal processes. This deposit was later remobilised during the Caledonian orogeny to produce many of the crosscutting features.

6.2 Summary of conclusions

In the present study of mineralogy and geochemistry of Parys Mountain sulphides and sulpho-salt minerals, the following conclusions are reached:

- 1) The mineralogy, paragenesis and association with a volcanic succession of rocks allow the interpretation that the deposit is both stratiform and conformable associated with volcanism. An earlier synsedimentary pyritic mineralisation has been enriched by an epigenetic

complex sulphide and sulpho-salt mineralisation.

- 2) The deviations in composition of the major sulphide minerals pyrite, chalcopyrite, sphalerite and galena from their stoichiometry are interpreted as due to presence of appreciable quantities of trace elements and complex substitutions.
- 3) Pyrite and chalcopyrite have relatively low trace element content and they mainly contain Co, Ni, Ba, As, Pb, Zn, also Cu in pyrite. The Co/Ni ratio in pyrites is generally > 1 . This is interpreted to indicate that the deposits are related to volcanism.
- 4) Sphalerite and galena are rich in As, Ag, Bi, Sb contained in solid solutions.
- 5) The iron content in sphalerite varies widely, and this is interpreted as being due to solid solution.
- 6) Measurements of cell edge of sphalerites, using both electron diffraction and X-ray diffraction techniques, showed it to vary linearly with iron content. Electron diffraction is thus an alternative method for measuring the iron content of sphalerites.
- 7) There is a good relationship between iron content and microhardness in sphalerite. However, this was found not to apply to the other sulphides, namely pyrite and chalcopyrite.
- 8) The chlorite group minerals, diabantite, ripidolite, grochauite, and aphrosiderite were formed in wall rocks at the contacts of the mineralisation. Chlorite 1b species was found in non-mineralised sections.

APPENDIX I

SAMPLE SELECTION AND PREPARATION

All the sulphide samples studies were taken from the diamond drill cores including some previously studied by Thanasuthipithak (1974), and only fresh looking material was selected. Two types of samples were required: a) sections of mineralised parts for polishing (reflected light microscopy, reflectivity, microhardness, and electron probe measurements); b) powdered sulphide minerals for chemical analyses, infrared and differential thermal studies. In the latter case, only mineral grains which were sufficiently coarse (average size $>$ about one mm) to be liberated with considerable amount of purity were selected. More finely grained minerals were analysed by electron probe on polished sections.

Sulphide mineral grains were liberated directly from the core specimen using an electrically vibrating needle. They were then thoroughly washed using acetone and distilled water and dried. They were examined under a binocular microscope and impurities were removed by hand. In some instances a heavy-liquid technique was used (Muller, 1967) to separate less coarse grained sulphides from fine grained gangue. In some cases the core chip was polished on a coarse grade abrasive paper to allow grain boundaries to be clearly seen before the grain was liberated. Most of the sphalerite samples were recovered in this way.

A certain amount of mineral impurity was, however, unavoidable. This was especially true of sphalerites and pyrites with some chalcopryrite exsolutions. Also some very fine grained gangue inclusions in sulphide minerals could not be separated.

APPENDIX 2

LABORATORY METHODS

2.1 Atomic Absorption Spectrophotometry (A. A. S.)

Solutions for A.A.S. were prepared by dissolving the sulphide samples in concentrated HCl and concentrated HNO_3 (Strasheim et al. 1960; in Angino and Billings, 1972). About 200 mg of powder was weighed accurately into a conical flask and 8 to 10 ml of concentrated HCl was added. This was allowed to stand for approximately one hour for the initial reaction to take place before adding 8 to 10 ml of concentrated HNO_3 . This method was used in preference to direct use of aquaregia to prevent basic nitrates being formed on the surface of the sulphide grains (Dolezal et al. 1968, in Ghosh, 1972). After adding HNO_3 some 3 hours were allowed for a clear solution to form. The solutions were stirred and then transferred to 150 or 250 ml volumetric flasks, made up to volume with double distilled water, and quickly transferred to polythene bottles. The solutions were analysed within three days of preparation because elements present in low concentrations are lost by absorption on to the sides of the bottle, if stored for longer periods.

Standards were prepared from stock solutions containing 1000 ppm of the element in each case. These stock solutions, except Mo were supplied from BDH Chemicals Limited. The Mo standard was prepared by dissolving 1.840g of ammonium paramolybdate ($(\text{NH}_4)_6\text{Mo}_7\text{O}_{24}\cdot 4\text{H}_2\text{O}$) in 1 litre of 1% ammonium hydroxide (NH_4OH), for 1000 ppm concentration.

Analyses for Cd, Co, Cu, Fe, Ni, Pb, Te and Zn were done using an air acetylene flame, and Mo and Ba were determined using a nitrous oxide acetylene flame. An integrated period of 0.5 seconds was allowed for each aspiration. At the beginning of each run, standard solutions were aspirated starting from lower concentration to higher concentration, followed by the sample solution. At least 4 readings were taken for each sample solution. The mean of these concentrations was taken and from it the weight % in the sample was calculated.

2.2 Electron probe microanalysis

Analyses were done on carbon coated polished sections and in some instances on the sections mounted in conducting bakelite. The standards used were either pure metals/elements or compounds (Table 41).

Analyses were done using a Cambridge Microscan V with a constant accelerating potential of 15 kV, a sample current of 0.3 mA and a beam current of 0.05 mA. The crystals used were PET (Pentaerythritol) and LiF (Lithium fluoride). Both crystals were used because readings were obtained simultaneously in two separate channels thus allowing two elements to be determined simultaneously. Counting rates were measured for intervals of 10 seconds. Peak intensities for various elements determined in each grain were read at least twice, and the mean taken. Similarly background readings also were taken at least twice.

A dead time correction was applied for counts more than 2000/second, though for count rates below 10,000 counts /second, the error is considered to be less than 1% (Adler, 1970). Dead counts were read from the graph supplied and were added to the measured counts. The concentration after applying dead time was calculated using the formula

$$\text{Wt \%} = \frac{\text{Peak-Background} + \text{Dead time (counts/second) of specimen} \times C}{\text{Peak-Background} + \text{Dead time (counts/second) of standard}}$$

where C is the weight percentage of the element in the standard.

The measured concentrations were subjected to corrections described by Long (1967), Adler (1970). Corrections for Atomic Number (Z), Fluorescence and Absorbance, were made using a computer programme produced in the Department of Metallurgy, University of Aston.

2.3 Reflectivity

Measurements of reflectivity were made on a Reichert Zetopan Ore Microscope equipped with a reflex microphotometer (Singh, 1965). Comparative quantitative measurements were made against Tungsten Titanium Carbide (WTiC) and silicon carbide (SiC), standards with reflectivity being calculated from the formula

$$R_{\lambda} \% \text{ of Mineral} = \frac{\text{Deflection Value of Mineral}}{\text{Deflection Value of Standard}} \times K$$

where K = calibrated reflectivity % of standard

λ = monochromatic wave length

R% = Reflectivity percentage

All measurements unless otherwise specified were made at a wave length of 589 nm in air. A glare correction was applied before calculating R% to compensate for reflections from the back of the objective (Bowie and Henry, 1964).

2.4 Indentation microhardness

Measurements of microhardness were made with a Leitz Durimet Microscope with an attached indenter. Varying loads of 50, 200 and 300 gm were applied to obtain a sharp indentation and an indentation time of 30 seconds was allowed for each specimen. The diagonals of the projected impression on the polished surface were measured using a travelling micrometer ocular. The hardness number was calculated using the formula

$$\text{VHN} = \frac{1854.4 \times L}{d^2}$$

where VHN = Vickers microhardness number in kg/mm^2

L = Load applied

d = Indentation diagonal

2.5 Infrared Absorption Spectroscopy

Samples for infrared studies were prepared by potassium bromide pellet method (Tuddenham and Lyon, 1959; and Lyon, 1967). Spectra were obtained on a Perkin-Elmer 237 Grating Infra red Spectrophotometer in the wave number region $600\text{-}4000\text{ cm}^{-1}$.

2.6 Differential Thermal Analysis

Analyses were made on samples of pyrite and chalcopyrite on a Dupont-900 Differential Analyser using a sample preparation technique described by McLaughlin (1967). Glass beads were used as standard. A heating rate of $50^\circ\text{C}/\text{minute}$ was applied, with the scale for chart paper of $100^\circ/\text{inch}$.

Sulphides contain corrosive elements such as S and As (Kopp and Kerr, 1957). Special techniques of diluting the samples with alumina to avoid corrosion by S or As were not employed because the maximum temperature reached was only 600°C .

REFERENCES

- Adler, I., (1970) X-ray emission spectrography in geology: in Methods in geochemistry and geophysics: Elsevier Publishing Company, Amsterdam, London and New York.
- Anderson, C. A., and Nash, J. T., (1972) Geology of the massive sulphide deposits at Jerome, Arizona - a re-interpretation: Econ. Geol., V. 67, pp. 845-863.
- Angino, E. E. and Billings, G. K., (1972) Atomic absorption spectrometry in geology: in Methods in geochemistry and geophysics: Elsevier Publishing Company, Amsterdam, London and New York.
- Angus, J. G. and Davis, G. R., (1976) Base metal enrichment in volcanic sublimates and secondary alteration products from Vesuvius and Vulcano: Mineralog. Mag., V. 40, pp. 481-486.
- Barnes, H. L. and Czernansky, G. K., (1967) Solubilities and transport of ore minerals: in Barnes, H. L., ed., Geochemistry of hydrothermal ore deposits: pp. 334-378. Holt, Rinehart and Winston Inc., New York/Chicago.
- Barton, P. B. and Skinner, B. J., (1967) Sulphide mineral stabilities: in Barnes, H. L., ed., Geochemistry of hydrothermal ore deposits: pp. 236-326. Holt, Rinehart and Winston, Inc., New York/Chicago.
- Bates, D. E. B., (1966) The geology of Parys Mountain: Welsh geol. quart., V. 2, pp. 27-29.
- Berry, L. G., (1940) Studies of mineral sulpho-salts IV: Galenobismuthite and 'lillianite': Am. Mineralogist, V. 25, pp. 726-734.
- Berry, L. G., (1974) Selected powder diffraction data for minerals. Joint Comm. Powder Diffraction Standards, Swarthmore, Penn., U. S. A.
- Bishara, W. W., (1966) Studies on trace and minor elements in sphalerite and galena from the Northern Pennine Ore field: Ph. D. thesis, Leeds University.
- Bowie, S. H. U. and Henry, N. F. M., (1964) Quantitative measurements with the Reflecting Polarising Microscope: Trans. Instn. of Min. Met., V. 73, pp. 467-478.
- Bowie, S. H. U. and Taylor, K., (1958) A system of ore mineral identification: Min. Mag., V. 99, pp. 265-277.

- Boyle, R. W. and Jambor, J. L., (1963) The geochemistry and geothermometry of sphalerites in the lead-zinc-silver lodes of the Keno Hill - Galena Hill area, Yukon: *Can. Min.*, V. 7, pp. 479-496.
- Campbell, F. A. and Ethier, V. G., (1974) Sulphur isotopes, iron content of sphalerites and ore textures in the Anvil ore body, Canada: *Econ. Geol.*, V. 69, pp. 482-493.
- Chang, L. L. Y. and Bever, J. E., (1973) Lead sulpho-salt minerals: Crystal Structures, stability relations and paragenesis: *Minerals, Sci. & Eng.*, V. 5, pp. 181-191.
- Constantinou, G., and Govett, G. J. S., (1973) Geology, geochemistry and genesis of Cyprus sulphide deposits: *Econ. Geol.* V. 68, pp. 843-858.
- Craig, J. R., (1967) Phase relations and mineral assemblages in the Ag-Bi-Pb-S system: *Miner. Deposita*, V. 1, pp. 278-306.
- Czemanske, G. K., and Hall, W., (1975) Mineralogy of the Darwin lead-silver-zinc deposit: *Econ. Geol.*, V. 70, pp. 1092-1110.
- El Shazly, E. M., (1951) The application of spectrographic analysis of minerals to the metallogenesis of lead-zinc ores: Ph. D. thesis, University of London.
- El Shazly, E. M., Webb, J. S. and Williams, D., (1957) Trace elements in sphalerite, galena and associated minerals from the British Isles: *Trans. Instn. Min. Met.*, V. 66, pp. 241-271.
- Evans, T. L., Campbell, F. A. and Krouse, H. R., (1968) A reconnaissance study of some Western Canadian lead-zinc deposits: *Econ. Geol.*, V. 63, pp. 349-359.
- Ferguson, J., and Lambert, I. B., (1972) Volcanic exhalations and metal enrichments at Matupi Harbour, New Britain, Territorial Protectorate of New Guinea: *Econ. Geol.*, V. 67, pp. 25-37.
- Fitton, J. G., and Hughes, D. J., (1970) Volcanism and plate tectonics in the British Ordovician: *Earth and Planetary Sci. Letters*, V. 8, pp. 223-228.
- Fleischer, M., (1955) Minor elements in some sulphide minerals: *Econ. Geol. 50th Anniv. Vol.*, pp. 970-1024.
- Frenzel, G., and Ottemann, J., (1967) Eine sulfidparagenese mit Kupferhaltigen Zonarpyrit von Nukundamu/Fiji: *Miner. Deposita*, V. 1, pp. 307-316.

- Ghosh, A.K., (1972) Trace element geochemistry and genesis of the copper ore deposits of the Singbhum shear zone, Eastern India: *Miner. Deposita* V. 6, pp. 292-313.
- Goosens, P.J., (1972) An exhalative volcanic iron sulphide stratabound deposit, near San Fernando, Azuay Province, Ecuador: *Econ. Geol.* V. 67, pp. 469-480.
- Gray, I.M., and Millman, A.P. (1962). Reflection characteristics of ore minerals: *Econ. Geol.* V. 51, pp. 325-349.
- Greenly, E., (1919) The geology of Anglesey: *Mem. Geol. Surv. Gt. Br.*, 2 vols.
- Hall, W.E., and Czernanske, G.K., (1972) Mineralogy and trace element content of the Wood River lead-silver deposits, Blaine County, Idaho: *Econ. Geol.*, V. 67, pp. 350-361.
- Hawkins, T.R.W., (1966) Bore holes at Parys Mountain near Amlwch, Anglesey: *Bull. Geol. Surv. Gt. Br.*, No. 24, pp. 7-18.
- Hey, H.M., (1954) A new review of the chlorites: *Mineralog. Mag.*, V. 30, pp. 277-292.
- Hunt, J.M., Wisherd M.P., & Bonham, L.C. (1950) Infrared absorption spectra of minerals and their inorganic compounds: *Analyt. chem.*, V. 22, pp. 1478-1497.
- Hutchinson, R.W., (1965) Genesis of Canadian massive sulphides re-considered by comparison to Cyprus deposits: *Can. Inst. Min. Met. Bull.*, V. 58, pp. 972-986.
- Hutchinson, R.W., (1973) Volcanogenic sulphide deposits and their metallogenic significance: *Econ. Geol.*, V. 68, pp. 1223-1246.
- Jenks, W.F., (1975) Origins of some massive pyritic ore deposits of western Europe: *Econ. Geol.*, V. 70, pp. 488-498.
- Kahn, L.H., (1968) Principles and practice of atomic absorption: *Advances in Chemistry series*, No. 73, pp. 183-229.
- Kakar, S.K., (1971) A study of the trace elements associated with lead-zinc ores of mid-Wales: Ph. D. thesis, University of Wales.

- Kalliokoski, J., (1959) Sphalerite temperatures from the Brunswick and Nigadoo deposits, New Brunswick, Canada: (Abst) Geol. Soc. Am. Bull., V. 70, p. 1626.
- Kopp, O. C., and Kerr, P. F., (1957) Differential Thermal Analyses of sulphides and arsenides: Am. Mineralogist, V. 42, pp. 445-454.
- Krauskopf, K. B., (1967) Source rocks for metal bearing fluids: in Barnes, H. L., ed., Geochemistry of hydrothermal ore deposits: pp. 1-28, Holt, Rinehart and Winston, Inc., New York/Chicago.
- Kullerud, G., (1953) The FeS-ZnS system - a geological thermometer: Norsk. Geol. Tidsskr., V. 32, pp. 61-147.
- Lambert, I. B., and Sato, T., (1974) The kuroko and associated ore deposits of Japan: A Review of their features and metallogenesis. Econ. Geol., V. 69, pp. 1215-1236.
- Loftus-Hills, G., and Solomon, M., (1967) Cobalt, nickel and selenium in sulphides as indicators of ore genesis: Miner. Deposita, V. 2, pp. 228-242.
- Long, J. V. P., (1967) Electron probe microanalysis: in Zussman, J., ed., Physical methods in determinative mineralogy., pp. 215-260. Academic Press, London, New York.
- Lusk, J., (1972) Examination of volcanic exhalative and biogenic origins for sulphur in the stratiform massive sulphide deposits of New Brunswick: Econ. Geol., V. 67, pp. 169-183.
- Manning, W., (1959) The Parys and Mona mines in Anglesey: in Future of non-ferrous mining in Great Britain and Ireland: Proceedings of the Symposium, Inst. Min. Met., London.
- McConnell, J. D. C., (1967) Electron microscopy and electron diffraction: in Zussman, J., ed., Physical methods in determinative mineralogy, pp. 335-370, Academic Press, London and New York.
- McLaughlin, R. J. W., (1967) Thermal techniques: in Zussman, J., ed., Physical methods in determinative mineralogy, pp. 405-444, Academic Press, London and New York.
- McLaughlin, R. J. W., (1967) Atomic absorption spectroscopy: in Zussman, J., ed., Physical methods in determinative mineralogy, pp. 475-486, Academic Press, London and New York.

- Muller, L. D., (1967) Laboratory methods of mineral separation: in Zussman, J., ed., Physical methods in determinative mineralogy, pp. 1-30, Academic Press, London and New York.
- Nash, T., (1975) Geochemical studies in the Park city district: Econ. Geol., V. 70, pp. 1038-1049.
- Petruk, W., and staff (1971) Characteristics of the sulphides: in Berry, L.G., ed., The Silver-arsenide deposits of the Cobalt-Gowganda region, Ontario., The Canadian Mineralogist, V. 2., pp. 196-231.
- Ramdohr, P., (1969) Ore minerals and their intergrowths: Oxford, Pergamon Press.
- Rankama, K., and Sahama, Th.G., (1950) Geochemistry: University of Chicago Press, Chicago.
- Raybould, J.G., (1973) The study of framboidal pyrites: Lithos, V. 6, pp. 175-182.
- Riley, J. F., (1974) The tetrahedrite-freibergite series with reference to the Mount Isa Pb-Zn-Ag ore body: Miner. Deposita, V. 9, pp. 117-124.
- Roberts, R.G., (1975) The geological setting of the Mattagami Lake mine, Quebec: A volcanogenic massive sulphide deposit: Econ. Geol., V. 70, pp. 115-129.
- Ross, V., (1957) Geochemistry, crystal structure and mineralogy, of the sulphides: Econ. Geol., V. 52, pp. 755-774.
- Schermerhorn, L. J. G., (1970) The deposition of volcanics and pyrite in Iberian pyrite belt: Miner. Deposita, V. 5, pp. 273-279.
- Sillitoe, R. H., (1973) Environments of formation of volcanogenic massive sulphide deposits: Econ. Geol., V. 68, pp. 1321-1336.
- Sims, P.K., and Barton, P. B., Jr., (1961) Some aspects of the geochemistry of sphalerite, Central City district, Colorado: Econ. Geol., V. 56, pp. 1221-1237.
- Singh, D. S., (1965) Measurement of spectral reflectivity with the Reichert Microphotometer: Trans. Inst. Min. Met., V. 74, pp. 901-916.
- Skinner, B. J., (1961) Unit cell edges of natural and synthetic sphalerites: Am. Mineralogist, V. 46, pp. 1399-1411.

- Skinner, B. J., Luce, F. D., and Makovicky, E., (1972) Studies of the Sulfosalts of Copper III: Phases and Phase relations in the system Cu-Sb-S; *Econ. Geol.*, V. 67, pp. 924-938.
- Spence, C. D., (1975) Volcanogenic features of the Vauze sulfide deposit, Noranda, Quebec: *Econ. Geol.*, V. 70, pp. 102-114.
- Spence, C. D., and de Rosen Spence, A. F., (1975) The place of sulfide mineralisation in the volcanic sequence at Noranda, Quebec: *Econ. Geol.*, V. 70, pp. 90-101.
- Springer, G., (1969) Electron probe analyses of tetrahedrite: *Neues, Jahr. Min. Mt.*, pp. 24-32.
- Stanton, R. L., (1960) General features of the conformable 'pyritic' ore bodies, Parts I & II: *Canadian Min. Metall. Bull.*, No. 573, pp. 24-29 and No. 574, pp. 66-74.
- Stanton, R. L., (1965) Mineral interfaces in stratiform ores: *Trans. Inst. Min. Met.*, V. 74, pp. 46-79.
- Stanton, R. L., (1972) *Ore Petrology*: New York, McGraw-Hill.
- Stanton, R. L., and Gorman, H., (1968) A phenomenological study of grain boundary migration in some common sulphides: *Econ. Geol.*, V. 63, pp. 907-923.
- Strauss, G. K., and Madel, J., (1974) Geology of massive sulphide deposits in the Spanish-Portuguese pyrite belt: *Geol. Rundschau*, V. 63, pp. 191-211.
- Suffel, G. G., (1965) Remarks on some sulphide deposits in volcanic extrusives: *Can. Inst. Min. Met. Bull.*, V. 58, pp. 1057-1063.
- Thanasuthipithak, T., (1974) Relationship of mineralisation to petrology at Parys Mountain, Anglesey: Ph. D. thesis, University of Aston in Birmingham.
- Thurlow, J. G., Swanson, E. A., and Strong, D. F., (1975) Geology and litho geochemistry of the Buchans polymetallic sulfide deposits, New Foundland: *Econ. Geol.*, V. 70, pp. 130-144.
- Tuddenham, W. M., and Lyon, J. R. P., (1959) Relation of infrared spectra and chemical analysis for some chlorites and related minerals: *Analyt. Chem.* 31, p. 377.
- Uytenbogaardt, W., and Burke, E. A. J., (1971) Tables for microscopic identification of ore minerals: Elsevier Publishing Company, Amsterdam, London and New York.

- Vaughan, D. J., (1971) Aspects of structure and bonding in the iron sulphides and related minerals: D. Phil., thesis, University of Oxford.
- Vlosov, K. A., (1964) Geochemistry and mineralogy of rare elements and genetic types of their deposits: Vol. 1, Geochemistry of rare elements. Jerusalem: Israel programme for scientific translations.
- Volborth, A., (1969) Elemental analysis in geochemistry Part A. Major elements: Methods in geochemistry and geophysics. Elsevier Publishing Company, Amsterdam, London and New York.
- Wager, L. R., and Brown, G. M., (1960) Collection and preparation of material for analysis: in Smales, A. A., Wager, L. R., ed., Methods in geochemistry. Interscience Publishers Inc., New York and London.
- Weunsch, B. J., (1974) Determination, relationships and classification of sulphide mineral structures: in Ribbe, P. H. (editor) Sulphide mineralogy. Min. Soc. Amer. Short course Notes 1, pp. W1-W20.
- Wheatly, C. J. V., (1971a) Economic geology of the Avoca mineralised belt, S. E. Ireland, and Parys Mountain, Anglesey: Ph. D. thesis, University of London.
- Wheatly, C. J. V., (1971b) Aspects of metallogenesis within the Southern Caledonides of Great Britain and Ireland: Trans. Inst. Min. Met., V. 80, pp. B 211-223.
- Williams, K. L., (1965) Determinations of the iron content of sphalerite: Econ. Geol., V. 60, pp. 1740-1747.
- Williams, K. L., (1974) Composition of sphalerites at Zeehan, Tasmania: Econ. Geol., V. 69, pp. 657-672.
- Young, B. B., and Millman, A. P., (1964) Microhardness and deformation characteristics of ore minerals: Trans. Inst. Min. Metall., V. 73, pp. 437-466.
- Zussman, J., (1967) X-ray diffraction: in Zussman, J., ed., Physical methods in determinative mineralogy. Academic Press, London and New York., pp. 261-334.

Table 1 Stratigraphic sequence at Parys Mountain

Age	(Hawkins, 1966)		(Thanasuthipithak, 1974)	
	Lithology	Thickness	Lithology	Thickness
Silurian	Grey shales with graptolites		Dark-grey to black slates	
Ordovician	Fine-grained sediments with a few occurrences of tuff in felsitic zone of silicification	600 ft	unconformity ?	
			Rhyolitic volcanic rocks	200m
			Grey to greenish-grey slates	600m
	Parys shales	720 ft		
	Black shales			
	* Grey shales weathering to brown and green			
	Grey micaceous shales with beds of sedimentary breccia	1200 ft		
----- Carmel Head Thrust -----				
Pre-Cambrian	Amlwch beds Pale-green phyllites		Chlorite schists, micaceous and granitoid gneisses, quartzitic gneisses.	

* Note: These are the Parys Green Shales of Greenly

Table 2. Classification of Ore Types.

Author	Mineralisation Type	Host rock or matrix	Mineralogy		Example
			Major	Minor	
Wolfenden (1967) (in Thanasuthipithak 1974)	Copper ore	Northern rhyolites and its contacts	Pyrite Chalcopyrite	Sphalerite Galena	Great ore Opencast lode, Hill Side open case, Black rock lode
	Bluestone ore	Dacite, silicified silurian slates and in rhyolites in contact with Ordovician slates	Argentiferous galena, Sphalerite	Chalcopyrite Pyrite	Clay shaft lode Black rock lode
	Pyritic ore	Within rhyolitic rocks	Pyrite	Chalcopyrite	Golden venture lode Carreg-y-doll lode, Middle lode, South branch lode North discovery lode
	Low grade Galena-Sphalerite ore	Disseminated in Ordovician slates	Galena Sphalerite		Not mined because of low grade
Wheatly 1971a	Pyritic zone	Black shale (Ordovician slates)	Pyrite Chalcopyrite	Pyrrhotite Sphalerite Galena	Disseminated in shale units
	Siliceous zone	Shales and tuffs (silicified Silurian slates and rhyolitic tuffs + siliceous sinter)	Pyrite Chalcopyrite Sphalerite Galena	Pyrrhotite Tetra- hedrite Bismuth- inite Native Bismuth	Carreg-y-doll, Golden Venture lode Charlotte lode, North discovery lode.
	Lead-zinc zone	Shales and tuffs	Sphalerite Galena Pyrite Chalcopyrite	Tetra- hedrite Bournon- ite	Morfa-dee and Black rock lodes, clay shaft lodes (Bluestone)
	Veins	Shales, tuffs and lavas	Galena, Sphalerite Chalcopyrite	Tetra- hedrite	Great cross Cowis Carreg-y-doll lode.

Table 3 Summary of some mineral forms at Parys Mountain

Ore Type	Form	Description	Minerals		Grain size/dmsns	Matrix/host matrix
			Major	Minor		
Pyritic ore	a) Layered sulphide form	Continuous and discontinuous layers conformable with the quartz and chloritic matrix parallel to foliation of the host rock. Some layers have a lenticular shape, major lens made up of smaller lenses giving rise to enechelon arrangement	Pyrite Chalcopyrite	Sphalerite	Thickness of the layer 2mm-1 cm.	Quartz-chloritic rocks
	b) Disseminated form	Well developed euhedral and subhedral pyrite grains disseminated in host rock.	Pyrite	Chalcopyrite	0.3mm-2 mm	Black shale, Dacite
Copper ore	a) Massive form	Irregular, coarse granular intergrowths	Pyrite Chalcopyrite	Sphalerite Galena	0.5cm to even 2cm in case of pyrite	Quartz is the main matrix
	b) Vein and stockwork form	Intersecting continuous and discontinuous veins of chalcopyrite	Chalcopyrite	Pyrite	Average width of the vein about 5 mm	Siliceous rocks
Blue-stone ore	Fine-grained	Microscopic granular intergrowths	Sphalerite Galena Chalcopyrite Pyrite	Sulphosalts	Average size < 1 mm	Shales and tuffs (Siliceous/sinter)

Table 4 Table showing the ore minerals at Parys Mountain

Name	Form	Microhardness range (Kg/mm ²)	Reflectivity % range at 589nm (air)	Special association
Pyrite	Euhedral, subhedral anhedral and fram- boidal	1027 - 1483	45.9 - 56.5	Euhedral pyrite with rutile
Chalco- pyrite	Anhedral, allotrio- morphic	174 - 221	38.2 - 42.6	
Sphaler- ite	Anhedral, rounded and as intergrowths with chalcopyrite	148 - 240	16.3 - 22.1	
Galena	Anhedral, sometimes intergrows with sphalerite	61 - 201	37.3 - 41.3	
Arseno- pyrite	Euhedral to subhedral	-	-	
Pyrrho- tite	Anhedral, irregular	-	-	
Tetra- hedrite- Tennantite	Fracture and interstitial infillings mainly in pyrite	279- 328	34.3 - 36.5 (Tetra- hedrite) 29.5 - 31.7 (Tennan- tite)	Pyrite
Bourn- onite	Inclusions - white in colour and anisotropic	-	-	Sphalerite
Lead sulpho- salts	Inclusions and intergrowths with mainly sphalerite and galena	-	39.3 - 43.5	Sphalerite and galena
Bismuth sulpho- salts	Interstitial infillings in pyrite, sphalerite	-	-	

Table 5 Summary of Textures shown by ore minerals at Parys Mountain

Texture	Primary		Texture	Secondary	
	Description	Mineral/s		Description	Mineral/s
1) Panidiomorphic	Euhedral grains	Pyrite	1) Cataclastic	Fractures and other deformative features are present	Pyrite
2) Framboidal	A spherical or subspherical aggregate of pyrite granules or microcrysts	Pyrite	2) Vein filling	A distinct and narrow filling of pyrite in the matrix in the form of a vein	Pyrite
3) Allotriomorphic granular	Irregular and anhedral grains	Pyrite Chalcopyrite Sphalerite Galena & sulphosalts	3) Interstitial fillings	Later formed minerals are present in the interstitial spaces of the previously formed grains	Sphalerite in Pyrite Tetra- hedrite - Tennan- tite in Pyrite
4) Mutual intergrowths	The two minerals are usually intergrown with no distinct boundary between them		4) Replacement	Later formed minerals replace previously formed minerals along peripheries	Chalcopyrite replaces pyrite
			5) Recrystallisation and homogenisation	An aggregate of framboidal or euhedral grains homogenised at the centre, retaining their respective outlines at the periphery	Pyrites

Table 6 Simplified Paragenetic diagram of Primary Sulphides and Sulpho-salts at Parys Mountain

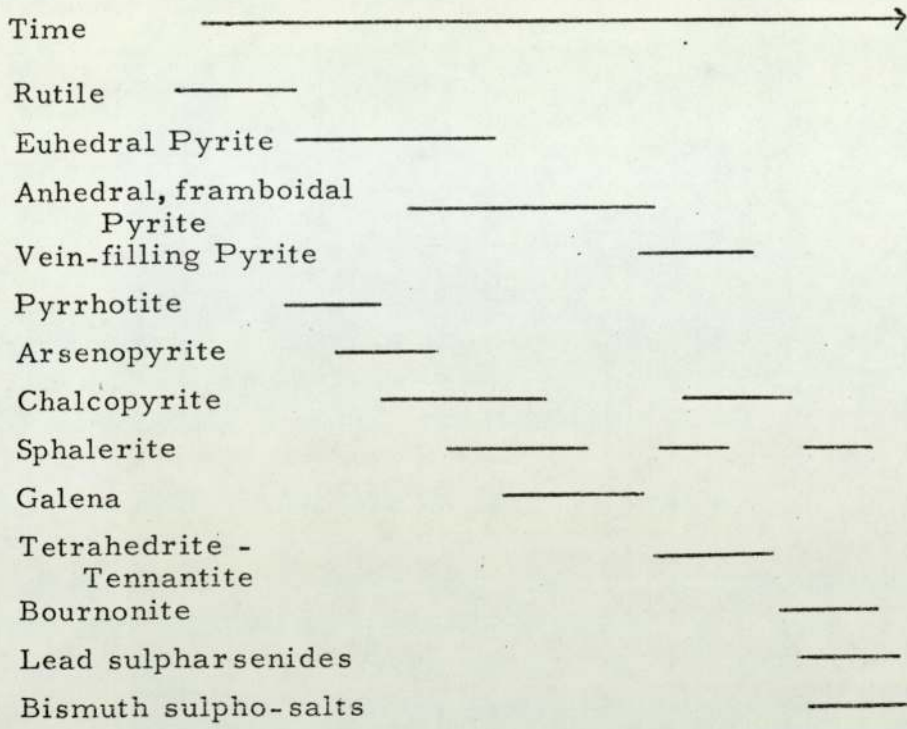


Table 7 Table to show the techniques employed and the nature of information obtained

Name of the technique	No. of samples	Minerals	Information
Reflected Light Microscopy	58	Sulphides and Sulpho-salts	Identification, Description and Paragenesis
Reflectivity	71 grains	a) Sulphides	a) Plotting of spectral reflectivity profiles.
		b) Sulpho-salts	b) For identification
Microhardness	56 grains	Sulphides	Quantitative measurement
X-ray diffraction (Powder Camera)	17	Sphalerite	Unit cell measurement
Electron diffraction	12	Sphalerite	Unit cell measurement
Atomic Absorption spectrophotometry	55	Sulphides	Major and trace element analysis
Electron Probe Microanalysis	74	Sulphides and Sulpho-salts	Major and trace element analysis
Infra-red absorption spectroscopy	13	Sulphides	To compare with published data and to see if related to composition
Differential thermal analysis	11	Pyrite, Chalcopyrite	To compare with published data and to see if related to composition

Explanation for Tables 8 - 12

A. A. S.	Atomic Absorption Spectrophotometry
EPMA	Electron Probe Microanalysis
A	Anhedral
F	Framboidal
E	Euhedral
S	Subhedral
X	Not determined
XX	Looked for but not detected
tr	traces

Results of EPMA are quoted in %

Results of A. A. S. are quoted in % for essential elements, and in parts per million for trace elements. Where EPMA and AAS analyses have both been done on the same sample, the analyses for essential elements are those done by EPMA and the trace elements unless quoted in % are those analysed by A.A.S.

Table 8 Table showing the essential and trace element composition of Pyrite

Sl. No.	Sample No.	Method	Type of grain	Fe	S	Total	As	Ba	Cd	Co	Cu	Mo	Ni	Pb	Te	Zn	Co/ Ni
1	A15/911	AAS	A	44.56	x	x	x	xx	xx	39	2873	xx	xx	107	49	414	-
2	A15/916	"	A	43.16	x	x	x	386	xx	66	1025	xx	46	208	52	502	1.43
3	A15/924	EPMA & AAS	F	43.98	54.65	0.16	xx	235	xx	1900	300	xx	400	xx	30	1400	4.75
4	A15/928	AAS	F	46.93	x	x	x	645	128	222	335	xx	37	38	133	41	6.00
5	A15/935	"	A	44.32	x	x	x	761	216	683	760	xx	47	429	15	22	14.53
6	A15/953	"	F	43.73	x	x	x	xx	xx	742	650	xx	349	1300	xx	141	2.13
7	A15/971	"	A	43.36	x	x	x	171	105	125	12715	46	158	808	xx	171	0.79
8	A15/980	"	E	44.84	x	x	x	108	91	340	454	37	253	535	23	874	1.30
9	A15/1193	"	A	43.55	x	x	x	150	76	206	348	193	16	411	xx	280	12.88
10	IM6/516' 6"	"	E	45.56	x	x	x	349	xx	xx	137	241.	97	390	68	289	-
11	IM6/770	"	S	44.97	x	x	x	148	xx	455	380	256	541	xx	xx	698	0.84
12	IM6/1044' 8"	"	S	44.64	x	x	x	205	xx	590	540	39	79	595	31	210	7.47
13	IM6/1101	"	S	47.15	x	x	x	103	xx	143	2575	xx	208	500	55	51	0.69
14	IM6/1108	"	S	46.33	x	x	x	xx	xx	105	120	13	84	873	88	30	1.25
15	IM6/1160	"	S	45.57	x	x	x	267	33	583	568	19	696	536	24	204	0.84
16	IM6/1179	"	A	44.96	x	x	x	105	xx	958	957	168	556	485	27	1854	1.72
17	IM6/1231	"	S	46.78	x	x	x	112	xx	487	479	xx	50	293	xx	325	9.74
18	IM6/1393	"	A	44.19	x	x	x	xx	45	795	2487	442	xx	316	xx	48	-
19	36A/1611	"	A	44.88	x	x	x	394	xx	36	2875	xx	xx	xx	128	71	-
20	36A/1617	"	A	45.23	x	x	x	268	xx	99	1563	xx	xx	xx	132	518	-
21	32-1108	"	E	45.71	x	x	x	827	275	697	340	xx	59	361	xx	108	11.81
22	32-1198	"	E	44.42	x	x	x	388	46	1486	379	xx	667	150	xx	190	2.23

Sl No.	Sample Number	Method	Type of grain	Fe	S	Total	As	Ba	Cd	Co	Cu	Mo	Ni	Pb	Te	Zn	Co/ Ni
23	HMA/1510	AAS	A	48.25	x	x	x	xx	xx	136	200	120	133	697	xx	629	1.02
24	H ₄ 3A/1837	"	A	47.65	x	x	x	130	xx	789	210	xx	50	804	xx	125	15.78
25	A14/1534	"	S	45.91	x	x	x	xx	xx	36	9767	xx	19	490	79	17	1.89
26	H14/186	EPMA & AAS	A	44.64	53.97	98.61	x	125	xx	2075	10800	xx	185	305	230	3280	11.22
27	H14/265	"	A	43.60	55.38	98.98	0.21	xx	320	268	tr	xx	563	152	xx	202	0.48
28	IM9/264	EPMA	S	46.56	52.88	99.44	0.11	x	tr	tr	tr	tr	tr	tr	x	0.28	
29	IM9/269	"	A	44.89	53.61	98.50	tr	x	xx	tr	0.12	tr	tr	1300	x	tr	
30	IM9/285	"	A	44.30	54.62	98.92	tr	x	tr	tr	0.10	tr	tr	tr	x	tr	
31	IM9/288	AAS	A	43.75	x	x	x	xx	260	83	2875	230	552	156	39	148	0.15
32	IM9/292' 6"	EPMA & AAS	A	43.19	54.97	98.16	tr	x	249	160	1260	68	276	589	36	380	0.58
33	IM9/294' 6"	EPMA	A	43.61	54.82	98.43	tr	x	tr	tr	0.11	tr	tr	tr	x	tr	
34	IM9/364' 6"	AAS	S	44.85	x	x	x	195	180	69	tr	100	410	440	169	260	0.17
35	M10/1512	EPMA	A	44.11	54.53	98.64	tr	x	0.10	tr	0.12	tr	tr	tr	x	tr	
36	M10/1540	EPMA	A	45.53	54.17	99.70	tr	x	0.13	tr	tr	tr	tr	tr	x	tr	
37	M10/1548	"	A	44.73	53.34	98.07	tr	x	0.11	tr	tr	xx	tr	tr	x	tr	
38	M10/1589	"	A	44.89	53.28	98.17	tr	x	tr	tr	tr	xx	tr	tr	x	tr	
39	M10/1599	"	A	46.84	52.35	99.19	tr	x	0.10	tr	tr	xx	tr	tr	x	tr	
40	M10/1608	"	A	44.38	54.69	99.07	tr	x	tr	0.12	tr	xx	tr	xx	x	tr	
41	H4/456	"	F	45.37	55.07	100.44	tr	x	tr	tr	tr	xx	xx	xx	x	xx	
42	H4/464	"	F	44.72	53.34	98.06	tr	x	tr	tr	tr	xx	xx	xx	x	tr	
43	H4/465	"	F	44.77	53.66	98.43	tr	x	tr	tr	tr	xx	xx	tr	x	xx	
44	H4/474	"	F	45.96	54.68	100.64	tr	x	tr	tr	tr	xx	xx	xx	x	tr	
45	C4/960	"	A	45.19	54.37	99.56	xx	x	tr	tr	tr	tr	xx	tr	x	xx	

Table 9 Table showing the essential and trace element composition of Chalcopyrite

Sl. No.	Sample Number	Method	Cu	Fe	S	Total	As	Ba	Bi	Cd	Co	Mo	Ni	Pb	Te	Zn
1	A15/920	AAS	34.37	31.16	x	x	924	x	xx	133	28	41	xx	xx	680	
2	A15/965	AAS	36.11	29.36	x	x	276	x	xx	60	140	12	325	62	395	
3	A15/1193	EPMA & AAS	35.05	32.37	34.20	101.62	tr	576	xx	250	405	510	500	155	55	2140
4	M10/1410	AAS	34.59	29.92	x	x	1653	x	xx	440	260	690	410	xx	1790	
5	M10/1521	EPMA & AAS	34.73	27.73	35.96	98.42	0.27	1385	xx	tr	710	tr	726	xx	74	1895
6	M10/1589	EPMA	35.81	28.15	36.15	100.11	tr	x	0.13	tr	tr	xx	tr	tr	x	tr
7	A14/1534	AAS	33.87	30.98	x	x	260	x	180	275	405	122	820	192	1388	
8	IM6/762	"	33.70	30.12	x	x	742	x	235	344	280	215	285	xx	696	
9	IM6/1392	"	32.40	30.34	x	x	210	x	446	486	85	190	1045	xx	851	
10	IM6/1393	EPMA	33.66	31.19	34.85	99.70	0.12	x	xx	tr	tr	tr	tr	x	tr	
11	H4/464	EPMA & AAS	34.64	30.15	36.58	101.37	0.11	xx	tr	211	410	300	510	tr	xx	345
12	H4/465	EPMA	34.72	25.80	36.49	97.01	tr	x	tr	tr	tr	tr	tr	tr	x	2100
13	H4/491	EPMA & AAS	34.54	27.75	36.61	98.90	tr	165	0.24	198	625	tr	446	656	xx	911
14	H4/581	EPMA	35.19	32.12	33.29	100.60	tr	x	tr	tr	tr	xx	tr	tr	x	0.38
15	IM9/264	"	32.07	29.25	36.93	98.25	tr	x	tr	xx	tr	xx	tr	tr	x	0.27
16	IM9/269	"	37.09	28.76	35.61	101.46	tr	x	0.13	xx	tr	xx	tr	tr	x	0.56
17	H14/171	AAS	32.27	30.69	x	-	x	368	x	98	290	xx	1060	316	xx	1100
18	H14/186	EPMA	35.25	32.81	32.81	100.54	xx	x	xx	tr	tr	xx	tr	tr	x	0.47
19	H43A/855	AAS	35.25	28.55	x	x	1526	x	xx	236	xx	xx	xx	313	xx	1295

Table 10 Table showing the essential and trace element composition of Sphalerite

Sl No.	Sample number	Method	Zn	Fe	S	Total	As	Fa	Bi	Cd	Co	Cu	Mn	Mo	Ni	Pb	Te	Type
1	H4/456	EPMA & AAS	58.99	4.21	35.27	98.47	0.12	2189	tr	0.17	206	2980	tr	xx	xx	1468	105	Exsolutions of Chalcopyrite present
2	H4/460	"	64.74	1.12	34.63	100.49	0.10	7222	tr	0.12	668	15360	tr	285	433	1286	xx	"
3	H4/467	AAS	53.01	13.77	x		x	1383	x	876	967	3157	x	xx	385	315	16	"
4	H4/473	EPMA	61.70	1.16	35.59	98.45	tr	x	xx	0.15	tr	0.33	xx	xx	xx	0.11	x	"
5	H4/474	"	54.87	12.47	32.23	99.57	tr	x	xx	0.13	tr	2.28	0.10	0.12	xx	0.14	x	"
6	H4/481	"	56.12	9.12	35.83	101.07	tr	x	0.14	0.13	tr	0.26	xx	0.12	xx	xx	x	"
7	H4/491	EPMA & AAS	51.68	14.21	35.28	101.17	tr	174	0.11	0.28	tr	4600	tr	2100	tr	286	149	"
8	IM9/283	EPMA	64.31	1.65	34.33	100.29	tr	x	tr	tr	tr	0.65	tr	tr	tr	0.12	x	"
9	IM9/285	"	60.43	2.75	37.08	100.26	tr	x	tr	0.11	tr	0.30	tr	tr	tr	tr	x	"
10	IM9/285'2"	EPMA & AAS	61.84	2.86	35.67	100.37	tr	1088	tr	388	tr	2870	tr	tr	tr	tr	x	"
11	IM9/292'6"	EPMA	62.66	1.59	35.19	99.44	0.12	x	tr	tr	xx	0.18	tr	xx	xx	tr	x	"
12	IM9/294'	"	62.07	5.09	33.94	101.10	tr	x	tr	tr	xx	0.40	tr	xx	xx	tr	x	"
13	IM9/294'6"	EPMA & AAS	61.87	2.96	36.15	100.98	tr	569	tr	215	135	1088	xx	565	340	85	260	"
14	IM6/1160	EPMA	54.56	11.58	35.61	101.75	xx	x	xx	0.12	xx	0.22	tr	xx	xx	0.12	x	No exsolutions
15	IM6/1392	EPMA	52.11	10.65	38.16	100.92	tr	x	xx	0.14	tr	0.10	tr	xx	xx	tr	x	"
16	M10/1548	"	62.78	3.73	32.97	99.48	0.37	x	xx	0.11	0.10	0.13	tr	tr	tr	tr	x	Exsolutions present
17	M10/1589	"	52.91	10.87	36.91	100.69	tr	x	tr	0.12	tr	2.75	tr	tr	xx	tr	x	"
18	A15/971	"	53.81	12.56	35.58	101.95	tr	x	tr	tr	tr	1.08	0.13	tr	xx	tr	x	"
19	A15/1193	"	58.56	2.39	38.66	99.61	tr	x	tr	tr	tr	tr	tr	tr	xx	tr	x	No exsolutions
20	A15/1194	AAS	57.91	2.19	x	-	x	168	x	228	886	330	x	384	xx	190	53	"
21	27-145	EPMA	55.26	11.78	32.98	100.02	tr	x	tr	tr	tr	0.47	tr	tr	xx	tr	x	Exsols pre-sent
22	H14/265	EPMA & AAS	63.82	2.77	33.74	100.33	tr	413	tr	1600	tr	4020	0.10	tr	tr	990	x	"

Table 11 Fe and Cd contents of Sphalerites

Sample	Fe%	Cd%
H 4/581	2.03	< 0.1
IM 9/269	18.32	0.33
IM 6/1044'8"	8.77	0.11
M 10/1512	1.69	0.18

Table 12. Table showing the essential and trace element composition of Galena

Sl. No.	Sample Number	Method	Pb	S	Total	Ag	As	Ba	Bi	Cd	Co	Cu	Fe	Mo	Ni	Sb	Sn	Te	Zn
1	H4/464	EPMA	81.61	14.87	96.48	0.12	2.33	x	1.18	0.11	xx	1.17	0.39	0.11	xx	0.21	tr	x	0.29
2	H4/474	"	83.88	15.75	99.63	0.11	1.78	x	0.34	tr	tr	0.10	0.12	0.12	tr	0.11	tr	x	0.21
3	H4/491	EPMA & AAS	83.12	15.65	98.77	tr	0.10	233	0.27	xx	xx	0.29	0.12	6.80	tr	0.10	tr	xx	0.59
4	H4/581	EPMA	80.15	15.13	95.28	tr	2.85	x	0.37	tr	tr	0.38	tr	xx	tr	0.15	tr	x	0.54
5	IM9/269	AAS	84.77	x		x	x	xx	x	xx	238	359	487	xx	xx	x	x	27	3188
6	IM9/283	AAS	85.14	x		x	x	455	x	775	xx	5680	1025	xx	xx	x	x	69	1164
7	IM9/294'6"	EPMA & AAS	85.19	14.60	99.83	0.28	1.26	xx	0.98	683	497	6100	913	386	145	0.19	0.13	15	2200
8	H14/265	EPMA	82.28	14.87	97.15	0.15	0.17	x	3.49	tr	tr	tr	0.11	xx	xx	0.37	tr	x	0.18
9	19-424	"	83.68	14.81	98.49	tr	2.24	x	0.38	tr	tr	0.14	tr	tr	tr	0.16	tr	x	0.15
10	A15/1193	AAS	87.75	x		x	x	396	x	412	xx	933	1236	xx	210	x	x	19	2130
11	M10/1584	EPMA	81.25	13.85	95.10	tr	1.18	x	3.17	0.11	tr	1.65	tr	tr	xx	0.14	0.13	x	0.26
12	M10/1589	"	83.19	14.67	97.86	tr	tr	x	1.07	tr	xx	0.14	tr	xx	xx	0.41	0.11	x	0.12

Table 13. Table showing the statistical data of Pyrite (in p.p.m. & %)

	Fe%	S%	As	Ba	Cd	Co	Cu	Mo	Ni	Pb	Te	Zn
Mean	45.01	54.14	-	314	395	523	1946	138	264	482	78	528
Minimum	42.83	52.35	-	103	33	30	120	13	16	38	15	17
Maximum	48.25	55.38	-	827	1300	2075	1,271	442	696	1300	230	3280

Table 14. Table showing the statistical data of Chalcopyrite (in p.p.m. & %)

	Cu%	Fe%	S%	As	Ba	Bi	Cd	Cc	Mo	Ni	Pb	Te	Zn
Mean	34.50	29.85	35.38	-	737	0.16%	231	401	217	410	481	95	1907
Minimum	32.40	25.80	32.48	-	165	1000	-	60	28	12	1000	55	1000
Maximum	37.09	32.81	36.93	-	1653	0.24%	446	710	510	1060	1045	192	5600

Table 15. Table showing the statistical data of Sphalerite (in p.p.m. & %)

	Cu%	Fe%	S%	As	Ba	Bi	Cd	Co	Cu	Mn	Mo	Ni	Pb	Te
Mean	58.46	6.43	35.29	0.17%	1651	0.12%	1190	588	5996	1157	951	382	874	116
Minimum	51.68	1.12	32.23	1000	168	1000	215	206	3.30%	1000	285	340	190	16
Maximum	64.74	18.32	38.66	0.37%	7222	0.13%	2780	1000	2.75%	1300	2100	433	1468	260

Table 16 Table showing the statistical data for Galena (in p. p. m. & %)

	Pb(%)	S(%)	Ag	As	Ba	Bi	Cd	Co	Cu	Fe	Mo	Ni	Sb	Sn	Te	Zn
Mean	83.50	14.91	16.50	1.48%	361	1.25%	820	367	4310	1378	841	202	0.20%	0.12%	33	2674
Minimum	80.15	13.85	1000	1.68%	233	0.27%	412	238	359	487	386	145	0.10%	1000	15	1164
Maximum	87.75	15.75	2800	2.85%	455	3.49%	1130	497	1.65%	3900	1200	260	0.37%	0.12%	69	5860

Table 17 Table showing the measured and calculated cell edges of Sphalerite

Sl. No.	Sample Number	Measured edge in Å	Calculated edge Å	Difference Å
1	H4/456	5.4146	5.4135	-0.0011
2	H4/460	5.4113	5.4107	-0.0006
3	H4/467	5.4221	5.4211	-0.0010
4	H4/473	5.4120	5.4108	-0.0012
5	H4/474	5.4194	5.4202	+0.0008
6	H4/481	5.4162	5.4172	+0.0010
7	H4/491	5.4201	5.4220	+0.0019
8	H4/581	5.4135	5.4109	-0.0026
9	IM6/1044'8"	5.4206	5.4169	-0.0037
10	IM6/1160	5.4198	5.4193	-0.0005
11	IM9/269	5.4249	5.4259	+0.0010
12	IM9/283	5.4118	5.4107	-0.0011
13	IM9/285'2"	5.4125	5.4118	-0.0007
14	IM9/292'6"	5.4114	5.4106	-0.0008
15	IM9/294'6"	5.4127	5.4118	-0.0009
16	M10/1512	5.4106	5.4114	+0.0008
17	H14/265	5.4152	5.4124	-0.0028

Table 18 Table showing the differences in measured cell edges of Sphalerite by X-ray diffraction and electron diffraction

Sl, No.	Sample number	X-ray diffraction Å	Electron diffraction Å	Difference Å
1	H4/456	5.4146	5.4284	0.0138
2	H4/460	5.4113	5.4226	0.0113
3	H4/491	5.4171	5.4248	0.0077
4	IM9/269	5.4249	5.4367	0.0118
5	IM9/283	5.4118	5.4320	0.0202
6	IM9/285'2"	5.4125	5.4177	0.0052
7	IM9/292'6"	5.4114	5.4236	0.0122
8	IM9/294'6"	5.4127	5.4381	0.0254
9	H14/265	5.4202	5.4207	0.0005
10	M10/1512	5.4106	5.4242	0.0136
11	19-424	* 5.4240	5.4196	0.0044
12	A15/1193	* 5.4115	5.4224	0.0109

* calculated edges

Table 19 Microhardness values of Pyrite

Sl. No.	Sample number	VHN kg/mm ²	Sl. No.	Sample number	VHN kg/mm ²
1	A15/916	1031	9	M10/1548	1097
2	A15/924	1037	10	M10/1589	1123
3	A15/971	1052	11	H14/186	1118
4	IM6/1044'8"	1063	12	M10/1599	1155
5	IM6/1160	1185	13	C4/960	1110
6	36A/1617	1123	14	H4/464	1168
7	H43A/1837'	1483	15	H14/265	1107
8	M10/1540	1089	16	32-1108	1063

Table 20 Microhardness values of Chalcopyrite

Sl. No.	Sample number	VHN kg/mm ²	Sl. No.	Sample number	VHN kg/mm ²
1	A15/920	203	7	IM9/264	221
2	A15/1193	210	8	M10/1548	197
3	A14/1534	201	9	M10/1589	187
4	M10/1521	201	10	H4/465	174
5	M10/1512	187	11	H4/491	194
6	H14/186	194	12	H4/171	210

Table 21 Microhardness values of Sphalerite

Sl. No.	Sample number	VHN kg/mm ²	Sl. No.	Sample number	VHN kg/mm ²
1	A15/971	230	11	IM9/288	206
2	IM6/1160	215	12	M10/1589	195
3	IM9/269	237	13	H4/465	148
4	19-424	203	14	M10/1548	175
5	M10/1512	161	15	H4/481	190
6	A15/1194	172	16	H4/474	210
7	H4/474	195	17	IM9/294'6"	172
8	H4/491	240	18	IM9/285	186
9	IM9/285'2"	168	19	H4/456	203
10	M10/1584	198			

Table 22 Microhardness values of Galena

Sl. No.	Sample number	VHN kg/mm ²	Sl. No.	Sample number	VHN kg/mm ²
1	19-424	61.7	5	H4/491	67.7
2	H4/464	107	6	M10/1584	201
3	H4/474	104	7	IM9/283	96.5
4	A15/1194	77.9	8	H14/265	87.8

Table 23 Table showing the spectral reflectivity values of Pyrite (R% air)

Section No.	400	420	440	460	480	500	520	540	560	580	589	600	620	640	660	680	700
A15/924	41.05	46.1	47.5	50.05	51.8	52.0	52.7	55.0	55.15	56.23	56.45	57.8	56.2	57.3	57.6	57.8	57.7
A15/980	42.5	45.20	45.5	45.18	47.5	48.2	49.3	49.6	49.8	50.25	52.1	52.5	52.6	53.8	53.9	53.8	53.7
A15/971	35.05	36.8	37.9	40.10	42.5	43.2	45.05	46.8	47.5	49.0	49.8	50.15	51.2	52.5	54.1	54.6	55.3
A14/1534	36.10	37.6	39.8	42.5	43.6	46.0	47.5	49.0	49.65	49.75	51.38	52.1	53.4	55.6	55.2	55.3	55.25
27-145	42.5	44.3	47.0	48.3	49.5	50.25	50.05	51.2	52.1	52.1	52.3	52.1	52.5	53.2	53.8	54.0	54.8
H43A/1855	34.8	36.7	37.2	38.3	41.8	42.9	45.6	47.5	48.3	50.6	52.1	52.35	53.68	54.8	54.95	55.0	54.86
32-1108	34.3	37.9	40.15	41.6	42.65	45.73	46.85	46.65	46.75	46.89	47.5	50.05	50.10	50.10	5.05	50.05	51.00
32-1198	36.0	37.5	39.8	42.5	45.05	47.8	48.5	50.05	50.10	50.5	52.01	52.25	52.20	51.85	51.80	51.8	50.75
H14/265	32.5	36.2	37.3	39.4	40.03	41.6	42.5	43.6	45.80	47.2	47.8	48.3	49.6	49.5	49.9	50.05	50.20
H4/456	36.2	41.8	42.6	43.2	45.05	46.7	47.5	48.3	50.15	52.6	53.9	54.8	55.05	55.10	55.20	55.15	55.20
H14/	36.25	37.5	37.8	40.16	41.68	42.5	43.6	45.2	46.25	46.8	47.6	47.8	49.3	50.2	52.6	52.3	52.2
19-424	38.12	40.10	42.3	42.7	44.3	45.6	46.2	47.6	48.3	48.9	49.2	50.12	50.15	49.8	50.2	49.5	50.05
A15/953	42.5	43.4	47.5	48.2	51.6	52.6	54.8	55.1	55.2	56.2	56.3	56.8	56.4	52.5	57.2	57.6	57.3
A15/950	37.0	37.5	39.5	40.25	45.06	46.3	47.5	49.3	47.25	50.15	50.30	52.2	55.0	55.25	55.6	55.3	55.75
A15/	34.8	35.2	36.8	36.9	37.5	40.2	41.5	42.2	43.8	45.0	46.3	49.8	51.3	52.6	52.7	52.6	53.9
32-1269	33.6	37.6	39.5	42.5	45.0	47.5	50.2	51.8	52.5	52.8	53.6	54.9	55.2	55.1	55.3	55.6	55.4
IM6/1101	35.0	37.8	41.8	44.8	47.5	47.8	51.3	51.85	52.6	53.6	52.8	55.05	55.61	55.3	55.4	55.6	55.0
A15/1193	32.6	34.6	39.6	42.5	45.0	47.2	49.6	49.8	50.1	51.2	51.8	52.5	52.6	52.7	52.9	54.0	55.0
IM6/1160	32.5	35.6	40.04	42.6	45.10	47.5	49.8	50.1	50.25	52.5	52.7	54.0	55.0	55.2	55.05	55.10	55.2
A15/941	36.8	37.5	39.8	42.3	42.8	46.8	47.9	50.0	50.10	50.15	51.28	52.20	52.5	52.8	52.4	52.3	52.0
IM6/231	34.3	35.0	36.2	37.2	40.02	40.35	42.5	42.6	44.8	46.35	47.21	47.75	48.3	48.4	48.2	48.3	49.5
A15/916	38.35	40.05	44.3	47.5	48.3	50.1	50.2	52.5	52.7	53.6	54.8	55.0	55.6	55.2	54.9	54.8	54.6
IM6/1392	34.8	35.0	40.35	42.6	46.3	46.2	47.5	47.8	47.9	50.25	50.20	53.2	52.5	53.2	53.1	53.6	53.78
H4/474	33.6	35.0	36.2	37.8	38.3	40.5	42.5	45.0	45.8	46.9	46.92	46.85	47.25	47.05	46.55	47.2	47.4
A15/935	33.8	36.8	38.6	42.6	47.5	48.9	51.6	52.6	53.78	54.2	53.98	54.5	55.2	55.1	52.8	52.3	52.6

	400	420	440	460	480	500	520	540	560	580	589	600	620	640	660	680	700
IM6/779	34.85	37.5	40.2	42.5	45.1	47.5	48.6	49.3	49.35	50.6	50.53	51.26	52.5	52.7	52.8	52.3	52.6
IM 9/364'2"	32.15	34.68	37.3	39.8	41.9	42.5	44.6	45.7	45.6	46.8	47.6	47.8	48.4	49.6	50.2	50.2	50.3
M10/1548	36.18	37.39	40.15	42.5	45.2	45.6	47.8	47.5	49.5	50.2	50.3	52.5	52.6	53.4	54.8	53.6	53.2
A15/965	33.5	35.7	37.8	40.2	42.5	43.6	44.2	45.6	45.2	45.7	45.9	50.2	51.2	52.3	50.25	50.15	51.2
36.A/1611	32.3	35.2	37.5	38.2	39.6	46.1	41.8	42.6	42.75	44.5	44.8	45.6	45.8	47.3	48.4	49.5	49.8
H4/491	32.2	35.0	37.5	41.5	42.6	44.2	45.5	47.5	48.4	50.5	51.6	52.5	53.6	53.8	53.65	53.78	53.6
M10/1610	34.8	34.6	40.2	42.6	46.8	47.5	50.2	51.8	52.6	54.6	54.5	54.7	55.2	55.3	55.0	55.2	55.4
IM9/292'6"	32.6	35.0	37.5	39.8	42.5	46.8	47.2	47.5	48.6	50.2	52.3	52.2	54.8	54.6	53.8	53.2	53.5

Table 24 Table showing the spectral reflectivity values of Chalcopyrite (R% air)

Section No.	400	420	440	460	480	500	520	540	560	580	589	600	620	640	660	680	700
32-1198	24.48	27.54	29.04	31.71	34.58	37.11	38.23	39.45	40.05	40.25	41.33	41.39	40.66	39.68	39.45	38.66	38.73
A15/1193	25.92	28.85	31.00	33.44	35.40	36.49	37.44	37.79	38.81	39.12	40.36	39.60	38.31	36.8	36.65	36.03	35.93
IM6/1393	22.75	24.26	26.28	28.54	29.91	31.13	31.32	33.38	34.56	36.15	38.21	38.66	37.81	36.65	36.2	34.75	34.2
A15/924	28.7	29.10	31.8	32.7	34.10	35.71	37.19	38.14	38.37	39.83	40.36	41.18	38.31	36.8	36.5	36.2	35.85
A15/943	21.91	22.95	24.60	27.45	30.10	34.76	35.68	36.61	37.31	38.25	38.65	39.30	40.31	39.58	37.61	37.5	36.31
H14/186	25.10	28.78	29.9	30.31	31.15	32.36	35.29	35.86	36.16	36.24	38.34	39.47	40.69	39.68	39.32	38.58	36.8
A15/965	20.40	22.56	25.08	27.81	30.44	32.38	33.98	34.39	36.35	37.12	38.88	38.56	37.34	38.31	36.62	36.12	35.2
IM6/779	28.15	29.28	30.36	31.38	32.67	34.73	36.01	37.28	37.92	39.13	40.62	39.47	40.31	39.8	38.86	38.05	36.9
H4/456	23.53	28.01	29.36	30.35	31.29	32.75	33.51	35.91	37.53	38.62	40.55	39.47	40.31	41.4	40.38	39.68	39.7
H43A/ 1855	27.35	28.45	28.86	29.81	30.34	33.76	35.29	36.94	37.92	39.6	41.35	40.44	40.75	40.4	40.2	39.65	39.3
H4/491	26.16	27.36	28.71	29.30	30.16	31.35	33.69	34.85	32.83	39.65	41.02	41.37	40.31	40.6	40.4	40.2	39.3
M10/1410	23.6	24.2	26.8	29.80	30.34	33.76	36.29	38.94	39.92	40.15	42.61	43.85	43.05	42.83	42.65	41.85	40.38

Table 25 Table showing the spectral reflectivity values of Sphalerite (R% in air)

Section No.	400	420	440	460	480	500	520	540	560	580	589	600	620	640	660	680	700
IM9/294' 6"	16.85	16.9	17.01	17.55	17.42	17.96	17.53	17.55	17.00	17.25	17.05	19.57	18.36	20.3	19.8	19.6	18.9
H4/456	19.2	18.9	18.8	18.9	18.62	18.78	17.53	17.6	17.37	17.25	17.60	18.85	18.64	18.32	18.8	20.3	20.6
IM9/285' 2"	18.35	18.2	17.85	17.83	17.79	16.52	16.32	15.89	15.81	16.35	17.7	16.32	17.8	19.32	20.3	19.46	19.3
A15/980	16.85	16.73	16.15	15.84	14.85	14.86	15.25	15.4	15.92	15.66	16.35	17.94	15.87	14.53	14.83	15.63	14.89
27-145	18.85	18.80	18.68	18.62	18.07	17.65	17.79	17.74	17.83	17.72	17.89	19.65	18.13	20.3	19.8	19.6	19.3
32-1198	22.24	22.20	22.16	22.04	21.95	21.87	22.31	22.04	22.29	22.25	22.13	23.92	22.67	23.07	20.32	19.87	19.6
19-424	16.85	16.76	16.64	16.58	16.11	16.66	16.40	16.50	16.07	16.95	16.98	17.08	15.87	14.53	13.53	13.6	13.3
A15/1193	19.31	19.25	19.05	18.72	19.91	18.80	17.93	18.28	18.79	17.72	17.92	17.65	18.13	19.23	20.3	19.6	19.4
IM6/1393	18.4	18.3	17.4	16.78	16.4	16.11	15.21	15.86	15.92	15.66	16.78	17.08	15.87	14.83	15.33	13.53	13.53
H14/265	19.15	19.03	18.8	18.6	18.6	17.89	17.35	17.63	17.65	17.43	17.35	17.28	16.87	16.47	17.15	17.6	17.6

Table 26 Table showing the spectral reflectivity values of Galena (R% air)

Section No.	400	420	440	460	480	500	520	540	560	580	589	600	620	640	660	680	700
H4 A14/456	32.95	33.45	32.80	32.8	32.15	32.00	31.92	32.38	34.16	35.86	37.31	37.31	38.15	37.7	35.57	34.2	33.2
19-424	43.31	43.15	43.05	42.66	40.65	38.85	39.29	38.91	38.37	37.83	38.3	39.6	37.39	41.4	40.8	41.2	40.5
A15/1193	45.92	45.24	45.15	45.05	45.24	43.95	42.38	41.71	40.57	39.45	40.25	41.18	36.13	36.8	36.5	37.2	36.68
H4/491	43.93	43.65	43.35	42.84	42.64	41.96	41.35	41.39	41.08	40.68	41.32	42.36	43.06	46.0	45.8	45.63	44.83
M10/1584	38.75	38.65	38.3	36.09	35.19	35.69	33.26	32.79	32.73	32.74	32.47	31.87	33.22	34.42	36.35	33.2	31.2

Table 27

Composition of Arsenopyrite

	M 10/1599 %	M 10/1608 %	Theoretical composition %
Fe	36.06	37.11	34.30
As	42.78	43.23	46.01
Co	tr	tr	
Ni	tr	tr	
Cu	tr	tr	
Pb	tr	tr	
Zn	tr	tr	
S	20.76	21.25	19.69
Total	99.60	101.59	100.00

Table 28 List of Sulpho-salts found at Parys Mountain

General classification	Name	Theoretical formula
Copper Sulpho-salts	Tetrahedrite-Tennantite	$(\text{Cu Fe Zn Hg})_{12}$ $(\text{Sb As})_4\text{S}_{13}$
Copper-Lead Sulpho-salt	Bournonite	Pb Cu Sb S_3
Lead Bismuth Sulpho-salts	Galenobismuthite Kobellite	$\text{Pb Bi}_2\text{S}_4$ $\text{Pb (Bi, Sb)}_2\text{S}_5$
Lead Sulpharsenides	Lead Sulpharsenide	Pb-As-S (varying)

Table 29 Composition of Tetrahedrite - Tennantites

Sample No.	1	2	3	4	5	6	7	8	9	10	11	12	13
Element Cu	H4/473	H4/464	H4/456a	H4/456b	27-145	H4/474	27-145	H4/491	M10/1548				
	34.35	36.12	33.76	36.31	39.67	32.39	37.88	31.61	28.78	34.7	32.6	34.4	34.9
Ag	0.1	tr	0.31	tr	0.55	tr	0.23	1.28	xx	3.1	5.4	1.8	2.6
Fe	9.54	8.42	10.18	9.61	6.05	4.31	7.04	8.31	3.16	1.7	1.3	4.9	3.9
Zn	2.38	1.29	5.36	2.23	4.24	8.18	4.69	5.15	1.29	5.7	6.1	2.6	2.5
Sb	24.77	28.52	23.35	22.85	22.12	23.67	tr	1.38	0.12	25.1	28.2	29.8	29.8
As	2.1	3.2	2.1	4.48	1.18	3.28	22.16	24.29	41.57	2.7	0.8	1.1	0.8
Bi	0.32	0.89	0.67	tr	xx	xx	1.42	0.87	xx	-	-	-	-
S	25.45	23.25	26.18	25.03	23.32	26.66	27.47	24.63	25.12	25.2	24.5	25.0	24.7
Total	99.01	98.69	101.91	100.51	97.75	98.49	100.91	97.52	100.04	98.2	98.9	99.6	99.2

tr - traces xx not detected

- 1 - 6 Parys Mountain Tetrahedrites (Present Study)
- 7 - 9 Parys Mountain Tennantites (Present Study)
- 10 Parys Mountain Tetrahedrite Hill Side open cast, Bluestone adit dump (Analyst: Wheatly 1971a)
- 11 Parys Mountain Tetrahedrite, Morfa-du Ida Shafi dump (Analyst:Wheatly 1971a)
- 12 West Avoca Tetrahedrite, South Lode. (Analyst: Wheatly 1971a)
- 13 East Avoca Tetrahedrite (Analyst: Wheatly 1971a).

Table 30 Table giving the atomic proportions for Tetrahedrites-Tennantites (Present Study)

	T e t r a h e d r i t e s				T e n n a n t i t e s				
	H4/473	H4/464	H4/456a	H4/456b	27-145	H4/474	27-145	H4/491	M10/1548
Cu	8.66	9.23	7.99	10.59	9.33	8.59	8.99	8.10	10.27
Ag	0.01	-	0.04	-	0.07	-	0.03	0.19	-
Fe	2.73	2.44	2.74	1.05	1.62	1.30	1.90	2.42	1.28
Zn	0.58	0.32	1.23	0.37	0.97	2.10	1.08	1.28	0.45
Sb	3.49	3.33	3.44	3.03	3.53	3.26	0.00	0.13	-
As	0.48	0.61	0.50	0.97	0.47	0.74	3.90	3.82	3.99
Bi	0.02	0.06	0.06	-	-	-	0.09	0.05	0.00
S	12.93	11.37	12.79	13.95	11.54	13.90	12.48	11.42	11.50

Table 31 Composition and atomic proportions of Bournonite

	Composition						Atomic Proportions	
	1	2	3	4	5	6	1	2
Cu	15.22	20.72	13.0	13.6	14.2	12.3	1.37	1.58
Pb	39.81	43.86	42.4	44.6	43.8	42.9	1.10	1.03
Sb	22.84	16.17	24.9	22.7	22.7	25.3	1.07	0.64
As	2.49	3.67	-	-			0.19	0.24
Bi	0.12	0.22	-	-			0.00	0.00
Fe	xx	0.25	-	-			-	0.02
Zn	0.16	0.14	-	-			0.01	0.01
S	18.17	15.62	19.7	19.3	20.5	19.6	3.25	2.46
Total	98.81	100.65	100.0	100.2	101.2	100.1		

1. Parys Mountain, H4/465 (Present Study)
2. Parys Mountain, M10/1548 (Present Study)
3. Theoretical Composition
4. East Avoca, Tigroney (Analyst: Wheatly, 1971a)
5. No. 1A, draw point, Avoca (Analyst: Wheatly, 1971a)
6. Wood river Lead Silver deposit, Idaho (Analysts: Hall and Czernanske, 1972)

Table 32 Composition and atomic proportions of Kobellite

	Composition				Atomic Proportions	
	1	2	3	4	1	2
Pb	40.26	43.18	44.4	47.1	5.51	8.77
Cu	2.86	2.19	-	0.9	1.27	1.45
Bi	30.22	32.15	29.9	32.1	4.10	6.47
Sb	6.12	4.23	8.6	4.5	1.43	1.46
Fe	3.12	1.29	-	-	0.65	0.97
As	1.31	0.88	-	-	0.05	0.00
S	17.18	16.19	17.2	15.7	15.20	21.25
Total	101.07	100.11	100.1	100.3		

1. Parys Mountain H4/474
2. Parys Mountain M10/1548
3. Theoretical Composition
4. West Avoca (Analyst: Wheatly, 1971a)

Table 33 Composition and atomic proportions of Galenobismuthite

	Composition				Atomic Proportions
	1	2	3	4	1
Bi	43.16	55.5	54.69	58.0	1.47
Cu	3.18	-			0.36
Pb	26.47	27.5	27.65	24.7	0.83
Zn	10.12				1.10
Fe	0.39				0.00
S	13.78	17.0	17.35	17.0	3.06
	97.10	100.0	99.69	99.7	

1. Parys Mountain H4/474
2. Theoretical Composition
3. Type Material (Analyst: Sjogren (1878) in Berry, 1940)
4. Bally Coog, Avoca (Analyst: Wheatly, 1971a)

Table 34 Composition and atomic proportions of Lead Sulpharsenides

	Composition		Atomic Proportions	
	1	2	1	2
Cu	0.18	0.28	0.03	0.06
Pb	69.68	68.18	3.17	4.21
Sb	0.13	0.05	0.01	0.00
As	13.24	15.37	1.66	2.63
Fe	0.16	0.38	0.03	0.09
Zn	1.88	0.19	0.27	0.04
Bi	xx	xx		
S	13.82	14.38	4.06	5.75
Total	99.09	98.83		

1. Parys Mountain 19-424
2. Parys Mountain M10/1589

Table 35 X-ray Powder diffraction data for Diabantite

d Å (from Tables 7-171)	hkl	d Å measured
7.08	002	7.081
3.541	004	3.541
2.458	132, 20 $\bar{3}$	2.458
2.271	132, 20 $\bar{4}$	2.276
1.829	13 $\bar{6}$, 205	1.829
1.550	33 $\bar{1}$, 060	1.542
1.360	334, 065, 336	1.368

Table 36 X-ray Powder diffraction data for Ripidolite

d Å (from Tables 7-76)	hkl	d Å measured
14.1	001	14.119
7.07	002	7.076
4.724	003	4.720
3.537	004	3.534
2.599	(131, 20 $\bar{2}$)	2.600
2.450	132, 20 $\bar{3}$	2.452
1.826	13 $\bar{6}$, 205	1.826
1.665	13 $\bar{7}$, 206	1.666
1.547	33 $\bar{1}$, 060	1.546

Table 37 X-ray Powder diffraction data for Clinocllore

d Å from Tables 19-749	hkl	d Å measured
14.3	001	14.348
7.12	002	7.115
3.56	004	3.559
2.435	132	2.438
2.255	133	2.256
1.535	24 $\bar{5}$, 060	1.536

Table 38 X-ray Powder diffraction data for Aphrosiderite

d Å from Tables 2-243	hkl	d Å measured
7.05	002	7.047
3.52	004	3.527
2.83	005	2.822
2.67	200	2.672
1.559	060	1.559

Table 39 X-ray Powder diffraction data for Grochautite

d Å from Tables 7-165	hkl	d Å measured
14.0	001	14.029
7.08	002	7.081
3.545	004	3.545
2.543	13 $\bar{2}$, $\bar{2}$ 01	2.544
2.842	005	2.844

Table 40

X-ray powder data for Chlorite 1b

$d(\text{\AA})$ from Tables 16-351	hkl	$d \text{\AA}$ measured
14.4	001	14.392
7.15	002	7.155
2.475	$20\bar{3}$	2.470
2.29	$20\bar{4}$	2.287
1.548	060	1.549

- 35 36A/1617 (Pyrite with little chalcopyrite), IM6/1044'8" (Pyrite), 36A/1611 (Pyrite)
- 36 36A/1670 (Pyrite), M10/1630 (Pyrite), A15/941 (Pyrite with little chalcopyrite), M10/1410 (Chalcopyrite with some pyrite)
- 37 IM9/269 (Sphalerite with some pyrite), 32-1198 (Pyrite with little sphalerite)
- 38, 39 IM6/1231 (Pyrite), IM6/1365 (Pyrite, Chalcopyrite with little sphalerite; in this section only grochaultite is present)
- 40 IM6/1359, 36A/1525, 6-527, H17A/1510, H43A/1845 (non-mineralised sections).

Table 41

Standards used for Microprobe Analysis

Element	Standard	Radiation
Ag	Pure Metal	Ag K_{α}
As	Pure Element	As K_{α}
Bi	Pure Metal	Bi L_{α}
Cd	Pure Metal	Cd L_{α}
Co	Pure Metal	Co K_{α}
Cu	Pure Metal	Cu K_{α}
Fe	FeS ₂ 46.55% Fe	Fe K_{α}
Mn	Pure Metal	Mn K_{α}
Mo	Pure Metal	Mo L_{α}
Ni	Pure Metal	Ni K_{α}
Pb	PbS 86.62% Pb	Pb M_{α}
S	FeS ₂ 53.45% S	S K_{α}
Sb	Pure Element	Sb L_{α}
Se	No Standard available	-
Sn	Pure Metal	Sn K_{α}
Zn	Pure Metal	Zn K_{α}

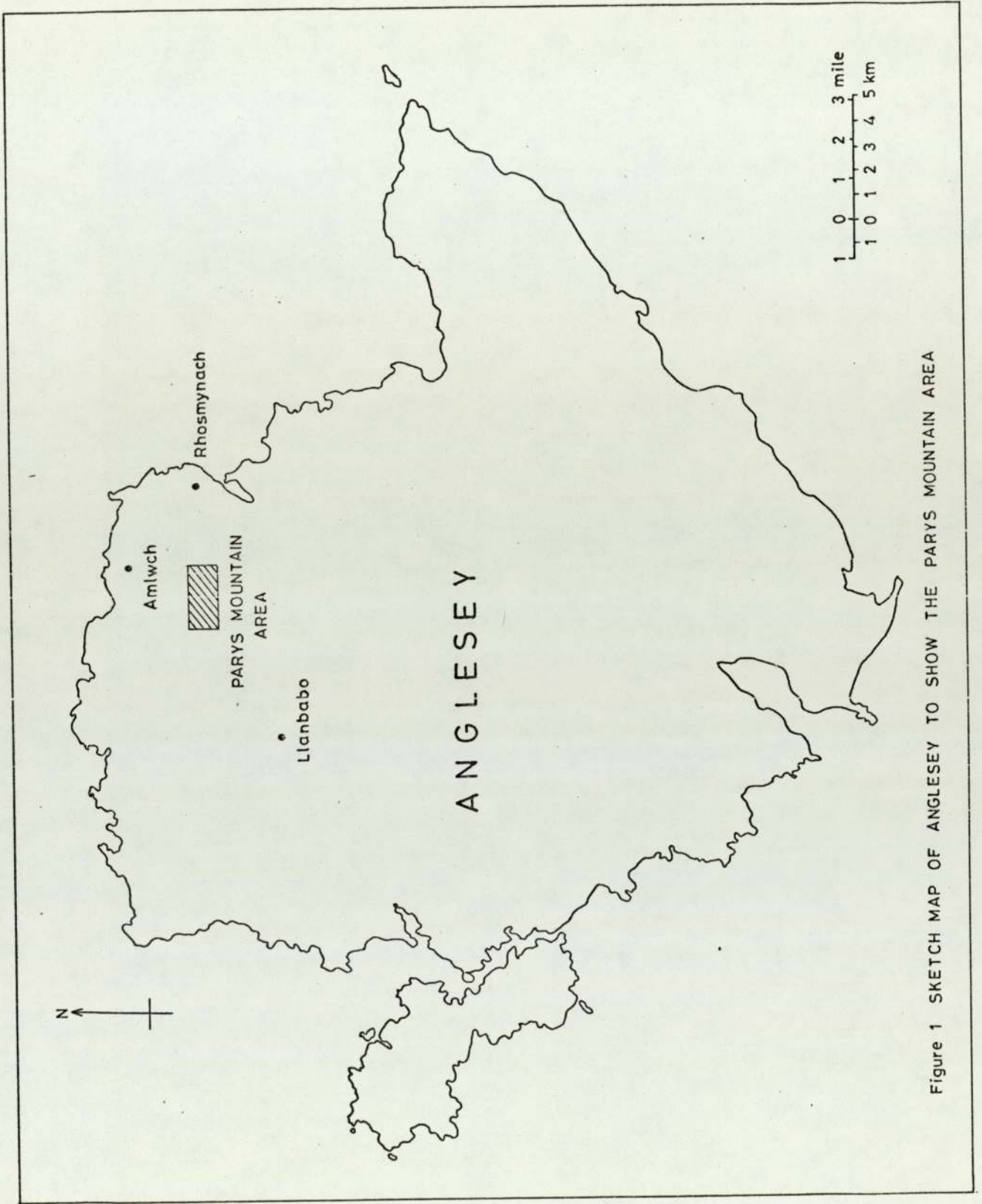
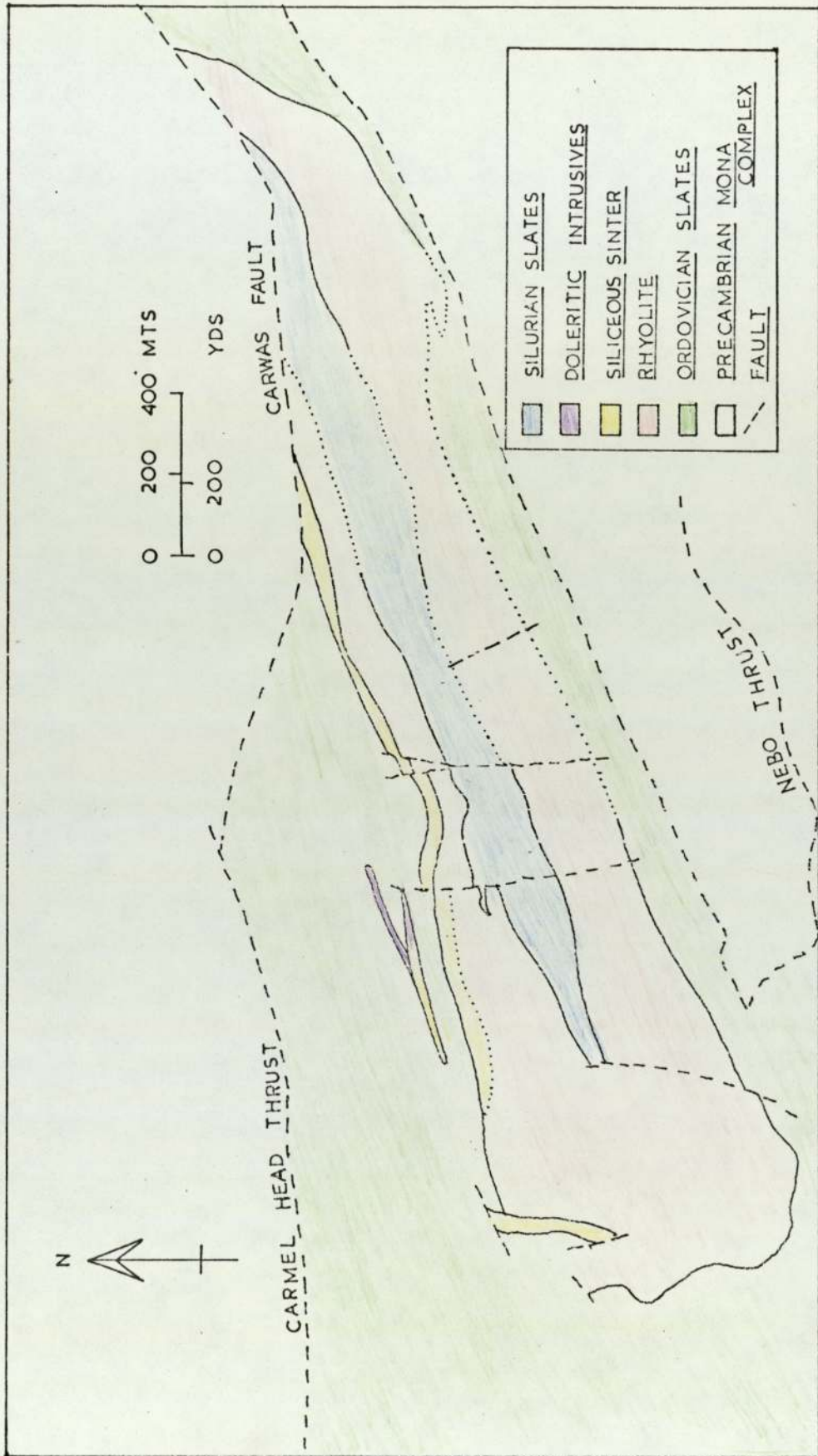


Figure 1 SKETCH MAP OF ANGLESEY TO SHOW THE PARYS MOUNTAIN AREA

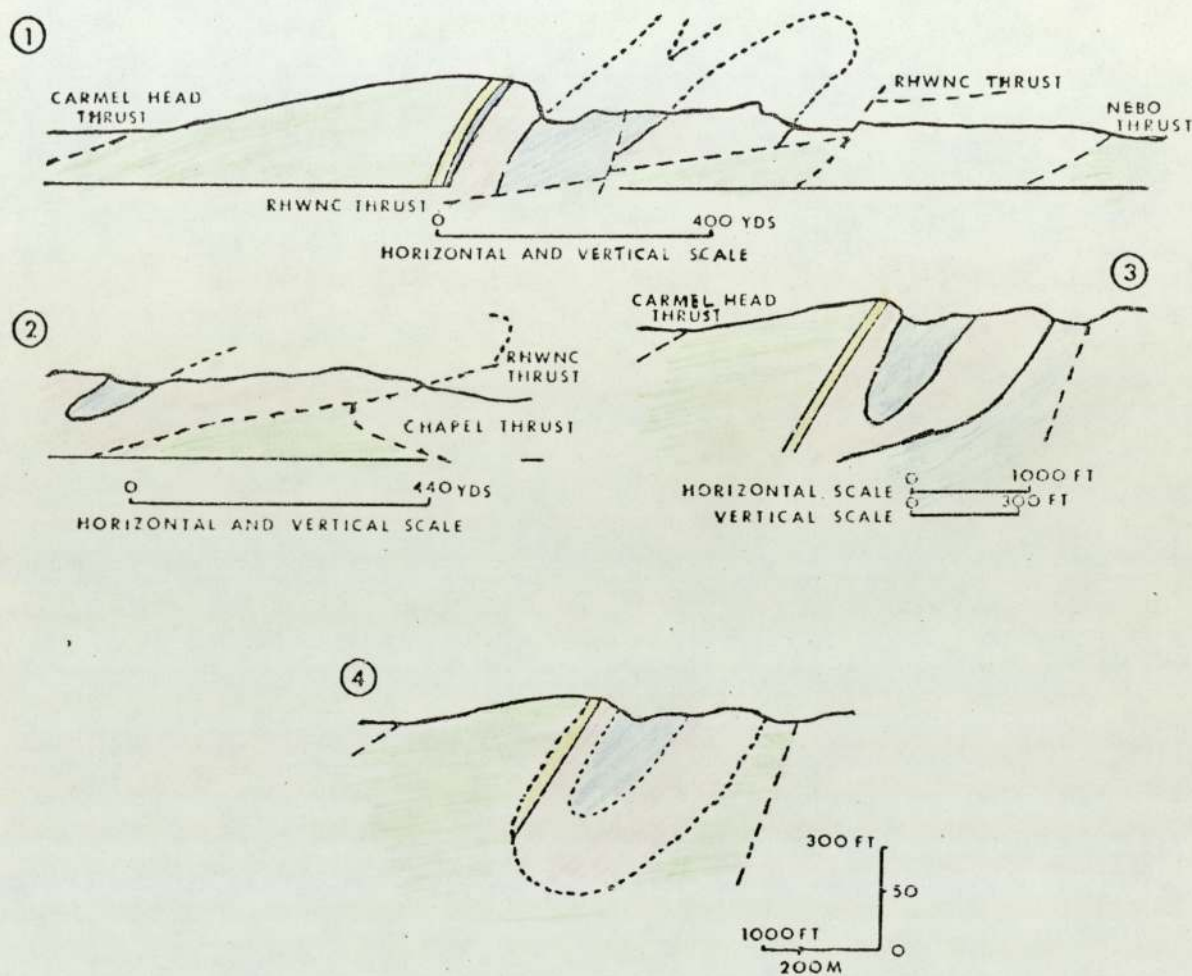
FIGURE 2



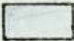
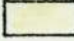
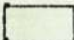
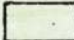

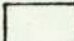
Simplified Geological map of Parys Mountain Area (after Thanasuthipithak, 1974)

FIGURE 3

CROSS SECTIONS ILLUSTRATING THE STRUCTURAL INTERPRETATIONS
OF PARYS MOUNTAIN



- ① SECTION THROUGH THE CENTRAL PART OF PARYS MOUNTAIN (AFTER GREENLY 1919)
- ② SECTION THROUGH THE WESTERN END OF PARYS MOUNTAIN (AFTER GREENLY 1919)
- ③ SECTION THROUGH THE CENTRAL PART OF PARYS MOUNTAIN (AFTER MANNING 1959)
- ④ SECTION THROUGH THE CENTRAL PART OF PARYS MOUNTAIN AFTER THANASUTHIPITHAK 1974
(cf. WHEATLEY, 1971)

	SILURIAN SLATE		SILICEOUS SINTER
	DACITE		ORDOVICIAN SLATE
	RHYOLITE		PRECAMBRIAN MONA COMPLEX

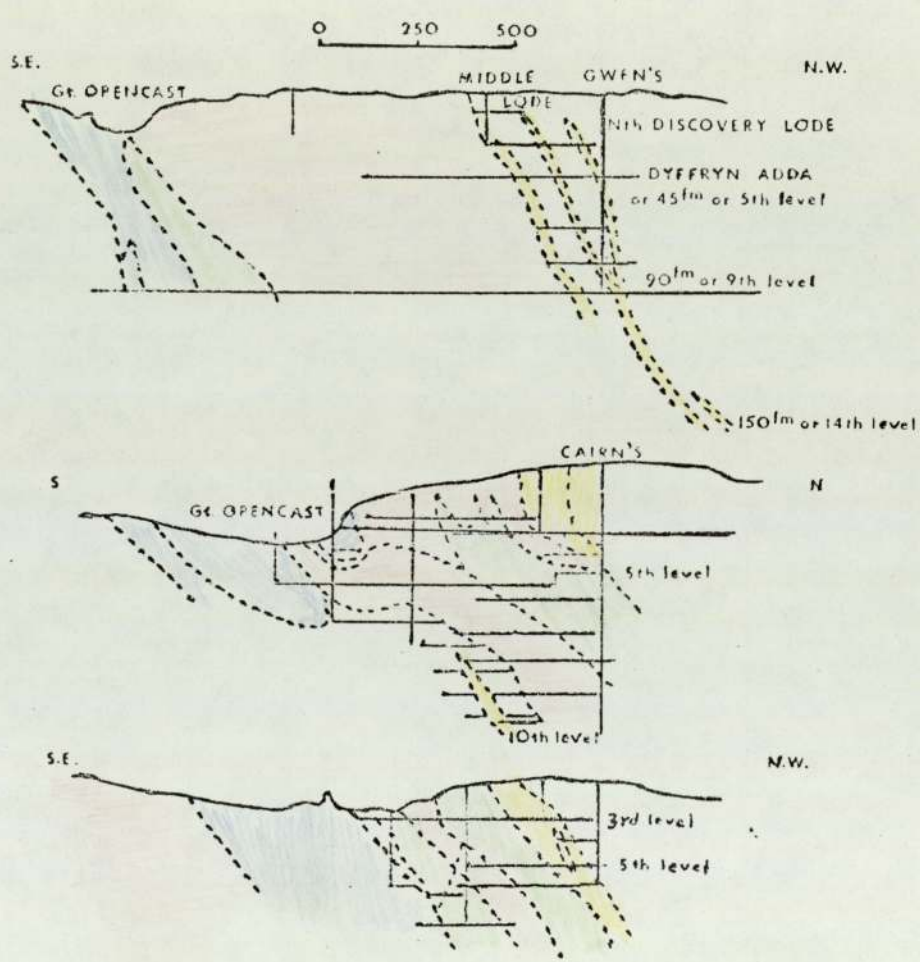
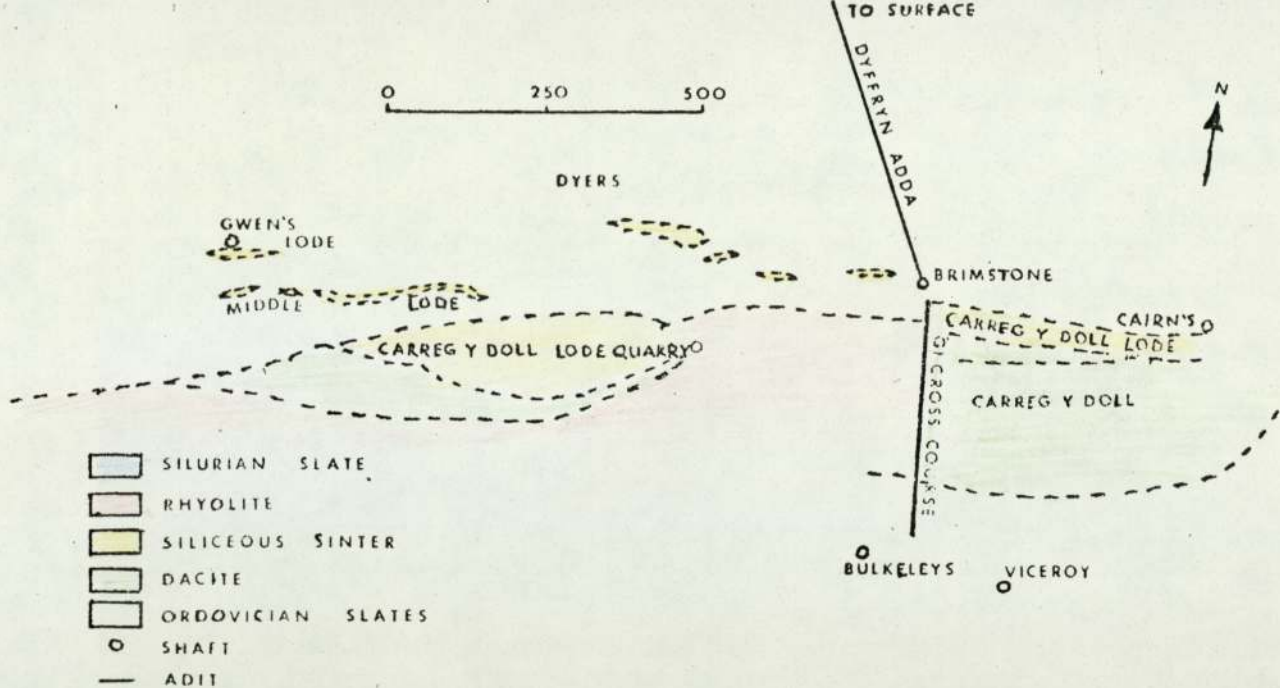
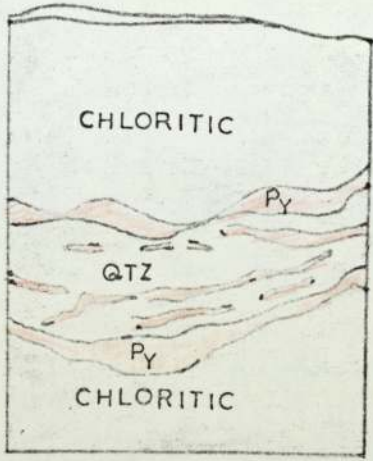


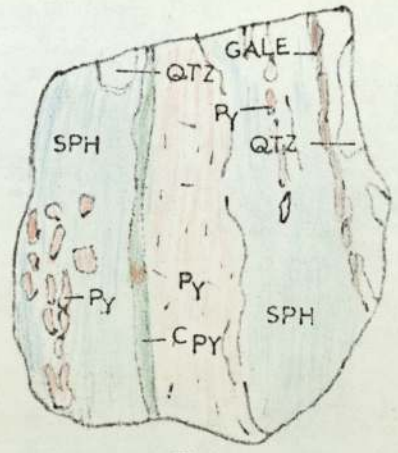
Figure 4

Sections illustrating the various lodes (after Manning, 1959)

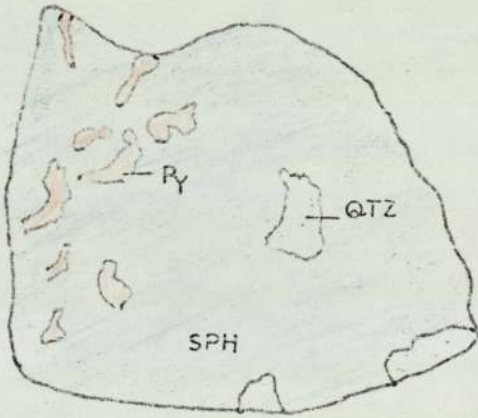
FIGURE 5



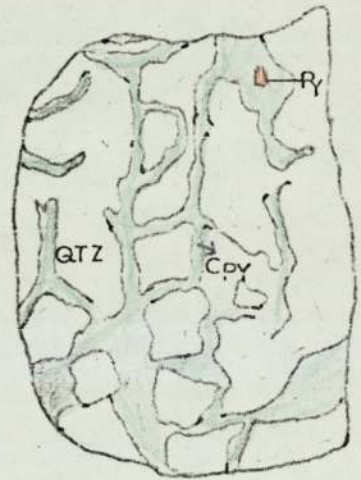
A



B



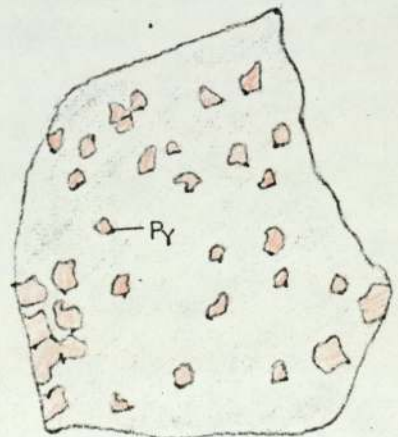
C



D



E



F

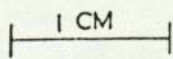


Fig. 6a

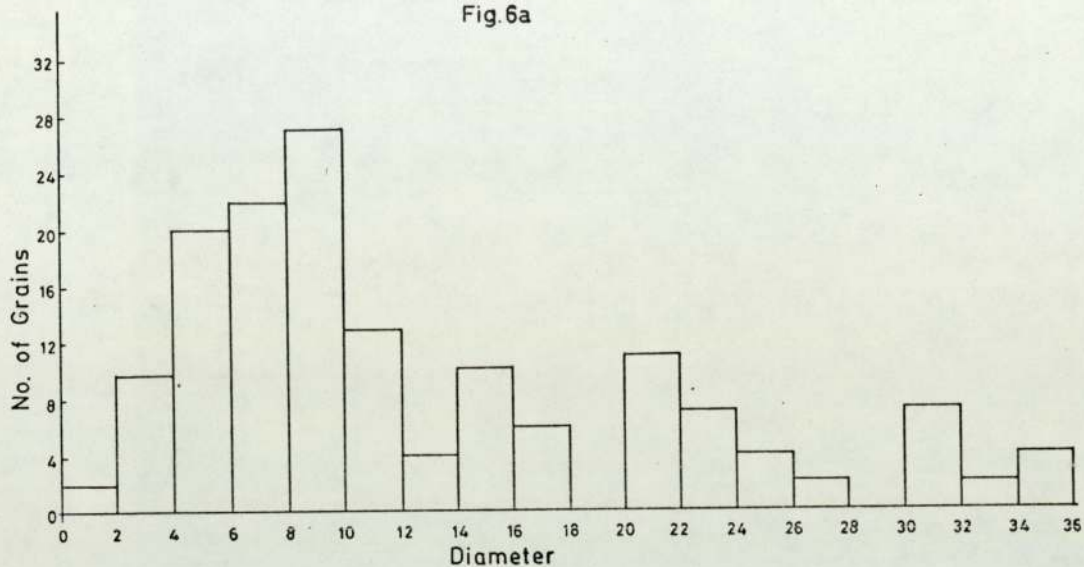


Fig. 6b

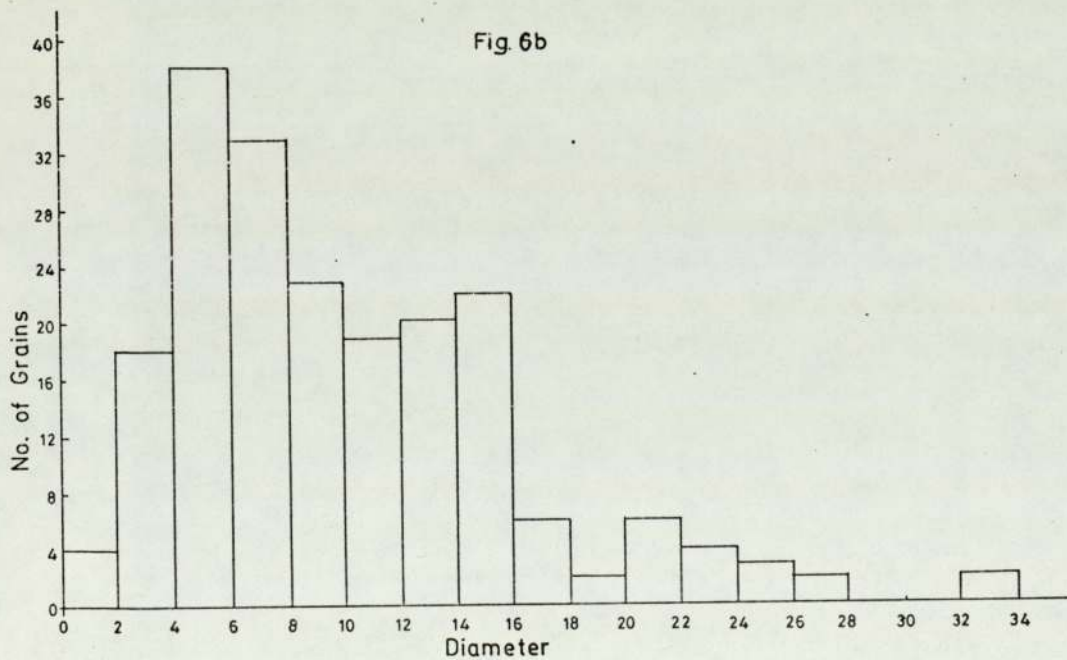


Fig. 6a Size distribution of framboidal pyrites in sample A15/920 (180 frambooids)

Fig. 6b Size distribution of framboidal pyrites in sample A15/941 (160 frambooids)

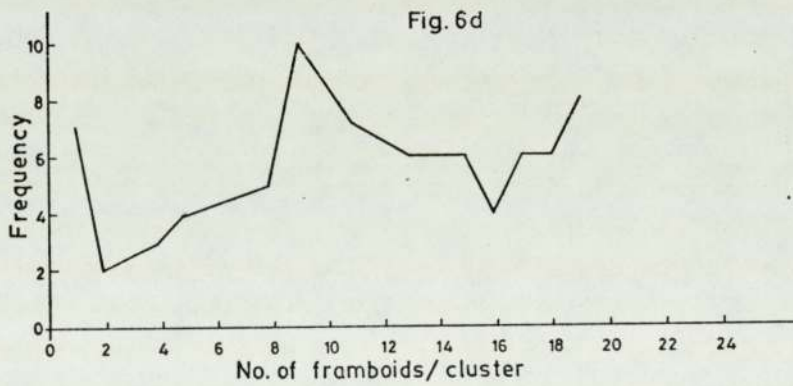
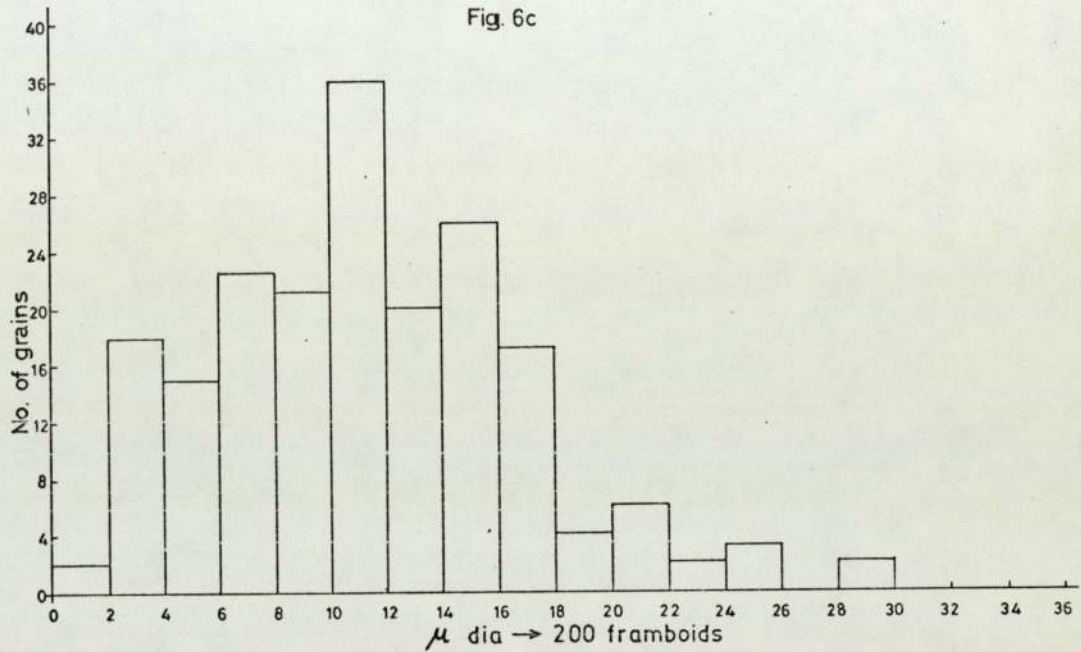


Fig. 6c Size distribution of framboidal pyrites in samples H4/460 and H4/474

Fig. 6d Plot of frequency against number of frambooids/cluster (sample H4/464)

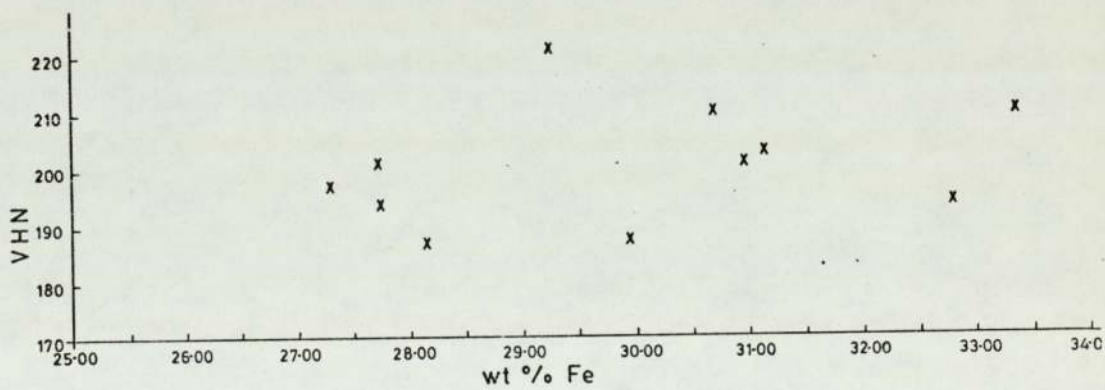
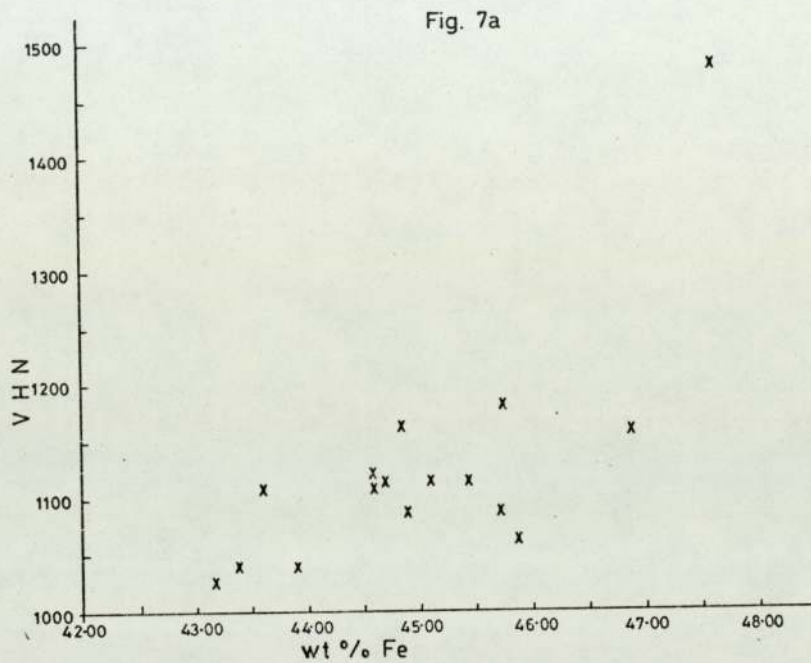


Fig. 7a Plot of microhardness (VHN) against wt% Fe in pyrite
 Fig. 7b Plot of microhardness (VHN) against wt% Fe in chalcopyrite

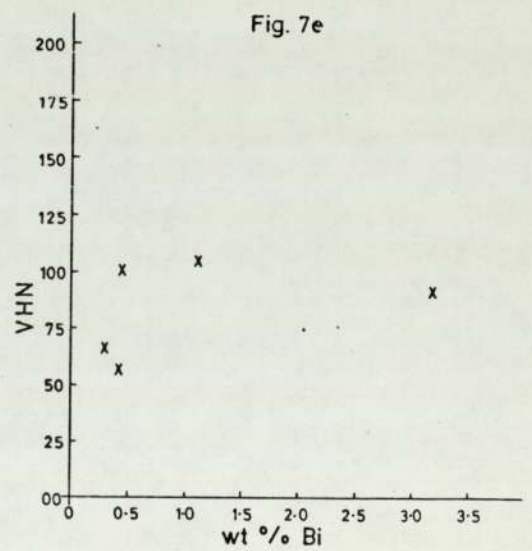
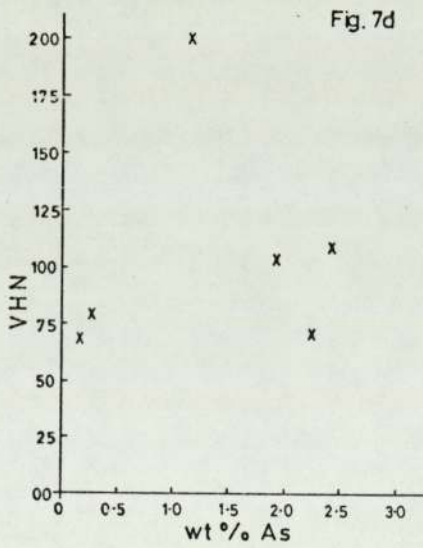
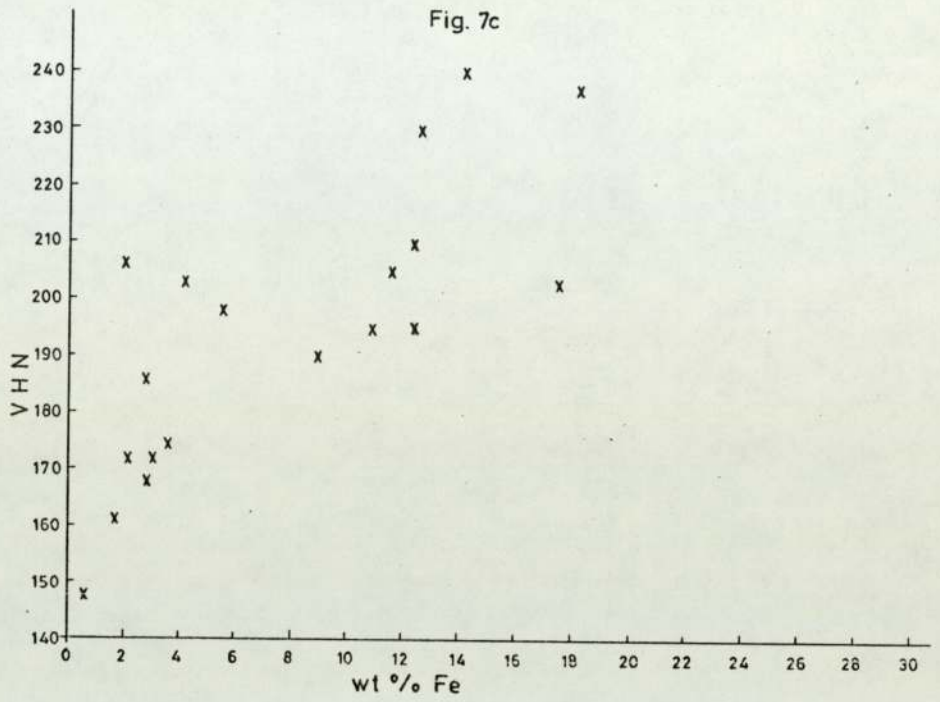


Fig. 7c Plot of microhardness (VHN) against wt% Fe in sphalerite
 Fig. 7d Plot of microhardness (VHN) against wt% As in galena
 Fig. 7e Plot of microhardness (VHN) against wt% Bi in galena

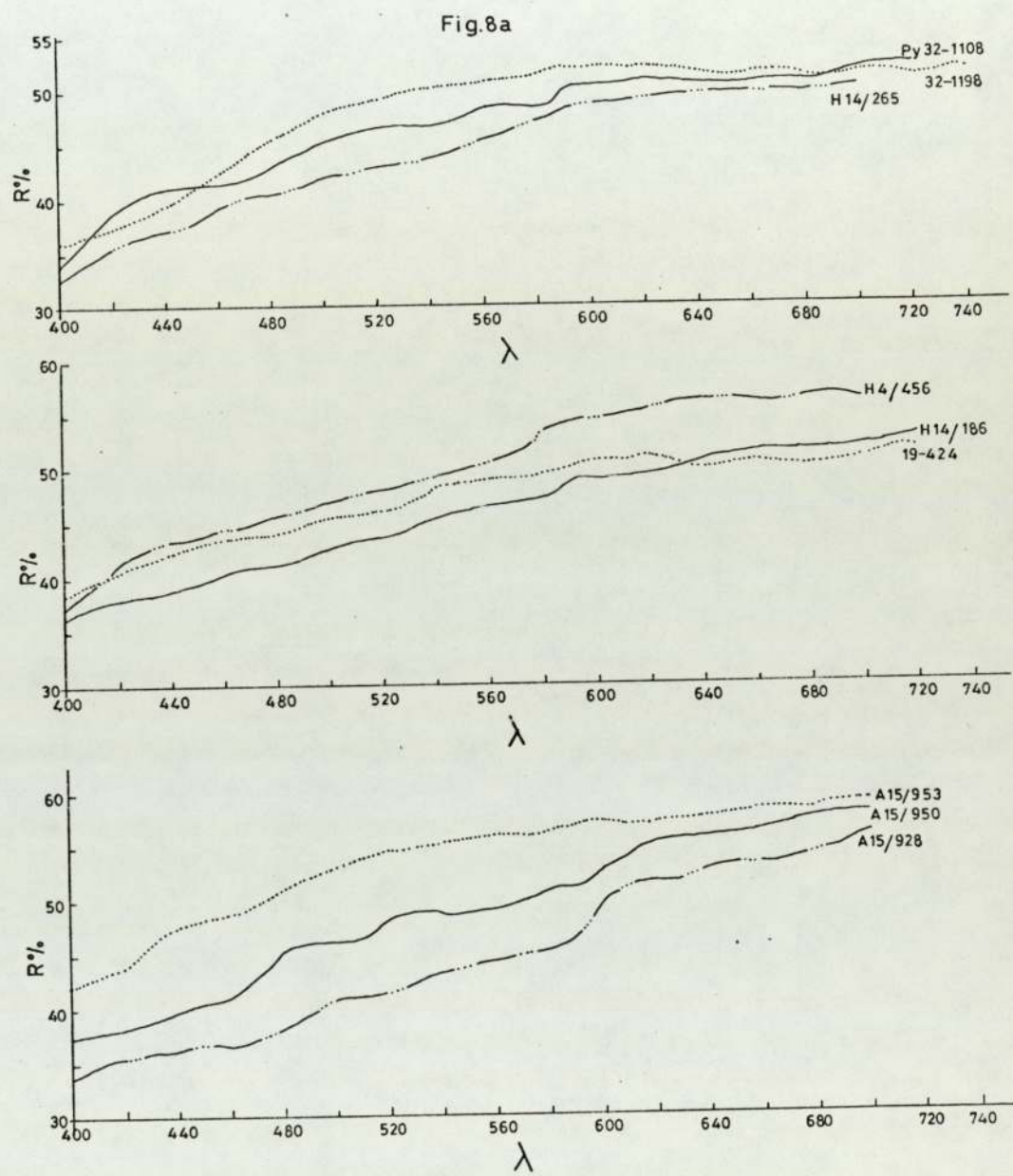


Fig. 8a Spectral reflectivity profiles of pyrite R% - Reflectivity; (air)
 λ - wave length
 32-1108, 32-1198 Euhedral pyrites; H 14/265, H14/186, 19-424,
 A 15/950, M 10/1630, all anhedral pyrites; H 4/456, A 15/953,
 A 15/928 Framboidal pyrites

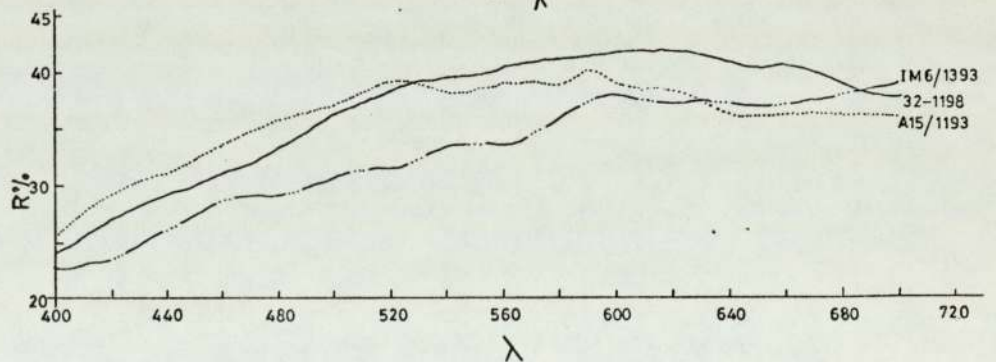
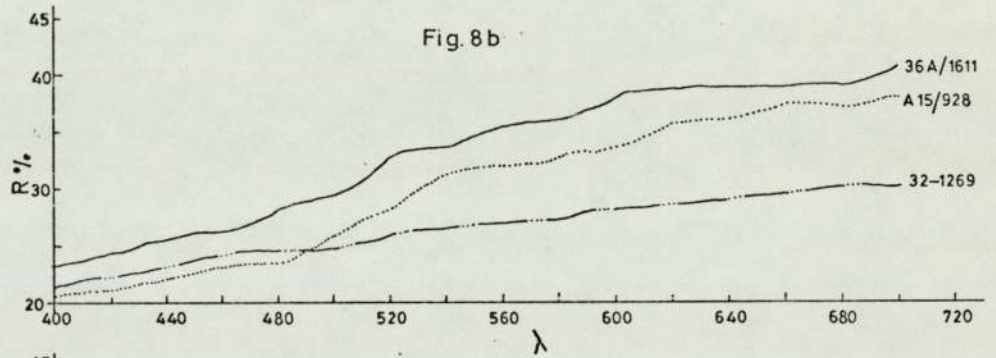
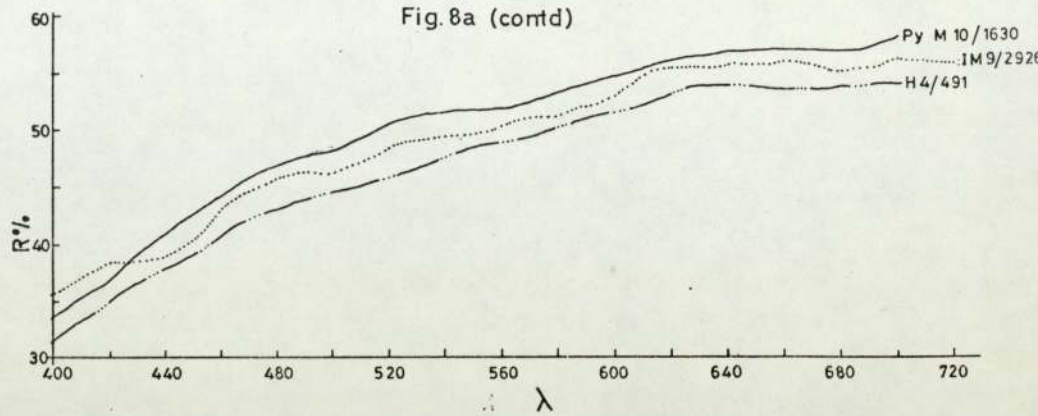


Fig. 8b Spectral reflectivity profiles of chalcopyrite (sample number is given at the end of each curve)
 R% - Reflectivity (air)
 λ - Wave length

Fig. 8c

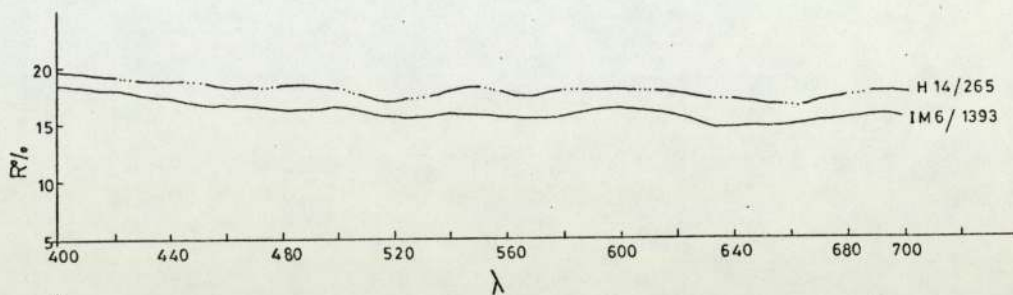


Fig. 8d

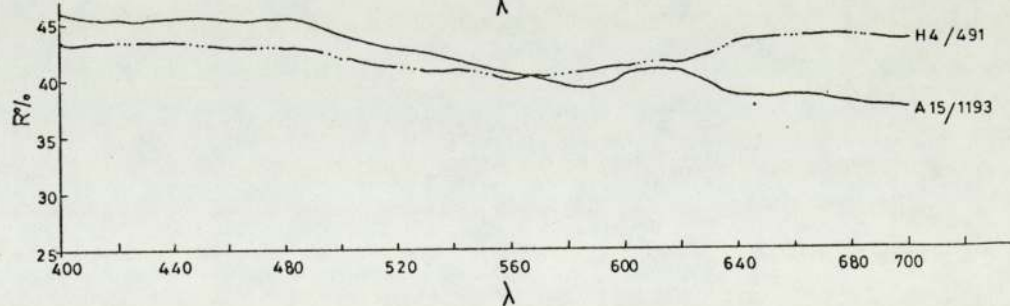
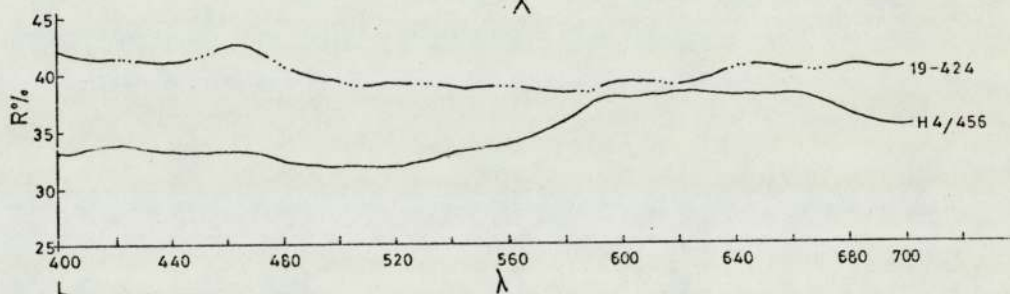
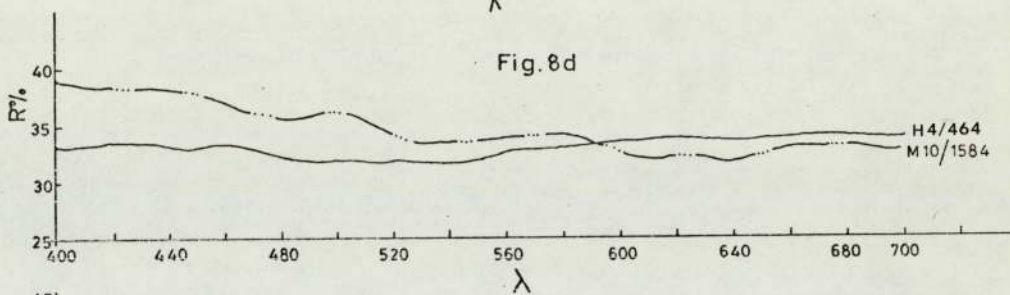


Fig. 8c Spectral reflectivity profiles of sphalerite
Fig. 8d Spectral reflectivity profiles of galena
R% - Reflectivity (air)
λ - Wave length
Sample number is given at the end of each curve.

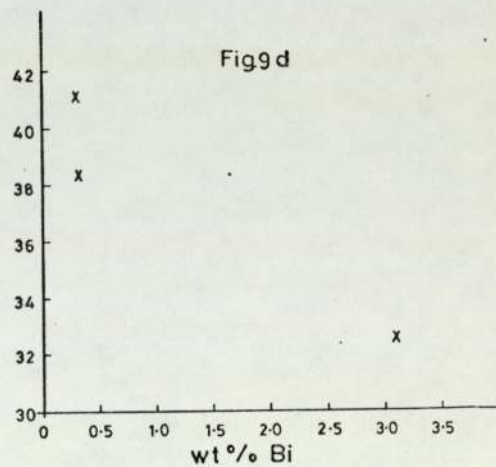
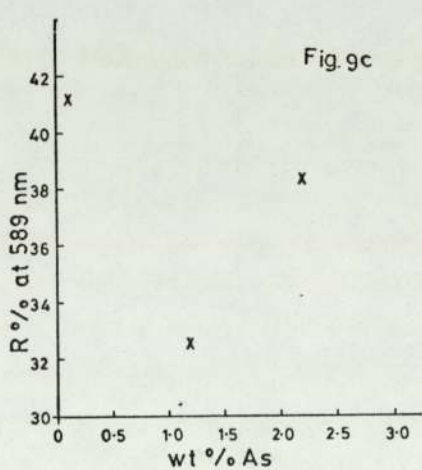
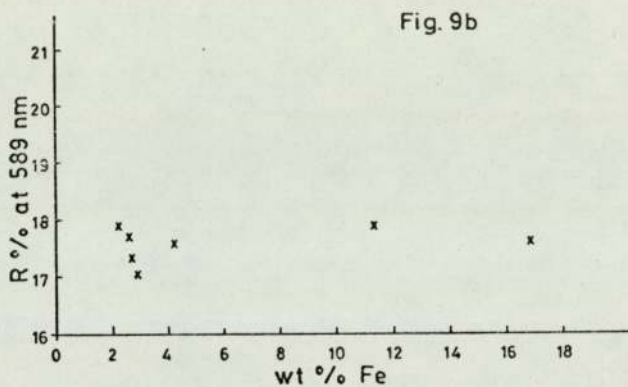
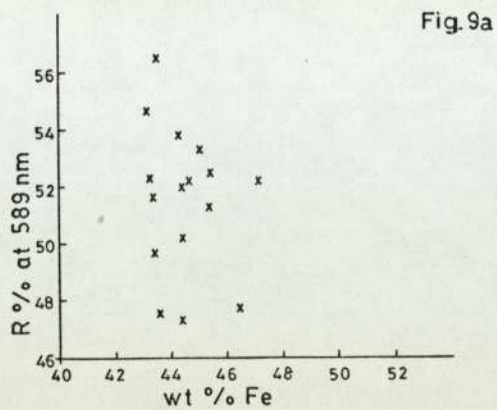
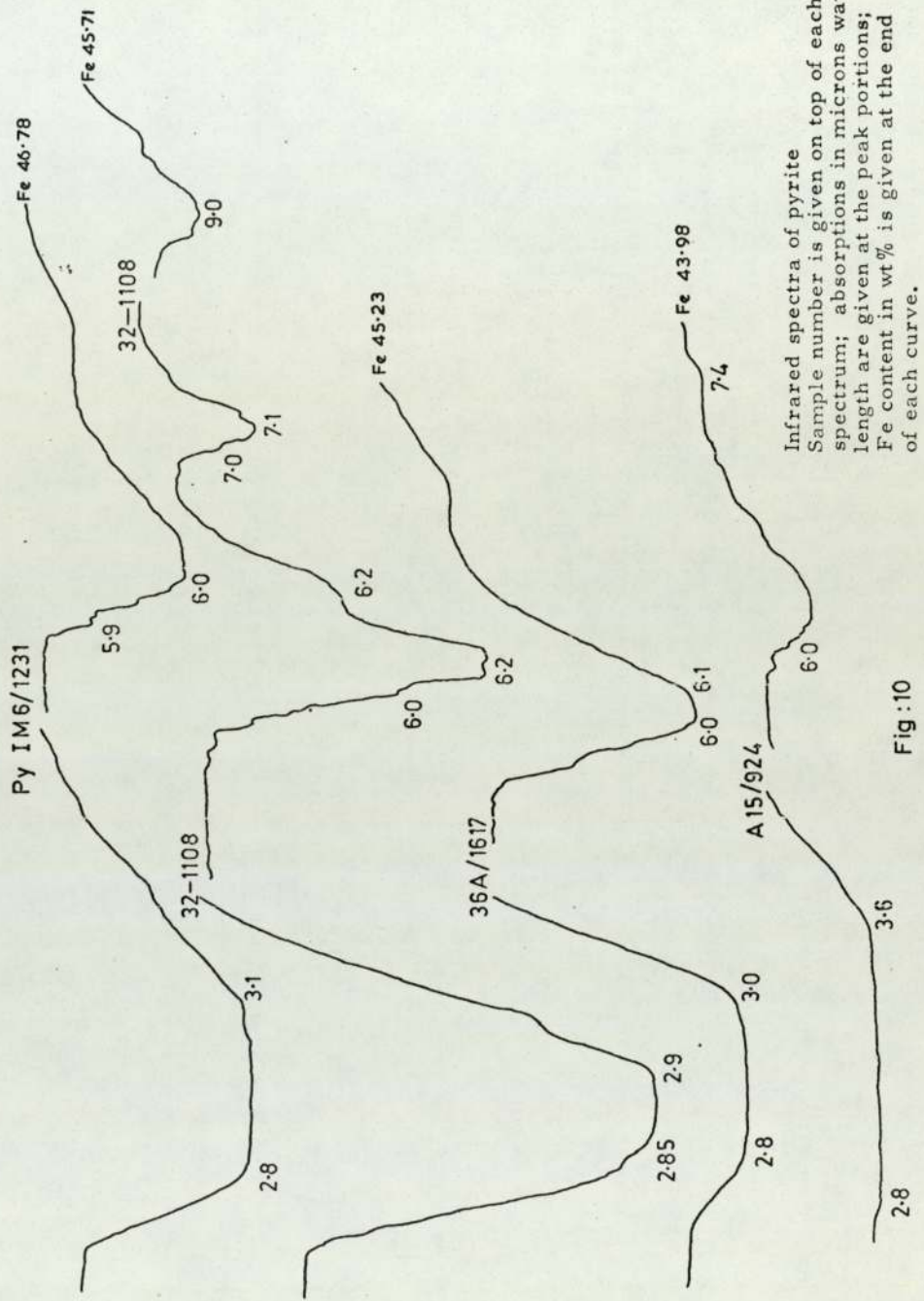


Fig. 9a Plot of Reflectivity (R%) at 589nm against wt% Fe in pyrite
 Fig. 9b Plot of Reflectivity (R%) at 589nm against wt% Fe in sphalerite
 Fig. 9c Plot of Reflectivity (R%) at 589nm against wt% As in galena
 Fig. 9d Plot of Reflectivity (R%) at 589nm against wt% Bi in galena



Infrared spectra of pyrite
 Sample number is given on top of each
 spectrum; absorptions in microns wave
 length are given at the peak portions;
 Fe content in wt% is given at the end
 of each curve.

Fig:10

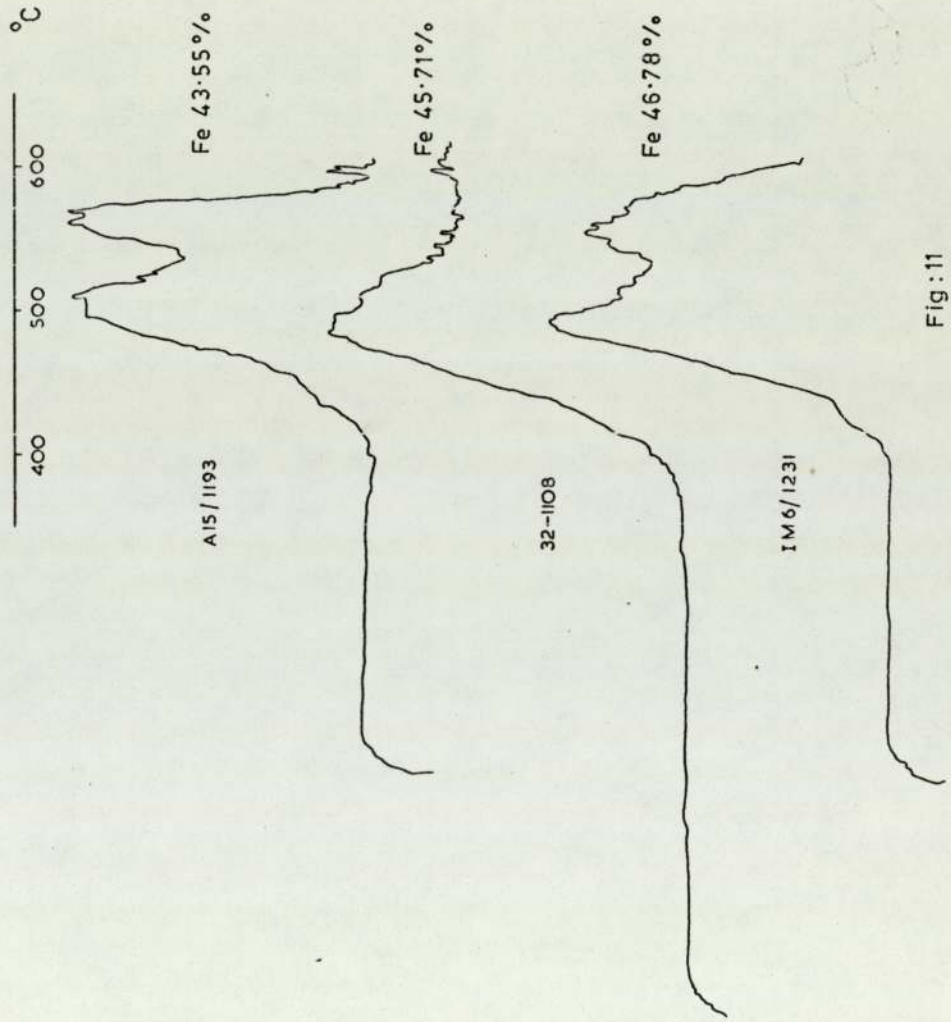
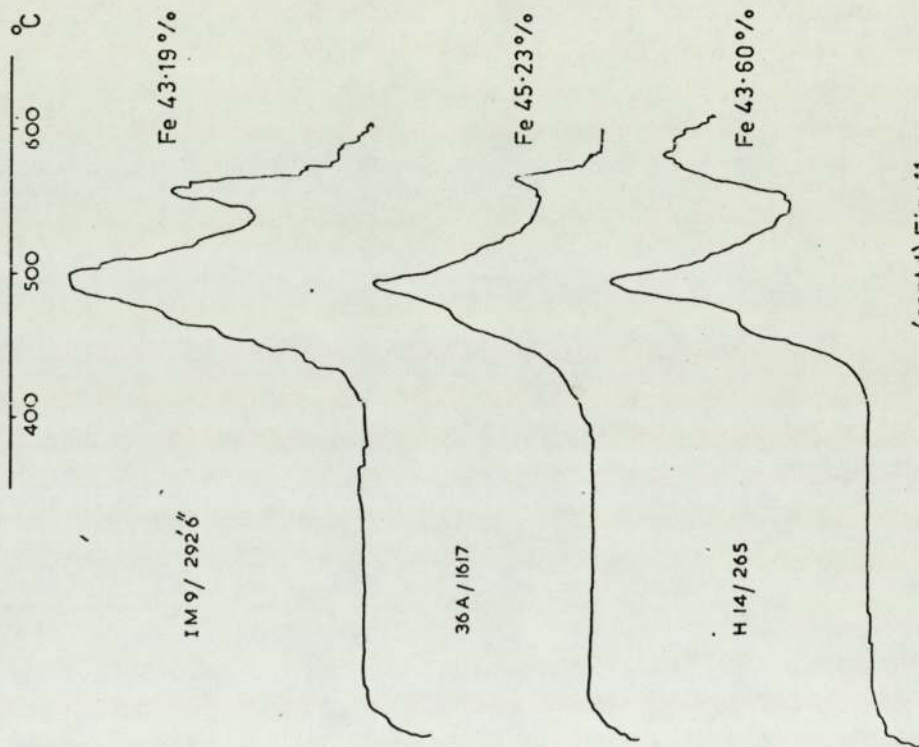


Fig: 11

D.t.a. curves of pyrite. Sample numbers are given at the left hand side of each curve; Fe content in wt% is given at the right hand side of each curve.



(contd) Fig : 11

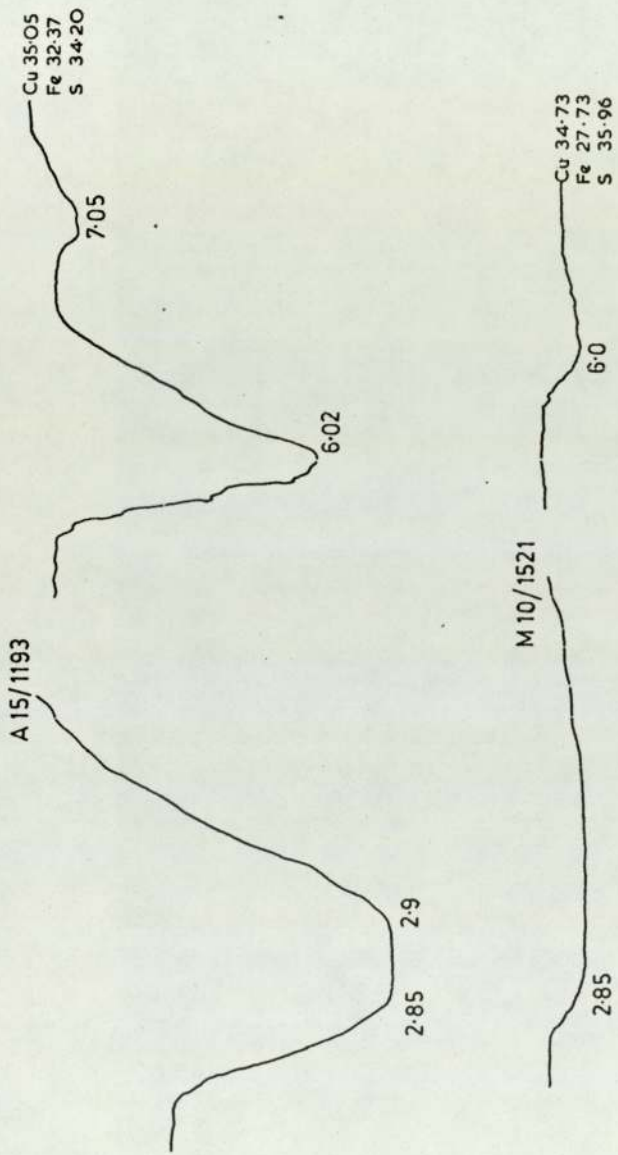


Fig :12

Infrared spectra of chalcopyrite. Sample number is given on top of each spectrum. Absorptions in microns wave length are given at peak portions. Composition in wt% is given at the end of each spectrum.

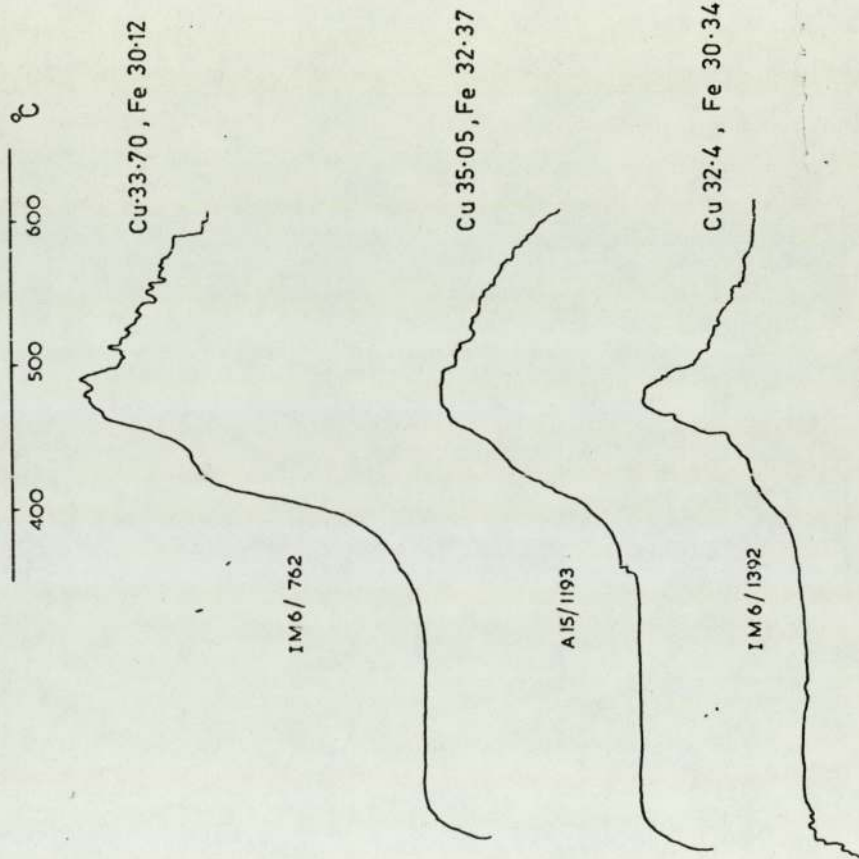
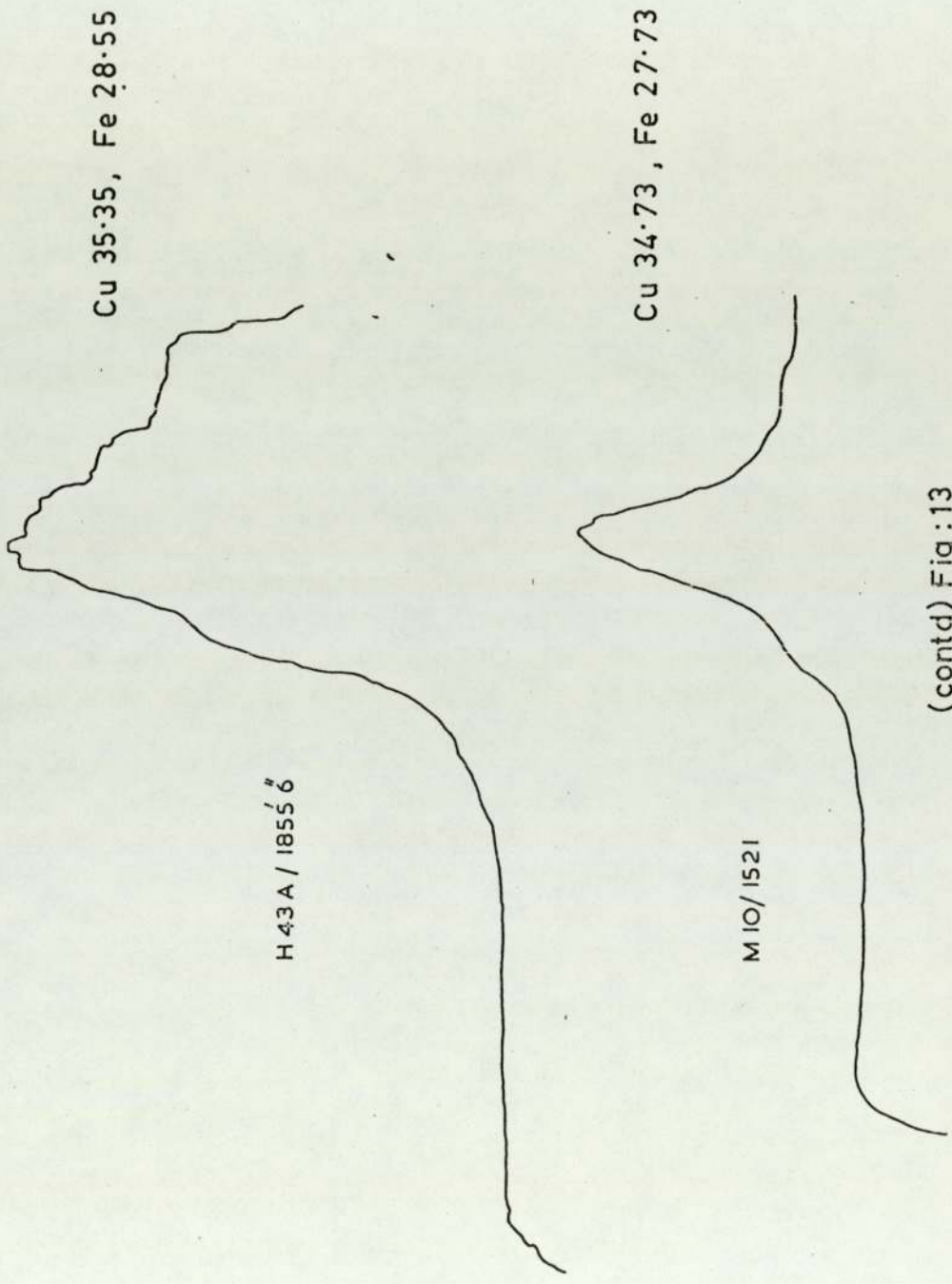


Fig:13

D. t. a. curves of chalcopyrite. Sample number is given at the left hand side of each curve. Wt% Cu and Fe are given at the right hand side of each curve.

400 500 600 °C



(contd) Fig:13

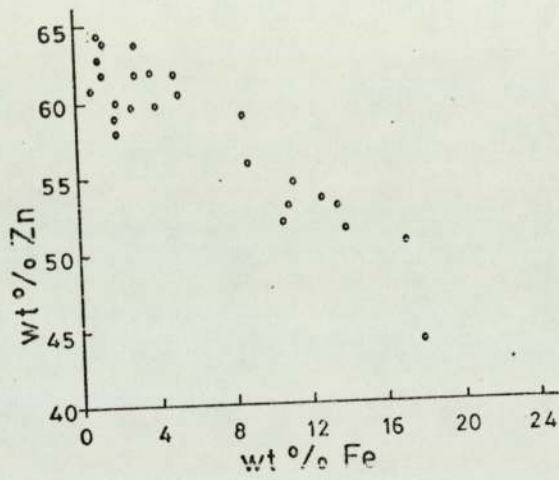


Fig.14

Plot of wt% Zn against wt% Fe in sphalerite

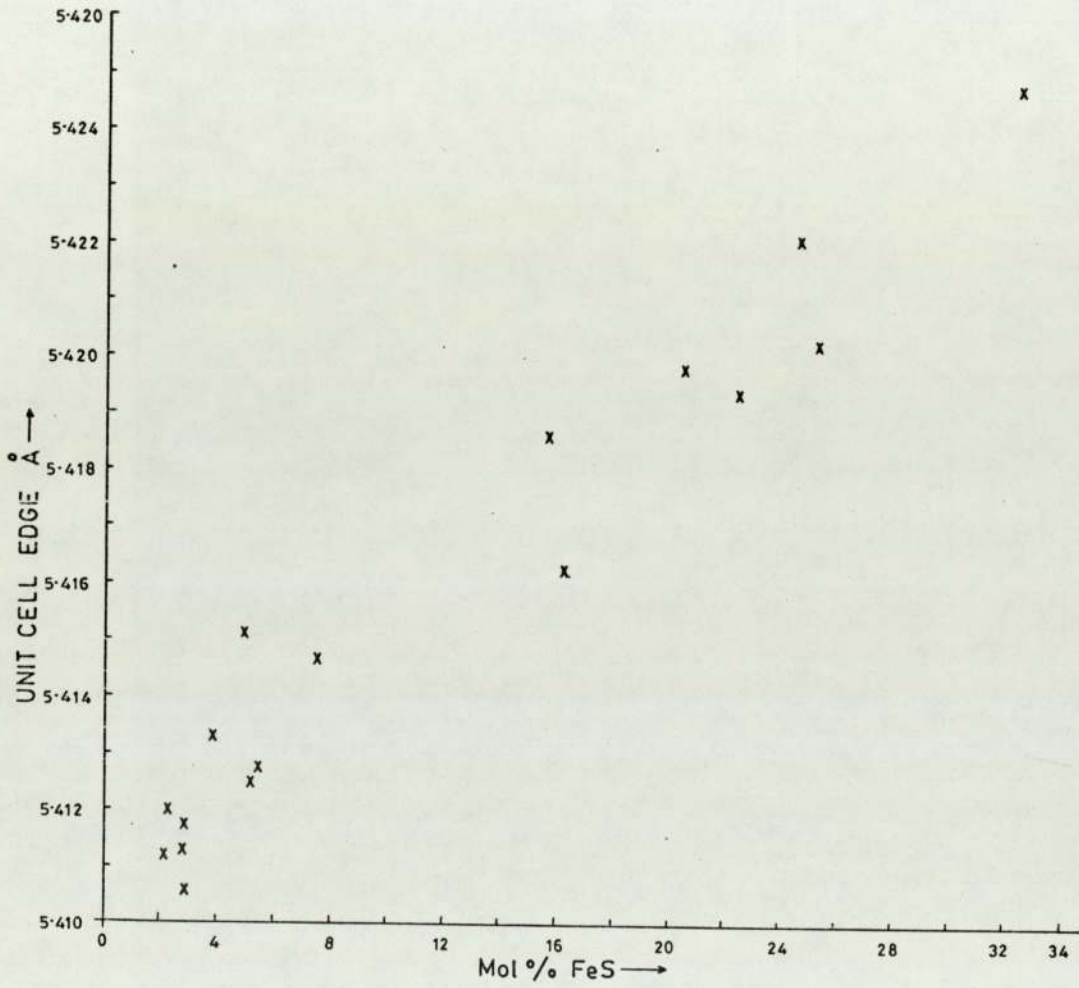


Fig. 15

Plot of Mol % FeS against unit cell edges of sphalerite

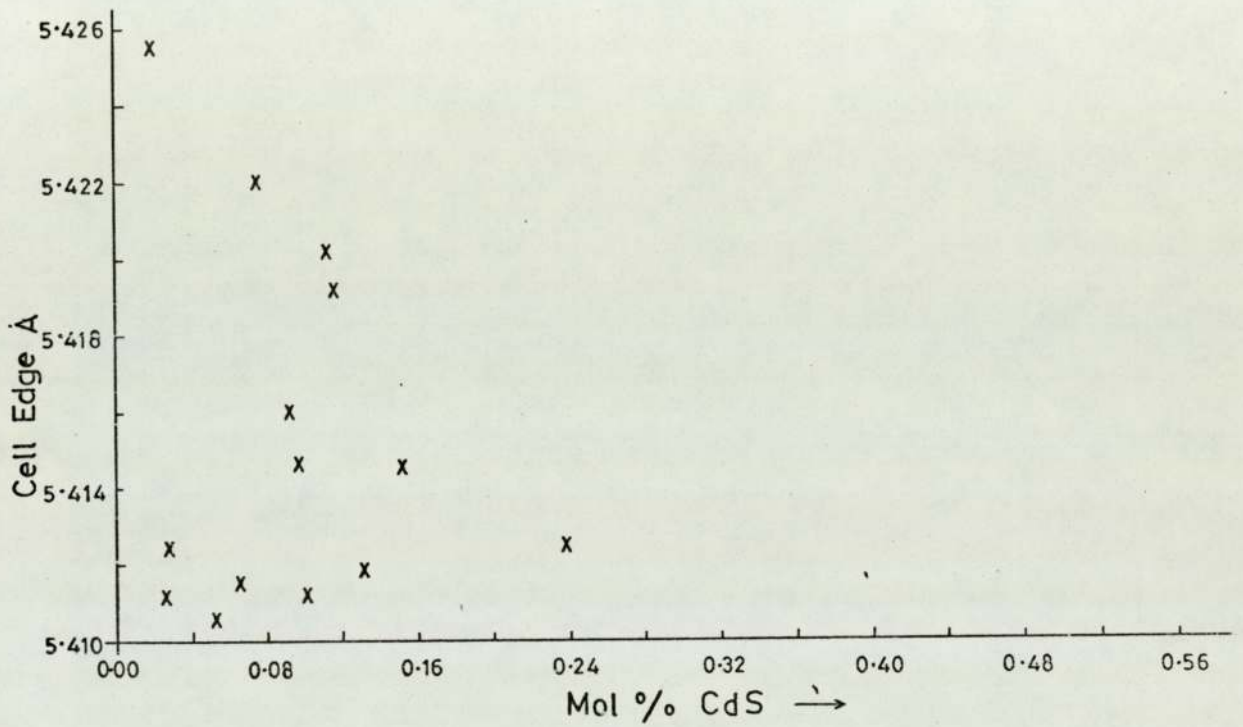
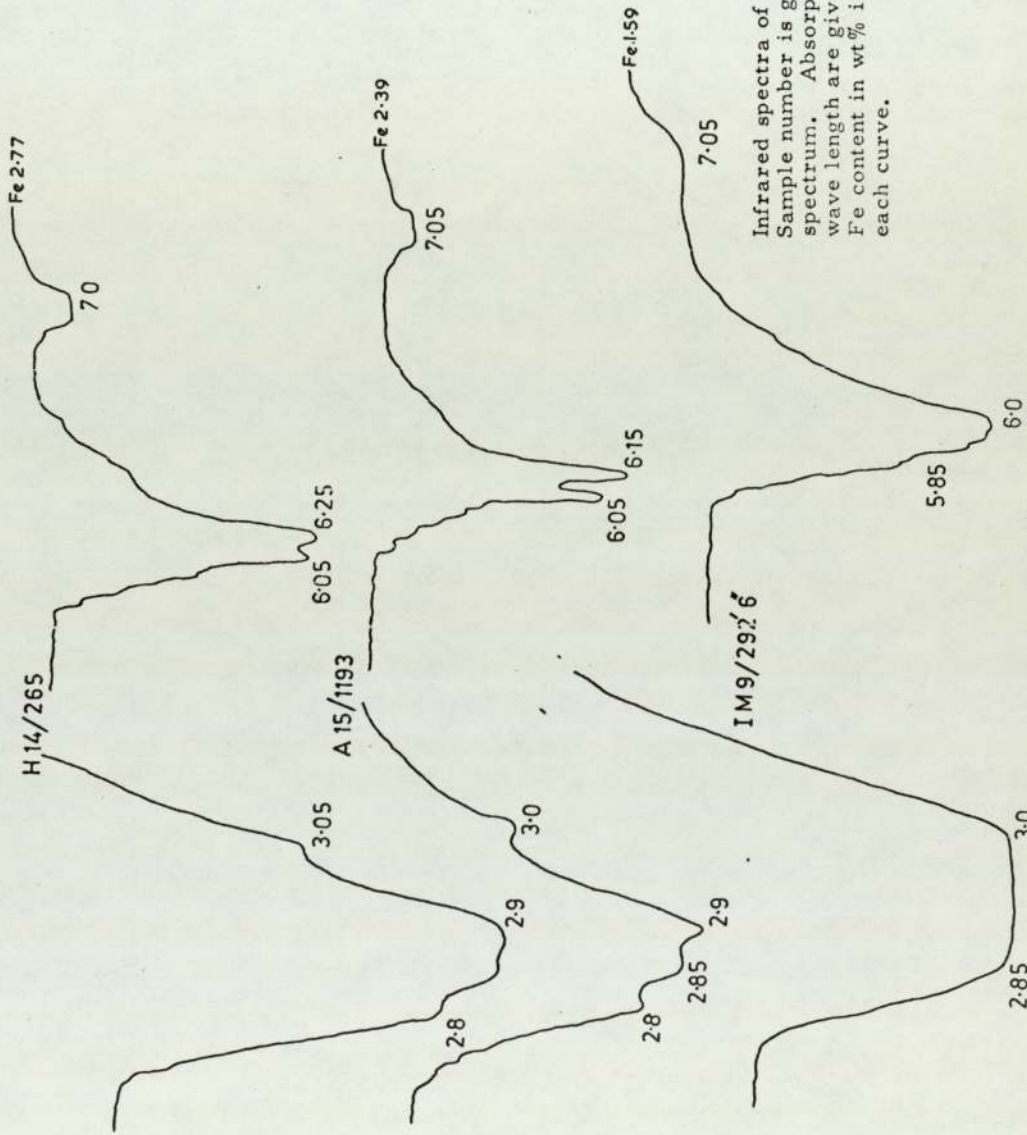


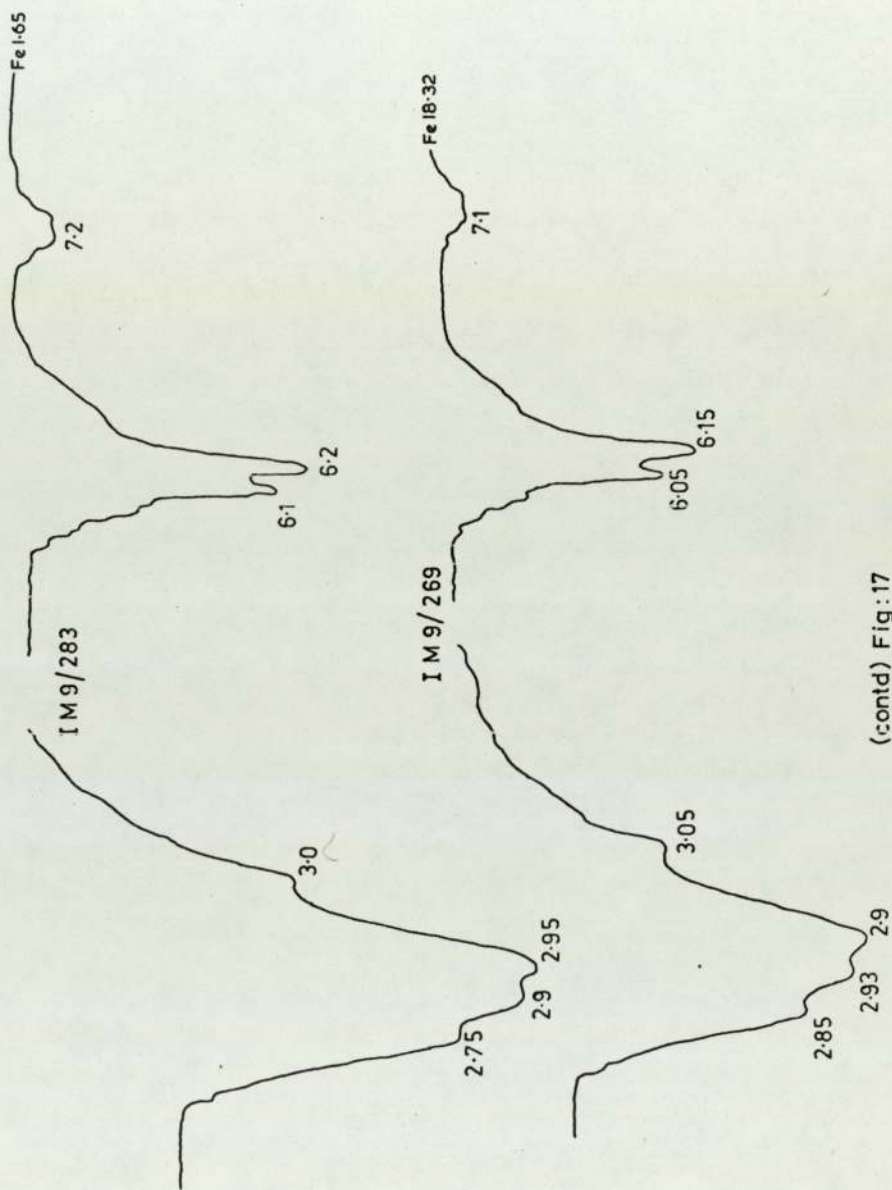
Fig. 16

Plot of Mol% CdS against unit cell edges of sphalerite



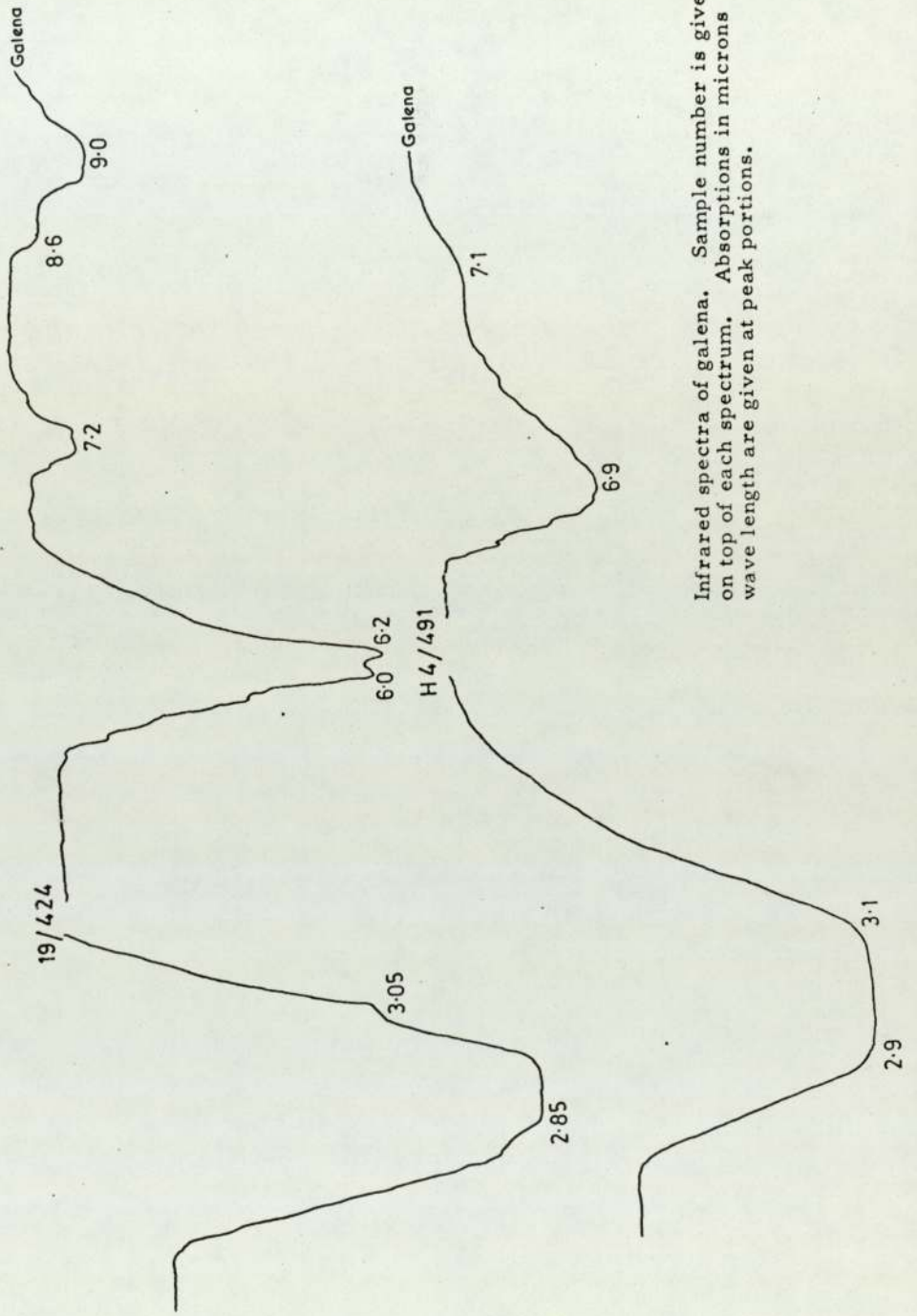
Infrared spectra of sphalerite.
 Sample number is given on top of each spectrum. Absorptions in microns wave length are given at the peak portions. Fe content in wt% is given at the end of each curve.

Fig:17



(contd) Fig: 17

Fig: 18



Infrared spectra of galena. Sample number is given on top of each spectrum. Absorptions in microns wave length are given at peak portions.

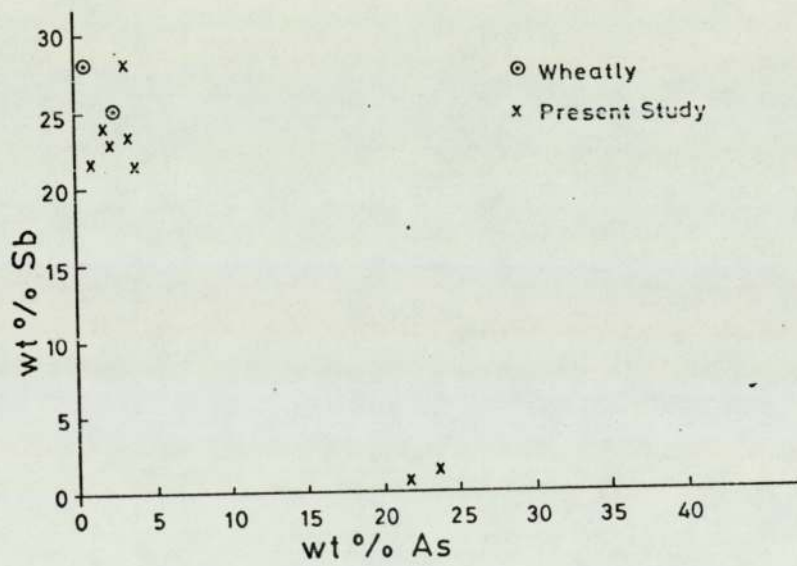
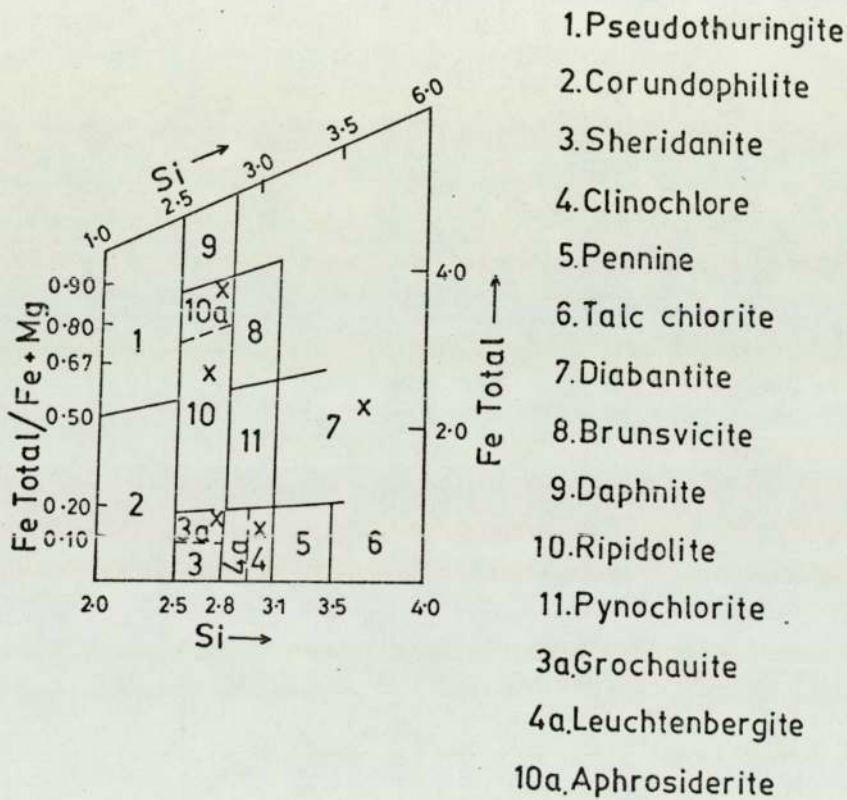


Fig.19

Plot of wt% Sb against wt% As in tetrahedrite-tennantites showing the compositional break.

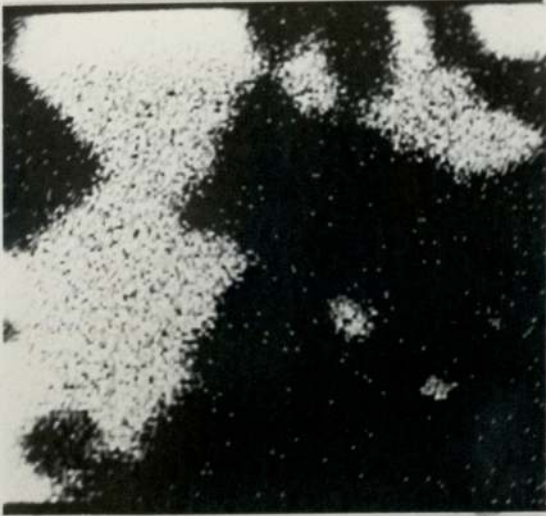
Fig. 20



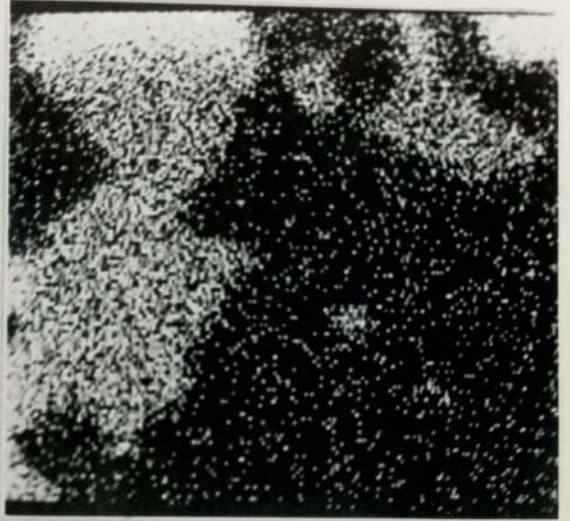
Orthochlorites showing the species and variety boundaries (after Hey, 1954)
 X - shows the Parys Mountain Species

PLATE IV

A



B



C



D

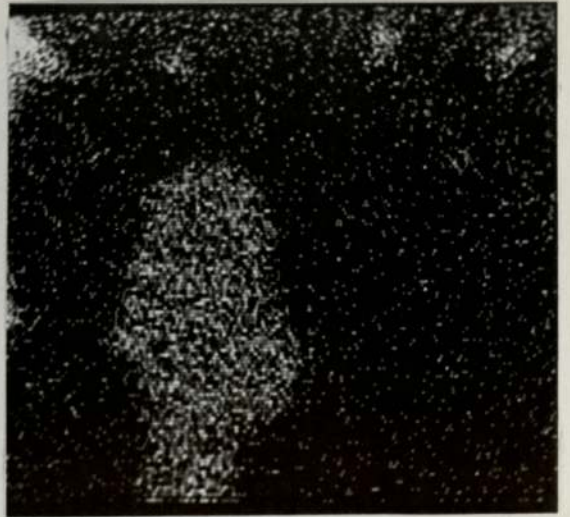


Plate IV X-ray images

A-B Tetrahedrite in sample 27-145

A - Sb L_α

B - As K_α

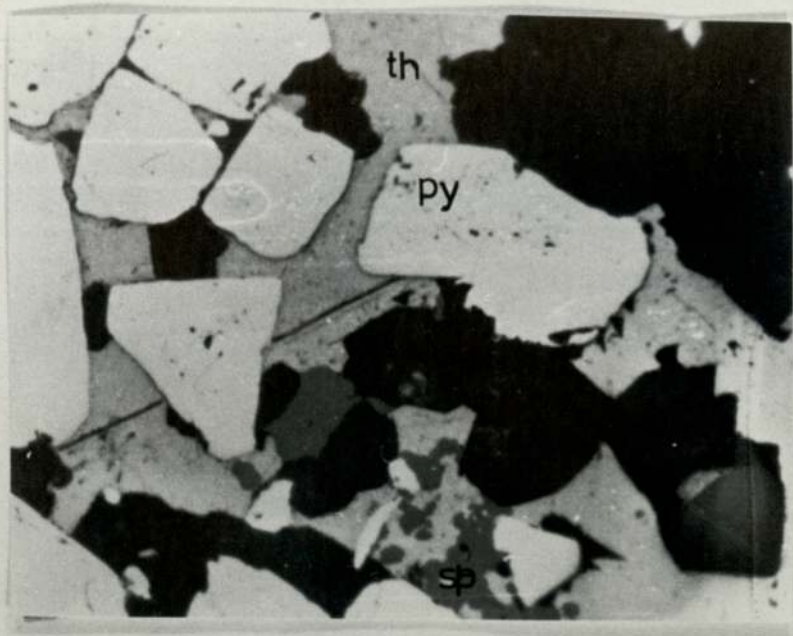
C-D Tennantite in sample 27-145

C - As K_α

D - Sb L_α

PLATE III

A



B

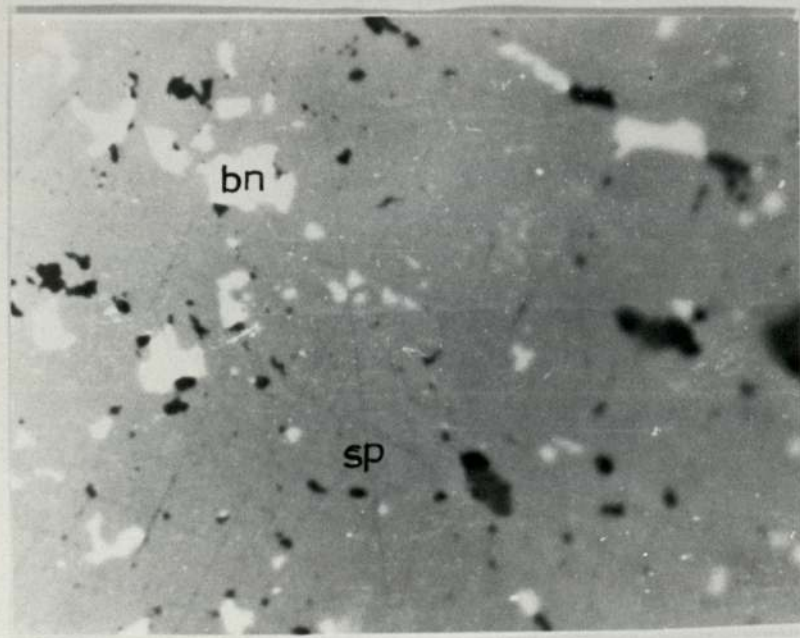
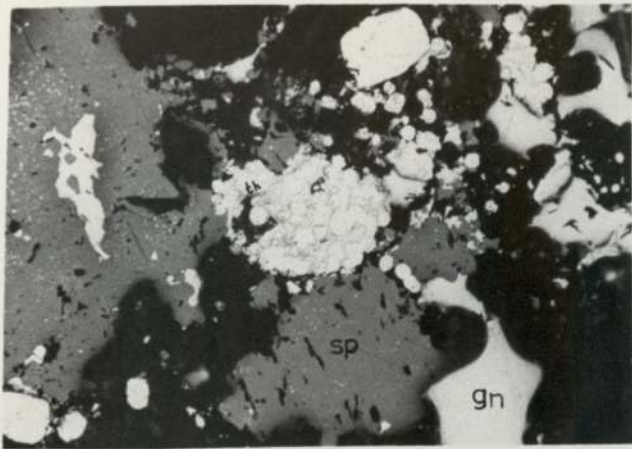


Plate III Photomicrographs

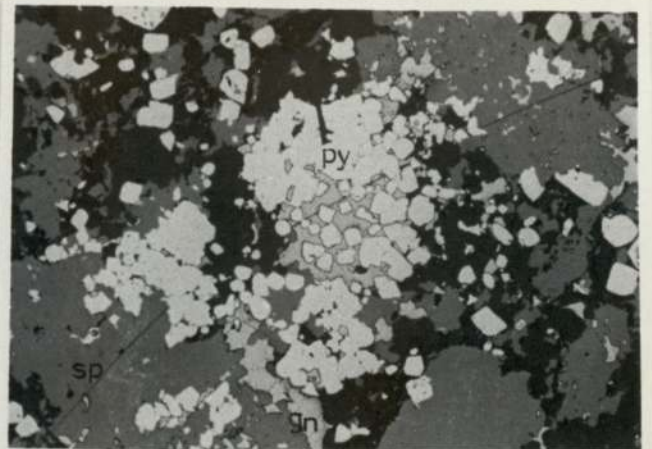
- A Sample from bore hole 27 at 145 feet depth. Tetra-
hedrite (th) forming the interstitial and fracture
infillings of pyrite. 16 x (air)
- B Sample from bore hole H4 at 465 feet depth.
Sphalerite (sp) with inclusions/infillings of
bournonite (bn). 40 x (oil)

PLATE II

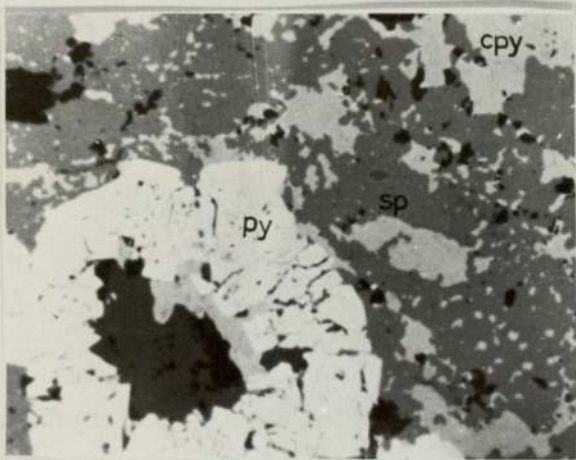
A



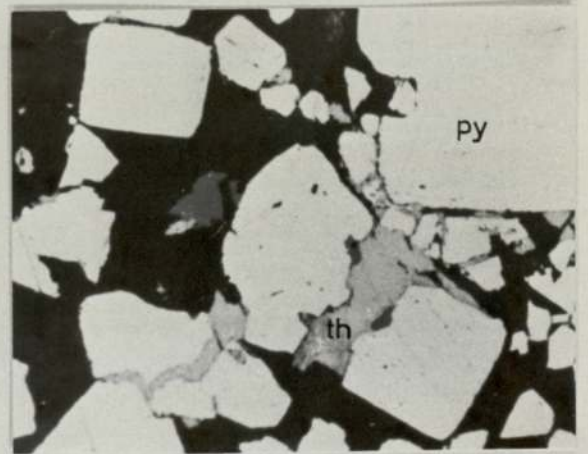
B



C



D



E

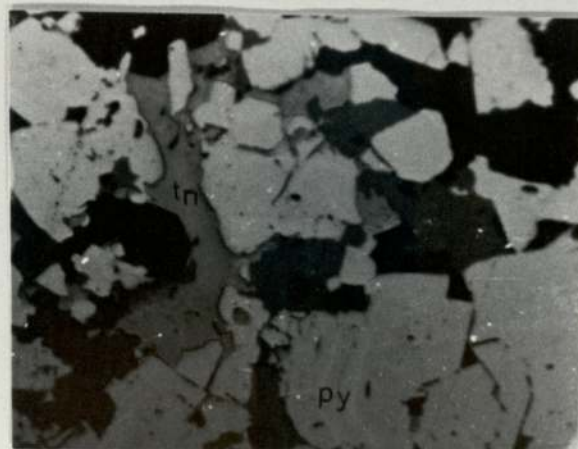
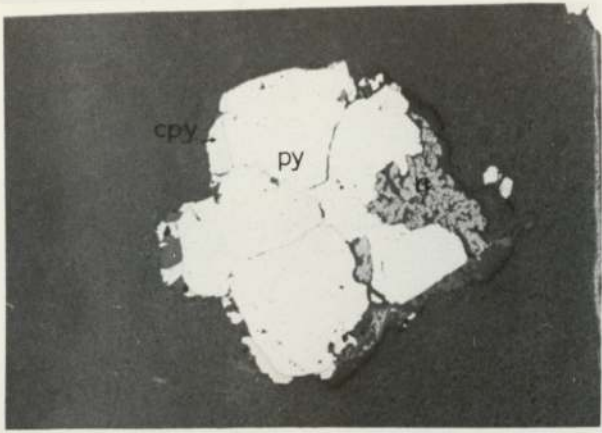


Plate II Photomicrographs

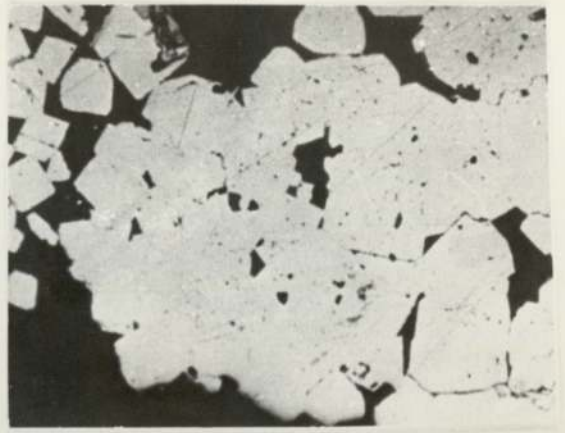
- A-B Sample from bore hole H4 at 474 feet depth. Sphalerites (sp) showing intergrowths with galena (gn). Galena and tetrahedrites forming interstitial matrix for pyrites. 16 x (oil)
- C Sample from bore hole IM6 at 1392 feet depth. Pyrite (py) showing the radiating texture. Chalcopyrite (cpy) and sphalerite (sp) show intergrowth textures. Chalcopyrite is also seen replacing the core of the pyrite and filling in its fractures. 16 x (air)
- D Sample from bore hole 27 at 145 feet depth. Tetrahedrite (th) forming the interstitial and fracture infillings of pyrite. 16 x (air)
- E Sample from bore hole 27 at 145 feet depth. Pyrite (bottom centre) showing zoning. Tennantite (tn) is filling in the interstitial spaces of pyrite. 16 x (air)

PLATE I

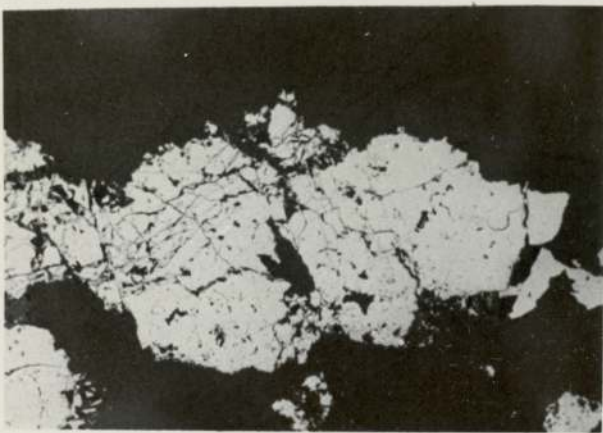
A



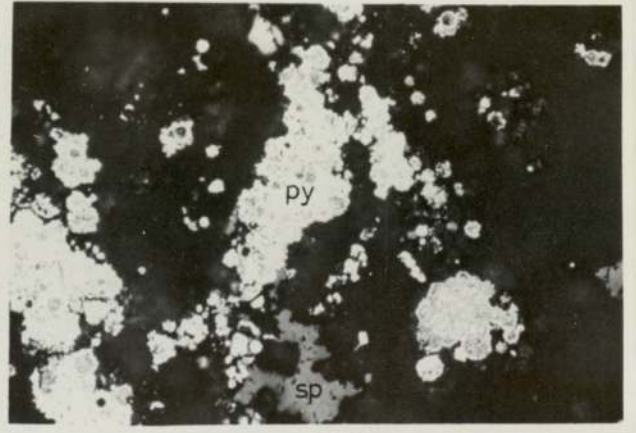
B



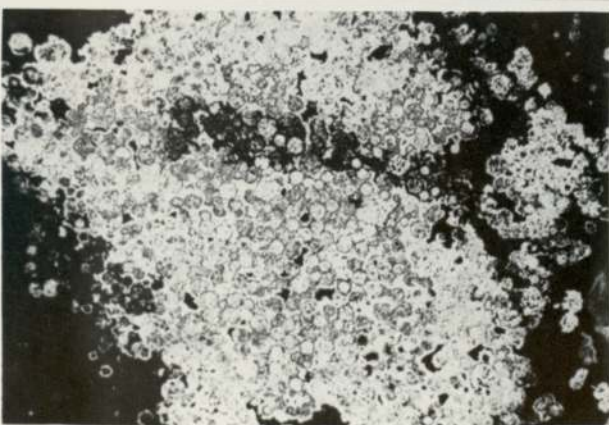
C



D



E



F

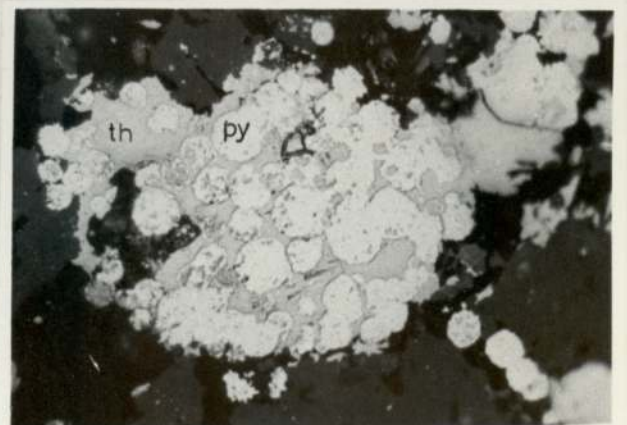
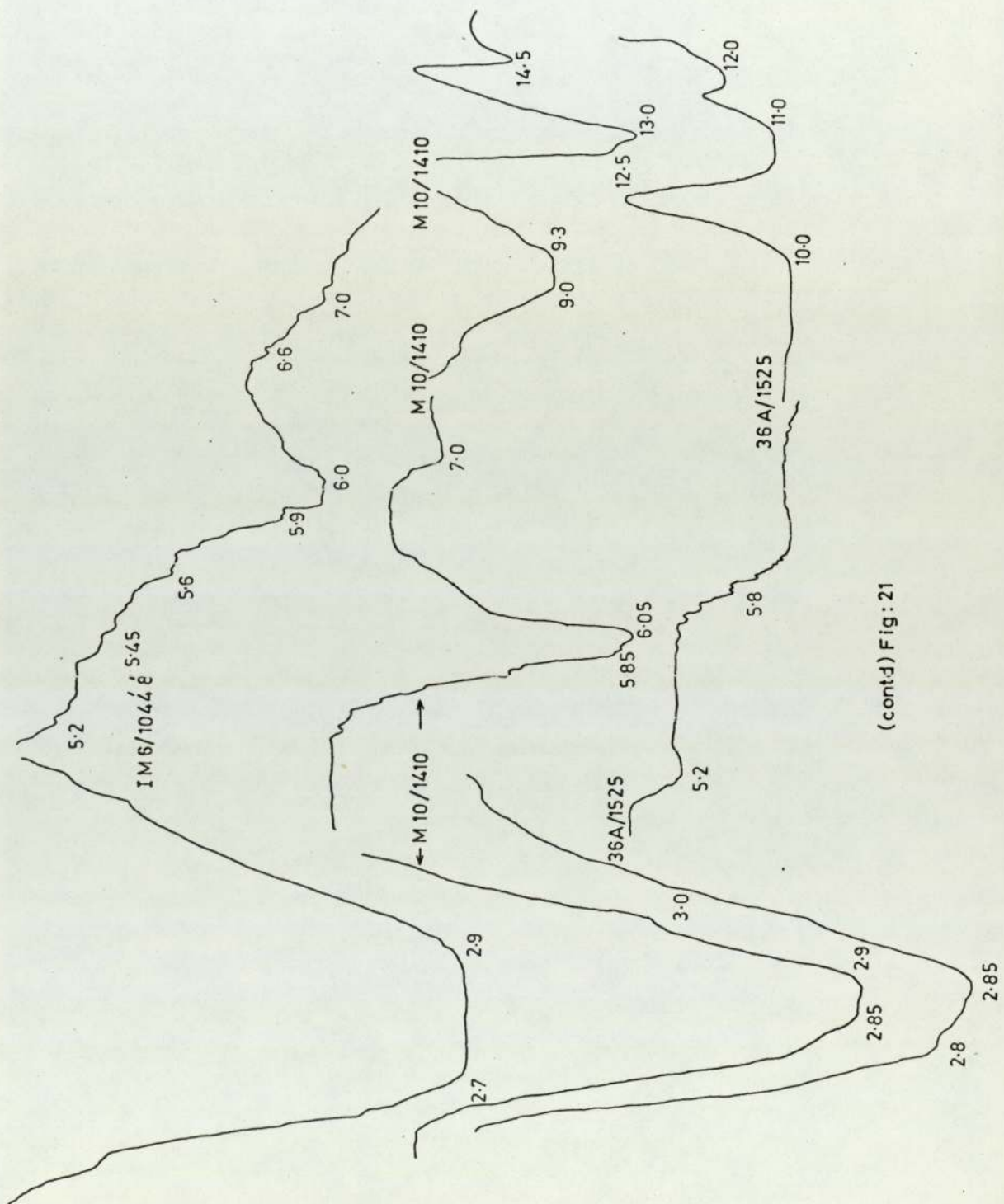
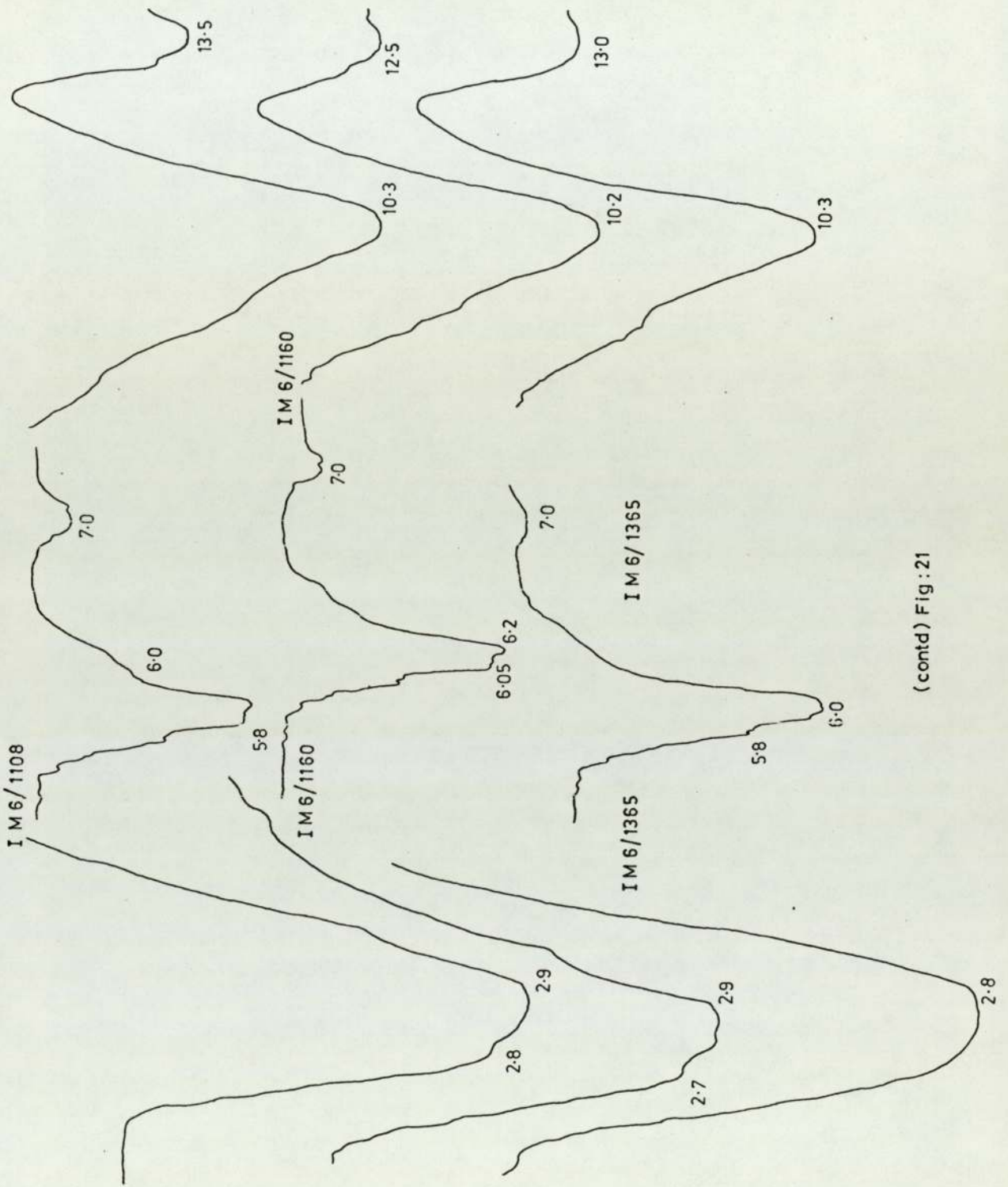


Plate I Photomicrographs

- A Sample from bore hole 32 at 1198 feet depth. Pyrite (py) associated with rutile (rt). Chalcopyrite rims pyrite and replaces it at grain boundaries.
4 x (air)
- B Sample from bore hole 27 at 145 feet depth. Aggregate of euhedral pyrites homogenised at the centre of the aggregate but retaining the cubic outlines at the periphery.
4 x (air)
- C Sample from bore hole A 15 at 1193 feet depth. Pyrite showing intense fractures developed due to cataclasis.
4 x (air)
- D Sample from bore hole H 4 at 464 feet depth. Framboidal pyrites (py) forming clusters. Sphalerite (sp) is also seen.
16 x (oil)
- E Sample from bore hole H4 at 464 feet depth. Framboidal pyrites showing atoll textures with tetrahedrite-tennantite forming the interstitial infillings.
16 x (oil)
- F Sample from bore hole H4 at 474 feet depth. Framboidal pyrites (py) with interstitial infillings of tetrahedrite (th).
16 x (oil)



(contd) Fig: 21



(contd) Fig : 21

Fig. 21 Infrared spectra of chlorites.
36A/1670, A15/946, M10/1410 Ripidolite
36A/1617, IM6/1044'8" Diabantite
IM6/1359, 36A/1525 Chlorite 1b
IM6/1365 Aphrosiderite and grochauite
IM6/1108, IM6/1160 Chlorites (species not identified)

Sample number is given on top of each spectrum; absorptions in microns wave length are given at the peak portions.